UNITED STATES AIR FORCE

SUMMER RESEARCH PROGRAM -- 1996

HIGH SCHOOL APPRENTICESHIP PROGRAM FINAL REPORTS

VOLUME 15A

WRIGHT LABORATORY

RESEARCH & DEVELOPMENT LABORATORIES

5800 Uplander Way

Culver City, CA 90230-6608

Program Director, RDL
Gary Moore

Program Manager, AFOSR
Major Linda Steel-Goodwin

Program Manager, RDL
Scott Licoscos

Program Administrator, RDL
Johnetta Thompson

Program Administrator, RDL
Rebecca Kelly

Submitted to:

AIR FORCE OFFICE OF SCIENTIFIC RESEARCH

Bolling Air Force Base

Washington, D.C.

December 1996

REPORT DOCUMENTATION PAG

Form Approved
OMB No. 0704-0188

AFRL-SR-BL-TR-00-

0747

1. AGENCY USE ONLY *(Leave blank)*	2. REPORT DATE	
	December, 1996	

4. TITLE AND SUBTITLE
1996 Summer Research Program (SRP), High School Apprenticeship Program (HSAP), Final Reports, Volume 15A, Wright Laboratory

5. FUNDING NUMBERS
F49620-93-C-0063

6. AUTHOR(S)
Gary Moore

7. PERFORMING ORGANIZATION NAME(S) AND ADDRESS(ES)
Research & Development Laboratories (RDL)
5800 Uplander Way
Culver City, CA 90230-6608

8. PERFORMING ORGANIZATION REPORT NUMBER

9. SPONSORING/MONITORING AGENCY NAME(S) AND ADDRESS(ES)
Air Force Office of Scientific Research (AFOSR)
801 N. Randolph St.
Arlington, VA 22203-1977

10. SPONSORING/MONITORING AGENCY REPORT NUMBER

11. SUPPLEMENTARY NOTES

12a. DISTRIBUTION AVAILABILITY STATEMENT
Approved for Public Release

12b. DISTRIBUTION CODE

13. ABSTRACT *(Maximum 200 words)*

The United States Air Force Summer Research Program (USAF-SRP) is designed to introduce university, college, and technical institute faculty members, graduate students, and high school students to Air Force research. This is accomplished by the faculty members (Summer Faculty Research Program, (SFRP)), graduate students (Graduate Student Research Program (GSRP)), and high school students (High School Apprenticeship Program (HSAP)) being selected on a nationally advertised competitive basis during the summer intersession period to perform research at Air Force Research Laboratory (AFRL) Technical Directorates, Air Force Air Logistics Centers (ALC), and other AF Laboratories. This volume consists of a program overview, program management statistics, and the final technical reports from the HSAP participants at the Wright Laboratory.

14. SUBJECT TERMS
Air Force Research, Air Force, Engineering, Laboratories, Reports, Summer, Universities, Faculty, Graduate Student, High School Student

15. NUMBER OF PAGES

16. PRICE CODE

17. SECURITY CLASSIFICATION OF REPORT	18. SECURITY CLASSIFICATION OF THIS PAGE	19. SECURITY CLASSIFICATION OF ABSTRACT	20. LIMITATION OF ABSTRACT
Unclassified	Unclassified	Unclassified	UL

GENERAL INSTRUCTIONS FOR COMPLETING SF 298

The Report Documentation Page (RDP) is used in announcing and cataloging reports. It is important that this information be consistent with the rest of the report, particularly the cover and title page. Instructions for filling in each block of the form follow. It is important to ***stay within the lines*** to meet ***optical scanning requirements.***

Block 1. Agency Use Only *(Leave blank)*.

Block 2. Report Date. Full publication date including day, month, and year, if available (e.g. 1 Jan 88). Must cite at least the year.

Block 3. Type of Report and Dates Covered. State whether report is interim, final, etc. If applicable, enter inclusive report dates (e.g. 10 Jun 87 - 30 Jun 88).

Block 4. Title and Subtitle. A title is taken from the part of the report that provides the most meaningful and complete information. When a report is prepared in more than one volume, repeat the primary title, add volume number, and include subtitle for the specific volume. On classified documents enter the title classification in parentheses.

Block 5. Funding Numbers. To include contract and grant numbers; may include program element number(s), project number(s), task number(s), and work unit number(s). Use the following labels:

C - Contract
G - Grant
PE - Program Element
PR - Project
TA - Task
WU - Work Unit Accession No.

Block 6. Author(s). Name(s) of person(s) responsible for writing the report, performing the research, or credited with the content of the report. If editor or compiler, this should follow the name(s).

Block 7. Performing Organization Name(s) and Address(es). Self-explanatory.

Block 8. Performing Organization Report Number. Enter the unique alphanumeric report number(s) assigned by the organization performing the report.

Block 9. Sponsoring/Monitoring Agency Name(s) and Address(es). Self-explanatory.

Block 10. Sponsoring/Monitoring Agency Report Number. *(If known)*

Block 11. Supplementary Notes. Enter information not included elsewhere such as: Prepared in cooperation with....; Trans. of....; To be published in.... When a report is revised, include a statement whether the new report supersedes or supplements the older report.

Block 12a. Distribution/Availability Statement. Denotes public availability or limitations. Cite any availability to the public. Enter additional limitations or special markings in all capitals (e.g. NOFORN, REL, ITAR).

DOD - See DoDD 5230.24, "Distribution Statements on Technical Documents."
DOE - See authorities.
NASA - See Handbook NHB 2200.2.
NTIS - Leave blank.

Block 12b. Distribution Code.

DOD - Leave blank.
DOE - Enter DOE distribution categories from the Standard Distribution for Unclassified Scientific and Technical Reports.
Leave blank.
NASA - Leave blank.
NTIS -

Block 13. Abstract. Include a brief *(Maximum 200 words)* factual summary of the most significant information contained in the report.

Block 14. Subject Terms. Keywords or phrases identifying major subjects in the report.

Block 15. Number of Pages. Enter the total number of pages.

Block 16. Price Code. Enter appropriate price code *(NTIS only)*.

Blocks 17. - 19. Security Classifications. Self- explanatory. Enter U.S. Security Classification in accordance with U.S. Security Regulations (i.e., UNCLASSIFIED). If form contains classified information, stamp classification on the top and bottom of the page.

Block 20. Limitation of Abstract. This block must be completed to assign a limitation to the abstract. Enter either UL (unlimited) or SAR (same as report). An entry in this block is necessary if the abstract is to be limited. If blank, the abstract is assumed to be unlimited.

PREFACE

Reports in this volume are numbered consecutively beginning with number 1. Each report is paginated with the report number followed by consecutive page numbers, e.g., 1-1, 1-2, 1-3; 2-1, 2-2, 2-3.

Due to its length, Volume 15 is bound in three parts 15A, and 15B. Volume 15A contains #1-27. Volume 15B contains reports #28-58. The Table of Contents for Volume 15 is included in all parts.

This document is one of a set of 16 volumes describing the 1996 AFOSR Summer Research Program. The following volumes comprise the set:

VOLUME	TITLE
1	Program Management Report
	Summer Faculty Research Program (SFRP) Reports
2A & 2B	Armstrong Laboratory
3A & 3B	Phillips Laboratory
4	Rome Laboratory
5A , 5B & 5C	Wright Laboratory
6	Arnold Engineering Development Center, Wilford Hall Medical Center and Air Logistics Centers
	Graduate Student Research Program (GSRP) Reports
7A & 7B	Armstrong Laboratory
8	Phillips Laboratory
9	Rome Laboratory
10A & 10B	Wright Laboratory
11	Arnold Engineering Development Center, United States Air Force Academy, Wilford Hall Medical Center, and Wright Patterson Medical Center
	High School Apprenticeship Program (HSAP) Reports
12A & 12B	Armstrong Laboratory
13	Phillips Laboratory
14	Rome Laboratory
15A&15B	Wright Laboratory
16	Arnold Engineering Development Center

HSAP FINAL REPORT TABLE OF CONTENTS i-xiv

APPENDICIES:

HSAP FINAL REPORTS

SRP Final Report Table of Contents

SRP Final Report Table of Contents

SRP Final Report Table of Contents

SRP Final Report Table of Contents

SRP Final Report Table of Contents

SRP Final Report Table of Contents

SRP Final Report Table of Contents

SRP Final Report Table of Contents

SRP Final Report Table of Contents

SRP Final Report Table of Contents

SRP Final Report Table of Contents

SRP Final Report Table of Contents

INTRODUCTION

The Summer Research Program (SRP), sponsored by the Air Force Office of Scientific Research (AFOSR), offers paid opportunities for university faculty, graduate students, and high school students to conduct research in U.S. Air Force research laboratories nationwide during the summer.

Introduced by AFOSR in 1978, this innovative program is based on the concept of teaming academic researchers with Air Force scientists in the same disciplines using laboratory facilities and equipment not often available at associates' institutions.

The Summer Faculty Research Program (SFRP) is open annually to approximately 150 faculty members with at least two years of teaching and/or research experience in accredited U.S. colleges, universities, or technical institutions. SFRP associates must be either U.S. citizens or permanent residents.

The Graduate Student Research Program (GSRP) is open annually to approximately 100 graduate students holding a bachelor's or a master's degree; GSRP associates must be U.S. citizens enrolled full time at an accredited institution.

The High School Apprentice Program (HSAP) annually selects about 125 high school students located within a twenty mile commuting distance of participating Air Force laboratories.

AFOSR also offers its research associates an opportunity, under the Summer Research Extension Program (SREP), to continue their AFOSR-sponsored research at their home institutions through the award of research grants. In 1994 the maximum amount of each grant was increased from $20,000 to $25,000, and the number of AFOSR-sponsored grants decreased from 75 to 60. A separate annual report is compiled on the SREP.

The numbers of projected summer research participants in each of the three categories and SREP "grants" are usually increased through direct sponsorship by participating laboratories.

AFOSR's SRP has well served its objectives of building critical links between Air Force research laboratories and the academic community, opening avenues of communications and forging new research relationships between Air Force and academic technical experts in areas of national interest, and strengthening the nation's efforts to sustain careers in science and engineering. The success of the SRP can be gauged from its growth from inception (see Table 1) and from the favorable responses the 1996 participants expressed in end-of-tour SRP evaluations (Appendix B).

AFOSR contracts for administration of the SRP by civilian contractors. The contract was first awarded to Research & Development Laboratories (RDL) in September 1990. After

completion of the 1990 contract, RDL (in 1993) won the recompetition for the basic year and four 1-year options.

2. PARTICIPATION IN THE SUMMER RESEARCH PROGRAM

The SRP began with faculty associates in 1979; graduate students were added in 1982 and high school students in 1986. The following table shows the number of associates in the program each year.

YEAR	SRP Participation, by Year			TOTAL
	SFRP	GSRP	HSAP	
1979	70			70
1980	87			87
1981	87			87
1982	91	17		108
1983	101	53		154
1984	152	84		236
1985	154	92		246
1986	158	100	42	300
1987	159	101	73	333
1988	153	107	101	361
1989	168	102	103	373
1990	165	121	132	418
1991	170	142	132	444
1992	185	121	159	464
1993	187	117	136	440
1994	192	117	133	442
1995	190	115	137	442
1996	188	109	138	435

Beginning in 1993, due to budget cuts, some of the laboratories weren't able to afford to fund as many associates as in previous years. Since then, the number of funded positions has remained fairly constant at a slightly lower level.

3. RECRUITING AND SELECTION

The SRP is conducted on a nationally advertised and competitive-selection basis. The advertising for faculty and graduate students consisted primarily of the mailing of 8,000 52-page SRP brochures to chairpersons of departments relevant to AFOSR research and to administrators of grants in accredited universities, colleges, and technical institutions. Historically Black Colleges and Universities (HBCUs) and Minority Institutions (MIs) were included. Brochures also went to all participating USAF laboratories, the previous year's participants, and numerous individual requesters (over 1000 annually).

RDL placed advertisements in the following publications: *Black Issues in Higher Education, Winds of Change,* and *IEEE Spectrum.* Because no participants list either *Physics Today* or *Chemical & Engineering News* as being their source of learning about the program for the past several years, advertisements in these magazines were dropped, and the funds were used to cover increases in brochure printing costs.

High school applicants can participate only in laboratories located no more than 20 miles from their residence. Tailored brochures on the HSAP were sent to the head counselors of 180 high schools in the vicinity of participating laboratories, with instructions for publicizing the program in their schools. High school students selected to serve at Wright Laboratory's Armament Directorate (Eglin Air Force Base, Florida) serve eleven weeks as opposed to the eight weeks normally worked by high school students at all other participating laboratories.

Each SFRP or GSRP applicant is given a first, second, and third choice of laboratory. High school students who have more than one laboratory or directorate near their homes are also given first, second, and third choices.

Laboratories make their selections and prioritize their nominees. AFOSR then determines the number to be funded at each laboratory and approves laboratories' selections.

Subsequently, laboratories use their own funds to sponsor additional candidates. Some selectees do not accept the appointment, so alternate candidates are chosen. This multi-step selection procedure results in some candidates being notified of their acceptance after scheduled deadlines. The total applicants and participants for 1996 are shown in this table.

1996 Applicants and Participants			
PARTICIPANT CATEGORY	TOTAL APPLICANTS	SELECTEES	DECLINING SELECTEES
SFRP	572	188	39
(HBCU/MI)	(119)	(27)	(5)
GSRP	235	109	7
(HBCU/MI)	(18)	(7)	(1)
HSAP	474	138	8
TOTAL	1281	435	54

4. SITE VISITS

During June and July of 1996, representatives of both AFOSR/NI and RDL visited each participating laboratory to provide briefings, answer questions, and resolve problems for both laboratory personnel and participants. The objective was to ensure that the SRP would be as constructive as possible for all participants. Both SRP participants and RDL representatives found these visits beneficial. At many of the laboratories, this was the only opportunity for all participants to meet at one time to share their experiences and exchange ideas.

5. HISTORICALLY BLACK COLLEGES AND UNIVERSITIES AND MINORITY INSTITUTIONS (HBCU/MIs)

Before 1993, an RDL program representative visited from seven to ten different HBCU/Mis annually to promote interest in the SRP among the faculty and graduate students. These efforts were marginally effective, yielding a doubling of HBCI/MI applicants. In an effort to achieve AFOSR's goal of 10% of all applicants and selectees being HBCU/MI qualified, the RDL team decided to try other avenues of approach to increase the number of qualified applicants. Through the combined efforts of the AFOSR Program Office at Bolling AFB and RDL, two very active minority groups were found, HACU (Hispanic American Colleges and Universities) and AISES (American Indian Science and Engineering Society). RDL is in communication with representatives of each of these organizations on a monthly basis to keep up with the their activities and special events. Both organizations have widely-distributed magazines/quarterlies in which RDL placed ads.

Since 1994 the number of both SFRP and GSRP HBCU/MI applicants and participants has increased ten-fold, from about two dozen SFRP applicants and a half dozen selectees to over 100 applicants and two dozen selectees, and a half-dozen GSRP applicants and two or three selectees to 18 applicants and 7 or 8 selectees. Since 1993, the SFRP had a two-fold applicant

increase and a two-fold selectee increase. Since 1993, the GSRP had a three-fold applicant increase and a three to four-fold increase in selectees.

In addition to RDL's special recruiting efforts, AFOSR attempts each year to obtain additional funding or use leftover funding from cancellations the past year to fund HBCU/MI associates. This year, 5 HBCU/MI SFRPs declined after they were selected (and there was no one qualified to replace them with). The following table records HBCU/MI participation in this program.

SRP HBCU/MI Participation, By Year				
YEAR	SFRP		GSRP	
	Applicants	Participants	Applicants	Participants
1985	76	23	15	11
1986	70	18	20	10
1987	82	32	32	10
1988	53	17	23	14
1989	39	15	13	4
1990	43	14	17	3
1991	42	13	8	5
1992	70	13	9	5
1993	60	13	6	2
1994	90	16	11	6
1995	90	21	20	8
1996	119	27	18	7

6. SRP FUNDING SOURCES

Funding sources for the 1996 SRP were the AFOSR-provided slots for the basic contract and laboratory funds. Funding sources by category for the 1996 SRP selected participants are shown here.

1996 SRP FUNDING CATEGORY	SFRP	GSRP	HSAP
AFOSR Basic Allocation Funds	141	85	123
USAF Laboratory Funds	37	19	15
HBCU/MI By AFOSR (Using Procured Addn'l Funds)	10	5	0
TOTAL	188	109	138

SFRP - 150 were selected, but nine canceled too late to be replaced.
GSRP - 90 were selected, but five canceled too late to be replaced (10 allocations for the ALCs were withheld by AFOSR.)
HSAP - 125 were selected, but two canceled too late to be replaced.

7. COMPENSATION FOR PARTICIPANTS

Compensation for SRP participants, per five-day work week, is shown in this table.

1996 SRP Associate Compensation

PARTICIPANT CATEGORY	1991	1992	1993	1994	1995	1996
Faculty Members	$690	$718	$740	$740	$740	$770
Graduate Student (Master's Degree)	$425	$442	$455	$455	$455	$470
Graduate Student (Bachelor's Degree)	$365	$380	$391	$391	$391	$400
High School Student (First Year)	$200	$200	$200	$200	$200	$200
High School Student (Subsequent Years)	$240	$240	$240	$240	$240	$240

The program also offered associates whose homes were more than 50 miles from the laboratory an expense allowance (seven days per week) of $50/day for faculty and $40/day for graduate students. Transportation to the laboratory at the beginning of their tour and back to their home destinations at the end was also reimbursed for these participants. Of the combined SFRP and

GSRP associates, 65 % (194 out of 297) claimed travel reimbursements at an average round-trip cost of $780.

Faculty members were encouraged to visit their laboratories before their summer tour began. All costs of these orientation visits were reimbursed. Forty-five percent (85 out of 188) of faculty associates took orientation trips at an average cost of $444. By contrast, in 1993, 58 % of SFRP associates took orientation visits at an average cost of $685; that was the highest percentage of associates opting to take an orientation trip since RDL has administered the SRP, and the highest average cost of an orientation trip. These 1993 numbers are included to show the fluctuation which can occur in these numbers for planning purposes.

Program participants submitted biweekly vouchers countersigned by their laboratory research focal point, and RDL issued paychecks so as to arrive in associates' hands two weeks later.

In 1996, RDL implemented direct deposit as a payment option for SFRP and GSRP associates. There were some growing pains. Of the 128 associates who opted for direct deposit, 17 did not check to ensure that their financial institutions could support direct deposit (and they couldn't), and eight associates never did provide RDL with their banks' ABA number (direct deposit bank routing number), so only 103 associates actually participated in the direct deposit program. The remaining associates received their stipend and expense payments via checks sent in the US mail.

HSAP program participants were considered actual RDL employees, and their respective state and federal income tax and Social Security were withheld from their paychecks. By the nature of their independent research, SFRP and GSRP program participants were considered to be consultants or independent contractors. As such, SFRP and GSRP associates were responsible for their own income taxes, Social Security, and insurance.

8. CONTENTS OF THE 1996 REPORT

The complete set of reports for the 1996 SRP includes this program management report (Volume 1) augmented by fifteen volumes of final research reports by the 1996 associates, as indicated below:

1996 SRP Final Report Volume Assignments

LABORATORY	SFRP	GSRP	HSAP
Armstrong	2	7	12
Phillips	3	8	13
Rome	4	9	14
Wright	5A, 5B	10	15
AEDC, ALCs, WHMC	6	11	16

APPENDIX A – PROGRAM STATISTICAL SUMMARY

A. Colleges/Universities Represented

Selected SFRP associates represented 169 different colleges, universities, and institutions, GSRP associates represented 95 different colleges, universities, and institutions.

B. States Represented

SFRP -Applicants came from 47 states plus Washington D.C. and Puerto Rico. Selectees represent 44 states plus Puerto Rico.

GSRP - Applicants came from 44 states and Puerto Rico. Selectees represent 32 states.

HSAP - Applicants came from thirteen states. Selectees represent nine states.

Total Number of Participants	
SFRP	188
GSRP	109
HSAP	138
TOTAL	435

Degrees Represented			
	SFRP	GSRP	TOTAL
Doctoral	184	1	185
Master's	4	48	52
Bachelor's	0	60	60
TOTAL	188	109	297

SFRP Academic Titles	
Assistant Professor	79
Associate Professor	59
Professor	42
Instructor	3
Chairman	0
Visiting Professor	1
Visiting Assoc. Prof.	0
Research Associate	4
TOTAL	188

Source of Learning About the SRP		
Category	Applicants	Selectees
Applied/participated in prior years	28%	34%
Colleague familiar with SRP	19%	16%
Brochure mailed to institution	23%	17%
Contact with Air Force laboratory	17%	23%
IEEE Spectrum	2%	1%
BIIHE	1%	1%
Other source	10%	8%
TOTAL	100%	100%

APPENDIX B -- SRP EVALUATION RESPONSES

1. OVERVIEW

Evaluations were completed and returned to RDL by four groups at the completion of the SRP. The number of respondents in each group is shown below.

Table B-1. Total SRP Evaluations Received

Evaluation Group	Responses
SFRP & GSRPs	275
HSAPs	113
USAF Laboratory Focal Points	84
USAF Laboratory HSAP Mentors	6

All groups indicate unanimous enthusiasm for the SRP experience.

The summarized recommendations for program improvement from both associates and laboratory personnel are listed below:

A. Better preparation on the labs' part prior to associates' arrival (i.e., office space, computer assets, clearly defined scope of work).

B. Faculty Associates suggest higher stipends for SFRP associates.

C. Both HSAP Air Force laboratory mentors and associates would like the summer tour extended from the current 8 weeks to either 10 or 11 weeks; the groups state it takes 4-6 weeks just to get high school students up-to-speed on what's going on at laboratory. (Note: this same argument was used to raise the faculty and graduate student participation time a few years ago.)

2. 1996 USAF LABORATORY FOCAL POINT (LFP) EVALUATION RESPONSES

The summarized results listed below are from the 84 LFP evaluations received.

1. LFP evaluations received and associate preferences:

Table B-2. Air Force LFP Evaluation Responses (By Type)

		How Many Associates Would You Prefer To Get ? (% Response)											
		SFRP				GSRP (w/Univ Professor)				GSRP (w/o Univ Professor)			
Lab	Evals Recv'd	0	1	2	3+	0	1	2	3+	0	1	2	3+
AEDC	0	-	-	-	-	-	-	-	-	-	-	-	-
WHMC	0	-	-	-	-	-	-	-	-	-	-	-	-
AL	7	28	28	28	14	54	14	28	0	86	0	14	0
FJSRL	1	0	100	0	0	100	0	0	0	0	100	0	0
PL	25	40	40	16	4	88	12	0	0	84	12	4	0
RL	5	60	40	0	0	80	10	0	0	100	0	0	0
WL	46	30	43	20	6	78	17	4	0	93	4	2	0
Total	84	32%	50%	13%	5%	80%	11%	6%	0%	73%	23%	4%	0%

LFP Evaluation Summary. The summarized responses, by laboratory, are listed on the following page. LFPs were asked to rate the following questions on a scale from 1 (below average) to 5 (above average).

2. LFPs involved in SRP associate application evaluation process:
   a. Time available for evaluation of applications:
   b. Adequacy of applications for selection process:
3. Value of orientation trips:
4. Length of research tour:
5. a. Benefits of associate's work to laboratory:
   b. Benefits of associate's work to Air Force:
6. a. Enhancement of research qualifications for LFP and staff:
   b. Enhancement of research qualifications for SFRP associate:
   c. Enhancement of research qualifications for GSRP associate:
7. a. Enhancement of knowledge for LFP and staff:
   b. Enhancement of knowledge for SFRP associate:
   c. Enhancement of knowledge for GSRP associate:
8. Value of Air Force and university links:
9. Potential for future collaboration:
10. a. Your working relationship with SFRP:
    b. Your working relationship with GSRP:
11. Expenditure of your time worthwhile:

(Continued on next page)

12. Quality of program literature for associate:
13. a. Quality of RDL's communications with you:
    b. Quality of RDL's communications with associates:
14. Overall assessment of SRP:

Table B-3. Laboratory Focal Point Reponses to above questions

	AEDC	*AL*	*FJSRL*	*PL*	*RL*	*WHMC*	*WL*
# Evals Recv'd	0	7	1	14	5	0	46
Question #							
2	-	86 %	0 %	88 %	80 %	-	85 %
2a	-	4.3	n/a	3.8	4.0	-	3.6
2b	-	4.0	n/a	3.9	4.5	-	4.1
3	-	4.5	n/a	4.3	4.3	-	3.7
4	-	4.1	4.0	4.1	4.2	-	3.9
5a	-	4.3	5.0	4.3	4.6	-	4.4
5b	-	4.5	n/a	4.2	4.6	-	4.3
6a	-	4.5	5.0	4.0	4.4	-	4.3
6b	-	4.3	n/a	4.1	5.0	-	4.4
6c	-	3.7	5.0	3.5	5.0	-	4.3
7a	-	4.7	5.0	4.0	4.4	-	4.3
7b	-	4.3	n/a	4.2	5.0	-	4.4
7c	-	4.0	5.0	3.9	5.0	-	4.3
8	-	4.6	4.0	4.5	4.6	-	4.3
9	-	4.9	5.0	4.4	4.8	-	4.2
10a	-	5.0	n/a	4.6	4.6	-	4.6
10b	-	4.7	5.0	3.9	5.0	-	4.4
11	-	4.6	5.0	4.4	4.8	-	4.4
12	-	4.0	4.0	4.0	4.2	-	3.8
13a	-	3.2	4.0	3.5	3.8	-	3.4
13b	-	3.4	4.0	3.6	4.5	-	3.6
14	-	4.4	5.0	4.4	4.8	-	4.4

3. 1996 SFRP & GSRP EVALUATION RESPONSES

The summarized results listed below are from the 257 SFRP/GSRP evaluations received.

Associates were asked to rate the following questions on a scale from 1 (below average) to 5 (above average) - by Air Force base results and over-all results of the 1996 evaluations are listed after the questions.

1. The match between the laboratories research and your field:
2. Your working relationship with your LFP:
3. Enhancement of your academic qualifications:
4. Enhancement of your research qualifications:
5. Lab readiness for you: LFP, task, plan:
6. Lab readiness for you: equipment, supplies, facilities:
7. Lab resources:
8. Lab research and administrative support:
9. Adequacy of brochure and associate handbook:
10. RDL communications with you:
11. Overall payment procedures:
12. Overall assessment of the SRP:
13. a. Would you apply again?
    b. Will you continue this or related research?
14. Was length of your tour satisfactory?
15. Percentage of associates who experienced difficulties in finding housing:
16. Where did you stay during your SRP tour?
    a. At Home:
    b. With Friend:
    c. On Local Economy:
    d. Base Quarters:
17. Value of orientation visit:
    a. Essential:
    b. Convenient:
    c. Not Worth Cost:
    d. Not Used:

SFRP and GSRP associate's responses are listed in tabular format on the following page.

Table B-4. 1996 SFRP & GSRP Associate Responses to SRP Evaluation

	Arnold	Brooks	Edwards	Eglin	Griffis	Hanscom	Kelly	Kirtland	Lackland	Robins	Tyndall	WPAFB	average
# res	6	48	6	14	31	19	3	32	1	2	10	85	257
1	4.8	4.4	4.6	4.7	4.4	4.9	4.6	4.6	5.0	5.0	4.0	4.7	4.6
2	5.0	4.6	4.1	4.9	4.7	4.7	5.0	4.7	5.0	5.0	4.6	4.8	4.7
3	4.5	4.4	4.0	4.6	4.3	4.2	4.3	4.4	5.0	5.0	4.5	4.3	4.4
4	4.3	4.5	3.8	4.6	4.4	4.4	4.3	4.6	5.0	4.0	4.4	4.5	4.5
5	4.5	4.3	3.3	4.8	4.4	4.5	4.3	4.2	5.0	5.0	3.9	4.4	4.4
6	4.3	4.3	3.7	4.7	4.4	4.5	4.0	3.8	5.0	5.0	3.8	4.2	4.2
7	4.5	4.4	4.2	4.8	4.5	4.3	4.3	4.1	5.0	5.0	4.3	4.3	4.4
8	4.5	4.6	3.0	4.9	4.4	4.3	4.3	4.5	5.0	5.0	4.7	4.5	4.5
9	4.7	4.5	4.7	4.5	4.3	4.5	4.7	4.3	5.0	5.0	4.1	4.5	4.5
10	4.2	4.4	4.7	4.4	4.1	4.1	4.0	4.2	5.0	4.5	3.6	4.4	4.3
11	3.8	4.1	4.5	4.0	3.9	4.1	4.0	4.0	3.0	4.0	3.7	4.0	4.0
12	5.7	4.7	4.3	4.9	4.5	4.9	4.7	4.6	5.0	4.5	4.6	4.5	4.6
Numbers below are percentages													
13a	83	90	83	93	87	75	100	81	100	100	100	86	87
13b	100	89	83	100	94	98	100	94	100	100	100	94	93
14	83	96	100	90	87	80	100	92	100	100	70	84	88
15	17	6	0	33	20	76	33	25	0	100	20	8	39
16a	-	26	17	9	38	23	33	4	-	-	-	30	
16b	100	33	-	40	-	8	-	-	-	-	36	2	
16c	-	41	83	40	62	69	67	96	100	100	64	68	
16d	-	-	-	-	-	-	-	-	-	-	-	0	
17a	-	33	100	17	50	14	67	39	-	50	40	31	35
17b	-	21	-	17	10	14	-	24	-	50	20	16	16
17c	-	-	-	-	10	7	-	-	-	-	-	2	3
17d	100	46	-	66	30	69	33	37	100	-	40	51	46

4. 1996 USAF LABORATORY HSAP MENTOR EVALUATION RESPONSES

Not enough evaluations received (5 total) from Mentors to do useful summary.

5. 1996 HSAP EVALUATION RESPONSES

The summarized results listed below are from the 113 HSAP evaluations received.

HSAP apprentices were asked to rate the following questions on a scale from 1 (below average) to 5 (above average)

1. Your influence on selection of topic/type of work.
2. Working relationship with mentor, other lab scientists.
3. Enhancement of your academic qualifications.
4. Technically challenging work.
5. Lab readiness for you: mentor, task, work plan, equipment.
6. Influence on your career.
7. Increased interest in math/science.
8. Lab research & administrative support.
9. Adequacy of RDL's Apprentice Handbook and administrative materials.
10. Responsiveness of RDL communications.
11. Overall payment procedures.
12. Overall assessment of SRP value to you.
13. Would you apply again next year? Yes (92 %)
14. Will you pursue future studies related to this research? Yes (68 %)
15. Was Tour length satisfactory? Yes (82 %)

	Arnold	Brooks	Edwards	Eglin	Griffiss	Hanscom	Kirtland	Tyndall	WPAFB	Totals
# resp	5	19	7	15	13	2	7	5	40	113
1	2.8	3.3	3.4	3.5	3.4	4.0	3.2	3.6	3.6	3.4
2	4.4	4.6	4.5	4.8	4.6	4.0	4.4	4.0	4.6	4.6
3	4.0	4.2	4.1	4.3	4.5	5.0	4.3	4.6	4.4	4.4
4	3.6	3.9	4.0	4.5	4.2	5.0	4.6	3.8	4.3	4.2
5	4.4	4.1	3.7	4.5	4.1	3.0	3.9	3.6	3.9	4.0
6	3.2	3.6	3.6	4.1	3.8	5.0	3.3	3.8	3.6	3.7
7	2.8	4.1	4.0	3.9	3.9	5.0	3.6	4.0	4.0	3.9
8	3.8	4.1	4.0	4.3	4.0	4.0	4.3	3.8	4.3	4.2
9	4.4	3.6	4.1	4.1	3.5	4.0	3.9	4.0	3.7	3.8
10	4.0	3.8	4.1	3.7	4.1	4.0	3.9	2.4	3.8	3.8
11	4.2	4.2	3.7	3.9	3.8	3.0	3.7	2.6	3.7	3.8
12	4.0	4.5	4.9	4.6	4.6	5.0	4.6	4.2	4.3	4.5
Numbers below are percentages										
13	60%	95%	100%	100%	85%	100%	100%	100%	90%	92%
14	20%	80%	71%	80%	54%	100%	71%	80%	65%	68%
15	100%	70%	71%	100%	100%	50%	86%	60%	80%	82%

The Creation of a Shell Program to Interface to Confor

Jesse Anderson

Chaminade-Julienne High School
505 South Ludlow Street
Dayton, OH 45402

Final Report for:
High School Apprenticeship Program
Wright Laboratories

Sponsored by:
Air force Office of Scientific Research
Bolling Air Force Base, DC

and

Wright Laboratories

August 1996

The Creation of a Shell Program to Interface to Confor

Jesse Anderson

Abstract

A program was developed in C++ to be used as an interface, file translator, and control mechanism to the Ukrainian developed program Confor, enabling the user to run Confor multiple times using files in a format common in the United States.

The Creation of a Shell Program to Interface to Confor

Jesse Anderson

Introduction

In recent years the sharing of scientific data, ideas, and projects between the United States and the former Soviet Union has increased dramatically. One such shared project is a program entitled Confor, developed in the Ukraine by Victor Gladun as an implementation of hie Pyramidal Net Classification Theory, and later sold for use in the United States. One problem with the use of this program, however, is its interface, which has proven difficult and cumbersome to use after being introduced to US computers and translated into English. The task of this project was to develop a system whereby Confor's ease of use could be enhanced, by creating a program to translate standard data files into those used by Confor and then running Confor in a "shell" program, requiring of the user only necessary input.

Methodology

This part of the paper will be split into two sections. The first will deal with the problem of the conversion of files from a common format used to store data in the office to that required as input by Confor. The other will concern itself with the creation of the shell program to run Confor automatically.

It should be noted that the author only had one year's experience programming computers, and that year was spent in the study of Pascal. A large amount of time spent on the programs was spent learning new programming techniques. Not only was C++ to be used, but many parts of the program required procedures at very low levels and in machine code.

The file conversion preformed to format files to Confor specifications was done before the introduction of this project by a simple macro under Microsoft Excel. This macro was written in Visual Basic, and, while working sufficiently, it had some drawbacks, including low speed, which made it infeasible for daily use by the office.

The data files received to turn into Confor data files were basically formatted as follows:

```
8
D    0    2043  2044  4552  4553  10200 10201 36400
A    0.1  1     1.001 2     2.001 3     3.001 4
```

[more entries here ...]

304

NAME	D	A	B	C	AW	TK	XD		
Ca5Pb3	5097	1.623	1.623	0.704	821.99		1400	4414	0.199
BiCs3	5000	0.931	0.931	0.931	607.6967	923	5000	0.984	

[more entries here..]

The first line in the file contains the number of pairs of "bin" numbers, those numbers contained in the table following. This table contains a letter or name, called an attribute, and then appropriate bin definitions. From these a file was created that gave each bin a letter. For instance, in attribute D, bin "a" would be 0-2043, "b" 2044-4552, etc.

Then the attributes of the compounds after the table were given a bin letter instead of a number, and formatted as need by Confor. For the first Compound, Ca5Pb3, the attribute "D" would be given bin "c". All these things were incidental to the creation of the program though, and only give examples of the tasks needing accomplishment. Other files used by Confor were translated in similar ways.

The second part of the project proved to be the more irregular as well as the harder part to write. The exact nature of the task itself took some weeks to define. Basically the problem that needed to be solved involved sending keystrokes to the program at points where Confor required input to continue.

Originally, it was hoped Confor could be run in a shell under Microsoft Windows, indeed the file conversion program was written as both a DOS and as a Windows application. Time was spent determining whether Windows could even pass keystrokes to a program in a DOS application. Programs such as Microsoft Recorder simply could not do the required tasks, for whatever reason. Extensive searching of the Internet was done, as well as multiple postings to relevant Usenet newsgroups, but no answer was found.

The task was set then, to run Confor under a DOS program in DOS. From previous programming experience, it was known that it was possible to send keystrokes to the DOS keyboard buffer from a program, or "fake" keystrokes. The only way to accomplish this however, was to load the buffer with the program and then exit the program, letting the keystrokes come

out of the buffer, load up Confor, and do the required tasks. Also, the buffer cold only hold 16 keystrokes, not enough to complete all the tasks in Confor. So it was determined that what was required was a terminate-stay resident program, that would send keystrokes to the buffer, go resident, and then take over again when more keystrokes were required by Confor. This part of the program was written, with some difficulties, as DOS was neither extremely receptive to the TSR or to the loading of the keyboard buffer. Originally this part of the implementation was written in C++, but the executable that sat in memory was much too large, so it was rewritten in Pascal, taking advantage of Pascal's smaller executable size, as well as the programmer's previous experience in writing such specific and low-level programs in Pascal.

The TSR was able to load keystrokes and begin Confor, but no method could be devised to keep track of when Confor required more input. The process took more time for larger data files, and since it was written in DOS, no information about the program running was available on a system level. It was attempted to have the TSR pop-up when the interrupt to poll for a keystroke was called by Confor, indicating that it required more input. For some reason, this was ineffective, and a disassembly of Confor showed no presence of that interrupt in the executable. Nor was the interrupt that Confor called to get another keystroke determined, so that tactic could not be relied upon to provide a way to activate the TSR. The only thing that was without a doubt available to show that Confor required input was the screen prompt for input. The TSR was rewritten to periodically poll video memory to see if certain character slots contained certain colors or text indicating that Confor was ready for more input. The rest of the required keystrokes were supplied this way, and the Confor shell program was able to be fully written to automatically run Confor.

The program was also written to enable multiple runs of Confor made from a single command. The usefulness of this was as a statistical measure of Confor's ability to reliably supply the same answers. After a program run, the results were saved and then the input files scrambled, so that the data for each compound was the same but the order of the compound changed. Through many runs, differences in output based on differences in input could be determined.

All that the program required at that point was an interface to connect the user to the program. The programmer spent a time devising a system of dialog boxes and windows for use under DOS that would make the program as user friendly as possible. It enabled the user to

convert any files necessary as well as running Confor as many times as necessary.

Results

The program was completed as required, though many conflicts during its writing and debugging impaired the amount of time spent on the project. Little time was allotted for debugging of the program because of the immensity of the task and the small time allotted to it. For this reason, many of the parts of the project were prematurely labeled finished and later showed they had problems. The program did work and do what was required of it, all fairly reliably.

A STUDY OF THE GENERALIZATION AND CLASSIFICATION ABILITIES OF A BACKPROPAGATION NEURAL NETWORK

Mark A. Bartsch

Carroll High School
4524 Linden Ave.
Dayton, OH 45432

Final Report for:
High School Apprenticeship Program

Wright Laboratory
Avionics Directorate
WL/AACF

Sponsored by:
Air Force Office of Scientific Research
Bolling Air Force Base, DC

and

Wright Laboratory

August 1996

A STUDY OF THE GENERALIZATION AND CLASSIFICATION ABILITIES OF A BACKPROPAGATION NEURAL NETWORK

Mark A. Bartsch
Carroll High School

Abstract

The generalization abilities of a backpropagation neural network simulation were examined in three stages. The first stage statistically tested the network's ability to perform 5-bit binary negation under varying network sizes and extents of the training set. It was found that a two layer network was the most accurate, yielding no errors with a training set of sixteen cases. The second stage tested the ability of a network to classify music based on melody. The third stage tested the ability of a network to determine whether or not a point in a matrix was "surrounded" by other matrix elements, based on a partially ambiguous set of rules. Both stage two and stage three were inconclusive because of too few training examples.

A STUDY OF THE GENERALIZATION AND CLASSIFICATION ABILITIES OF A BACKPROPAGATION NEURAL NETWORK

Mark A. Bartsch

Introduction

The field of artificial neural networks has often been regarded with awe to the outsider; many "experts" have made claims of amazing feats of computer ability far beyond what any normal computer programmer, much less anyone less familiar with computers, could imagine. "Look at this!" say the proverbial neural network experts, "It can recognize patterns! It can predict stuff! It can learn!" The general public tends to "ooh" and "ah" over these results temporarily before ignoring them (and spinning off some rather quaint pop-culture AI flicks), but the computer programmer hears this and more: "Look at this! It doesn't need to be told how to do it! It can even, in some cases, do it without any human intervention at all!" These last comments tend to cause the programmer to begin to drool, his eyes glazing over (while the public, hearing the last statement, proceeds to spin off several more quaint pop-culture flicks, these about evil and maniacal computers taking over the world).

Artificial neural networks (ANNs), to their credit, can in fact do these things (well, they can't take over the world just *yet*...), and generally with a good bit more ease than standard programming techniques. Still, the ANN is not a magical technique for solving the world's problems; rather, it is a specialized technique for solving certain types of problems which are difficult to solve otherwise. Actually, ANNs can do just about anything normal computational methods can, but they are not suited to those problems. Instead, the ANN is suited for classification, pattern recognition, data representation, and similar problems which are the focus of the general excitement.

Because of the extent of the field of neural networks, this introduction will focus only on the ANN used in this study and the theories behind it: the feedforward network trained on a backpropagation algorithm. The backpropagation network is a basic type of ANN with comparatively simple workings. This ANN is, like most ANNs, composed of a number of units or nodes which are connected by weighted connections. In the backpropagation network (henceforth referred to as a "backprop net"), the units are arranged in layers and connected to every unit in the preceding and succeeding layers. The first layer is the input layer, and the last layer is the output layer. A network with only these two layers is known as a *perceptron* (made famous by a book of the same name by Minsky and Papert, "famous" because of some sweeping negative statements about the capabilities of ANNs in general which have been proven grossly incorrect). If one or more layers lie between the input and output layers, these extra layers are known as hidden layers.

Each unit performs its own simple calculations. Generally these calculations involve the summation of all weighted inputs, followed by that result being input into an activation function. Popular activation functions are linear or sigmoidal. The latter, which is employed in the network used in this study, provides for a bounded but continuous and differentiable output while allowing any input. Theoretically, if a neural net was constructed in hardware rather than simulated on a computer, each unit could run in parallel to every other unit, increasing the speed of the net.

During the training stage, the input from each training case in the training set is fed forward through the network. At the output, an accumulated total error for all cases is calculated, and this error is then propagated backwards through the network. The adjustment to each unit's weight is based on its "error," which in turn is based on the errors of the nodes it is connected to, and so on. The adjustment is also multiplied by the derivative of the activation function to alter the speed of training and a learning rate value. This process is repeated until the network reaches convergence, at which point the error is acceptably small.

Unlike the perceptron, which can only solve problems which are linearly separable, such as the AND or OR function, but not the XOR function (Braspenning, Thuijsman, Weijters), a three-layer network can theoretically model any function which can be modeled, given a proper number of training cases (White). "Any lack of success in applications must arise from inadequate learning, insufficient numbers of hidden units, or the lack of a deterministic relationship between input and output" (White, 20). This is a sweeping claim, but it has been proven mathematically. Perhaps the proverbial ANN experts have reason to be so positive. Still, neural networks, and especially backprop nets, are not miracle machines; several problems arise which must be addressed.

The first and most obvious problem with backprop nets is the rate of training. Convergence occurs slowly, and simple adjustments (such as to the learning rate) tend to prevent the network from converging at all. The learning rate must be kept reasonably small, especially towards the end of training, to prevent the network from overshooting its goal. Additionally, a sigmoidal activation function given a very large (positive or negative) activation will train slowly because its derivative is small, even if its output is wildly incorrect (Skapura, 36). Another problem is the occurrence of local minima in the solution space. If the network should become caught in one of these minima, it may not converge satisfactorily even if there exists a satisfactory solution. Several methods have been implemented to avoid or minimize these problems, including momentum and the adaptive back-propagation algorithm. The backprop program used for this study includes an adaptive learning rate algorithm which may be a version of this later method. Unfortunately, the workings of this algorithm are cryptic; it does seem to speed convergence, but what it actually does and how it does it remains a mystery. This algorithm seems to have the unfortunate effect of occasionally randomizing the weights again if convergence is not forthcoming; a safeguard weight-dump procedure was added to save any progress up to that point.

Methodology, Stage I

This study revolves around the use of a backpropagation network simulation program called "Bounded Dynamic Backpropagation," written by Professor J. L. Noyes in Turbo Pascal in 1992. The study began with an effort to translate this program from Turbo Pascal into C++. The translation was necessary for several reasons, including the ability to incorporate the more portable C++ code into future developments, the improved speed of the C++ programming language, and the ability to port the code to other computers to make use of available resources.

The initial translation of the code needed testing, so what was to become the first stage of the study began. In order to test (and learn about) the program, the program was run with a set of initial parameters provided by an external source who was knowledgeable about the code. The initial goal of the network was to perform binary negation on five-bit numbers. During initial testing, a three layer network, with five nodes each, was used. Once the program was debugged to a satisfactory degree, a statistical study of the network's ability to perform these binary negations was conducted.

The goal of this stage was to determine the effects of network size and extent of training on the performance of binary negation. First, a set of standard, randomly selected training sets and testing sets were generated. The training sets were generated using either four, eight, twelve, sixteen, and twenty training cases per set. For each number of training cases, ten different sets were generated. Each training set had a corresponding test set, consisting of eight untrained cases

With this established set of fifty pairs of training and test sets, each of the pairs was run through eight networks of different sizes, ranging from a simple two layer perceptron to a five layer network with ten units on each hidden layer. Input and output layers, to allow use of the same training files, all contained five nodes.

Results were collected in two forms. The first was the "output parameter error" which the original program counted. This counted every output which was not within 0.1 of the actual value. The second was an added error measurement, the "actual error" measurement. This value counts every error which is not within 0.5 of the actual value. This provides for the ability of the user of the output data to round to the nearest integer. Each grouping of ten training/testing sets were averaged together to yield the data below.

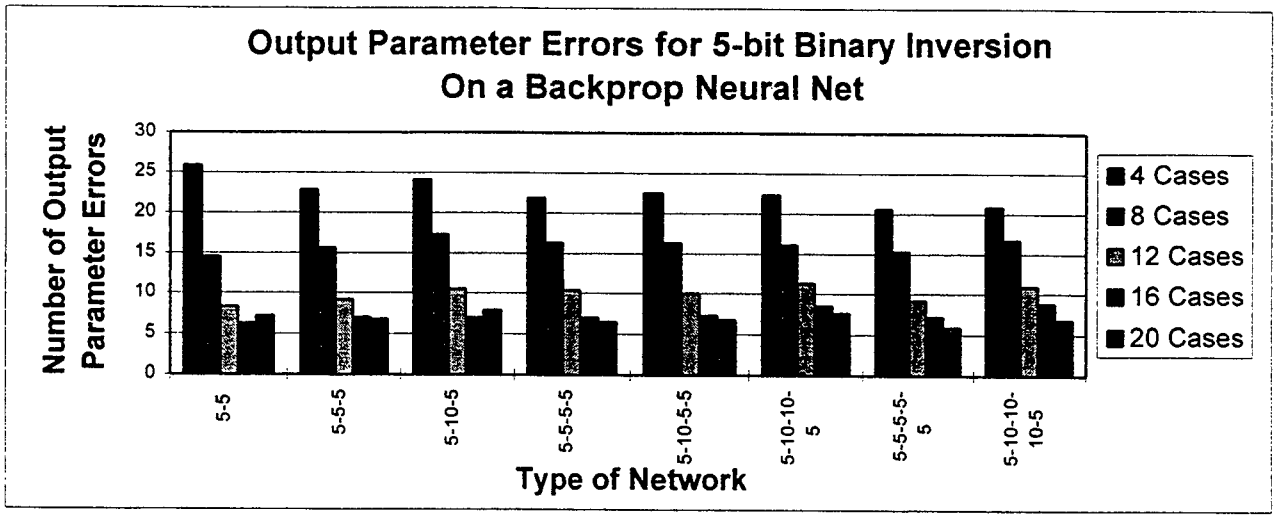

"Output Parameter" errors for the inversion network based on network size and training extent.

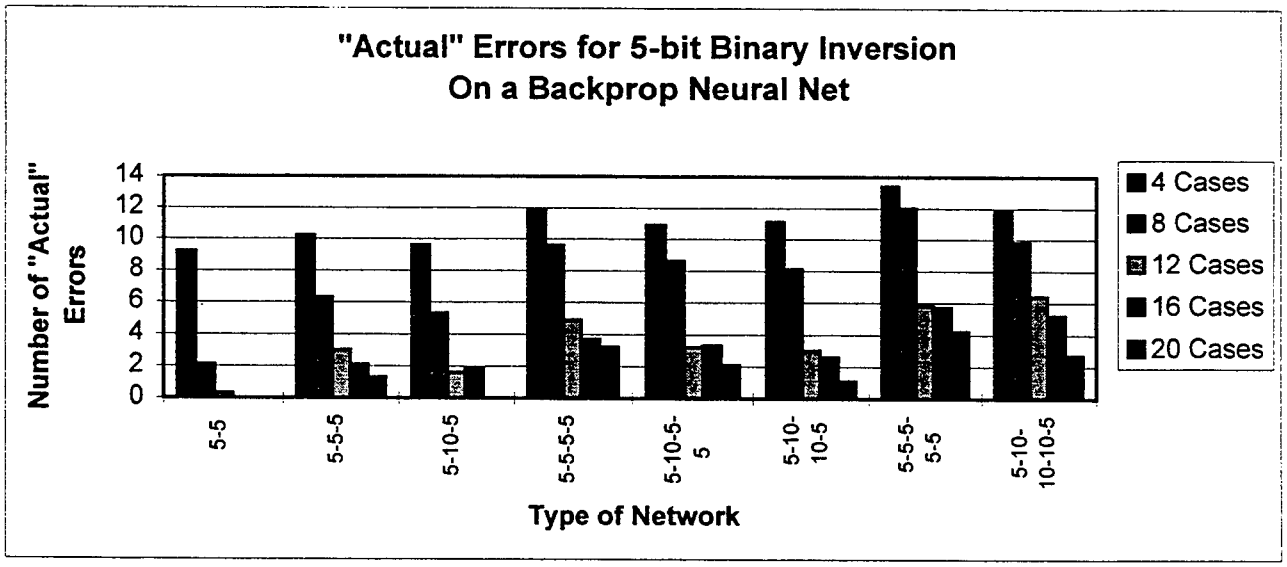

"Actual" errors for the inversion network based on network size and trainining extent.

These data show the averages of each grouping of ten training/testing sets for each network size and with each number of training cases.

Results and Conclusions, Stage I

The output parameter error measurements reveal little about the behaviors of the various networks. With very few training cases, larger networks performed slightly better than the smaller networks. This pattern did not hold for more training cases.

The "actual" error measurements, however, show a very definite pattern. Networks with fewer layers returned fewer errors than those with more layers. Additionally, for networks with the same number of layers, an increase in number of hidden layers reduces the number of "actual" errors somewhat.

Since the perceptron performed the best under "actual" error measurements, this implies that binary negation is a linearly separable problem.

In conclusion, this stage of the study reveals that, for simple problems, smaller networks are better. This likely holds over to more complex problems as well. If a network is too large, it will not be able to represent its target function with as great an accuracy as a smaller network with the same number of example sets.

Methodology, Stage II

The second stage of this study examined the capabilities of the backprop net to generalize and classify complex and somewhat ambiguous data sets. The sets of data chosen were melodies from music of various styles. Given the restraints on time and computing power, the network was limited to the examination of a twenty-five note "window." Each note was represented by one byte, with five bits indicating the note value (or a rest) and three bits indicating the note's duration. This resulted in the use of a three layer network: the first layer contained two hundred nodes for input and the last layer contained eight nodes, which was the maximum number of musical categories included. The hidden layer was given fifty nodes, a number more or less arbitrarily assigned.

Music was collected as standard MIDI files and the melodies were extracted. The music was separated into eight categories and each category was divided up into training and testing sets. "Windows" of data were extracted by removing as many windows as possible without overlap of more than one note. A number of training sessions were begun. The first used all eight categories plus a ninth group of music which was placed between two other categories in value. During the second session, this ninth grouping, which seemed to only confuse the network, and one of the categories, which had very few examples, were dropped. During the third session, two more categories were dropped and the remaining categories were concentrated into three more broad categories.

The size of the training sessions ranged from more than six hundred cases to about two hundred and fifty cases. During training, the network only converged on session three. On the first two sessions,

the minimum error reached lay between twenty and thirty. Results were calculated by averaging together all of the node outputs for all of the testing sets under one category.

Data, Stage II

The data shown here are from the second and third training sessions. The data from the second training session is located in the grouping of seven graphs; the smaller grouping of three graphs represents the data from the third training session. In both sets, the high, dark bars represent the goal output for that category, while the shorter bars show the actual output.

The titles of the graphs are the categories which they represent. These titles are probably of chief interest to those with musical background who wish to examine connections between various types of music.

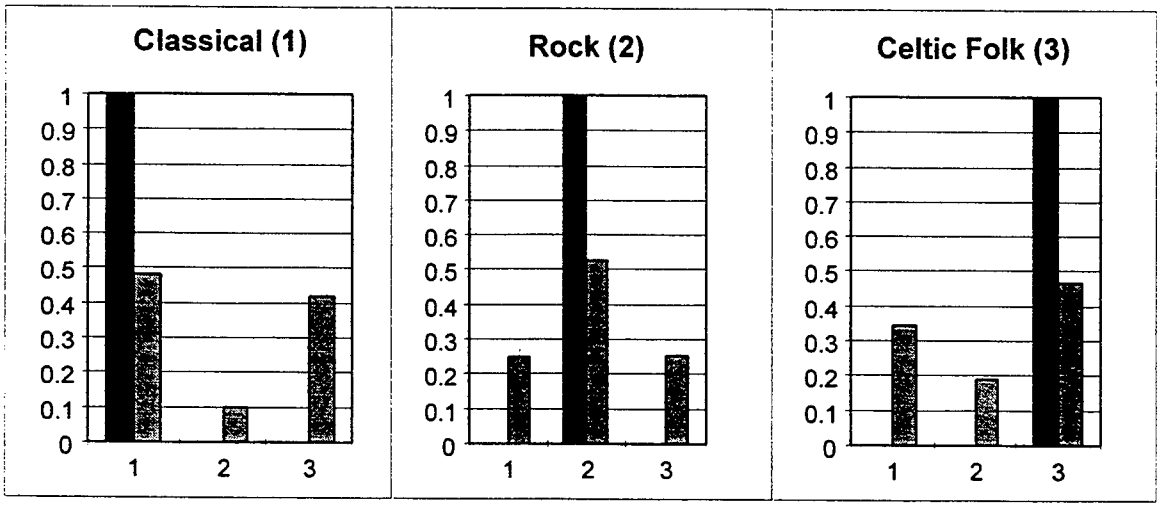

Stage II Session 3 Test Results. The dark bar represents expected output, the light bar represents actual output.

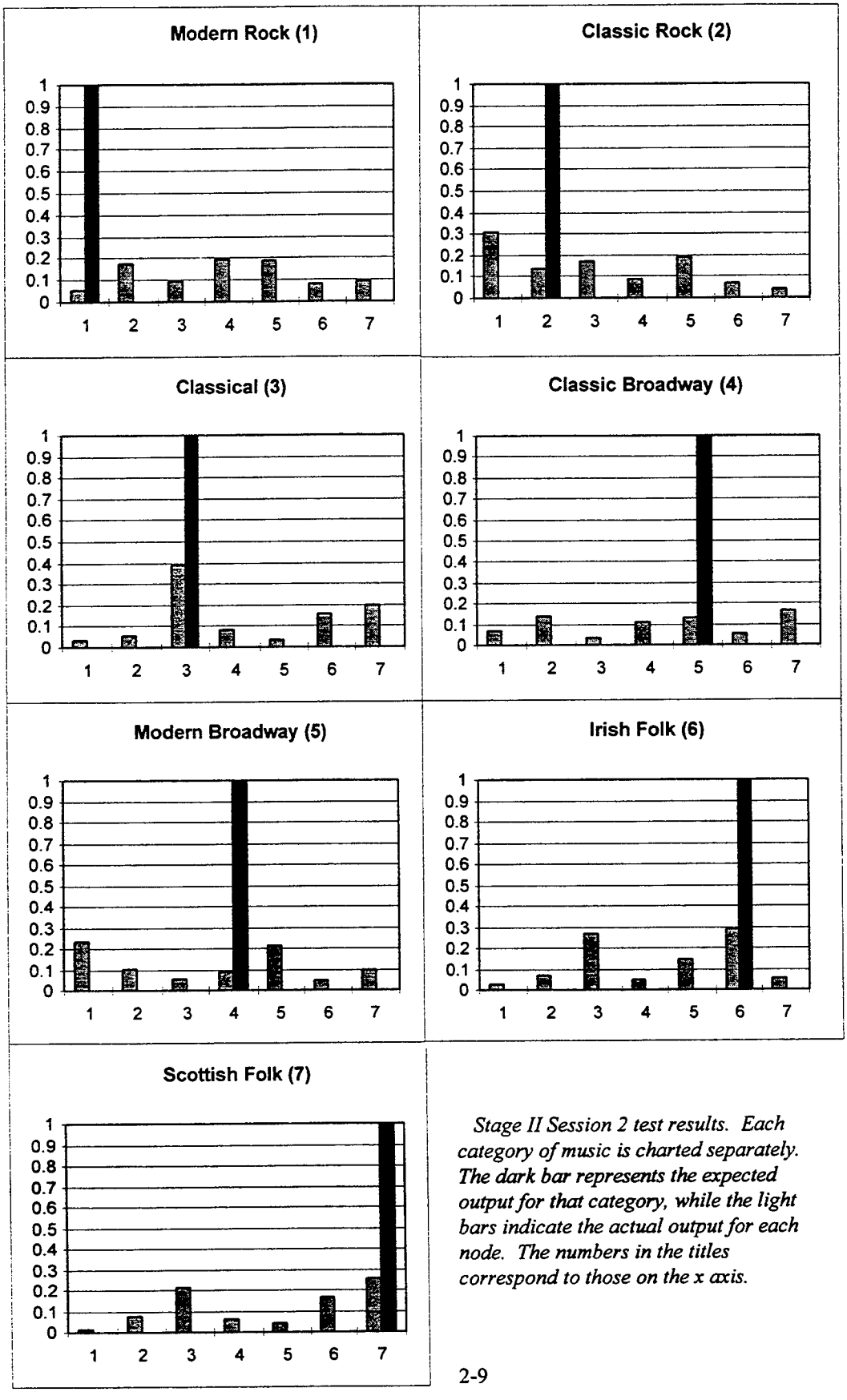

Stage II Session 2 test results. Each category of music is charted separately. The dark bar represents the expected output for that category, while the light bars indicate the actual output for each node. The numbers in the titles correspond to those on the x axis.

Conclusions and Results, Stage II

Though the data was not included here, results of session number one were very similar to those of session number two, with a few differences. The first category (which was dropped for session number two) had too little data to properly classify much of anything. This led to confusion of the network, claiming many things to be a part of that category. These results indicated that that category (which included "American Patriotic" music) was musically ambiguous. Also, the "multiple output" category, attached to the categories labeled three and six under session two, seemed to confuse the categories that it was attached to. On its own, however, it tended to reflect the dual categories accurately. (This category was the music of Irish bard Turlough Carolan, whose music has been classified as a mix of both classical and Irish folk).

Most of the results applying to session number two also applied to session number one. First, the category most correctly identified was category number three (category numbers can be found in the larger chart under *Data, Stage II*). Categories six and seven reported correct identification more often than any other single output, but some confusion existed between the categories (for number seven) and also with category three. Categories one, two, four and five were, on the whole, not identified correctly with any consistency.

A musical analysis of the categories used shows that, perhaps, categories number one and two are too similar to be separate; this also applies to categories six and seven. Categories number four and five are musically ambiguous, not constrained to any particular style. Thus, for session number three, categories one and two were combined, as were categories six and seven; categories four and five were dropped altogether, and category three was transferred without alteration. (Note that for discussion of session three, the categories were renumbered, as per the smaller chart under *Data, Stage II.* Category three became category one; categories one and two became category two; and categories six and seven became category three).

During session number three, category two was most consistently identified correctly. Categories one and three averaged a correct classification more often than any other single output, but some confusion seemed to exist between them. Still, these categories tended not to be classified as category two.

Because all of the data analyzed were averages, the data could most accurately be viewed as the probability of any given output (though the outputs do not always add up to one) for each category. This process masks most of the wild inaccuracies which occurred between note windows even on the same song. Output tended to jump between categories from one window to the next, even if the positional difference between the windows was only one or two notes. Overall, the network performed rather poorly on its classification efforts. Still, a great deal of evidence is shown that classification was occurring.

Referring back to White, "any lack of success in applications must arise from inadequate learning, insufficient numbers of hidden units, or the lack of a deterministic relationship between input and output." The first is most likely to be true; the variety of music which was used was small and often of poor quality. The lack of a deterministic relationship could also have been a problem. Melodies may not vary enough between styles to be classified solely on the melodies themselves. To combine these two conclusions, more music with more information (i.e., a harmony line or figured bass) should be used in the future. Though it does not seem that the network suffered from too few hidden units, this has not been verified.

One interesting result which was reflected throughout the training sessions was the correspondence between "classical" and the various "(Celtic) folk" categories. During session one this result was dismissed as a fault of the "dual output" category, but the result persisted throughout sessions two and three as well. Because of its recurrence, this seems to indicate an outside relationship between "classical" melodies and "(Celtic) folk" melodies rather than an error in the network. Though only of minimal interest to the computer science community, this might interest those in the fields of musical theory and musical history. Alternately, this could simply be a faulty result of inadequate training resources.

Methodology, Stage III

The third stage of this study regards the ability of the network to generalize information from a matrix of data, as a visual display might provide. During this stage, an eight-by-eight grid was set up to train the network to recognize whether or not a particular point is "surrounded" by elements of the grid. This application could be expanded to determine this for every point on the matrix, and it would approximate an edge-finding algorithm.

The first test of the third stage involved an eight-by-eight matrix filled with binary elements (that is, either on or off). This binary matrix and the location of one point on the matrix was given to the network as input. Expected output was a single node which indicated whether the point was surrounded. In this test, the term "surrounded" became somewhat ambiguous and subject to human judgment. This is due to the fact that the edges of the matrix can be included in "surrounding" an area, but a point on an empty matrix is not considered "surrounded." With this definition of "surrounded," there are really no hard-and-fast rules to be applied (which suits this test to the neural network), but rather a faith in the human trainer's consistency of judgment. Below are presented some examples of "surrounding."

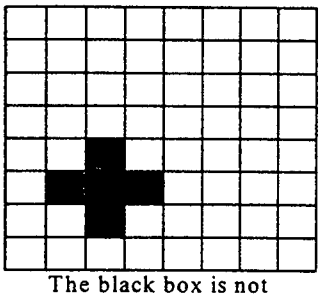

The black box is not "surrounded."

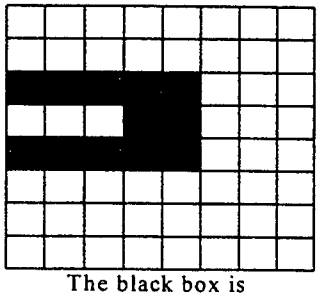

The black box is "surrounded."

When creating the training set for the network, not only was each selected matrix included, but so was each of that matrix's seven rotations and reflections. This inclusion was implemented to lower the time required generating training examples while at the same time increasing the number of examples the network would be trained on. This also addresses directly the rotations problem indicated by Skapura. The final training set included 640 training examples.

The ambiguity of the "surrounded" definition was initially unintended in the first test, so a second test was developed to increase the complexity of the test while decreasing (but not eliminating) this ambiguity. This was accomplished by adding a second type (or "color," referring to the colors used in the program which assisted in the creation of the training set) of element to the matrix. In this case, for an area to be surrounded, the area must be completely surrounded by only one color (though again, the edges can be used as boundaries as well). If any element of the other color is included in the "surrounded" area, the area is not "surrounded." Again, some ambiguities exist (though much fewer). In this test, a point in a blank matrix is still not surrounded, nor is a point in a matrix blank but for a ring of one color (which the point is not inside). Examples of test number two are shown below.

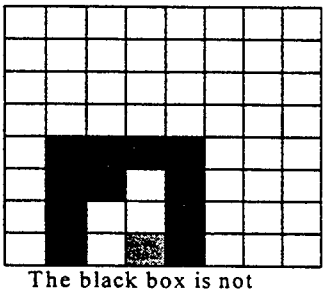

The black box is not "surrounded" by either light or dark gray.

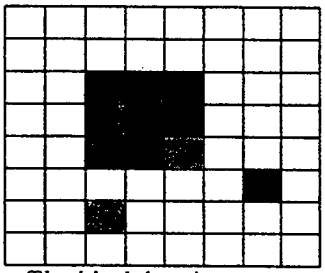

The black box is not "surrounded" by either light or dark gray.

Data, Stage III

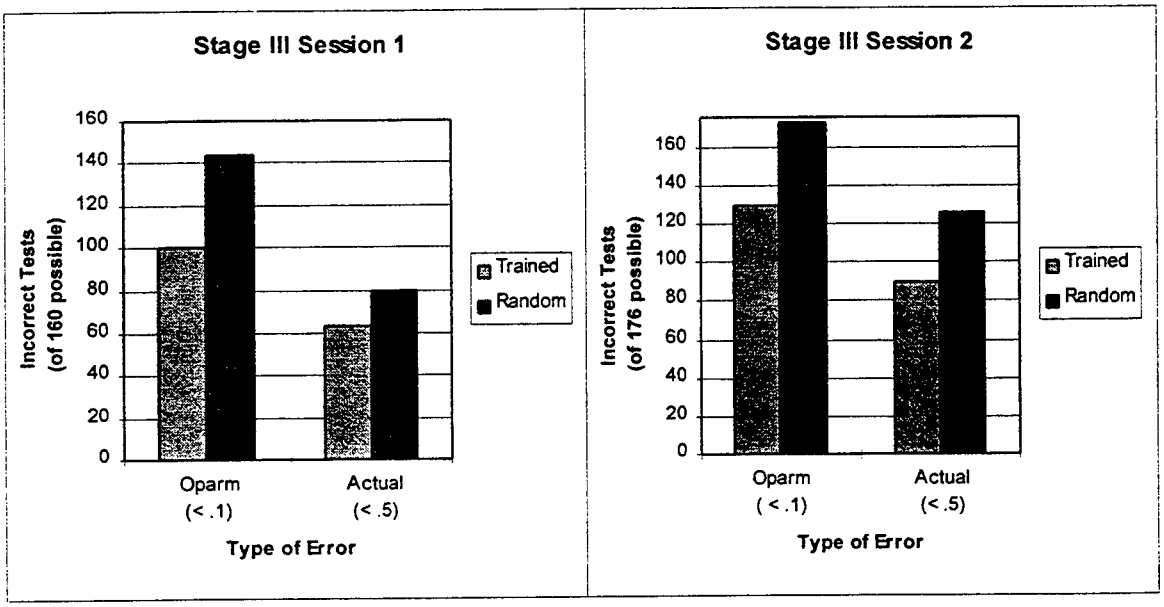

Data for Stage III Sessions 1 and 2. Both charts reflect incorrect tests rather than incorrect nodes.

These charts compare the number of incorrect tests resulting from each session with the number of incorrect tests resulting from random output (calculated based on probability laws and confirmed by actual pseudo-random tests).

Conclusions and Results, Stage III

As can be seen by the number of incorrect results, both of these sessions performed quite poorly. Still, the trained sessions were more accurate than their random counterparts. This poor performance can be attributed to a couple of factors. First, there were probably too few training files. Also, the ambiguities of the not-quite rule based system of judgment may have confused the network. Most likely the correction of the first problem would rectify the second on its own.

Another factor that is interesting to note: despite the training on rotations of each training case, similar rotations in the testing cases yielded much different results from rotation to rotation. This is probably due to the lack of true convergence (the training was stopped at an error around twenty).

Overall Conclusions, Recommendations, and Points For Future Thought

In general, the most important conclusion resulting from this study is this: training sets absolutely *must* be extensive enough to train the network sufficiently. How to assure this, though, is unknown. One method is to arbitrarily pick a number of training cases with the understanding that this number will increase as necessary. This requires (as will any other acceptable method) that the trainer have sufficient access to or ability to generate training cases (the lack of which was the problem in this study's second stage) as well as enough time to train the network several times with increasing numbers of training cases (the lack of which was the problem in this study's third stage). If, however, the trainer has the ability to automatically generate training cases with the proper output, what is the necessity of the neural network? This is a potentially serious fault of backpropagation neural networks, that the networks must be "supervised" in some way.

Stage one seems to have something to say about the question of number of training cases. The most accurate network, the perceptron, did not reach high (perfect) accuracy until nearly half of the possible cases were given to it for training. Less accurate networks never reached that peak accuracy. Could the 1:2 training-to-possible ratio carry over to larger networks and larger problems? Hopefully this is not the case. If so, needing to generate half of 2^{100} possible inputs before the network can generate consistently accurate results from a net of that size essentially negates the usefulness of the network in the first place. If the first half of so many training cases can be generated, why not generate the second half as well and use a standard lookup routine rather than taking the time and effort to train the network? The examination of this accuracy ratio is left to future (or past) studies to disprove.

The Bounded Dynamic Backpropagation program is in need of two future adjustments. First, if it is ever to be used on an PC-Compatible machine in the future, it must either be rewritten to make full use of available memory or it must be compiled by a 32-bit flat-memory model compiler. Second, it should be adjusted to aim for outputs of 0.1 and 0.9 rather than 0 and 1. This would improve the quality of convergence as well as its speed. It would also expand the allowable error and perhaps eliminate the need for two measures of error.

Plans have been made to continue stage three of this study. Should such a continuation be attempted, one part of it should be altered. Training files must be generated automatically to produce them in sufficient quantity that the network might be properly trained. This, unfortunately, essentially kills the "ambiguous judgment" part of the study, but it is more or less necessary. In order to automate the production of training cases, it is necessary to strictly define the rule system which defines "surrounded." This could be done by preventing the edges of the matrix from "surrounding" the point. The network would then essentially test for exclusion from the edges of the matrix (and, if the second session of stage three should be continued, the second "color" of matrix element). The program generating training files would simply need to create a matrix, select points within it randomly, and use some sort of a "flood-fill" routine to test if the point is surrounded.

References

Braspenning, P.J., Thuijsman, F., and Weijters, A.J.M.M. (ed.) *Artificial Neural Networks: An Introduction to ANN Theory and Practice*. Berlin: Springer, 1991

Hossoun, Mohamad H. *Fundamentals of Artificial Neural Networks*. Cambridge: MIT Press, 1995

Sarle, Warren S. *comp.ai.neural-net Frequently Answered Questions*. Cary, NC: SAS Institute Inc., 1996

Skapura, David M. *Building Neural Networks*. New York: ACM Press, 1996

White, Halbert, *Artificial Neural Networks: Approximation and Learning Theory,* Oxford: Blackwell, 1992

COMPRESSOR TESTING

Amy E. Beam

Beavercreek High School

2600 Dayton-Xenia Rd.

Beavercreek, Ohio 45434

Final Report for:

High School Apprentice Program

Wright Laboratory

Sponsored by:

Air Force Office of Scientific Research

Bolling Air Force Base, DC

and

Wright Laboratory

Wright Patterson Air Force Base, Ohio

August 1996

COMPRESSOR TESTING

Amy E. Beam

Compressor Research Facility

Beavercreek High School

Abstract

The Compressor Research Facility (CRF) at Wright Patterson Air Force Base, in Ohio, has been testing a compressor for General Electric. Three steps of this testing were done and are written about in the following. A simple and efficient way of adding error bars to data was found. This was important because the accuracy of the data needed to be found quickly. A Pressure Sensitive Paint (PSP) is being developed to replace probes on the rotor blades. The paint is significant in finding the pressure difference inside the compressor. Lastly a new piece was designed for the facility. It is to be placed in the test rig so that the PSP is able to be viewed optically.

COMPRESSOR TESTING

Amy E. Beam

Introduction

The engine is the key element to all future military aircraft system. The engine is important, it provides thrust and power for all onboard subsystems. These subsystems include the electrical power generation necessary to run the plane, environmental control systems, to cool the pilot, and hydraulic and phenumatic systems, for flight control. There are two classes of engines, reciprocating and non-reciprocating. The futuristic airplane is expected to use a non-reciprocating engine. Non-reciprocating aircraft engines, all of which operate on the principle of jet propulsion, include the turbojet, the turboprop, the ramjet, and the rocket engine. The turboprop, turbojet, and turbofan engines, figure #1, are gas turbine engines, in which the air that enters the intake of the engine is first compressed in a compressor. Fuel is then added to burn the oxygen in the air, increasing the gas temperature and its volume. The high pressure gases are then partially expanded through a turbine which drives the compressor (and the propeller in a turboprop engine). The residual gas that is now at intermediate pressure is accelerated by expansion through a rear-facing nozzle, to produce a high leaving velocity and, with it, the desired thrust. Turboprop engines are efficient for medium-sized planes at speeds up

to about 480 to 640 km/hr (about 300 to 400 mph). At higher speeds, turbojet or turbofan engines perform better. The performance of a propeller reaches such a low level of efficiency that jet engines are used exclusively on aircraft that operate above 800 km/hr (about 500 mph).

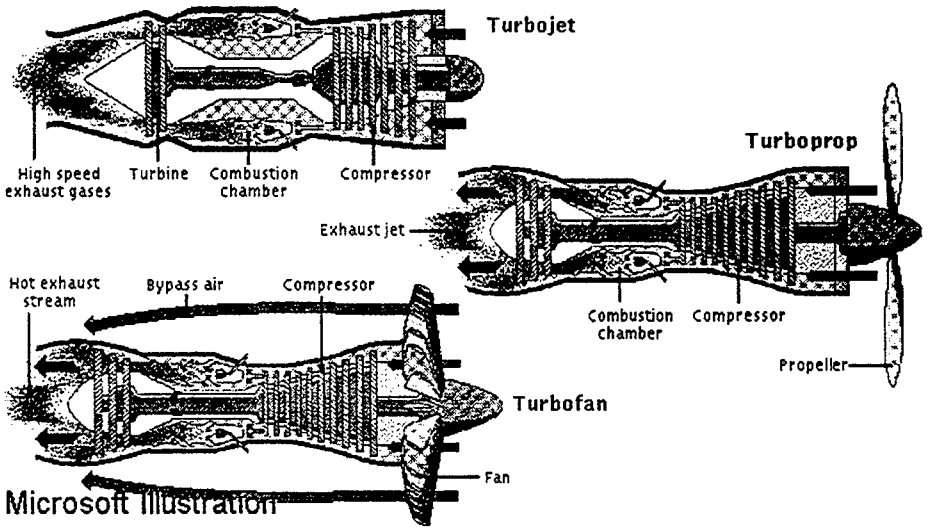

Figure #1

The above illustrations are replicas of the three types of engines.

Discussion of Problem

The CRF has been working on a new compressor for the General Electric Swept Fan Assessment Rig (GESFAR). A performance test of this compressor has been conducted and it was the laboratory's job to correlate the data to the expected theoretical results. The data did not match the predicted results and additional testing is required to resolve this difference. An easy way of correlating the error bars was needed. A special paint was also essential but not yet designed. When the paint was ready it needed a way to be viewed on the blade itself.

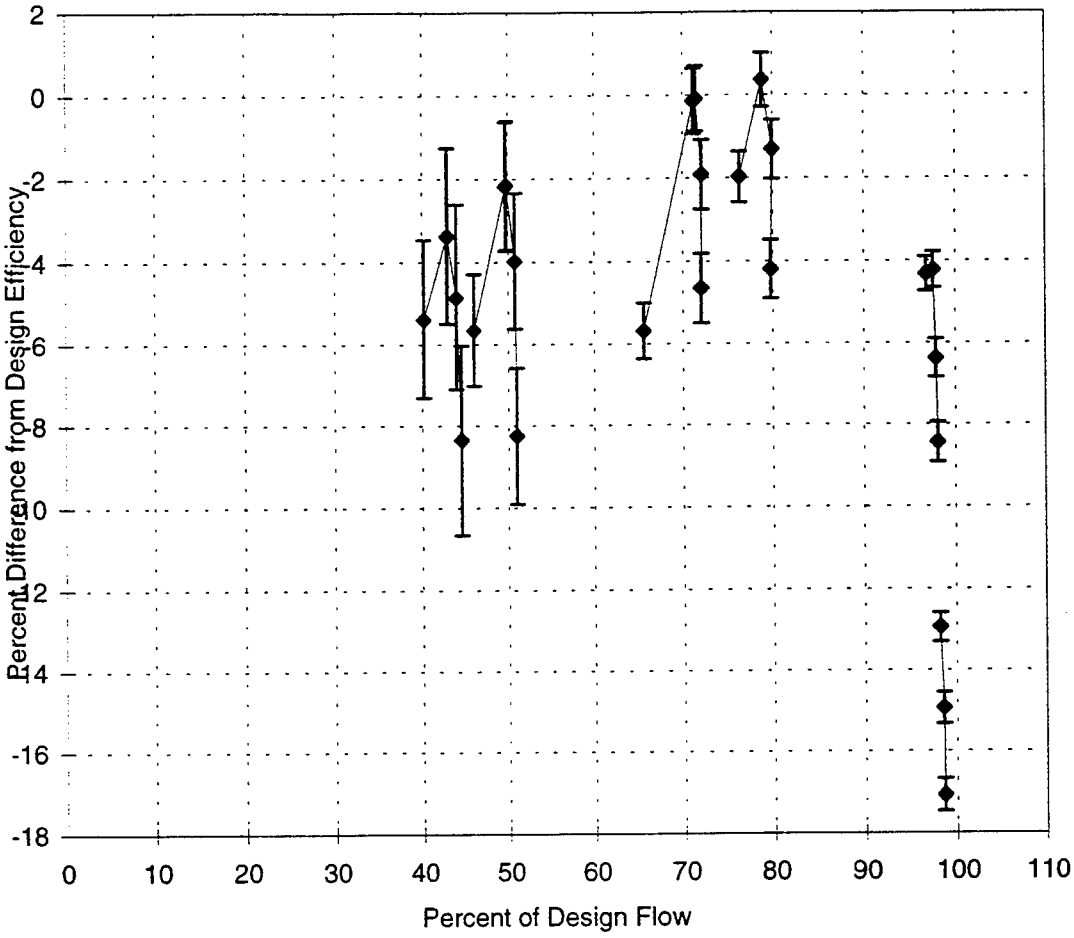

Figure #2

This chart is establishing the design flow efficiency.

Methodology

The CRF had collected data earlier in the year for the GESFAR project. This data needed to show varying error bars. The Microsoft Excel program was studied and a simple way of transforming data into error bars was found. Figure #2 shows the data that the lab collected, the new procedure that was to be designed was used to insert the error

bars. Subsequently the error span was larger then expected and the lab resolved that there needed to be a way to measure the internal airflow pressure more accurately.

In addition to making pressure measurements with probes, surface pressure measurement techniques using an optical sensitive paints were also investigated. This is an important capability, because rotating blades of a compressor do not have enough room for probes to obtain the data. The surface coating or paints would be used instead of a probe. To investigate this novel technique, sample disks ere painted. The paint sensitivity to pressure was evaluated. As shown in figure #3 the test runs as follows. A sample disk was inserted into a vacuum chamber. As the air is evacuated and then replenished again a light source scanned the sample and the reflected light intensity was taken. Figure #4 shows the correlation of the reflectance and pressure. During these checks, it was important that the change of light intensity, a function of pressure, be repeatable. In addition the sensitivity of light needed to be large enough to record pressure changes as small as .5 psi.

Figure #5 is the compressor shroud that was designed to support the PSP development. This case was needed to use PSP in a transonic compressor rotor. The new case will take the place of two old parts, so that the overall length of the compressor does not change. The design changed many times, but finally ended up to include two windows that allow the blades, covered in PSP, to be viewed easily. The group came to this conclusion after a life size model was created using cardboard. Due to economical concerns the shroud was designed to be made from half an inch thick steel, rolled and

welded to make the tube. The end sections will then be welded onto the tube. Then the piece will be complete and ready for testing.

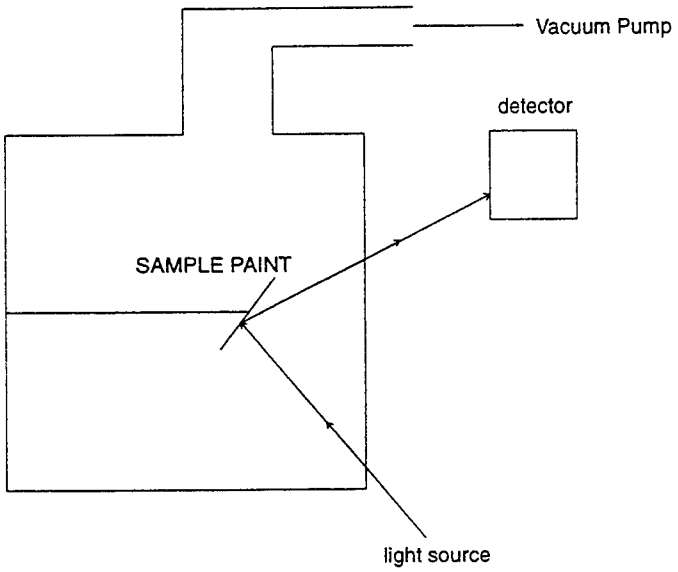

Figure #3

This diagram is demonstrating the procedure of the test rig for testing a PSP.

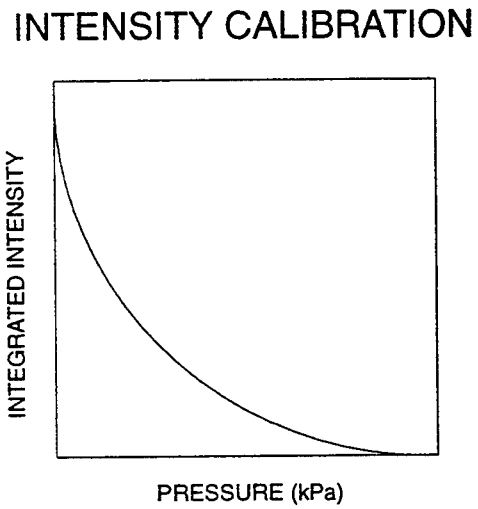

Figure #4

This is a simple replica of a data chart used in PSP testing.

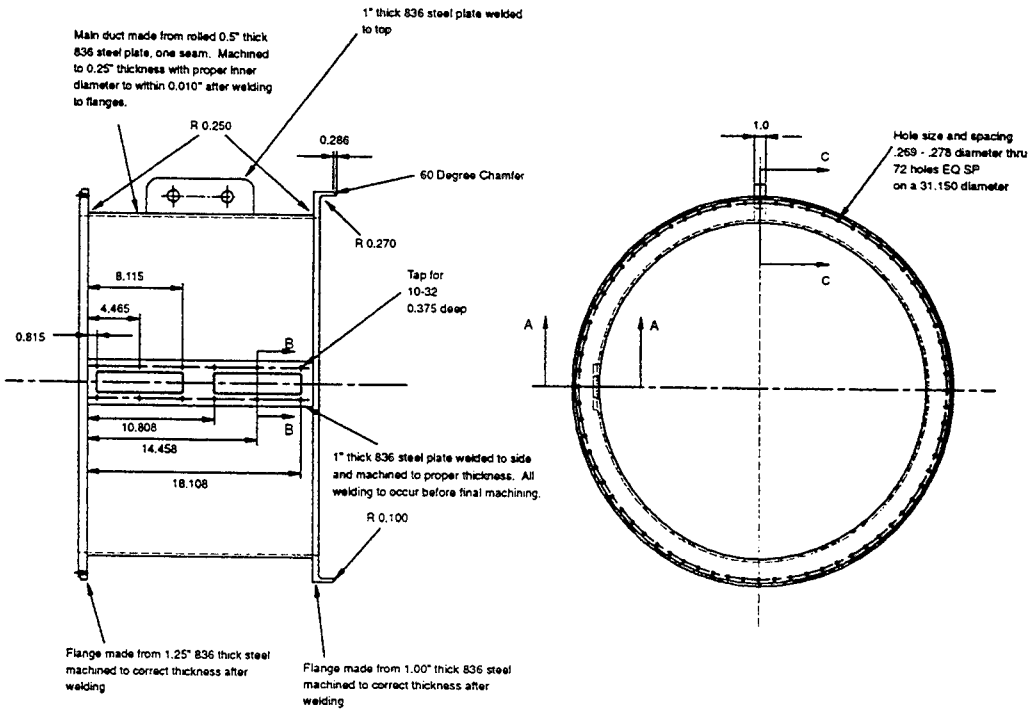

Figure #5

This is the design for a new piece in the GESFAR project.
This piece will be used for viewing the rotor blades with PSP on them.

Conclusions

The GESFAR speedline uncertainty data was correlated and was determined to have differing error bars. The Excel program was used to report this. The pressure sensitive paint acquired a calibration curve that identified pressure changes in association to light intensity changes. The surface pressure can now be achieved on rotating components of the compressor. The compressor shroud was redesigned using the Tommy

CAD designer program. All of the blades for the transonic compressor rotor test are able to be viewed optically using the two windows in this compressor shroud. It is recommend that the CAD program is used wherever useful.

References

"Airplane," Microsoft (R) Encarta. Copyright (c) 1994 Microsoft Corporation. Copyright (c) 1994 Funk & Wagnall's Corporation.

A STUDY OF THE EFFECTS OF VARYING CHAIN LENGTH SURFACTANTS ON POLYMER DISPERSED LIQUID CRYSTAL HOLOGRAPHIC GRATINGS

Crystal Bhagat

Dayton Christian High School
325 Homewood Avenue
Dayton, OH 45405

Final Report for:
High School Apprentice Program
Wright Laboratories, Materials Directorate

Sponsored by:
Air Force Office of Scientific Research
Bolling Air Force Base, DC

and

Wright Laboratory

August 1996

A STUDY OF THE EFFECTS OF VARYING CHAIN LENGTH SURFACTANTS ON POLYMER DISPERSED LIQUID CRYSTAL HOLOGRAPHIC GRATINGS

Crystal Bhagat
Dayton Christian High School

Abstract

The focus of this investigation was to study the effect of varying chain length surfactants on polymer dispersed liquid crystal (PDLC) gratings. This included propylpentanoic acid, hexanoic acid, heptanoic acid, lauric acid, and octanoic acid. Also observed was the effect of varying percent weight amounts of the liquid crystal E7 on PDLC gratings. The percents used for this were 30%, 50%, 70%, and 79% E7 weight amounts in the PDLC syrups. PDLC grating samples representing the different E7% syrups and the syrups with the varying surfactants were constructed. They were then characterized by measuring diffraction efficiency and transmission with a helium neon laser at 633nm. Samples representing gratings with the different surfactants were characterized in *s* and *p* polarizations. Switching voltage was also conducted on several samples. Results showed that gratings containing the octanoic or hexanoic acid surfactant will have higher diffraction efficiencies compared to the others. Also, a 30% E7 amount in the PDLC syrup will have better diffraction efficiency, lower transmission, and a higher total light compared to the other percents of E7 experimented. Characterizing at *p* polarization will also give better grating results compared to the *s*.

A STUDY OF THE EFFECTS OF VARYING CHAIN LENGTH SURFACTANTS ON POLYMER DISPERSED LIQUID CRYSTAL HOLOGRAPHIC GRATINGS

Crystal Bhagat

Introduction & Background

Polymer dispersed liquid crystal conditions have recently been the focus of preparing Bragg gratings used in the area of holography. A hologram is a type of 3D photograph with a visible parallax. It is an exact recording of the light waves from an object. A polymer dispersed liquid crystal (PDLC) based plate records an interference pattern made by a reference beam and an object beam. The effects of two main constituents were studied in this report. They consist of varying chain length surfactants and the liquid crystal E7. Their influence on a PDLC syrup was the core of this investigation.

In the grating spacing (microns) of a sample, a liquid crystal substance resides in the region of deconstructive interference (dark channels), and dense polymer lies in the region of constructive interference (light channels). The morphology of a grating is related to the sample's performance. This is mainly described as the diffraction efficiency and transmission power observed when a laser beam is focused through the sample's grating. Diffraction efficiency is measured by the diffracted power divided by the calibrated factor, and the transmission is calculated by the transmitted power divided by the calibrated factor.

A PDLC syrup contains five main ingredients. The first one is the chain extender N-vinylpyrolidone (NVP). NVP is a cross-linking monomer and reinforces the grating by assisting in strengthening bonds in the polymer. The next ingredient is the liquid crystal E7. Liquid crystals (LC) exist in a phase between the solid and liquid phases and reserve characteristics of both. They are needed in the syrup's recipe because of their chemical structure and mobile nature. These qualities allow the LC to easily form droplets and travel to regions of low light intensity where less rapid polymerization occurs. Another component used is N-phenylglycine (NPG) which functions as a coinitiator. DPHPA works a another ingredient and stands for the monomer dipentaerythrol

hydroxy penta acrylate. The last constituent is the photo initiator dye, Rose Bengal (RB). Also known as bis(triethylammonium)salt, this dye is used for its display of a broad absorption spectrum. The chemical bond structures of these materials can be found at the end of this section.

PDLC films can be switched from an opaque (scattering) state to an optically clear state. This is accomplished be applying an electric field to the sample. This method is known as using "switching voltage" on a sample.

The scanning electron microscope (SEM) can be used to look at the morphology of a grating. The sample film must first be soaked in methanol overnight. Then it is put in liquid nitrogen in order to fracture it. The sample piece can then be mounted and looked at through the microscope. The SEM works by sending an electron beam which scans the sample in a large chamber. A low voltage SEM shows the morphology of a grating as being made of periodic polymer dispersed liquid crystal planes. E7 microdroplets can be seen confined to the Bragg planes and having the size of about one-half the grating space. These droplets are observed as elongated and coalesced.

"Characterizing" is an essential method of recording diffraction efficiency and transmission as a function of voltage. It is defined as measuring optical properties of an optical material. A setup for characterizing samples looks as follows:

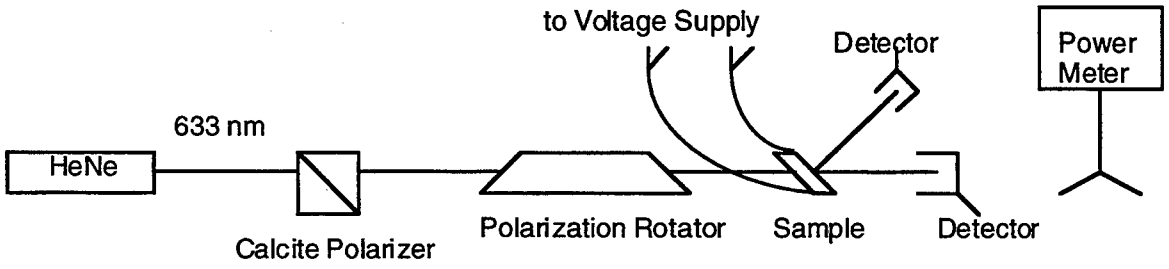

A helium neon laser (HeNe) with the wavelength of 633 nm is used as the coherent light source (unpolarized). Next is the calcite polarizer. This is used to separate horizontal and vertical polarization. The polarization rotator is then used to change the probe beam's polarization from horizontal to vertical. The sample comes next in line. It contains the PDLC holographic gratings. Silicon detectors connected to a power meter are then used to measure the power of the light diffracted or transmitted. Alligator clips can be attached to the electrodes on the sample to conduct

switching voltage. This characterization setup is the main one in which we used for characterizing my PDLC holographic gratings.

A good quality sample is usually clear like glass with no scattering of light. Large droplets of LC cause light scattering as well as causing the sample to look milky. Surfactants can be used in the syrup to make the E7 droplets smaller and therefore improving the quality with less scattering of light. Different chain length surfactants can be used to show this response including propylpentanoic acid, hexanoic acid, heptanoic acid, lauric acid and octanoic acid. A good grating sample will also have high diffraction efficiency, low transmission, and a low switching voltage. This report is a study of gratings prepared from syrups containing a varying percentage composition by weight of the liquid crystal E7 as well as the five different types of surfactants.

The picture above shows a magnified view of a 79% E7 sample. The large E7 droplets flowed when stressed. (Polarizing Optical Microscope)

PDLC Syrup Ingredients (not including E7)

N-vinyl Pyrrolidone

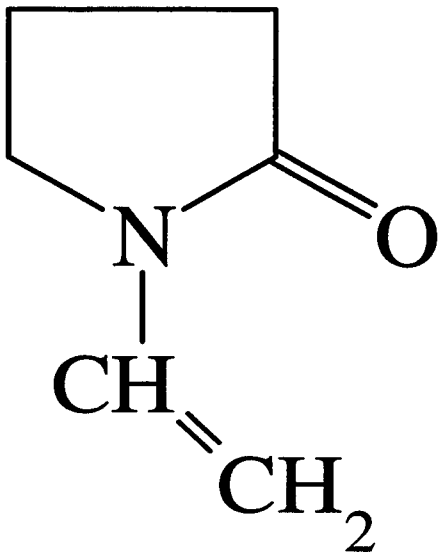

N-phenylglycine

$C_8H_9NO_2$

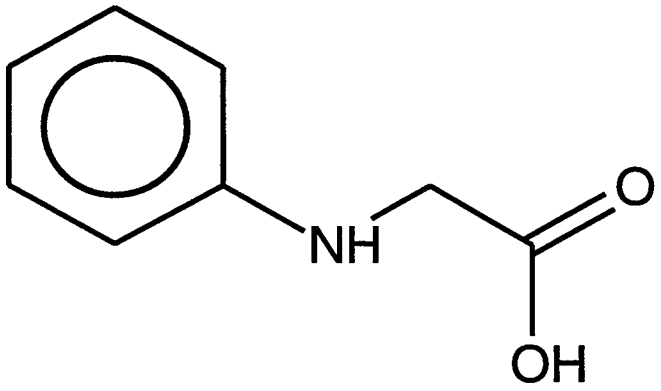

Dipentaerythrol Hydroxypenta Acrylate (DPHPA)

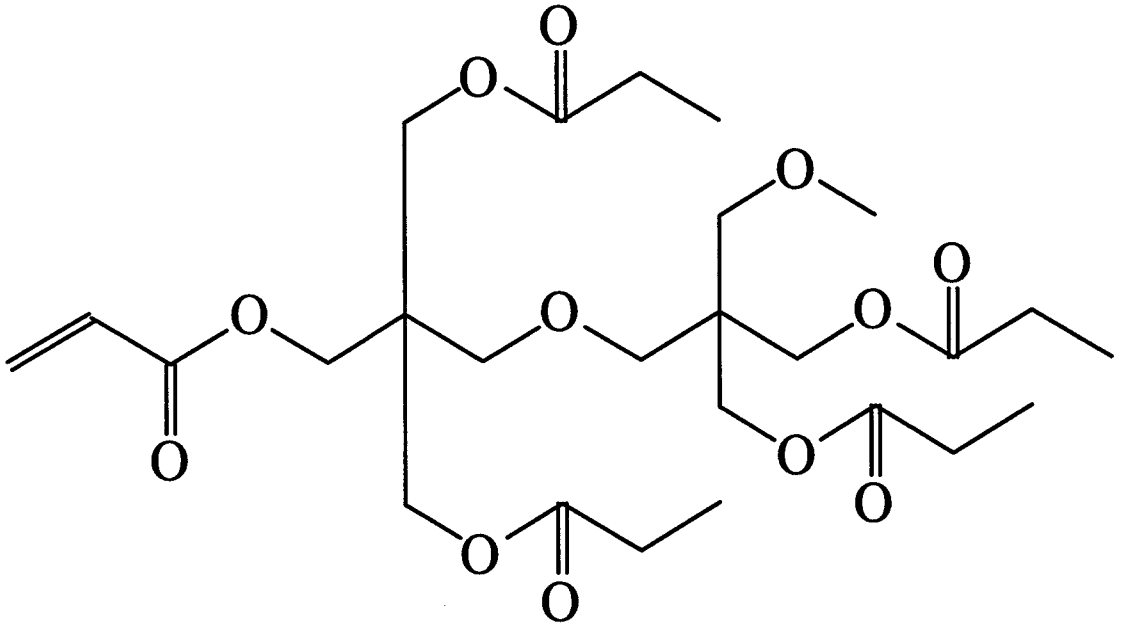

Rose Bengal

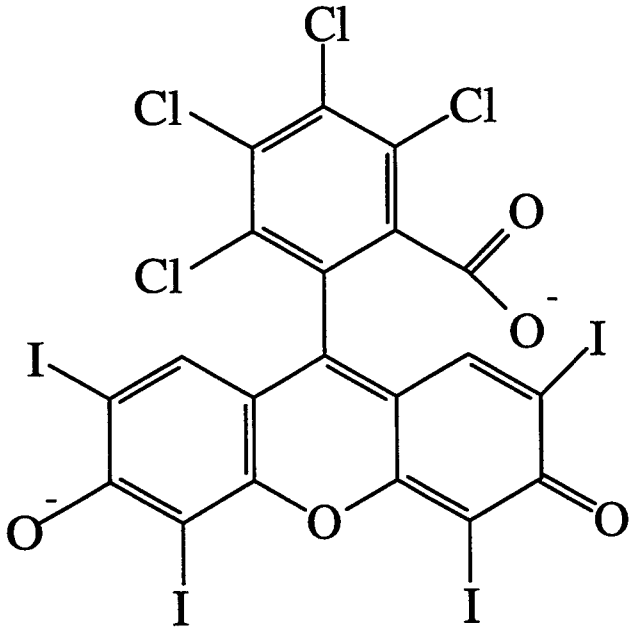

2 $(CH_3CH_2)_2NH^+$

Surfactants

Propylpentanoic Acid

$C_8H_{16}O_2$

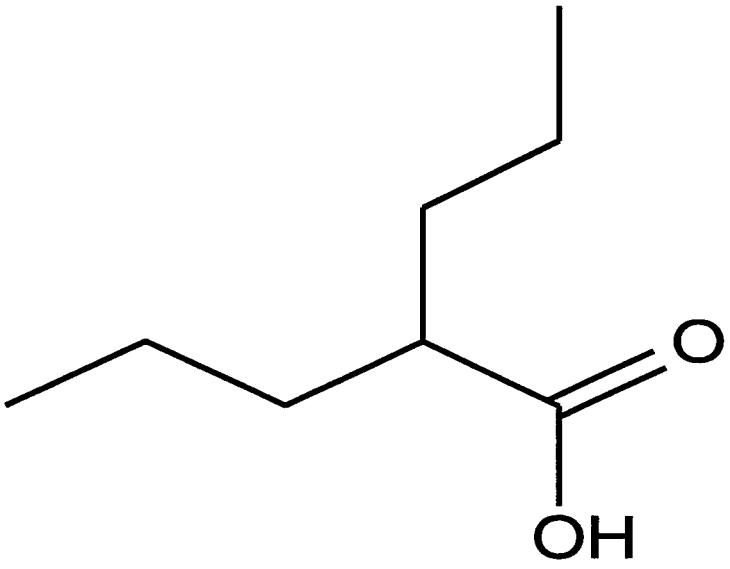

Hexanoic Acid

$C_6H_{12}O_2$

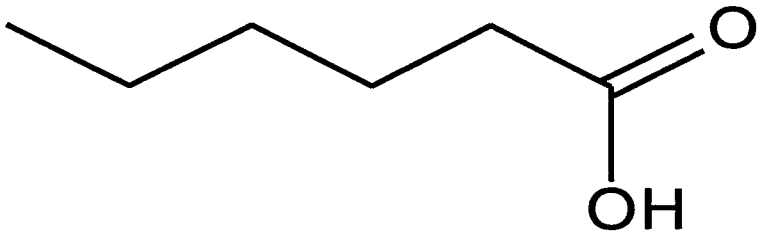

Heptanoic Acid

$C_7H_{14}O_2$

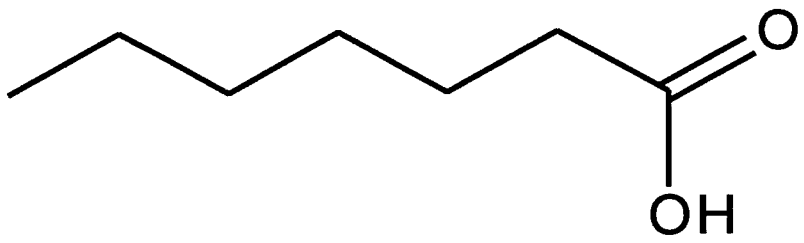

Lauric Acid

$C_{12}H_{24}O_2$

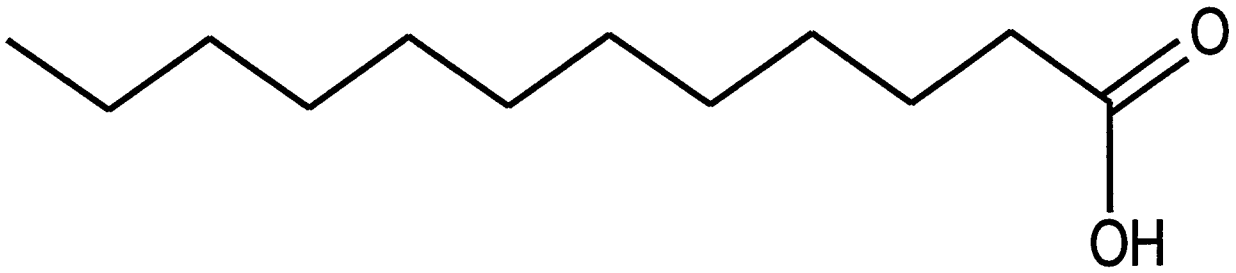

Octanoic Acid

$C_8H_{16}O_2$

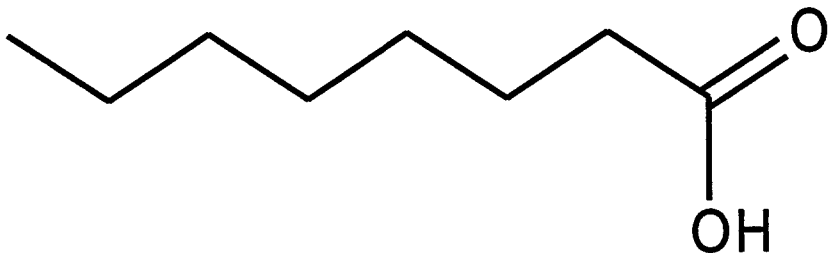

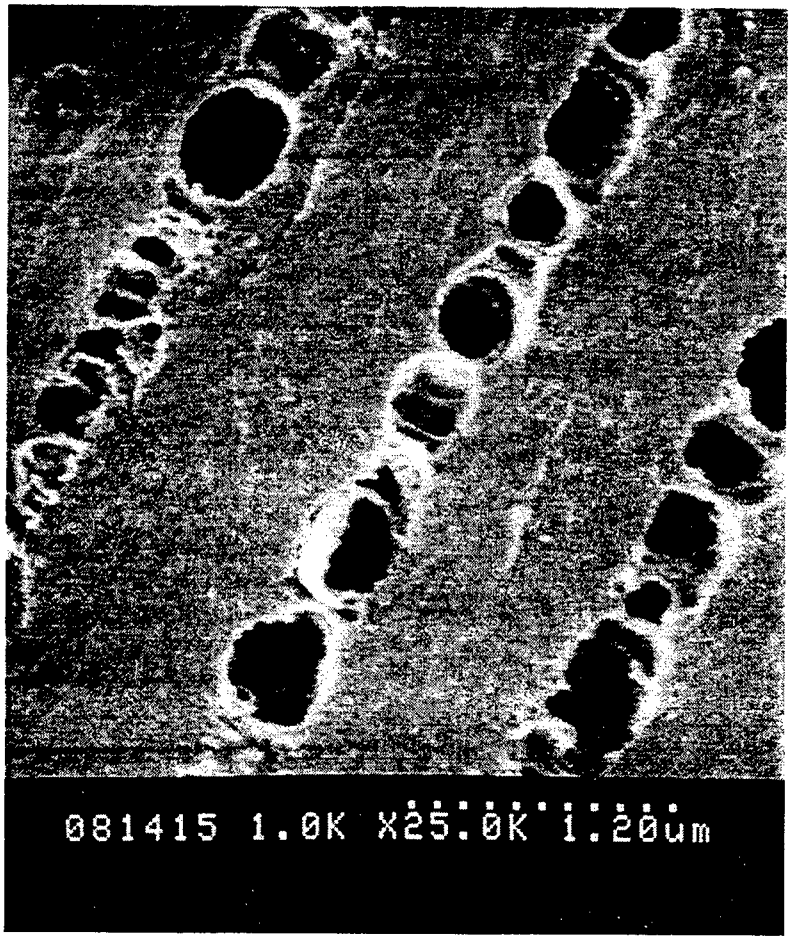

The picture above shows an in-plane view of a typical PDLC grating (SEM).

Methodology

This project relied on two main methods. The first was to make and characterize diffraction gratings consisting of prepolymer syrups with varying percent amounts of the liquid crystal E7. The latter was to make and characterize gratings made from five syrups each containing a different surfactant and a 32% E7 amount.

Four syrups were made all containing five different ingredients: N-vinylpyrrolidone (NVP), liquid crystal E7, N-phenylglycine (NPG), DPHPA, and the photoinitiator dye Rose Bengal (RB). Each syrup was made with a 30%, 50%, 70%, or 90% E7 weight amount. The syrups were then sonicated to ensure a well mixture. They were each contained in a glass vile and wrapped with aluminum foil because of the photo sensitive Rose Bengal dye. After nearly two weeks the 70% and 90% E7 solutions "went bad", and their mixtures were no longer homogenous. Two more syrups were made to replace these, a 70% E7 and 79% E7 solution. Samples were constructed using glass and ITO (Indium Tin Oxide) slides. Spacers 15 μm thick and a circular drop of the syrup were put in between the slides. OD filters were then placed on the sample using refractive index liquid. The sample was mounted and then exposed to blue laser at 514 nm for seven minutes. After that the sample was quickly put under an incandescent lamp to cure. The preparing, mixing, and transferring of syrup onto the slides were all done in the dark due to the photosensitivity of the syrup.

The next page shows a picture of a constructed sample.

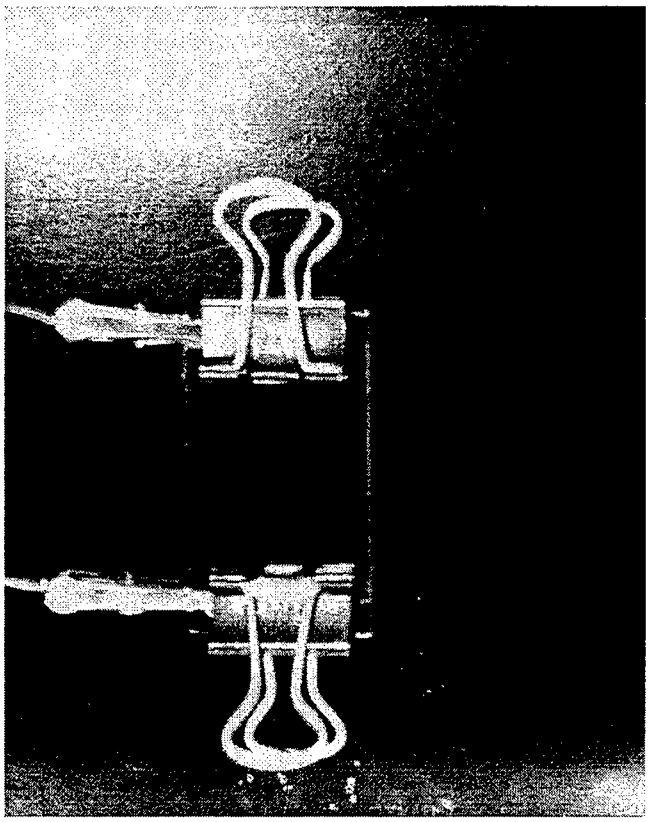

The latter part of the project required the same steps except this time we made recipes containing an additional ingredient. Five different surfactants were added to make five different syrups each containing only a 32% E7 weight amount. The surfactants used were propylpentanoic acid, hexanoic acid, heptanoic acid, lauric acid, and octanoic acid. These each contributed to a 6% weight in the recipe. One glass and three ITO samples were made for each of the five syrups, and the same procedures were followed as before.

The next step was to measure the diffraction efficiency and transmission of all the samples. The characterization setup diagram displayed in the *Introduction & Background* section of this report was used in the process using a helium neon laser at 633nm. The formulas used were:

$DE = (d/c)100\%$ and $T = (t/c)100\%$ where DE = Diffraction Efficiency,

d = diffracted power,

T = Transmission,

t = transmitted light, and

c = calibration factor (transmitted light w/a glass slide)

The grating samples containing surfactant were characterized in both *p* and *s* polarizations. Switching voltage data was also collected on several samples. This was done on the ITO samples by painting a thin strip of silver on the edges and then attaching alligator clips to these electrodes. The clips were then connected to the voltage supply. This applied an electric field to the sample which caused the PDLC films to switch from an opaque state to an optically clear state. A good grating sample was defined as having high diffraction efficiency, low transmission, and a low switching voltage. Diffraction efficiency, transmission, and switching voltage were all recorded and the results made accordingly.

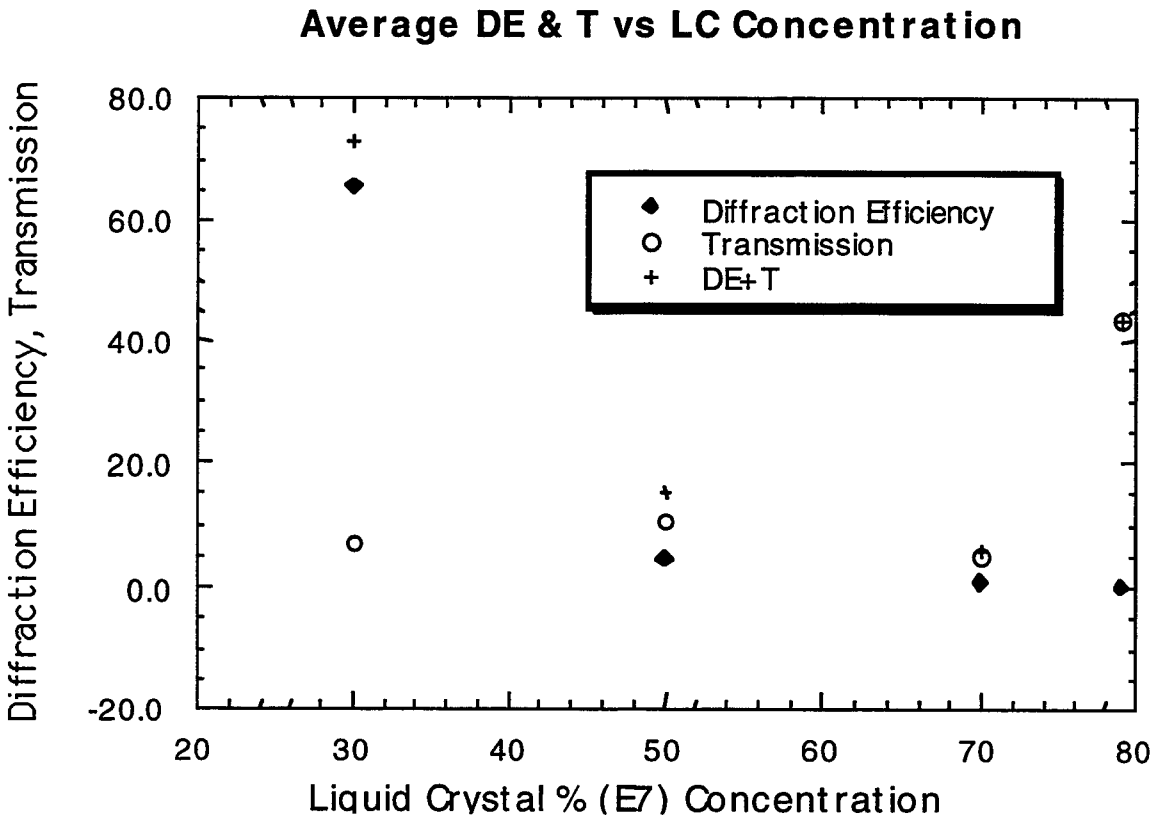
Average DE & T vs LC Concentration
Diffraction Efficiency, Transmission
80.0
60.0
40.0
20.0
0.0
-20.0
20
30
40
50
60
70
80
Liquid Crystal % (E7) Concentration
Diffraction Efficiency
Transmission
DE+T

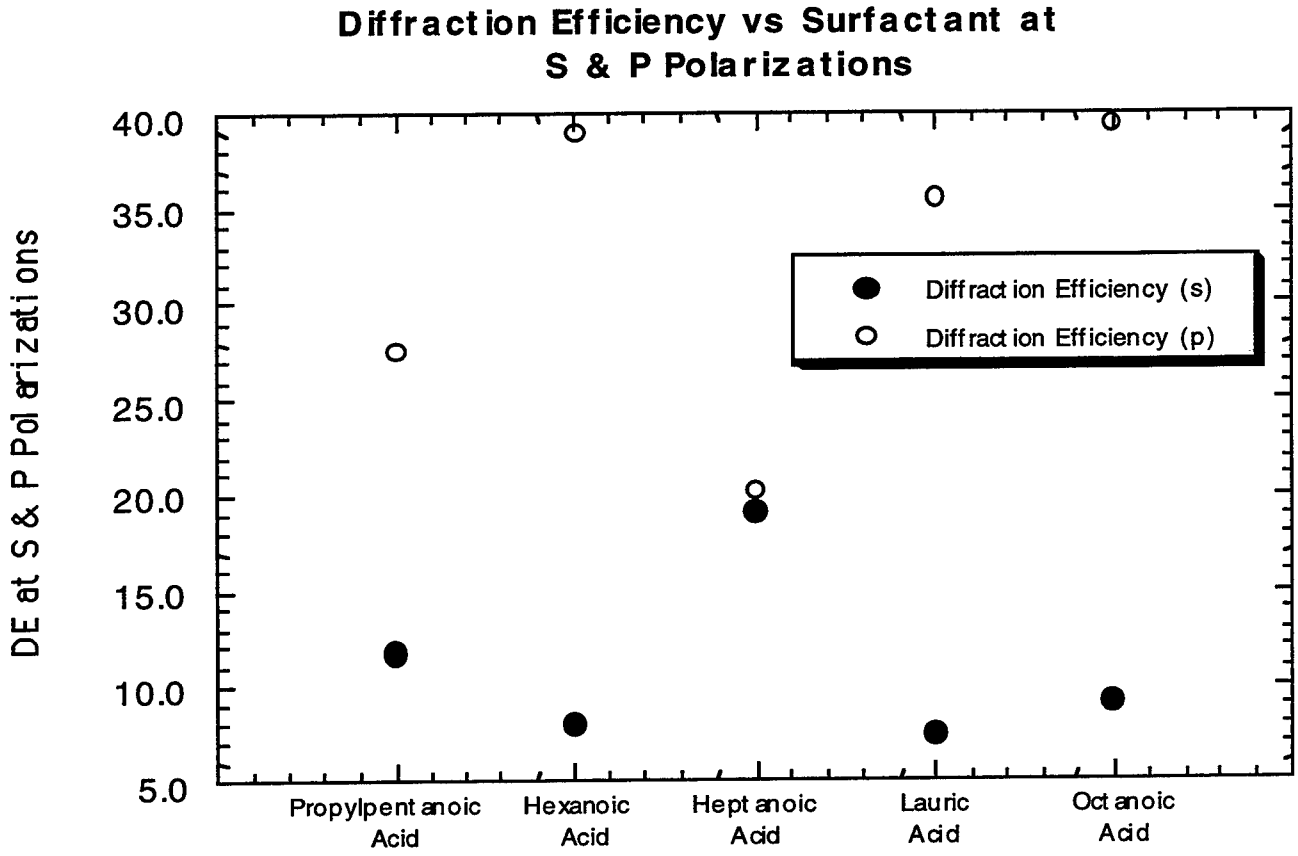
Diffraction Efficiency vs Surfactant at
S & P Polarizations
DE at S & P Polarizations
40.0
35.0
30.0
25.0
20.0
15.0
10.0
5.0
Diffraction Efficiency (s)
Diffraction Efficiency (p)
Propylpentanoic Acid
Hexanoic Acid
Heptanoic Acid
Lauric Acid
Octanoic Acid

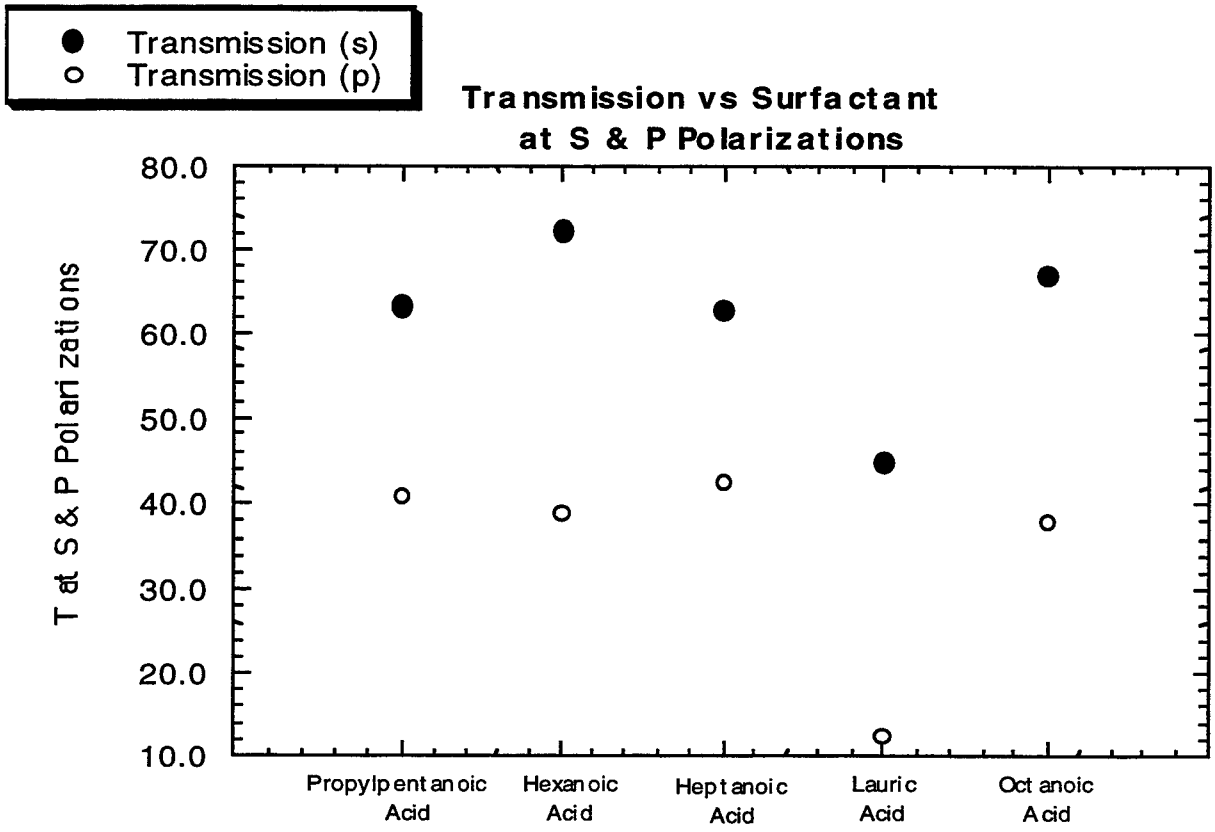
Transmission (s)
Transmission (p)
Transmission vs Surfactant
at S & P Polarizations
T at S & P Polarizations
80.0
70.0
60.0
50.0
40.0
30.0
20.0
10.0
Propylpentanoic Acid
Hexanoic Acid
Heptanoic Acid
Lauric Acid
Octanoic Acid

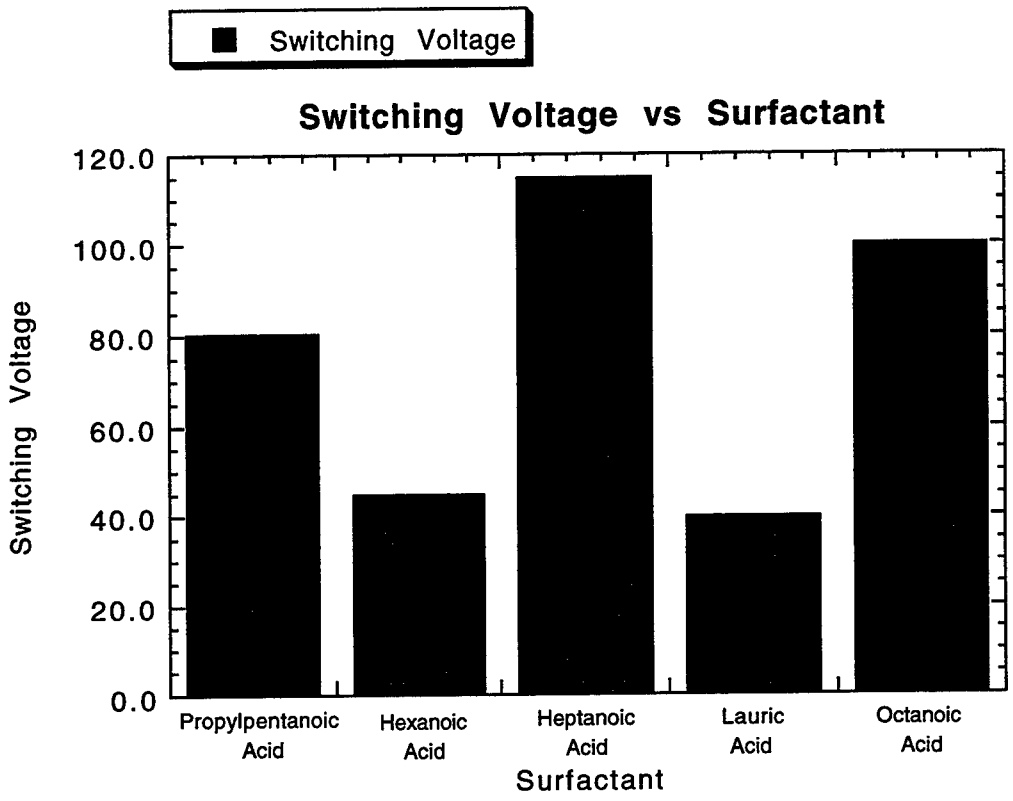
Switching Voltage
Switching Voltage vs Surfactant
120.0
100.0
80.0
60.0
40.0
20.0
0.0
Switching Voltage
Propylpentanoic Acid
Hexanoic Acid
Heptanoic Acid
Lauric Acid
Octanoic Acid
Surfactant

Results & Conclusions

The first graph shows the average diffraction efficiency and transmission versus the liquid crystal concentration. We see that the average 30% E7 gratings had good diffraction efficiency that were significantly higher than the transmission. The 50% E7 concentration had a slightly higher transmission than diffraction efficiency and the overall total light (DE+T) was low. The 70% was similar and had the lowest total light. The 79% had a much higher transmission compared to its diffraction efficiency. These samples were all characterized in *p* polarization. The second graph shows the diffraction efficiency versus the surfactant at *s* and *p* polarizations. Diffraction efficiency was higher at *p* polarization that at the *s* polarization except for the heptanoic acid which had similar DE at both polarizations. Octanoic acid then hexanoic acid showed the best (highest) diffraction efficiency at *p* polarization. The next graph shows the transmission versus the surfactant at *s* and *p* polarizations. Transmission was much higher at *s* polarization than at the *p* polarization. This was seen with all the varying surfactants. In the next graph showing switching voltage versus the surfactant it appears that lauric acid had the best (lowest) average switching voltage, and heptanoic acid had the highest switching voltage.

We can now conclude that characterizing grating samples at *p* polarization rather than at the *s* polarization will result in higher diffraction efficiency and lower transmission. Also in this polarization, octanoic acid and hexanoic acid grating samples will have the best diffraction efficiencies. We can also now assume that a 30% E7 weight will have higher diffraction efficiency compared to a 50%, 70%, or 79% E7 weight solution. The total light through a 30% E7 sample will also be higher.

Suggestions for Future Research

Further experimentation is suggested in testing the effects of varying chain length surfactants on PDLC holographic gratings. More syrups containing the 32% E7 and 6% surfactant weight amounts should be formed and this recipe maybe even a little varied. Several more ITO samples

could also then be constructed, characterized, and conducted with switching voltage. Morphology could also be further studied through the SEM. Overall, a further study dealing with the surfactants is recommended, one that will be thorough and given more time.

Acknowledgments

Special thanks to Dr. L. V. Natarajan, Dr. Richard Sutherland, and Vince Tondiglia for all their guidance and support. I am also grateful to Wright Laboratories which made this experience possible.

References

Adams, W. W, T. J. Bunning, L. V. Natarajan, R. L. Sutherland, and V. P. Tondiglia. "Electrically Switchable Volume Gratings in Polymer-Dispersed Liquid Crystals." *Applied Physics Letters*, 1993: 1074-1076.

Adams, W. W, T. J. Bunning, L. V. Natarajan, R. L. Sutherland, and V. P. Tondiglia. "Volume Holographic Image Storage and Electro-Optical Readout in a Polymer-Dispersed Liquid-Crystal Film." *Optical Letters*, 1995: 1325-1327.

Adams, W. W, T. J. Bunning, L. V. Natarajan, R. L. Sutherland, VP. Tondiglia, and D. L. Vezie. "The Morphology and Performance of Holographic Transmission Gratings Recorded in Polymer Dispersed Liquid Crystal." *Polymer*, 1995: 2699-2708.

Aldrich Catalog Handbook of Fine Chemicals. Milwaukee: Aldrich Chemical Company, Inc., 1994.

Bunning, T. J., L. V. Natarajan, R. L. Sutherland, and V. P. Tondiglia. "Bragg Gratings in an Acrylate Polymer Consisting of Periodic Polymer-Dispersed Liquid-Crystal Planes." *Chemistry of Materials*, 1993: 15331538.

Caulfield, H. John. "The Wonder of Holography." *National Geographic* March 1984: 365-377.

Green, Floyd J. The Sigma-Aldrich Handbook of Stains, Dyes, and Indicators. Milwaukee: Aldrich Chemical Company, Inc., 1990.

Schulte, Michael D. "Synthesis and Characterization of Chain Extending Monomers for Polymer Dispersed Liquid Crystal Systems." Wright Laboratory, 1995.

A Trial of Microencapsulated Phase Change Material of use in modern aircraft as an effective Thermal Barrier

Daniel A. Binkis

Beavercreek High School
Dayton-Xenia Rd
Beavercreek, OH 45385-9527

Final Report for:
High School Apprentice Program
Transparency and Thermal Laboratories

Sponsored by:
Air Force Office of Scientific Research
Wright Patterson Air Force Base

and

Transparency and Thermal Laboratories

August 1996

A Trial of Microencapsulated Phase Change Material of use in modern aircraft as an effective Thermal Barrier

Daniel A. Binkis
Beavercreek High School

Abstract

The objective of the Microencapsulated Phase Change Material (Micro PCM) Advanced Applications effort is to research PCM technologies so that quantitative evaluation of their benefits for innovative aircraft cooling applications can be assessed. This project will evaluate the thermal effectiveness and durability of Micro PCMs embedded in carbon composite structural panels. Micro PCM capsules will be mixed into the resin of composite panels in various concentrations and compared to baseline panels that contain no Micro PCM capsules in the resin. The thermal effectiveness of the panels will be evaluated by applying an external heat flux to the panels and measuring the transient temperature response through the panel. These temperatures will be compared to a one dimensional model of the system. The durability of the panels will be evaluated by thermally cycling the panels in the temperature chamber and observing the results. At the completion of the durability tests, thermal effectiveness tests may be conducted on selected panels to determine if the thermal cycling affected thermal performance. Mechanical property tests including tension and compression will be performed at the conclusion of the thermal cycling tests. The mechanical tests will be conducted by FIB in their facilities. The first phase of this testing will use a carbon composite panel devoid of any Micro PCM capsules in order to attempt to establish several base-line figures for comparison and model design.

A Trial of Microencapsulated Phase Change Material of
use in modern aircraft as an effective Thermal Barrier

Introduction

At times there is a need for thermal protection of certain areas of an aircraft from a brief yet intense burst of heat. A specific example of this need is for the Harrier Jet. Upon vertical takeoff and landing, while the plane is near the ground, the vectored thrust downward reflects off of the near ground and hits the bottom of the aircraft. The areas affected by this need some sort of thermal protection from this occurrence. Microencapsulated Phase Change material offers this protection. The material is formed into miniscule beads (about 50 microns in diameter) which is mixed in with a composite material. When the temperature of these beads rises above a certain temperature, they melt allowing for a lower conductance of the heat through the material, and protection for the underside of the composite.

Testing and Performance

For performance testing of the composite panels, a heat gun was used. In order to measure the temperature at different points within the composite material, two holes were drilled from the bottom of the sample to a specific distance from the top (One was drilled to 1/3 from the top, the other to 2/3 from the top). These were then filled with thermocouples. A thermocouple was attached underneath the sample material, and one was attached on top of the sample. In an attempt to measure solely the top surface temperature, without interference from the air temperature from the heat-gun, the top thermocouple was covered with epoxy. The composite material was placed on top of a heat sink, cooled, with a neslab chiller, to 50°F. In order to ensure good thermal conduction thermal grease was placed between the sample and the heat sink. A heat-flux sensor was attached to the top of the sample to measure Q, and a thermocouple was placed into the flowpath of the hot air so that air temperature could be recorded. The data from these sensors were fed into a computer running ViewDAC software, and then exported to Microsoft Excel for analysis. (See Diagram 1: Actual Test Setup)

Originally the test was quite simple. The decision was made to mark off 5 points (each an inch apart) at which to run the tests. After the setup had been completed, the platform would be adjusted to one of the 5 points to set a specific distance from the heat-gun. We made a quick check of the thermocouples to ensure precise and steady readings. Then the sample would be lined up under the heat gun. The computer was then set to start recording data, and the heat gun was turned on, and left on until the change of temperature would lessen to a great degree. This was altered after the second run of the tests, because of a great variance of the air temperatures, caused by the position of the sample under the heat gun. For the 3rd and 4th tests, the heat gun was started, and the sample adjusted underneath so that the sample was aligned into the path of the hot air. Then it would be allowed to cool, and the test would be run as above.

The test results for the tests were fairly consistent except for the few adjustments made. When the discrepancy between Test A's air temperature and Test B's air temperature was discovered, we altered the Test Procedure for Test C and Test D to ensure consistent air temperature input. In Test C and Test D, attempts were made to get a truer Top Surface Temperature, however these attempts appear to be unsuccessful in obtaining a usable Top Surface Temperature, despite improving the accuracy by over 100°F. This was first done by drilling a hole from bottom to top, and placing a thermal couple along the same plane as the top surface, then covering the hole with epoxy. Secondly, a hole was drilled almost to the top

surface, within 0.05mm. Q (Heat Flux) values would range from 1.07 Btu/sec to 0.605 Btu/sec over the 4 inch spread of platform positions. Temperature differences over this spread were less drastic, however, only varying about 40°F from the closest position to the furthest position. Temperature differences between the points in the material were made manageable by the addition of the heat sink underneath the sample, giving delta T's of 17.74 between the bottom surface and the thermocouple at 1/3 from the top. This allowed for fairly accurate conductivity (k) value calculations. These values were consistently in the 1 to 3.5 W/m·K range, and so an approximate average of 2.5 W/m·K was used for the analysis using the SINDA/FLUINT model created.

Using the Microsoft Windows front-end program SINAPS, a SINDA/FLUINT model was created in order to better analyze this test. (See Diagram 2: SINDA Model Network) The SINDA model forced many assumptions to be made concerning certain values that were required to correctly model the composite material to be modeled. The conductivity was assumed to be 2.5, obtained from the actual test. The specific heat used was 962.964. The dimensions of the piece modeled was 0.0485m x 0.0495m x 0.0025m, with a density of 1370 kg/cubic meters. The SINDA model consisted of a total of 15 nodes. Two of these 15 nodes were boundary nodes, one being the heat sink set to be maintained at 50°F and to transfer the heat over a conductor with a G value equal to (0.35*area)/(height of composite/4). This value was an estimation of the thermal transference of the thermal grease used in the actual test set-up. The other boundary node was set to the air temperature obtained by the thermocouple gathering air temperature so that a real-life experiment could be accurately portrayed in SINDA/FLUINT. The conductance from this node to the modeled composite was set equal to 85*area (or 90*area if attempting to model the closest platform setting), which was an estimation as well of the transference of heat from the air to the material. The other 13 nodes consisted of 9 diffusion nodes (each having specific heat values, and being modeled as an actual piece of the composite), and 4 arithmetic nodes (representing the thermocouples, these only read in temperature, and do not affect the transference of heat through the material. (See Diagram 3: SINDA Model Representation)

The results of the SINDA/FLUINT model created were very consistent with those obtained from the actual testing runs made with the heat gun. The only serious deviation from this was the top surface temperature, which SINDA/FLUINT calculated to be much lower than that actually obtained, and at a consistent delta T as the other points in the material. This coupled with the variation of Top Surface temperatures between tests lends to the fact that the SINDA/FLUINT model is more accurate then the actual measured temperatures. When checking the SINDA/FLUINT model, a calculated Q value was made, using the results of the model run and the assumed values, in order to compare between the SINDA/FLUINT model results and the results obtained from the actual test runs.

The 30% Micro PCM SINDA/FLUINT model differed greatly from the 0% Micro PCM model. Similar assumptions for certain values were made for the 30% model as the 0% model. The density and specific heat were altered to compensate for the addition of the Micro PCM material. Along with this change, the C_p needed to vary as the temperature changed. Using interpolation, SINDA was able to take 5 points, describing the change of C_p, and use those to determine the approximate C_p for any given temperature.

After running the experiments with the composite material, we created a new SINDA/FLUINT model in order to model a Micro PCM mixture in a coating over a composite material. Here we used data already gathered from a previous set of test runs in order to complete our model. Through the modeling of the 0% PCM mixture and the 60% PCM mixture,

and cross-comparing our data with that of the actual run of experiments, we discovered that SINDA was not accurately modeling the PCM during phase change, hence giving us completely unreliable results.

For the SINDA/FLUINT model created in order to model a PCM coating on top of a carbon composite for protection purposes, a variety of methods were tried in order to achieve accurate results. First, a baseline mixture was determined. Equations were then inputted in order to dynamically calculate the Cp, k, and density of the mixture based upon the differing percentages of PCM material to be mixed and tested. Once this was completed, the variables needed to be adjusted in order to obtain results consistent with the experimental data received 0.6 points along with the linear interpolation, creating a box graph, however, this met with similar results as the previous method. The next attempt was to use a similar method, however to apply negative heat to the nodes representing the coating mix. This was no more successful then the previous two attempts. The dimensions of the plate was 1 inch x 1 inch. The thickness of the coating varied from 0.01 to 0.1 inches thick. The convection coefficient varied in order to simulate the differing distances from the heat gun in the experiment (30.6, 27.7, and 22.0 Btu/hr-ft^2-°F). The k value used for the polyurethane was 0.31. Unfortunately the first method tried in order to model the PCM effect upon the conductivity of the coating, and the temperature of the sample was unsuccessful. Linear interpolation was used along with 5 points, creating a triangular graph, to adjust the C_p according to the temperature of the coating, thereby simulating the increased capacitance of the PCM when they melt at a certain temperature. The next approach to this problem was to use 6 points along with the linear interpolation, creating a box graph, however, this met with similar results as the previous method. The next attempt was to use a similar method, however to apply negative heat to the nodes representing the coating mix. This was no more successful then the previous two attempts.

This testing set up a baseline for which testing of composite materials with the Micro PCM Material blended inside may be compared against. It also established a Thermal model that will allow speculation upon the results of these experiments and another source of data not requiring an actual test to be run.

PREDICTION OF PARATROOP/WAKE VORTEX ENCOUNTERS DURING FORMATION AIRDROP

Matthew L. Blanton

Wayne High School
5400 Chambersburg Rd.
Huber Hts., OH 45424

Final Report for:
High School Apprentice Program
Wright Laboratory

Sponsored by:
Air Force Office of Scientific Research
Bolling AFB, DC

and

Wright Laboratory

August 1996

PREDICTION OF PARATROOP/WAKE VORTEX ENCOUNTERS DURING FORMATION AIRDROP

Matthew L. Blanton

Abstract

A modeling technique is described for predicting the relative locations of paratroops and trailing vortices for a formation of transport aircraft. The wake behind each vehicle is treated as a fully rolled up vortex pair with empirical relations used for the vortex decay. The technique is applied to two and six aircraft formations, with the objective being to maximize the distance between the vortices and paratroops, subject to numerous operational constraints. Nineteen sorties were flown using the formations developed. A total of 286 mannequins and 299 live troops were dropped with no paratroop/wake vortex interactions observed.

PREDICTION OF PARATROOP/WAKE VORTEX ENCOUNTERS DURING FORMATION AIRDROP

Matthew L. Blanton

Introduction

One of the more interesting wake vortex interaction problems is that of paratroops exiting from trail aircraft during multi-ship airdrops. The operational goal of putting as many troops on as compact a drop zone as possible in minimum time requires multiple transport aircraft in a low altitude tight formation. With an adverse crosswind, airdrops from these types of formations can lead to situations where a paratroop is likely to fall through a vortex generated from a ship upstream. The velocities generated by wake vortices can alter the descent path of a paratroop and affect the parachute in several ways, including complete collapse of a fully developed canopy. If an encounter occurs close to the ground, there may be insufficient time to recover and serious or fatal injuries can result.

Formation airdrops are not new. They were conducted extensively during World War II operations and have been done sporadically since, with the more recent experience in a training environment. However, span loading of military transports has increased significantly since World War II and the current generation of vehicles generate larger, more powerful vortices than their predecessors. In June 1995, a paratroop/vortex encounter occurred during operational testing of the C-17. Fortunately, there were no injuries. However, the incident prompted a re-examination of formation airdrop geometries and several new formations were developed and tested using both mannequins and live troops.

This paper will discuss the wake vortex modeling technique that was developed to support these tests and that is currently being used as an aid in defining suitable formations for multi-ship airdrop. The trailing wake behind each vehicle is modeled as a fully rolled up vortex pair. A time stepping analysis is used to track the vortices which includes interactions between vortices from other ships. Empirical expressions for the vortex decay and core radius are used. A simplified paratroop trajectory path is superimposed on the vortex paths, and predicted "vortex miss" distances are generated.

Nomenclature

A Wing aspect ratio

AGL Above ground level

b_{eff} Effective span of trailing vortices

b Wing span

C_L Lift coefficient

r_c Vortex core radius

W Vehicle weight

V_∞ Free-stream velocity

V_c Crosswind velocity

V_D Vortex descent velocity

V_θ Radial velocity

ρ Density

ν Kinematic viscosity

Γ Vortex circulation strength

Λ Wing quarter chord sweep angle

Wake Vortex Model

Paratroop/wake vortex interactions can be subdivided into two categories. In a short formation, with closely spaced ships (~ 1000 ft), the vortices are essentially full strength and their position can be estimated with some accuracy. From the paratroop perspective, the key question is "Where is the vortex ?". The second category is a long formation, with ships widely spaced (~ 10,000 ft). Here, it is not possible to determine the location of the vortices with any confidence, and vortex decay has started. The key question from the paratroop becomes "What is left of the vortex ?". To fully analyze these cases, a vortex position algorithm must be developed in conjunction with a reasonable decay model.

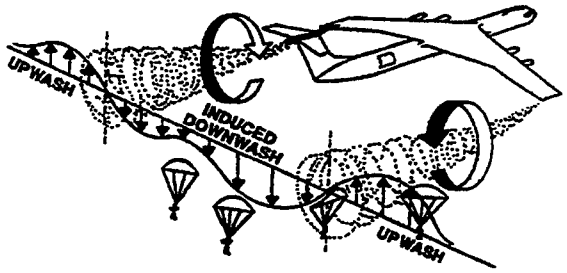

FIGURE 1 WAKE VORTEX FLOWFIELD

The flow behind a given vehicle is assumed to be represented by a pair of fully rolled up vortices (fig. 1). There is no modeling of the wake roll-up process, which typically takes several wings spans in distance. Spacing between aircraft for airdrop (>1000 ft) is beyond the point of wake rollup, so this assumption should be valid. As the trailing wake rolls-up, the vortices move inboard from the tip and are eventually separated by an effective span b_{eff}. For an elliptic loading this span is $(\pi/4)b$. The vortex strength is given by:

$$\Gamma_o = \frac{W}{\rho V_\infty b_{eff}} \qquad (1)$$

$$\Gamma_o = \frac{4W}{\pi \rho V_\infty b} \qquad \text{(elliptic load)}$$

Airdrop operations are conducted in essentially the approach condition, low speed with flaps down. Trailing edge flap deflections introduce additional vortices which interact with the primary tip vortices and promote vortex decay. This is accounted for using an empirical modification developed by Kurylowich [1]. The condition for decay and the resultant circulation strength are given by:

$$\Gamma = \Gamma_o \qquad t < 9.58\frac{bA}{V_\infty C_L}$$

$$\Gamma = 9.58\Gamma_o \frac{bA}{tV_\infty C_L} \qquad t < 9.58\frac{bA}{V_\infty C_L} \qquad (2)$$

$$= \frac{19.16 b^2}{\pi t} \qquad \text{(elliptic load)}$$

The radial velocity induced by the vortex is also taken from Kurylowich [1]:

$$V_\theta = \frac{\Gamma}{2\pi r}\left[1 - e^{-1.26(r/rc)^2}\right] \qquad (3)$$

with the vortex core radius given by:

$$r_c = 36.2\sqrt{\nu t / \cos^2\Lambda} \approx 0.5\sqrt{t} \qquad (4)$$

These equations can be combined to provide a relationship for the maximum vortex induced radial velocity as a function of time:

$$V_{\theta,\max} = \frac{0.190 b^2 \cos\Lambda}{\pi^2\sqrt{\nu}} t^{-1.5} \qquad (5)$$

An alternate vortex decay model, developed from DC-9, 707 and C-5 data, is given by Jenkins and Meyer [2]:

$$V_{\theta,\max} = 3.69\Gamma_o t^{-1.381} \qquad (6)$$

The time dependency of the models is similar with decaying exponents of -1.5 vs -1.381.

On a single aircraft, the velocity induced on one tip vortex due to the other is:

$$V_D = \frac{-\Gamma}{2\pi b_{eff}} \qquad (7)$$

$$= \frac{-8W}{\pi^3 \rho V_\infty b^2} \qquad \text{(elliptic load)}$$

This means that at a fixed vertical plane in space, the pair of trailing vortices moves downwards at a constant velocity. One means of addressing the formation flight problem is to simply track the vortices generated by each aircraft using eqs.(2,7) as a function of time. This approach suffers from one drawback, however. The influence of the vortices from one vehicle to another is not taken into account. If the vehicles are closely spaced, this influence can be greater than the influence of the vortices from a given vehicle on each other.

An efficient way to include the effects of all vortex-vortex interference in the analysis is to develop a time-stepping solution. This means solving for the trailing vortex strengths and positions as a function of time. These solutions are solved in the y-z plane (the vertical plane perpendicular to the flight path). For the present analysis, a coordinate system was established with the origin twenty ft aft of the wing trailing edge of the first aircraft. The time step is defined as a fraction of the longitudinal distance between the aircraft divided by the forward velocity:

$$\Delta t = \Delta x / V_\infty \qquad (8)$$

At a given plane, the induced velocity at each vortex core is calculated by summing the velocity components due to all other vortices:

$$v_k = \sum_{j=1}^{nv} \Gamma_j \frac{z_k - z_j}{2\pi r^2}\left[1 - e^{-1.26(r/rc)^2}\right] \qquad (9)$$

$$w_k = \sum_{j=1}^{nv} \Gamma_j \frac{y_k - y_j}{2\pi r^2}\left[1 - e^{-1.26(r/rc)^2}\right] \qquad (10)$$

where:

$$r = \sqrt{(y_k - y_j)^2 + (z_k - z_j)^2} \qquad (11)$$

At a given solution plane, vortices will exist is various states of decay, depending on how long ago they were generated. No attempt is made to account for vortex merging or destruction. After the velocity field is completely generated for a given solution plane, i.e. eqs.(9,10) have been applied to all vortices, the vortices are moved into place for the next time step. This involves shifting them by the following relations:

$$y_i = y_i + v_i \Delta t + V_C \Delta t \qquad (12)$$

$$z_i = z_i + w_i \Delta t \qquad (13)$$

The crosswind is assumed to be constant for the entire formation of aircraft. Uniform updrafts or downdrafts could be added in a similar manner.

Ground effect is not included in the current model, although it could be added in a straight-forward manner using image vortices. Ground effect does not begin to influence vortex trajectories until they descend to less than one wing span above the ground. Of the cases studied to date, the lowest airdrop altitude was 800 ft AGL. No vortices were predicted to descend more than 600 ft, so ground effect does not alter the results.

Several step sizes were studied to investigate the convergence properties of the model. A 200 ft step was chosen. Vortex cores were kept a minimum distance of twice the core radius of the oldest vortex from one another. This prevents excessive vortex movement in the y-z plane due to unrealistic induced velocities.

Paratroop Model

A very simple model was used for the drop path of the paratroops. They were assumed to drop at a constant rate of 20 ft/sec. Once the parachute is fully deployed, the lateral motion is with the crosswind. This was modeled by using zero

drift for the first 400 ft following exit from the vehicle, and 100% drift with crosswind thereafter. Computed paths of paratroops were obtained using ballistic models and did not deviate from the 20 ft/sec path by more than 10 ft for the first five seconds after drop.

Although not substantiated, prior studies [3,4] have indicated that vortices with radial velocities in excess of 30 ft/sec are sufficient to pose a hazard to paratroops while airborne. Near the ground and following impact, 22 ft/sec is considered sufficient to cause excessive dragging of troops along the ground. An effort to investigate vortex/jumper interactions to develop more precise guidelines is being conducted. Since the maximum induced velocity occurs at the edge of the vortex core, the expression used for the core radius becomes critical for this calculation. A more meaningful guideline may be the diameter or area of the region in space with velocity greater than 30 ft/sec. For this calculation, the vortex strength is the critical parameter; this should be more accurately known than the vortex core radius. In any event, for the short formations studied, the radial velocities were far in excess of 30 ft/sec, so their location relative to the paratroops is the critical parameter.

A series of flight tests [3,4] were conducted in 1988 using the C-130, C-141, and C-5 where mannequins and various types of equipment were intentionally dropped into the wake of an upstream aircraft. Only results from the simulated personnel drops will be discussed here. The lead aircraft flew approximately 1500 ft forward and 200 ft below the trail aircraft, out of which the parachutes were dropped. A laser reflector was attached to the parachute which allowed measurement of the descent rate during the drop. The test specimen was a 250 lb mannequin using a T-10B (28 ft diameter) parachute. The test results are summarized in Table 1 below.

TABLE 1 - VORTEX ENCOUNTERS

SIMULATED PERSONNEL DROPS

	C-130	C-141	C-5
Total drops	24	21	35
Drops with data	19	21	35
No vortex interaction	2	6	0
Vortex interactions	17	15	35
Pre-stabilization	6	0	1
Chute between cores	3	10	15
Descent speed, ft/sec	31-34	35-44	36-53
Chute outside cores	1	3	5
Descent speed, ft/sec	7	5-12	1-10
Core encounters	7	2	14

A pre-stabilization interaction means the parachute was not fully opened when it encountered the vortex. The majority of these occurred with the C-130, which has a vortex system which descends more slowly than the other aircraft.

The "standard" descent rate for the mannequin/ parachute combination used was 18.3 ft/sec. A landing with greater than 22 ft/sec rate is considered a "hard landing". The parachute descent rate effectively doubles when it falls through the strong downwash region between the vortices, while the descent nearly stops when it falls through the upwash region outside the vortex core. As the size of the vehicles generating the vortices increases, the relative number of vortex interactions increases as well as the magnitude of the change in descent rate. The descent rates did not return to normal until 5-10 seconds after the encounter. This means that almost any encounter within 400 ft of the ground is potentially hazardous. In all cases where the parachute encountered the core directly, the chute completely collapsed.

Assessment Using Tower Data

C-141 and C-5 data obtained by the National Oceanic and Atmospheric Administration [5] were used to assess the adequacy of the vortex model in an effort to gain confidence in its application to the C-17. Like the C-17, the C-141 and C-5 are high wing, four engine, military transports with a T-tail. The distinguishing features of the C-17 are a set of winglets and a powered lift system (externally blown flaps) for STOL capability. Otherwise, the basic wing planform characteristics are similar:

TABLE 2 - WING PLANFORM COMPARISON

	C-141	C-17	C-5
Wing area (ft2)	3228	3800	6200
Wing span (ft)	159.9	165	222.7
Aspect ratio	7.93	7.16	7.75
Taper ratio	0.37	0.25	0.37
Sweepback (c/4)	25.0	25.0	25.0
Flap chord ratio	0.25	0.30	0.25
Weight (lb)	237500	400000	450000
Span loading (lb/ft)	1485	2424	2019

Weights given in Table 2 were supplied by Air Mobility Command as representative airdrop gross weights. The C-5 is shown for reference only, it is not currently a formation airdrop platform. The C-47 transport, widely used for formation airdrop during World War II, had a span loading of about 270 lb/ft. Span loading, and the attendant increase in vortex strength and size, has almost increased by a factor of ten since that era.

The NOAA Tower, located in Idaho Falls, Idaho, is 200 ft tall with the base 4900 ft above sea level. The tower is four by six ft in cross section and is supported by wires at different heights. It sits in the middle of a flat plain which extends several miles in all directions, which minimizes distortion of vortices due to adverse terrain. Even so, most of the vortices

measured by the tower are influenced by the ground in some manner. How representative the data are of vortices generated at altitude is unknown.

Fifty hot film anemometers were located at intervals of every 3 ft from the top to a height of 101 ft, with 6 ft spacing below this level. Data were obtained at 0.01 sec intervals and at the instant of the occurrence of the maximum recorded velocity, a "snapshot" was taken of the speeds at all heights along the tower. Vortex age was calculated from the aircraft offset distance from the tower, the aircraft track, and the ambient wind speed/direction. To the extent possible, aircraft tracks were perpendicular to the ambient wind. Fifty two C-141 and sixty C-5 passes were made with 80 and 101 vortices measured respectively. The bulk of the unmeasured vortices passed over the tower (25) or dissipated (10).

Weight, speed, and flap setting varied for each vehicle during the tower tests. The calculated circulation strength (eq. 1) variation for the C-141 flights ranged from 3000 to 4000 ft^2/sec, while the C-5 values ranged from 4000 ft^2/sec to 8000 ft^2/sec.

Also shown are calculations using the two vortex models (eqs. 5,6) previously discussed. Circulation strengths of 3500 ft^2/sec for the C-141 and 6500 ft^2/sec for the C-5 were used for the predictions. Several vortices older than 2 minutes were measured for the C-141. These were observed in relatively calm winds. Stronger winds were present during the C-5 tests which more rapidly moved the vortices past the tower, so no long lived C-5 vortices were observed. For the purposes of this study, the desired vortex model should not pass through the center of the data points but rather define an upper bound. The Kurylowich model (eq. 5) satisfies this objective better than the Lockheed model (eq. 6) for both the C-141 and C-5. Both models predict much larger velocities than observed for vortices less than 30 seconds of age.

Results

On June 9, 1995, two paratroops from the trail ship of a two ship C-17 formation encountered the starboard vortex from the lead ship during descent. One jumper suffered a completely collapsed chute which never fully reinflated and resulted in a hard landing (no serious injuries). The chute of the other jumper did not collapse but rocked back and forth briefly, with no deleterious results. This wake vortex encounter was simulated using the model discussed above.

While it would always be desirable to have the trail ship in a two ship formation upwind of the lead ship, this cannot always be planned. The actual winds over the drop zone are not known until it has been reached. In the drops conducted, the trail ship was offset to starboard of the lead ship if the drift was within a given tolerance (3 degrees) while approach-ing the drop zone. With a greater drift in the adverse direction, the trail ship would move to the upwind position prior to reaching the drop zone.

Candidate two ship formations were studied with increased lateral separation and variations in longitudinal separation. Drop zone width limits the lateral separation to 500 ft, while the longitudinal separation is limited by the formation flying technique. The lead ship flies to the ground track of the drop zone while the trail ship maintains its position by visual contact with the lead. This is similar to the flying technique used by precision flight demonstration teams such as the USAF Thunderbirds. The smallest longitudinal separation considered attainable from this perspective was 1500 ft. This formation

was analyzed and the results are shown in figs. 6 and 7. The maximum adverse crosswind (7 Kts) was used for this case. While the side view shows a crossing of the vortex by paratroops 400 ft after the trail ship the formation, the top view shows a vortex miss distance of over 300 ft. This distance increases to 450 ft as the crosswind reduces to zero. These miss distances were considered safe, so a series of 12 two-ship flights dropping a total of 231 mannequins over a period of two weeks was conducted to assess the new formation. A wide range of wind conditions were present during this test series. These were completed without incident, so a live drop was conducted on June 22. A total of 97 troops were dropped with no vortex encounters.

The two ship drops were build-up tests towards a six ship demonstration drop. This demonstration represented a "slice" of a full brigade drop. The requirements of the six ship drop were:

a) Drop 60 tons of heavy equipment (four ship loads) and 204 paratroops (two ship loads) onto a 1000x15000 ft drop zone in 5 minutes.

b) Equipment drops from 1300-1500 ft AGL.

c) Personnel drops from 800-1300 ft AGL.

d) Equipment must land first.

e) No paratroop vortex encounters.

Requirement (d) places the ships with paratroops downstream of the ships carrying equipment. The two ships with paratroops were in the formation previously developed, where the vortex encounter problem was effectively solved. The new concern was avoidance of vortices from the ships carrying equipment.

Two strategies were used for the six ship formation to avoid potential vortex encounters. First, the ships carrying personnel were placed as far behind the ships carrying equipment as possible. This would give the vortices from the lead ships the maximum time to decay. Second, the ships carrying personnel were flown at the lowest altitude (800 ft AGL) while the ships carrying equipment were flown at the highest altitude (1500 ft AGL). The goal here was to have the vortices from the ships carrying equipment pass over the ships carrying personnel. The specifics behind these two strategies will be discussed in turn.

The drop zone used at Ft Bragg is a "1 minute" drop zone meaning that there is one minute for the troops or equipment to exit the aircraft once the drop zone has been reached. The four ships carrying heavy equipment were in two-ship elements, with 4000 ft between elements and 2000 ft between ships in an element. The ships carrying personnel were spaced 1500 ft apart. Using these spacings and the assumed drop rates (20 ft/sec for personnel, 28 ft/sec for equipment), an idealized time line for the drop was constructed. The maximum gap between the last ship carrying equipment and the first carrying personnel which meets the 5 minute drop requirement within this time line is about 2.5 minutes. The predicted maximum radial velocity as a function of time from the vortices generated by the ships carrying equipment can be calculated from eq.(5). No velocities greater than 30 ft/sec are predicted after 2 minutes time. The time line is shown below.

TABLE 3 - TIME LINE FOR SIX SHIP DROP

Time	Event
0:00	First ship (equipment) reaches drop zone
0:08	Second ship reaches drop zone
0:24	Third ship reaches drop zone
0:32	Fourth ship reaches drop zone
0:54	First piece of equipment reaches ground
1:26	Last piece of equipment reaches ground
3:02	Fifth ship (personnel) reaches drop zone
3:09	Sixth ship reaches drop zone
3:42	First troop (fifth ship) reaches ground
4:09	Last troop exits from sixth ship
4:49	Last troop (sixth ship) reaches ground

The uncertainty regarding the 30 ft/sec criterion and the applicability of the vortex decay model to the C-17 resulted in an additional measure being taken. This was to attempt to avoid the vortices completely by having the ships carrying personnel fly under them. The vortex tracking model was applied to the six ship configuration with the results shown in fig. 8.

For this case, a zero crosswind represents the worst case. A steady crosswind in either direction would blow the vortices away from the trail ships. The decay and mutual interactions between the vortices results in a complicated vortex pattern. A 200 ft margin of safety between the vortices from the lead ships and the trail ships is indicated. The uncertainties in this result are extremely large. A steady 1 Kt disturbance in any direction would shift the vortices by 300 ft by the time they reached the trail ships. The weather conditions at drop time also favored the lead ships high-trail ships low approach. The drop was scheduled for late morning on a hot humid day. It was hoped that thermals present under these conditions would assist in arresting the downward descent of the vortices from the lead ships over the 2.5 minute interval.

Two practice drops using the formation shown in fig. 8 were flown with a total of 48 mannequins dropped, with no observed vortex encounters. The flight demonstration program was concluded on June 27, 1995 with the successful six ship demonstration.

A summary of the flight test results using the formations discussed in this paper is given below. A total of 585 mannequins and personnel were dropped using the newly developed formations, with no vortex encounters.

TABLE 4

FLIGHT TEST SUMMARY - FT BRAGG TESTS

Formation	Ship No.	Passes	Total Drops	Vortex Encounters
2-ship				
Original	2	8 (M)	72	0
	2	1 (P)	102	2
Modified	2	12 (M)	238	0
	2	1 (P)	95	0
6-ship				
Modified	5	2 (M)	24	0
	5	1 (P)	102	0
	6	2 (M)	24	0
	6	1 (P)	102	0

NOTE: M: mannequin, P: live personnel

Conclusion

A wake vortex interaction problem of military significance is that of paratroops falling through the wake vortices of upstream aircraft in multi-ship airdrop formations. A wake vortex tracking model has been developed to aid in assessing candidate formation geometries. The problem is subdivided into "short" and "long" formation problems. For short formations, the vortices are strong and the primary concern is their location. For long formations, the position of the vortices is uncertain and the primary concern is their remaining strength. An empirical vortex decay model was used which compares favorably with C-141 and C-5 flight data.

The vortex tracking model was used to study multi-ship C-17 formations during operational testing. Over a dozen flight tests were conducted with both mannequins and live troops using formations developed with the model. No paratroop/wake vortex interactions were observed.

References

1. Kurylowich, G., "A Method for Assessing the Impact of Wake Vortices on USAF Operations," AFFDL-TR-79-3060, July 1979.

2. Jenkins, M.W.M., and Meyer, R.T., "Vortical Wake Hazard Advisory," AFFDL-TR-76-146, February 1977.

3. Johnson, Maj. D.J., "Operational Test and Evaluation of the Effects of C-130/C-141B Wake Vortices on the Drop Zone Environment," MAC Project 15-105-86, September 1988.

4. Johnson, Maj. D.J., and Reynolds, Capt J.K., "Operational Test and Evaluation of the Effects of C-5 Wake Vortices on the Drop Zone Environment," MAC Project 15-105-86, December 1988.

5. Clawson, K.L., et al,"Measurement of Wingtip Vortex Characteristics From C-130, C-141 and C-5A/B Aircraft," MAC Project 15-105-86, May 1988.

THE STUDY OF A BASIC LDV SYSTEM

Brian E. Brumfield

&

Matthew R. Rabe

Tippecanoe High School
555 North Hyatt Street
Tipp City, OH 45371

Carroll High School
4524 Linden Avenue
Dayton, OH 45424

Final Report for:
High School Apprenticeship Program
Wright Labratories/ POPT

Sponsered by:
Air Force Office of Scientific Research
Bolling Air Force Base, DC
and
Wright Labratories/ POPT

August 1996

THE STUDY OF A BASIC LDV SYSTEM

Brian E. Brumfield
Tippecanoe High School
&
Matt R. Rabe
Carroll High School

Abstract

The principle setup of an LDV system was researched and setup. LDV is a technique in which particles that are taggers in a fluid flow are illuminated by focused laser beams and become scattered sources of light. This causes a change in frequency (Doppler effect) in the scattered light due to the motion of the particles which the photomultiplier tube will receive and allows the particle velocity to be determined. The minimum requirements for such a system are as follows: A light source such as a laser, transmitting optics, receiving optics, photodetector, signal processor, and a data processor.

THE STUDY OF A BASIC LDV SYSTEM

Brian E. Brumfield
&
Matt R. Rabe

Introduction

LDV or laser Doppler velocimetry systems when properly setup can obtain data in many flow situations that cannot be achieved by other techniques (Fingerson 3/12, 83). There are more following pros such as having no probe in the flow, no velocity calibrations, velocity components are measured precisely, a small measuring volume, high frequency response, and a large dynamic range (Fingerson 3/12, 83). The types of flow environments in which an LDV setup can be used to gather data are liquid, transonic, separated, non-isothermal, high temperature, high turbulence intensity, and a very low flow velocity (Fingerson 3/12, 83). However, while working well in a straight flow situation, the particles that come at an angle or from side to side are measured inaccurately by an LDV system. This is because the particle is traversing the measuring volume from an angle. This makes a difference in the way it scatters light, and since the LDV works with the Doppler shift principle this will give you inaccurate readings on the particle's velocity. This problem can and is corrected by shifting one of the beams frequency while leaving the other unshifted.

Methodology

The minimum requirements for a dual beam system are as follows: The laser or light source, transmitting optics, receiving optics, photodetector, signal processor, and a data processor. The beam or beams must be realigned or altered in some way during several steps in the setup. This is to ensure a strong beam to provide a good signal when taking data.

The laser which was used was an Argon-Ion. This laser emits in the wavelengths of 476.5 violet, 488nm blue, and 514.5nm green. The laser produces it's light by light amplification from stimulated emission of radiation. This is achieved by placing electrodes in rings or adjacent to the disposed wall adjacent to the two ends of the plasma tube. This arrangement is required so electric discharge may occur between the electrodes, an arc discharge, while the column of light eventually produced is free to oscillate between the mirrors. Light is composed of quanta called photons and the photons are produced in the plasma tube when an arc discharge between the electrodes excite the electrons, in this case the electrons of argon atoms. These excited electrons raise

to a higher energy level, but cannot remain there indefinitely so they return to there ground state and radiate a photon with a specific frequency and wavelength which would be the specific signature of that atom. This photon will then strike another electron and raise it to a higher energy level and then the electron will go back to ground level and release a photon again of the exact same signature. When you add two mirrors to each end of the plasma tube it becomes a optical resonator chamber. The photons continue on their course hitting electrons and being reemitted while more are put into the system via the discharging electrodes. The photons hit the mirror and oscillate back and forth and continue this amplifying effect. If both mirrors were one-hundred percent reflective the amplifying effect would be so intense that the thermal energy would rupture the plasma tube. However the back mirror is one-hundred percent reflective while the mirror closest to the supposed exit of the beam is about forty to fifty percent transmissive. This allows some of the photons out to give you a coherent concentrated beam, due to the optical resonator which forces the atoms of the material to radiate in phase, of extreme directionality which can be further controlled by the collimator.

Coherence is the idea that all your electrons are radiating in phase as a whole, they are not oscillating independently of one another. While a laser produces coherent light a common light bulb does not. The light bulb excites atoms by providing a discharge of energy through a tungsten filament but the emission process is not controlled so they oscillate independent of one another. A laser maintains a constant phase relation over the oscillating electrons by stimulating their emission with a wave of the frequency to be radiated (Hallmark & Horn 94, 87). Spatial coherence is an instantaneous correlation of phase form point to point in space (Hallmark & Horn 94, 87). Temporal coherence is a consistent correlation in-phase at two neighboring points over a length of time (Hallmark & Horn 94, 87).

After the beam collimator a TSI colorburst unit was used. The colorburst unit by TSI actually has a beam splitter, then a shifter, and a color separator all in one which decreased the time required to setup the system. Normally for a dual beam system, using an argon-ion laser, you could use a conventional color separator and pick off the wavelength you required then split that beam into two separate beams. You could then shift the frequency of either one.

The colorburst unit has six openings on top with three on each side. One lane has all the unshifted colors from the argon-ion lasers beam and their shifted counterparts are on the other lane. Only two were to be used in the setup, the green shifted and unshifted light.

Fiber couplers were then mounted on the two ports. Each coupler had transverse motion knobs at the base, tilt knobs near the top, and a focusing module at the top. A fiber optic wire was connected to each that lead to another TSI component with a built in focusing lense to cross the beams to create the measuring volume.

Fiber optic cables, wires, etc. lead the beam on a confined path within the cable regardless of whither it is straight or bent. Inside a fiber optic cable there are a large number of transparent glass and plastic fibers, these gives the beam a medium to travel through. The beam is confined because the core of the cable has a higher refraction index that is greater than that of the cladding, the outer covering of the cable, therefore containing the light regardless of bends or curves in the wire. However it is not wise to bend them to such a great extent as to damage the fibers inside.

The fiber optic wires connected to the fiber couplers provided an exposed area to allow the laser light in. This requires alignment and a feedback mechanism to ensure a strong beam after it goes through the fiber optic cables. So a photodetector to read the power of each of the beams after the lense was used to help align the beams properly instead of by eye. First aligning it transversely, then the tilt, then focus provides the best order of aligning.

After the alignment and insurance of a fairly good beam intensity the TSI module connected to the end of the fiber optic cable was moved from the table it was mounted onto a table in an adjoining test cell pointing into the test section of a wind tunnel. The module was then position on the table to allow the beams to cross near the center of the inside of the test section, this is possible since the glass was transparent. On the other side of the window receiving optics were placed. Receiving optics take the two beams of scattered light and focuses them right onto the photomulitplier.

In an LDV system taggers are used in the fluid flow to scatter the light from the laser, therefore allowing the computer to derive the velocity of the tagged material. The devices that release taggers into the flow are commonly called seeders. The changing in the frequency of the scattered light due to the motion of these particles

when observed from a stationary position, the photomultiplier for instance, it allows the particle velocity to be determined. The computer processes the signal from the photomultiplier and can store moments, data, and derive mathematically the motion of the particle.

Results

No experiment was performed therefore no data was taken so no results can be posted.

Conclusion

The LDV system that was setup was a very basic, and easy to understand, dual beam laser anemometer, yet it could be used for many applications. LDV systems will continue to be used more widely because once they are setup additional or continuing data may be collected without much difficulty (Fingerson 4a, 66), and some techniques cannot gather the data required that an LDV can supply.

References

Hallmark, Clayton L., and Delton T. Horn. The Light Fantastic: Second Edition. Blue Ridge Summit, PA: Tab Books Inc., 1987.

Muncheryan, Hrand M., B. SC., E.E., M. SC. Principles & Practice of Laser Technology. Blue Ridge Summit, PA: Tab Books Inc., 1983.

Fingerson, Dr. Leroy M. "The Dual Beam Laser Velocimeter." Laser Velocimetry... Theory, Application & Techniques (1983): 3/12-4a

Stehling, Kurt R. Lasers and Their Applications. Cleveland, OH & New York, NY: The World Publishing Company, 1966.

A Study of Bending and Torsional Energies of Biphenyl

Jason Burris
Dayton Christian High School
Dayton, OH 45405

Final Report for
High School Apprentice Program
and
Wright Laboratory

Sponsored by:
Air force Office of Scientific Research
Bolling Air Force Base, DC

and

Wright Laboratory

September 1996

A STUDY OF THE BENDING AND TORSIONAL ENERGIES OF BIPHENYL

Jason M. Burris

Introduction

Biphenyl is an ideal model to understand deformations in oligomeric and polymeric materials containing polyphenylene units. Hence the rotation barrier and structure of biphenyl and its derivatives have received intense experimental and theoretical scrutiny. These results have been recently summarized by Tsuzuki and Tanabe [1]. The experimentally determined rotation barrier through the planar conformation is 1.4 kcal/mole[2-4], whereas the best theoretical value is 3.47 kcal/mole[1]. Though these seem close, the difference is somewhat disconcerting in view of the sophistication of the theory applied, namely *ab initio* MP4(SDQ)/6-31G*//RHF/6-31G* calculations. As part of our continued interest in aromatic polymers for high-performance and molecular electronic applications[5-7], we have investigated this issue and the problem of non-planar molecular deformations in biphenyl.

In previous work we reported that the inclusion of electron correlation has negligible impact on rotation barriers. For example, in N-phenyl benzthiazole the rotation barrier calculated at the RHF/6-31G* is 4.00, while addition of second order Moller-Plesset perturbation corrections for correlation give a value of 3.90 kcal/mole[6]. In biphenyl [1] these values are 3.34 kcal/mole (HF/6-31G*//HF/6-31G*) and 3.84 (MP2/6-31G*//HF/6-31G*). Not only is the effect of correlation larger in biphenyl, it increases the rotation barrier whereas correlation lowers the barrier in N-phenyl benznridezole. However, the planar geometry is the minium energy structure in N-Phenyl benzimidole, but it is the transition state in biphenyl.

What has not been explored is the impact of subtle geometrical changes. Generally, we have observed correlation increases C-H bond lengths, while it tends to even-out conjugated systems-lengthening double bonds while shortening single bonds. While such subtle changes are generally ignored when making comparisons with X-ray crystallographic results, they can have significant effects on electronic transition energies, in the range of 0.4 eV[8]. Our purpose in this portion of work was to obtain a correlated structure and rotation barrier to see if correlated structure refinements account for the

remaining discrepancies of the rotation barrier. In addition to correlation-structure effects, we have also investigated the importance of polarization in the C-H bonds in the correlated calculations.

A number of studies on the molecular dynamics of rigid-rod type polymers have now been reported. The overarching conclusion from these is that significant non-planar, distortions occur-contrary to the connotation implied in *rigid*-rod. The conventional wisdom has been that such polymers are exceedingly stiff, whereas the animation of molecular dynamics simulations clearly show substantial deviations from linearity in para-phenyl includes, for example. The underlying question is wether in the molecular dynamics simulations are realistic for such deformations or are such deformations artifacts of the parameterization schemes, Quantum chemical methods can be used to address this issue, and preliminary results [REF] have indicated such deformations are not particularly costly energetically. Herein we expand this work to consider, at an *ab intio* level, the rotation-bending potential energy surface of biphenyl.

Methodology

The Programs Gaussian 92 [12] and GAMESS [13] were used for the calculations reported herein. Guassian 92 was used in three modes to study the energy required to twist and bend biphenyl. The three modes were AM1, MP2 and Restricted Hartree Fock 6-31G*. A z-matrix was constructed with 3 imaginary points to find optimize geometry. First a bend was entered into the z-matrix and the energy calculated with optimized geometry. Next a torsion and bend together were entered into the z-matrix and the energy calculated with optimized geometry. Script files were used to keep one job from each torsion running at all times ie. a job with a torsion of 15 was running at the same time as a job with a torsion of 30 and so on. The first method started was an MP2 job at least one was kept continually running through out my experiment since they are so computer intensive and need a lot of time to finish. The next method started was AM1 which are the least computer intensive and take only a few minutes to complete, therefore many could be ran at the same time. After completing the full spectrum of AM1 jobs from a torsion of 0 and bend of 0 to a torsion of 90 and a bend of 10, Restricted Hartree Fock jobs were started. They take several hours each and are ***fairly computer intensive***. While running Restricted Hartree Fock jobs, the compilation of the AM1 results began. A scatter point graph and a surface graph, along with a data table were created to show the energies relative to the torsion and bend. The same graphs and tables

were then created with the Restricted Hartree Fock results too. The MP2/6-31G* and calculations require several cpu days on a state-of-the-art Silicon Graphics T-8000 based workstation.

Results

Structural parameters for biphenyl are shown in Figure 1 for the fully optimized (D2) symmetry, while parameters for the planar conformation are given in Figure 2. Torsional data are presented in Table 1, and Bending Energies are given in Table 2. Then torsion-bending potential energy surface calculated at the AM1 level of theory is shown in Figure 3, while the potential surface at the RHF/6-31G* level is shown in Figure 4.

Conclusion

We have shown that significant out of plane torsions in biphenyl are as energetically accessible as torsional rotations. This Supports the conclusions drawn from molecular dynamics simulations regarding the lack of rigidity in 'rigid-rod' polymers. Additionally, it suggests that rotations (racemizations for eventiomerically related conformers of biphenyl derivatives) are probable inhanced by substantial out of plane bending.

The work on the correlated-structre hypothesis is in inconcluseve. The cpu intensive nature of these caclulations did no allow their completion in the time allowed. Further work is in progress.

References

1). S. Tsuzuki and K. Tanabe, J. Phys. Chem., 95 (1991) 139

2). Almenningen, A.; Bastiansen, O.; Fernholt, L.; Cyvin, B. N.; Cyvin, S. J.; Samdal, S., J. Mol. Struct., 128 (1985) 59

3). Bastiansen, O.; Samdal, S., J. Mol. Struct., 128 (1985) 115

4). Carreira, L. A.; Towns, T. G., J. Mol. Struct., 41 (1977) 1

5). J. W. Connolly and D. S. Dudis, Mat. Res. Soc. Symp. Proc., 291 (1993) 591

6). S. Trohalaki and D. S. Dudis, Polymer., 36 (1995) 911

7). J. W. Connolly and D. S. Dudis, Polymer., 34 (1993) 1477

8). J. W. Connolly, D. S. Dudis and A. T. Yeates, Synth. Met., (in press).,

9). B. L. Farmer, D. S. Dudis and W. W. Adams, Polymer., 35 (1994) 3745

10). B. L. Farmer, B. R. Chapman, D. S. Dudis and W. W. Adams, Polymer., 34 (1993) 1588

11). S. Trohalaki and D. S. Dudis, Makromol. Chem., Macromol. Symp., 65 (1993) 163

12). *Gaussian* 92, Revision A, M. J. Frisch, G. W. Trucks, M. Head-Gordon, P. M. W. Gill, M. W. Wong, J. B. Foresman, B. G. Johnson, H. B. Schlegel, M. A. Robb, E. S. Replogle, R. Gomperts, J. L. Andres, K. Raghavachari, J. S. Binkley, C. Gonzalez, R. L. Martin, D. J. Fox, D. J. Defrees, J. Baker, J. J. P. Stewart, and J. A. Pople, Gaussian, Inc., Pittsburgh PA, 1992

13). M. W. Schmidt, K. K. Baldridge, J. A. Boatz, S. T. Elbert, M. S. Gordon, J. H. Jensen, S. Koseki, N. Matsunaga, K. A. Nguyen, S. J. Su, T. L. Windus, M. Dupuis, and J. A. Montgomery, J. Comput. Chem., 14 (1993) 1347

Table 1: Torsional Potential Energies of Biphenyl (D_2 Symmetry)

	MP2/6-31G*	RHF/6-31G*	AM1
0°	-460.245895	-460.2486263	0.0789031
44.52°	-460.251558		
90°		-460.2514957	0.0789374

Table 2:Bending Potential Energies of Biphenyl*

Tor 0° Bend:	Bending Potential RHF/6-31G*	AM1
0	-460.2486263	0.0789031
1	-460.2486144	0.0789101
2	-460.2485786	0.0789385
3	-460.2485191	0.0789857
4	-460.2484357	0.0790518
5	-460.2470309	0.0791367
6		0.0792407
7		0.0793635
8		0.0795052
9		0.0796659
10		0.0798456

* These start from a planar (D2h) geometry and maintain a zero torsion while the molecule is bent.

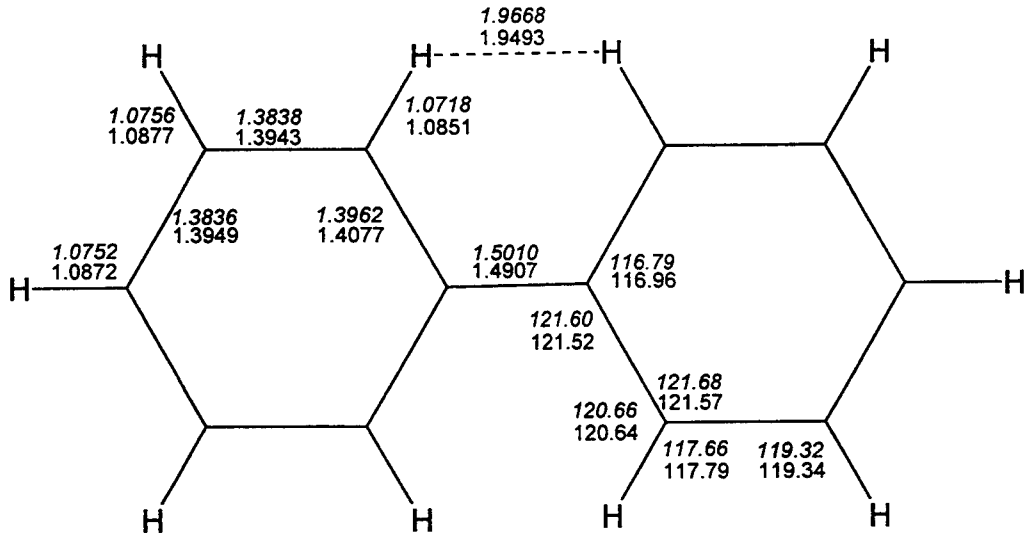

Figure 2: Correlated (MP2/6-31G*) and *Hartree-Fock (RHF/6-31G*, ref. 1)*

Planar (D_{2h}) Geometries of Biphenyl

LASER RADAR (LADAR) IMAGERY ANALYSIS TASK

Kimberly N. Cabral

Choctawhatchee High School
Fort Walton Beach FL 32548

Final Report for
High School Apprenticeship Program
Wright Laboratory

Sponsored by
Air Force Office of Scientific Research
Bolling Air Force Base FL

August 1996

LASER RADAR (LADAR) IMAGERY ANALYSIS TASK

Kimberly N. Cabral
Choctawhatchee High School

Abstract

Two tasks were undertaken in the analysis of ladar imagery. The first dealt with ladar data from a JAWG Captive Flight Test. Several flights containing Small Smart Bomb (SSB) and panel board targets were studied using a program which showed the data in terms of reflectance and range imagery. The objective was to determine the controls as well as the quantity and quality of useful data. It was observed that much of the data was of low quality, being that several of the images were dark and/or had excess noise.

The second task was materials data extraction. Material characteristics were analyzed so variations in reflectance data could be determined. The parameters considered were channel, field of view, discriminate function, and azimuth/elevation angle. Materials were viewed and extracted via a program designed for that specific function. Overall conclusions as to the reflectance results of the second task have yet to be drawn.

LASER RADAR (LADAR) IMAGERY ANALYSIS TASK

Kimberly N. Cabral

Discussion

Task I

In a five-day JAWG test, ladar data was collected on SSB targets and panel boards, then viewed. The SSB targets were the Duke Field Bunker, Duke Field Building, Duke Field Hangar, B-4 EW Radar Site, B-6 Firestation, B-6 Runway and B-12 SAM Site. The SSB targets were taken at three different altitudes: minimum (500 or 1000 feet), 1500 ft, and 2000 ft. The panel boards were taken in two scenarios, the first dealing with board separation and the second with tilt angles. Figures 1 and 2 illustrate the various target parameters that were used to log the data.

Altitudes	Headings
min	north
	south
	east
	southwest
1500	north
	south
	east
	southwest
2000	north
	south
	east
	southwest

Figure 1. SSB Target Parameters

Altitudes	Separation
min	6"
	12"
	max"
1500	6"
	12"
	max"

Altitudes	Tilt Angle
500	55
	70
	75
850	55
	70
	75
1640	55
	70
	75

Figure 2. Panel Board Scenarios 1 & 2.

Each target (all nine) viewed had two possible images: reflectance and range. The reflectance imagery was used to determine whether the target in question was fully visible, partially visible, or not visible at all. The range imagery better indicated the extent of noise. A JAWG Captive Flight Test data log was kept. The identity of the mission, flight number, frame number, target name, altitude, target visibility (full, partial, or not present), and observations were recorded. There were five categories of mission identification numbers, respective to the five days. There were 193 files in those flights, and 3152 frames (frames being the images themselves). The target visibility was significant, since those targets which were fully in view will be used for later analysis. The quality of that quantity was also significant. Those files with noise and darkness will not be accurate data for further investigation.

The images as a whole were not of high-quality. Not all passes contained the full targets in them. Also, several passes consisted of speckled regions denoting noise, darkness and/or poor detail. Such disturbance was most visible at the high and low extremes. Possible factors contributing to noise and darkness were incorrect gain settings

for the detectors in the sensor, insufficient power in the laser, and cloud cover. Figures 3 and 4 provide examples of reflectance imagery from the JAWG captive flight test.

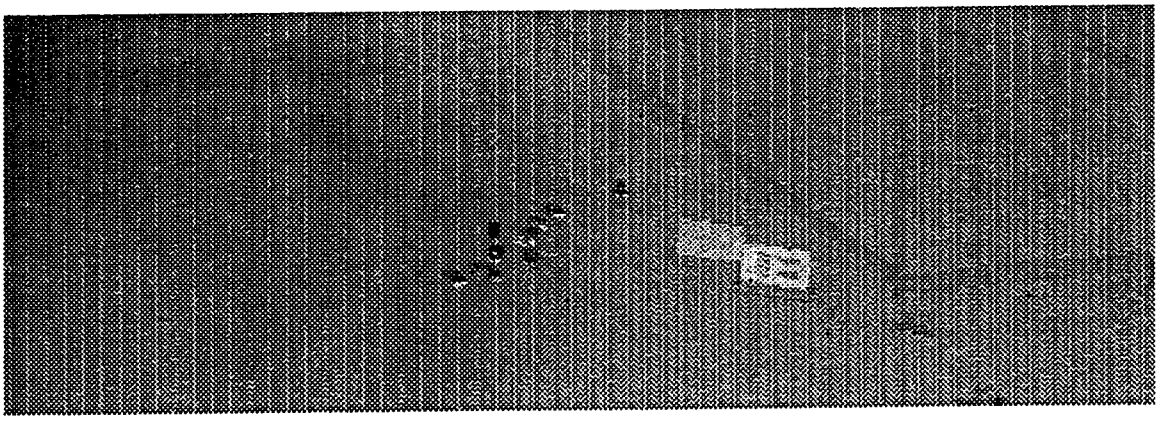

Figure 3. Panel Boards @ 1000 ft.

Figure 4. Navarre Bridge @ 1500 ft.

Task II

Two test panels and one control panel comprised the testing for materials data extraction. The panels contained various man-made and natural materials. The non-control panels were the two located on the outer extremes (see Figure 5).

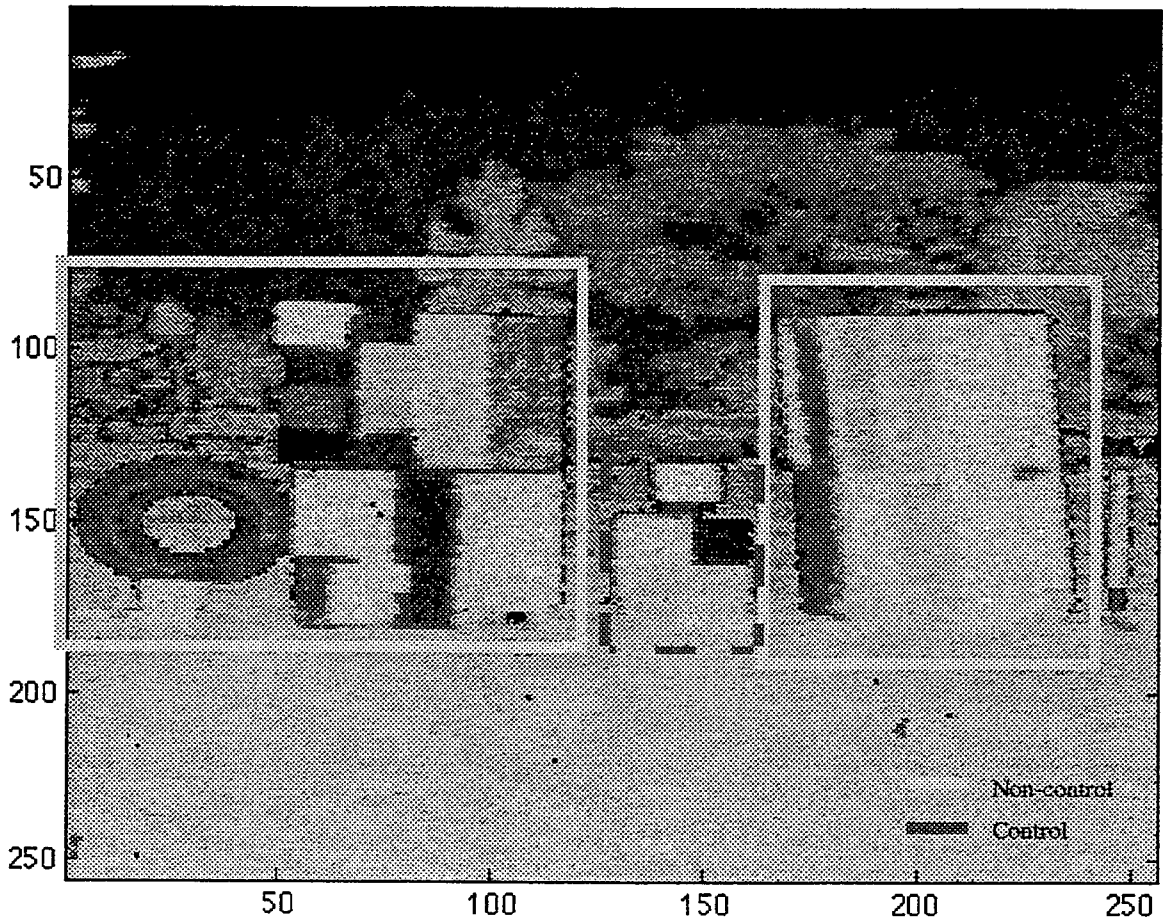

Figure 5. Example of Material Extraction Imagery

Although several control materials were used as non-control materials, there was significant difference in azimuth/elevation angles. The non-control materials were taken at several elevation angles: 0.0, 2.5, 5.0, 10.0, 20.0, 30.0, 45.0, 60.0, 70.0, 80.0, and 85.0 degrees. The control materials were consistently taken at 90 degrees. A list of the materials that were extracted are provided in Table 1.

Table 1. Control and Non-Control Materials (* indicates control materials).

Materials			
asphalt	auto glass	regular cardboard	black cardboard
concrete	delrina	gravel	paper
thick plastic	thin plastic	plexiglass	* regular plywood
* black plywood	polymer plastic	red sand	tan sand
* sand-blasted aluminum	* sand paper 1	sand paper 2	sidewall
sod	solar black	tread 1	tread 2
17038	36118	37038	f-16
f/g # 10	* c-3 target panel	* lab sphere panel	

The Extract program was used for the analysis process. Preliminary to the selection of a certain section of a panel board, one had to enter the appropriate parameters (corresponding to the records kept by those who carried out the experiment). The parameters were intensity channel 0 or 1, discriminate function linear or elliptical, 2 or 4 degree field of view, control or non-control material, specific azimuth/elevation angle, and specific material. Afterward, the region could be selected using the computer mouse. The statistics were then computed, based on average intensity and standard deviation. This enabled the creation of matrices containing this information. The determination of which matrix the information was stored in was as follows. If the particular material was in the control group, the information was carried to a *con* matrix, and if a non-control, then *mat*.

Using the binary system, the matrix storage locations are represented in terms of intensity channel (IC), discriminate function (DF), and field of view (FOV), where the IC is used to denote the most significant digit and FOV the least. Therefore, a storage location would be computed as follows:

$$\text{Location} = (IC \times 2^3) + (DF \times 2^2) + (FOV \times 2^1) \quad (1)$$

where Channel 0 = 0, Channel 1 = 1; linear discriminate = 0, elliptical = 1; 2 degree FOV = 0, 4 degree FOV = 1. Table 2 presents a hypothetical example to illustrate how the matrix locations are computed.

Table 2. Hypothetical Example

Program Parameters	Values
material	non-control
intensity channel	0
discriminate function	elliptical
field of view	4

By the material being non-control, its data goes into a *mat* matrix. Using Equation 1, the material information will be stored in *mat 3* since $011_2 = 3_{10}$.

After several statistics had been stored, one could view the data plots for the certain material with its specific parameters. The plot was the average intensity versus the azimuth/elevation angle, where the statistics were computed using the following parameters: material type, channel, discriminate function, and field of view. An example of a plot is shown in Figure 6.

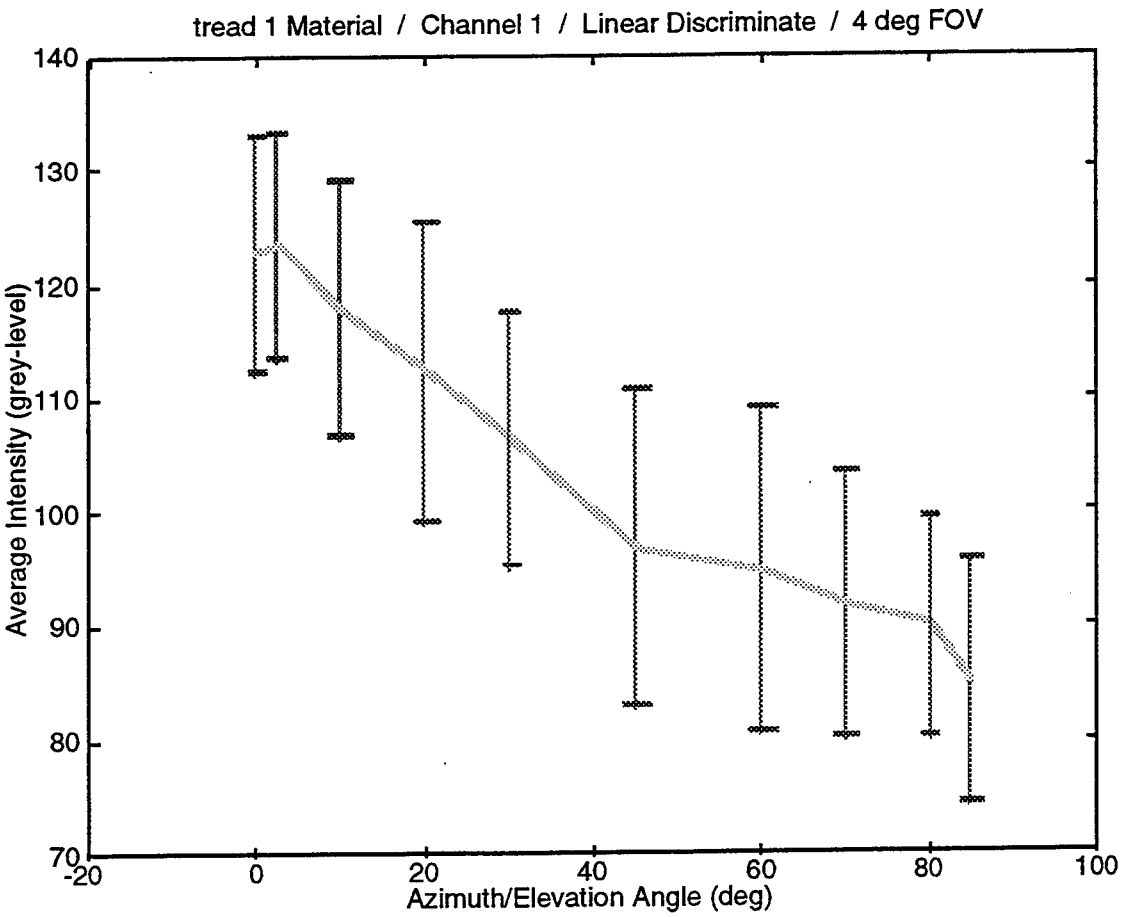

Figure 6. Plot of Material Data

Contributions

Task I- Evaluation of LADAR Data

I viewed all of the frames from five missions of the JAWG Captive Flight Test, recording observations in the flight test log. I then generated statistics for the quantity and quality of the data.

Task II- Extraction of Materials Data

I assisted in the design of Extract. Initially, I exercised the program to spot bugs. I also created a function to produce text for a program help window and a parameter information window. As I went through the program, I created a step-by-step methodology and also took note of aspects which might be confusing or that needed explanation. This information was then placed into the appropriate help windows. Additionally, I extracted regions of the data in order for various plots to be created.

Conclusions

As mentioned, finalized conclusions have not yet been drawn. Data from Task I was essentially of poor quality, and plots from Task II are presently in the process of being analyzed.

As for personal conclusions, I had the opportunity to learn a great deal this summer. For the first task, I became familiarized with the Khoros and SAOimage programs; in the second task, Matlab. Additionally, I was introduced to computer programming and other general computer knowledge. Overall, it was a worthwhile experience.

Acknowledgments

Karen Norris-Zachery

Don Harrison

Michael Deiler

Doug Ritchie

HSAP members

IPLers: especially Herline, Duane, Todd, Larry, Pam, Scott

A STUDY MEASURING THE ACCELERATION OF VIBRATING STRUCTURES USING A MICROPHONE

Sarah C. Calvert

Yellow Springs High School
420 E. Enon Rd.
Yellow Springs, OH 45387

Final Report for:
High School Apprentice Program
Wright Laboratory

Sponsored by:
Air Force Office of Scientific Research
Bolling Air Force Base, DC

and

Structural Dynamics Laboratory WL/FIBG
Building 24c Area B Wright Patterson AFB, 45433
(513) 255-5200

August 1996

A STUDY MEASURING THE ACCELERATION OF VIBRATING STRUCTURES USING A MICROPHONE

Sarah C. Calvert
Yellow Springs High School

ABSTRACT

Fatigue testing at high temperatures is becoming an important area of study, because of the need for increased durability of aircraft structures. Measurement methods that can be used in high intensity, high vibration areas at high temperatures will help designers predict and control cracking and other failures and ensure safe inexpensive flight vehicles. This report describes a method of using a non-contacting microphone and the sound radiating from a structure to define the surface acceleration. Test data are correlated with an accelerometer to determine that the relative accuracy of the use of a microphone is within 2 dB.

A STUDY MEASURING ACCELERATION OF VIBRATING STRUCTURES USING A MICROPHONE

Sarah C. Calvert

INTRODUCTION

Measurement of the motion of vibrating structural members is important in determining the dynamic properties of the structure itself and the fatigue life of the members. Especially important are the deflection, acceleration, and strains of aircraft structures. Defining and predicting aircraft structural failures are critical from the standpoint of human injuries and the immense cost with the need for light weight. With recent interest in the reusable reentry vehicles, the space plane, and many other concepts of high speed flight, the need for high temperature structures emerged. Measurement techniques that can determine the motions of these hot structures are being investigated. This effort investigates the possibility of using a microphone to determine accelerations in a local area of a vibrating coupon.

DISCUSSION OF PROBLEM

An accelerometer is usually used to measure the acceleration of a vibrating structure. Strain gages and microphones are also used to find more local strains and movements. Both accelerometers and strain gauges must be in contact with the structure in order to take measurements. By attaching an instrument to a structure, you add many variables which have to be accounted for when calculating data. A means of obtaining this data without contact would be valuable to the research of hot structures. The laser vibrometer is one new device that has proved useful for laboratory measurements of displacements. Unfortunately, the laser vibrometer is rather expensive. A cheaper method may be the use of a non-contacting microphone placed near the structural panel. Because the microphone is non-contacting, it does not have to withstand temperatures as high as the contacting devices. The microphone is able to be placed in an area that cannot be seen by the laser vibrometer. Because the microphone is placed extremely near the structure, it is able to distinguish between the sound from the structure and the background noise. The

laser vibrometer is placed at a distance where if the background noise is loud enough, it would not be able to make this distinction. Determining the local velocity and the mode shape of the panel is necessary in understanding the dynamic properties of a structure.

METHODOLOGY

Theory says that in the far acoustic field, the acoustic intensity is defined as {ref. 1}

$$I = pu$$

where p is the pressure, and u is the acoustic particle velocity at a point. It is interesting to look at the near field of a vibrating surface to determine if the pressure measurement can be used to obtain a level of local acceleration or velocity. The sound intensity level(SIL) is defined as

$$\mathrm{SIL} = 20\log\left(\frac{pu}{10^{-12}}watts/m^2\right)$$

We are far enough away from the coupon that the sound intensity level is equal to the sound pressure level(SPL) or SIL = SPL in dB.

Near the source of a sound, the "acoustic equations" do not strictly apply because of the boundary layer near the moving surface (viscous forces) , and the hydrodynamic flow area, which form the so called acoustic near field. Testing in the near field is difficult because you are so close to the material. In the near field you feel the air flow produced by the moving structure {ref. 2}. A little farther away is the geometric near field. In the geometric near field, you are able to distinguish from different vibrating regions, without the flow of air.

The flow field close to the source could be defined using computational methods and the Navier-Stokes equations. This is a very complicated method. The elegant part of the analysis is that we may be able to use acoustic near field measurement methods to describe the levels of displacement and acceleration for localized regions. With this, we may be able to relate these to the vibration inputs and acoustic loads without the difficult and tedious process of structural and flow modeling computations. And best of all, we will be able to do this without having to contact the structure. This becomes important when testing at extreme temperatures. If the measurements prove to be linear over a range of velocities and frequencies typically used in full scale thermal acoustic testing, then we will have a new instrument with many advantages over present devices.

An experiment was conducted using a cantilevered rectangular beam on a vibration shaker, shown in Figure 1. The elecrodynamic shaker can introduce any type of force into the base of the small coupon within 0 to 2000Hz frequency limitations and up to a force of 12000lb. A Gulton microphone, Endevco accelerometer, and a scanning laser vibrometer were installed to monitor the motion of the coupon. Figure 2 shows a closer view of the placement of the coupon, accelerometer, and microphone. The microphone was positioned 3/8 inch from the coupon surface at rest.

Sine sweeps from 0 to 500Hz were performed on the coupon to determine the resonant frequency and to take the acceleration and microphone level measurements. The scanning laser vibrometer could not measure the high velocity at the tip of the coupon, so an accelerometer had to be installed to record the tip accelerations. Three acoustic measurements were taken at different levels of acceleration.

Narrowband random force excitation was also used to check the results of the discrete frequency sweep data. The random input force was from 200 to 400Hz with a flat narrow band spectrum. The resultant acceleration and microphone levels were obtained for four levels of excitation.

RESULTS

The acceleration and microphone signals were captured on a digital storage system and spectrum analysis was performed on an Ono Sokki FFT Analyzer. The resultant acceleration and pressure spectral densities were plotted in Figure 5 for the sine sweeps. A sample of the narrowband random response is shown in Figure 6. The ordinate is displayed in dB with a reference of 1g for the acceleration and for the sound pressure level the standard $2X10^{-5}$ Newtons/m^2 is the reference pressure. The abscissa is expressed in frequency (Hz). These plots display the resonance peak at 319 Hz. The levels of acceleration, in dB, and sound pressure levels, in dB, were read approximately and tabulated. The data were displayed as a plot of acceleration versus SPL in Figure 7. The data does come close to a straight line within 2dB. The linear regression formula for the line is:

$$y = 1.1x - 85.6$$

or $$\text{ACCELERATION (dB)} = 1.1\text{X SPL (dB)} - 85.6 \quad \text{at 319 Hz,}$$

with a correlation coefficient of 0.956. Theory tells us that the equation should be

ACCELERATION (dB) = SPL +20 log f - 150 dB {ref. 3}

when f is frequency in Hertz. This coupon gives us a difference of 14.3 dB. This difference is not substantial when we look at the small size of the coupon, the closeness of the microphone to the surface of the coupon, and the hydrodynamic effect of the near field..

CONCLUSION

The technique of using a microphone to measure the acceleration of a vibrating coupon or panel seems to be within the accuracy of the microphone calibration and the accelerometer calibration. The linearity of the results shows that this method is feasible when testing at high acoustic or vibration levels, and at high temperatures.

ACKNOWLEDGMENTS:

I would like to express my sincere thanks to Ralph Shimovetz, Dr. Jon Lee, Cindy Shroyer, Ron Crumbacher, Maj. Kimberly Demoret and the rest of the WL/FIBGQ and WL/FIBGI staff for making this research project possible.

REFERENCES:

1. Beranek, Leo L. Noise and Vibration Control. New York: McGraw-Hill, 1971.

2. Morris, P. M. and Ingard, K. U. Theoretical Acoustics. McGraw-Hill, 1968.

3. Shimovetz, Ralph. Aerospace Engineer. Derived Equation, 1996.

SHAKER TEST ARRANGEMENT FOR MICROPHONE RESPONSE TESTS

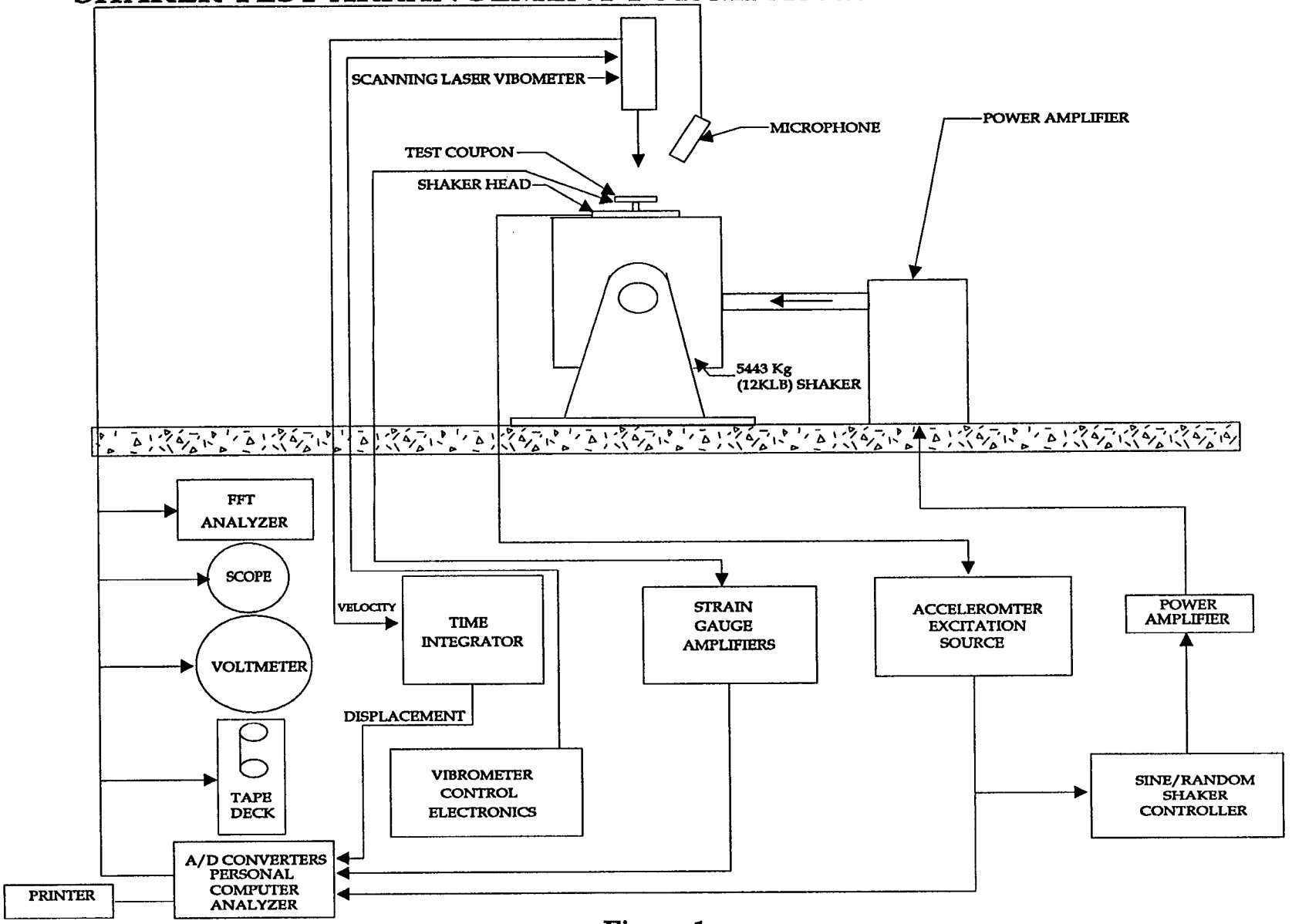

Figure 1

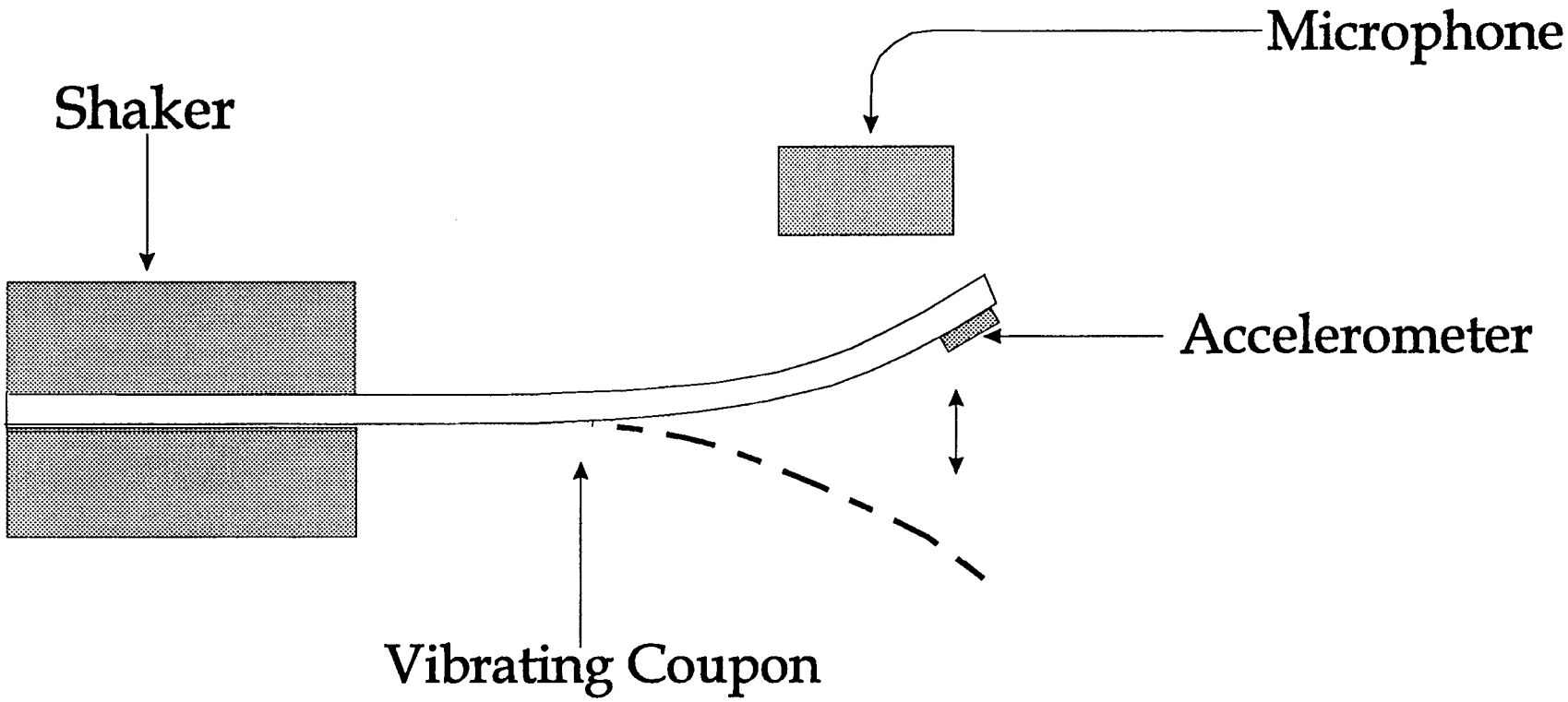

Figure 2

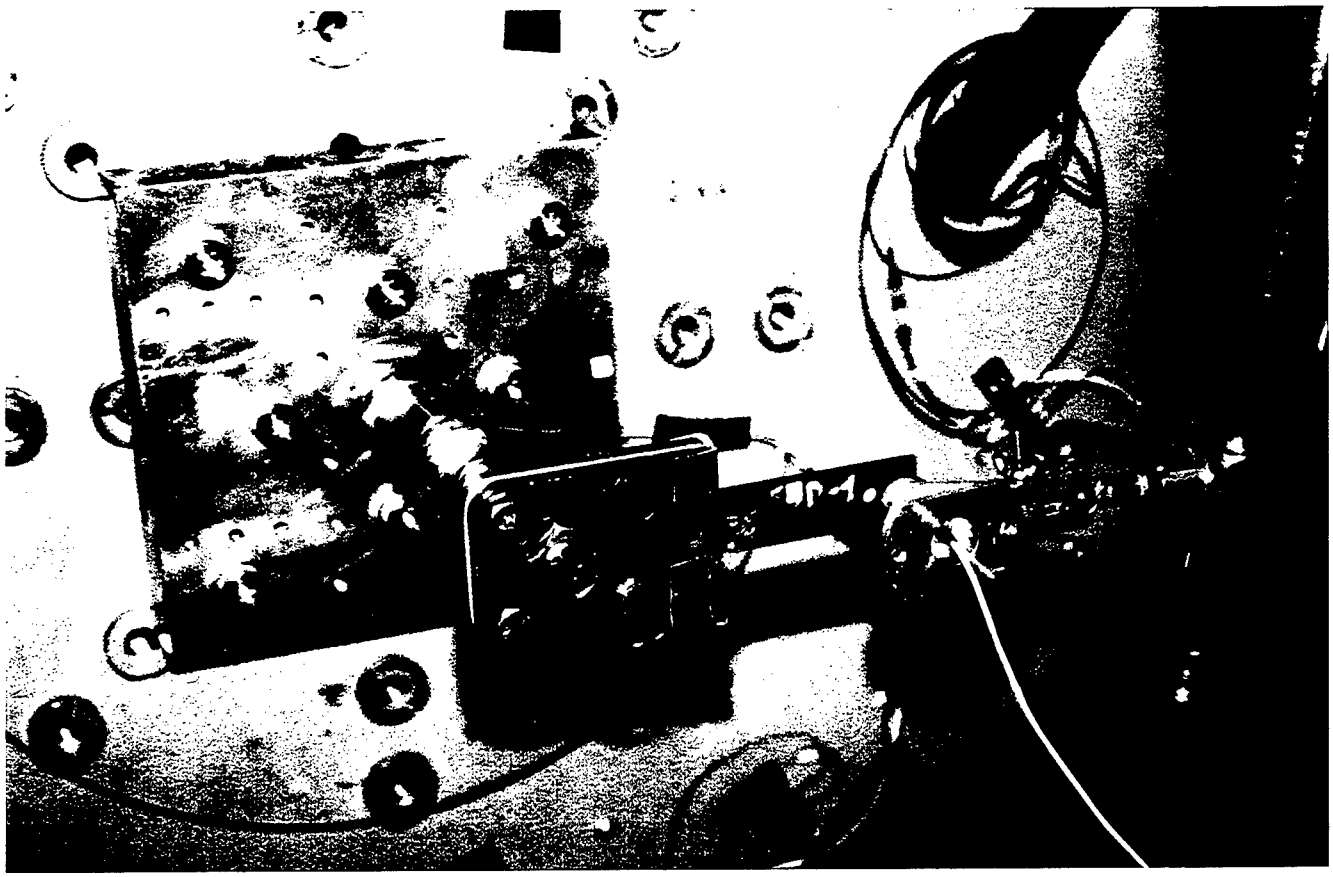

Figure 3

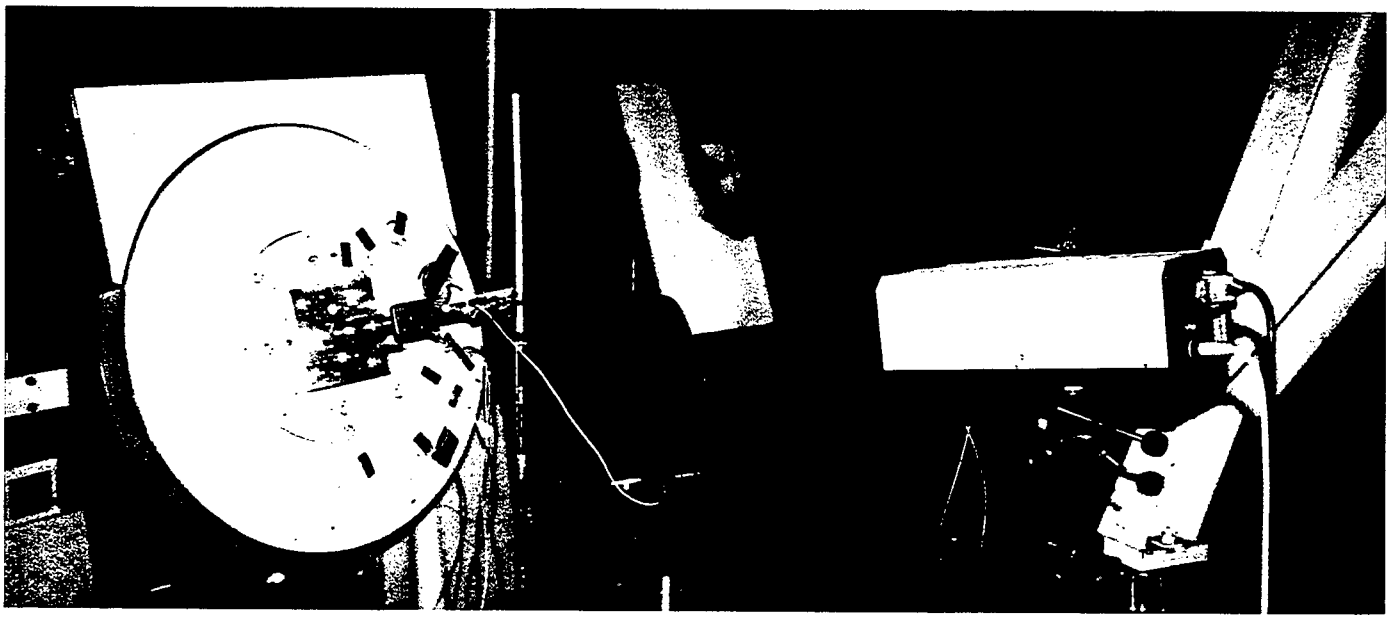

Figure 4

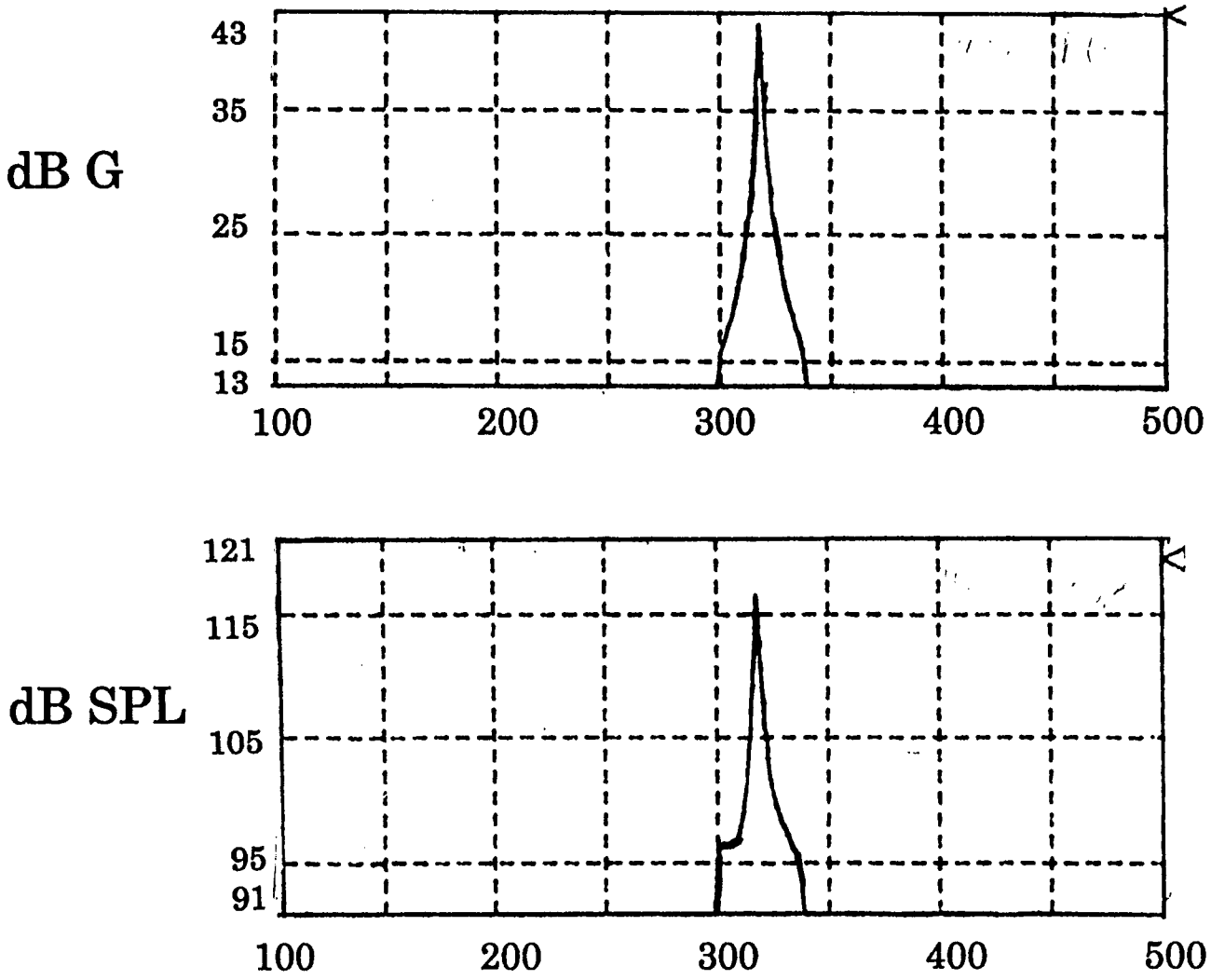

Sine Sweep Spectrum

Figure 5

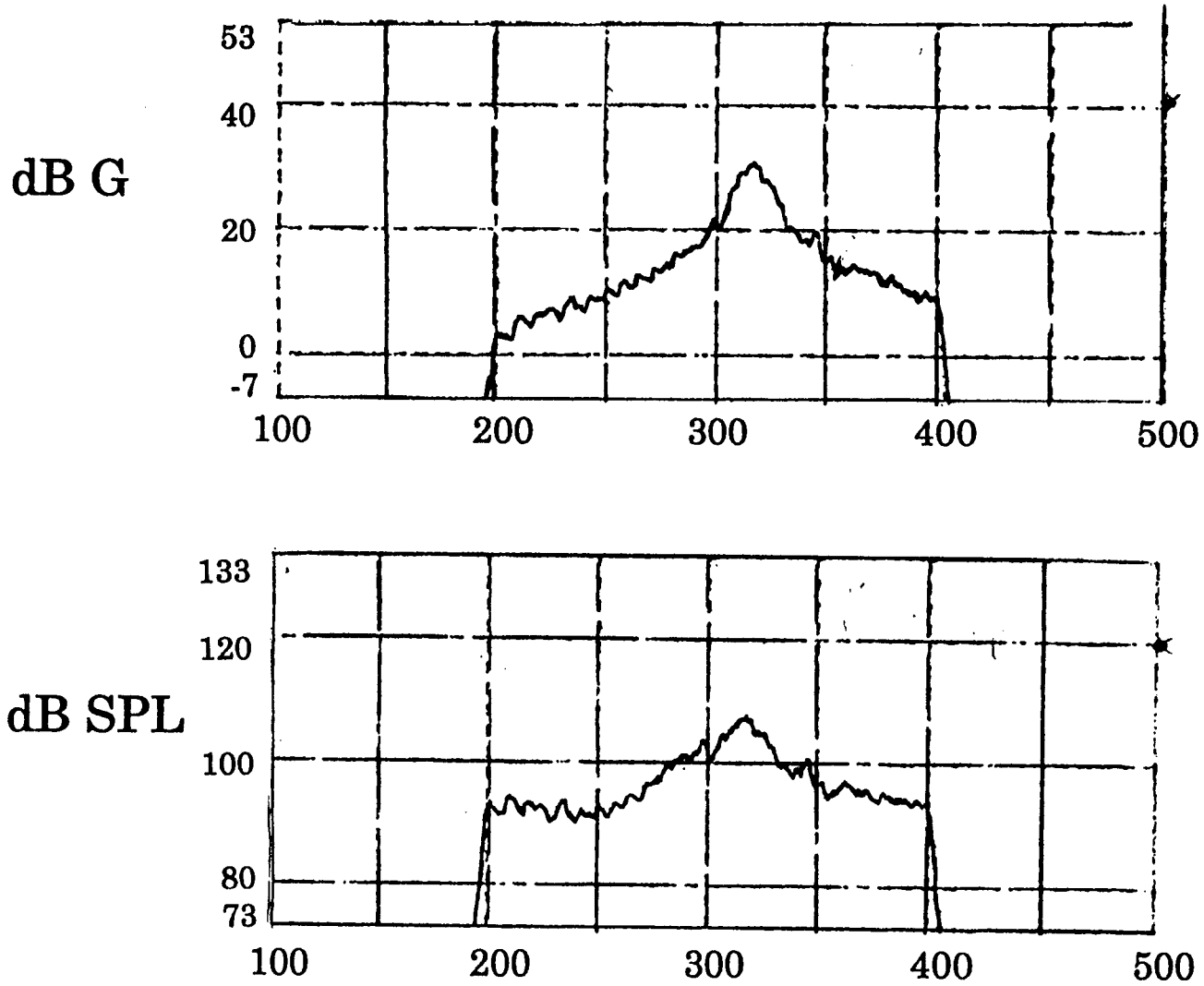

Narrow-Band Random Spectrum

Figure 6

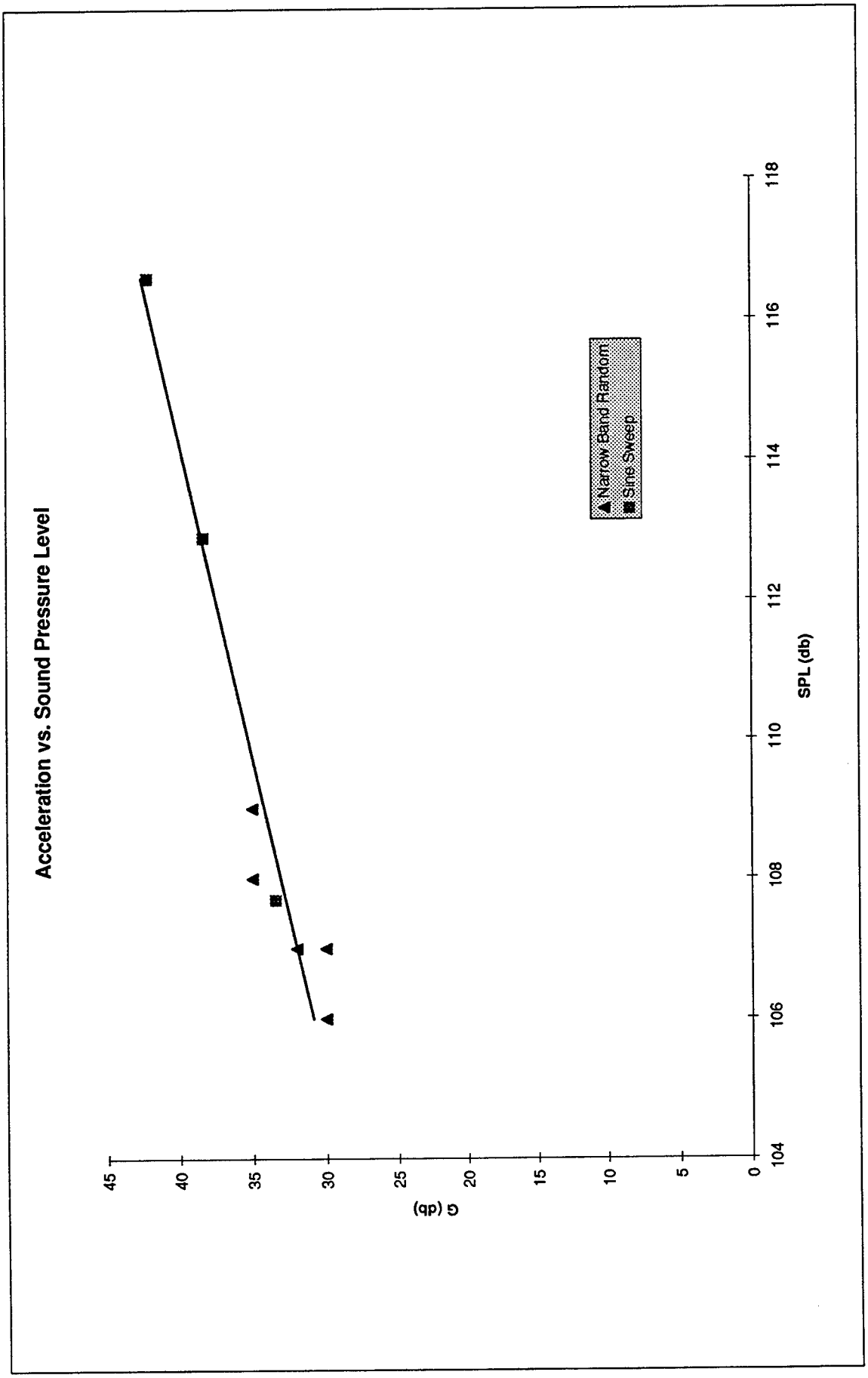
Acceleration vs. Sound Pressure Level
G (db)
SPL (db)
Narrow Band Random
Sine Sweep
0
5
10
15
20
25
30
35
40
45
104
106
108
110
112
114
116
118

Figure 7

AN INVESTIGATION INTO RED DYE CONTAMINATION OF AVIATION FUEL

Shannon M. Campbell

Carroll High School
4524 Linden Ave.
Dayton, OH 45432

Final Report For:
High School Apprentice Program
Wright Laboratory

Sponsored by:
Air Force Office of Scientific Research
Wright-Patterson Air Force Base, OH

and

Wright Laboratory

August 1996

AN INVESTIGATION INTO RED DYE CONTAMINATION OF AVIATION FUEL

Shannon M. Campbell
Carroll High School

ABSTRACT

Research was conducted to investigate how red dye contamination in aviation fuel affects the thermal stability of the fuel. A thermal oxidated test was performed on aviation fuel with and without the dye contamination by researchers in the fuel industry. The data was collected by an international coordination council. Several samples were run with different concentrations of dye and each sample's breakpoint temperature, test pressure, and color was recorded. An analysis of the data showed that the dye may not be the sole factor in the degradation of the thermal stability. High sulfur levels acquired from diesel fuel traces, or carbon and/or dye deposits left on the filter may be responsible for the lower breakpoints of the fuel.

TABLE OF CONTENTS

AN INVESTIGATION INTO RED DYE CONTAMINATION OF AVIATION FUEL

Shannon M. Campbell

INTRODUCTION/DISCUSSION OF PROBLEM

In 1991, environmental concerns propelled the EPA to initiate a program to replace high sulfur diesel fuel with a lower polluting low sulfur diesel fuel. The IRS later joined forces with the EPA, seizing an opportunity to tax consumers of the high sulfur fuel. Originally a blue dye was used to distinguish high sulfur diesel fuel from low sulfur diesel fuel, but it conflicted with blue avgas 100LL. To eliminate any confusion, the dye was changed to DPM 5160-1 Red with a requirement of 5.6 PTB (pounds per thousand barrel). However, red dye in aviation fuel was considered contaminated and banned from aircraft use.

Since the institution of this program, minute amounts of red dye have been found in aviation fuel. The problem is aviation fuel shares distribution pipelines with red dyed diesel fuel. Improper cleaning methods of the pipelines and the adherence of the dye on the pipe walls has been blamed for allowing the dye to contaminate the fuel.

Several interested parties, including the Air Force, have been conducting experiments to determine the adverse effects, if any, the dye has on the fuel's thermal stability. Until those conclusions are definite, the parties involved either agreed to have zero tolerance for contaminated fuel , or permit contaminated fuel for emergency situations if the fuel was retested to ASTM D1655, the commercial aviation fuel specification met all specification requirements, and contained less than 2.5% concentrate of the dye. Note the military will not allow the use of red dye aviation fuel for flying.

METHODOLOGY*

"Standard Test Method For Thermal Oxidation Stability of Aviation Turbine Fuels (JFTOT Procedure)," was used for rating the tendencies of fuel to deposit oxidative decomposition products within the fuel system. The test method was developed to simulate conditions present in real aircraft systems. To summarize the test procedure, approximately 600 mL of jet fuel is filtered, aerated, and then sealed in the JFTOT reservoir. After pressurizing the JFTOT system with nitrogen, the fuel is pumped at a constant flow rate over a restively heated aluminum heater tube and through a precision stainless steel filter for a given period of time. At the end of the test, the aluminum heater tube and pressure change across the filter are evaluated for decomposition products. Test conditions for the various fuels have been established in both commercial and military specifications. For commercial Jet A fuel, ASTM D 1655, states the evaluation of the aluminum heater tube may be performed by a tube deposit rater (TDR) or visual comparison to ASTM color standard. A TDR rating measures the maximum difference in reflected light from the aluminum heater tube before and after the test. The JFTOT test conditions for commercial Jet A Fuel are a heater tube temperature of 260° C, a system pressure of 3.45 MPa (500 psi), a fuel flow rate of 3.0 mL/min., and a test duration of 150 min.

*This methodology was developed by Patricia D. Liberio, Chemical Engineer at Wright-Patterson AFB, Dayton, OH.

RESULTS

ALL DATA COURTESY OF TEXACO, DEC. 1995
AND AMOCO, FEB. TO APRIL 1996

ALL JET A FUEL NOT THE SAME; EACH COMPANY SUPPLIED
IT'S OWN AVIATION FUEL

DIESEL FUELS PREPARED BY HOWELL HYDROCARBONS

JFTOT BREAKPOINT RESULTS

FUEL	T°C	VTR	ΔP, PSI	
1. Avjet A	285	<1	0.1	
	290	<4P	0.1	Breakpoint
2. Avjet A +	280	<1	0	
0.40mg/L red dye	285	<3P	0.1	Breakpoint
(0.14 PTB)	290	<4P	0	
3. Fuel 2+2.5 (v)%	235	<1	2.8	
undyed, high sulfur	240	<1	12.5	(test shut down)
No. 2 diesel fuel				Breakpoint

The concentration of dye (0.40mg/L =0.14 PTB) in sample No. 2 was not great enough to cause a degradation in the thermal stability of avjet A. However, in sample No. 3 the JFTOT breakpoint was decreased 50° C due to the dilution of the dyed fuel.

Avjet A = Jet A

JFTOT BREAKPOINT RESULTS

FUEL	% DYE	T ° C	VTR	ΔP, mm Hg
Jet A	0	300	4	>125
Jet A	0	290	<3	95.1
Jet A	0	285	<2	5.9
Jet A	0	280	<1	3.2
Jet A	2.5	290	4	>125
Jet A	2.5	285	<3	>125
Jet A	2.5	280	2	>125
Jet A	2.5	275	<2	>125
Jet A	2.5	270	<2	1.8
Jet A	2.5	260	<2	0.7
Jet A	2.5	250	<2	0.1
Jet A	2.5	240	1	0.4
Jet A	0.5	290	4	>125
Jet A	0.5	280	<3	>125
Jet A	0.5	270	<2	>125
Jet A	0.5	260	<2	>125
Jet A	0.5	255	1	0.4
Jet A	0.5	250	1	0.1
Jet A	0.5*	275	<2	9.4
Jet A	0.5*	270	<2	2.8
Jet A	0.5*	260	<2	0.2
*Condition repeated with new dye solution blend, same base fuel				

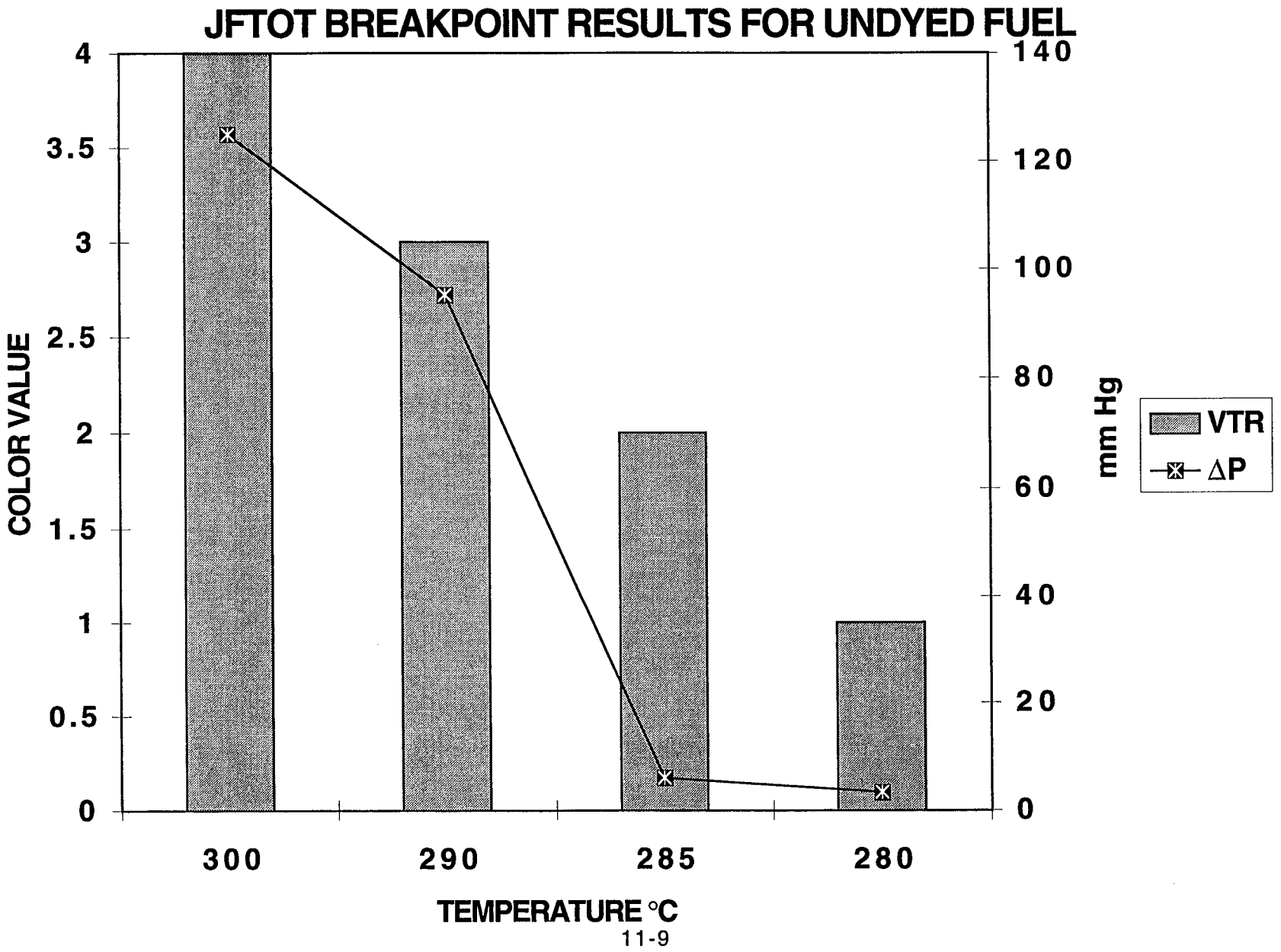
JFTOT BREAKPOINT RESULTS FOR UNDYED FUEL
COLOR VALUE
4
3.5
3
2.5
2
1.5
1
0.5
0
140
120
100
80
60
40
20
0
mm Hg
VTR
ΔP
300
290
285
280
TEMPERATURE °C

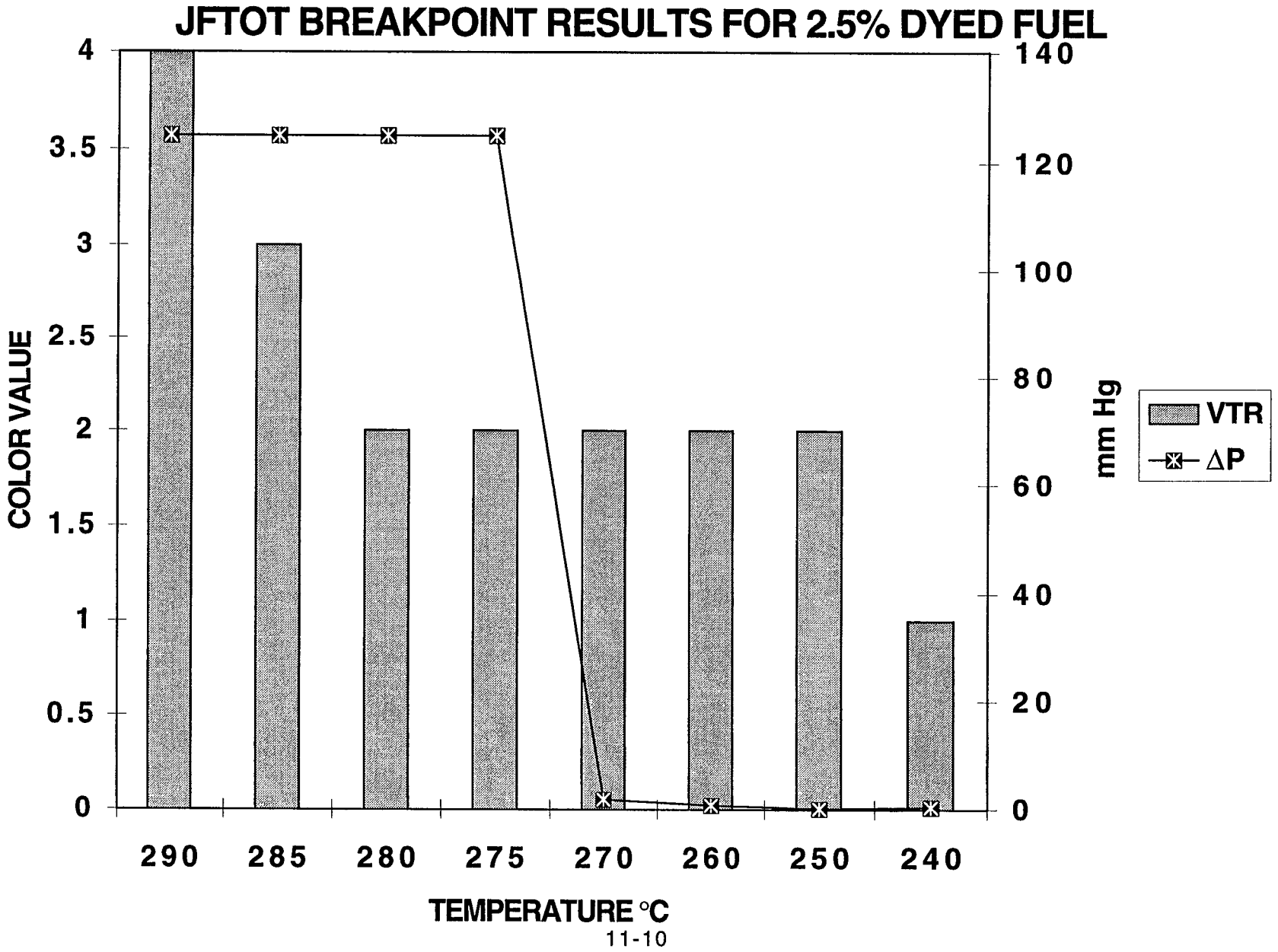
JFTOT BREAKPOINT RESULTS FOR 2.5% DYED FUEL
COLOR VALUE
4
3.5
3
2.5
2
1.5
1
0.5
0
140
120
100
80
60
40
20
0
mm Hg
VTR
ΔP
290
285
280
275
270
260
250
240
TEMPERATURE °C

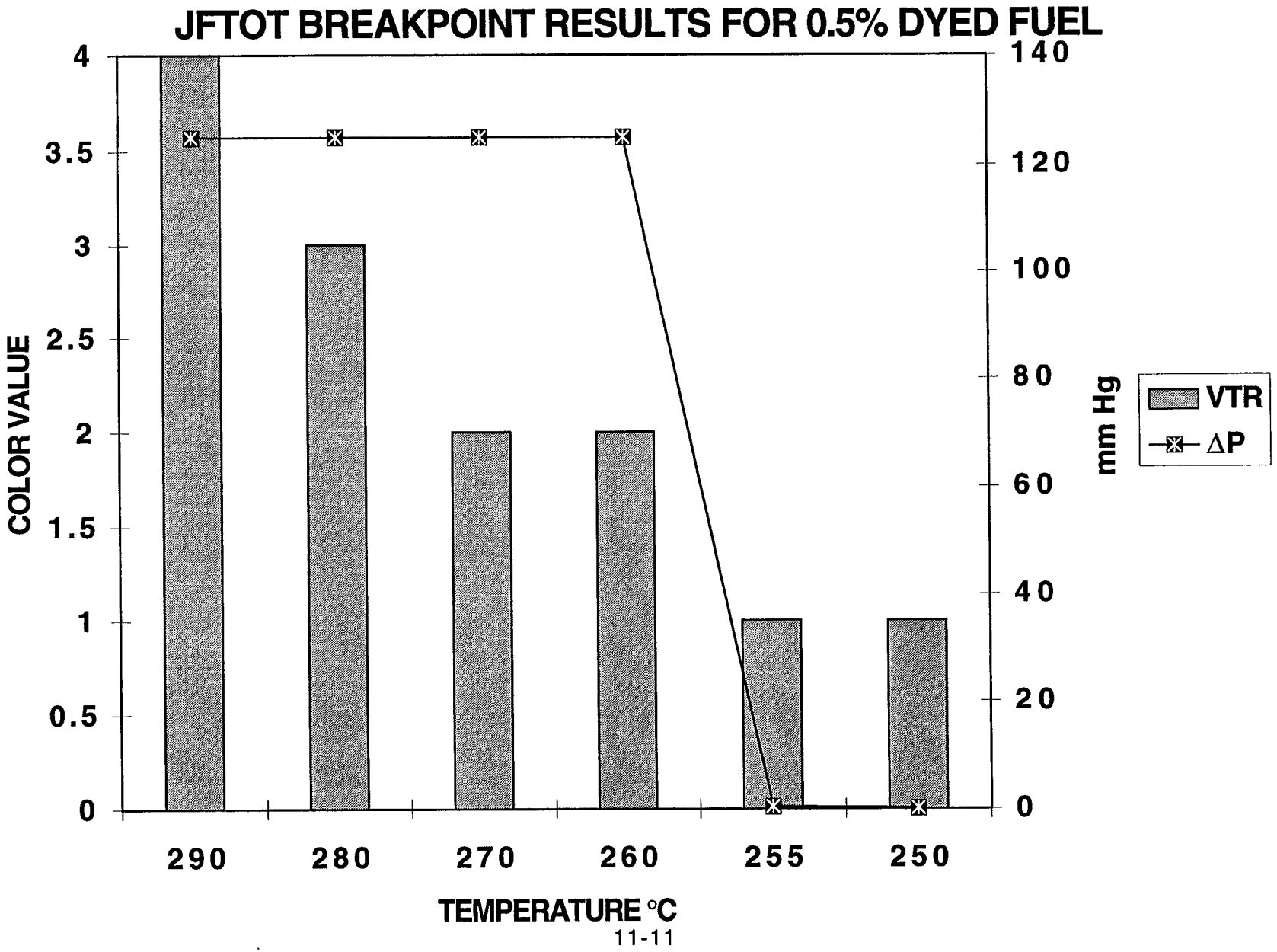
JFTOT BREAKPOINT RESULTS FOR 0.5% DYED FUEL
COLOR VALUE
4
3.5
3
2.5
2
1.5
1
0.5
0
140
120
100
80
60
40
20
0
mm Hg
VTR
ΔP
290
280
270
260
255
250
TEMPERATURE °C

JFTOT BREAKPOINT RESULTS FOR 0.5%* DYED FUEL

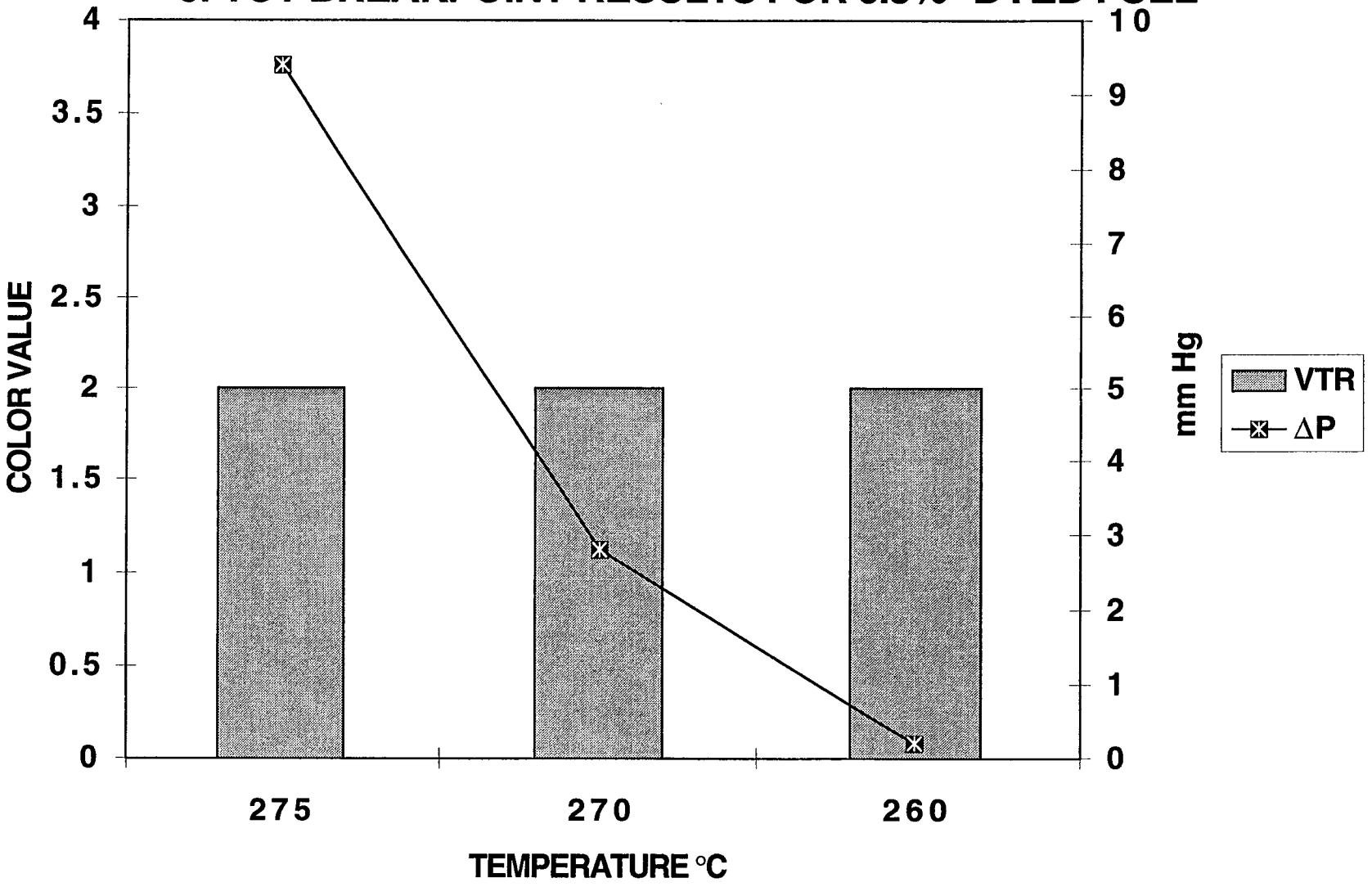

*Condition repeated with new dye solution blend, same base fuel

CONCLUSIONS AND RECOMMENDATIONS

The combined efforts of the Coordinating Research Council along with Texaco Inc. and Amoco Research and Development gave supportive evidence to the following conclusions: The results from Chart #1 (Texaco) indicated that the avjet A's thermal stability was not degraded because of the dye, but rather was degraded as the result of the addition of high sulfur diesel fuel. Sample number 2 produced a slightly lower breakpoint temperature than the pure avjet A (sample number 1). However, when diesel fuel was added to the pure aviation fuel, the breakpoint temperature decreased dramatically by 50°C. This suggested that the sulfur level was the primary reason for the deterioration of the thermal stability in the jet fuel.

Even though the diesel fuel contamination affected the breakpoint of the aviation fuel during the JFTOT testing, it may not be the only factor reducing thermal stability. From data gathered by Amoco, the solubility of the dye in the fuel was questionable. Some samples of the Amoco data failed due to an unexpected increase in pressure. Possible reasons for this are particles of either dye or carbon have dropped out of the fuel and deposited onto the filter, thus causing an increase in the pressure or the dye is affecting fuel chemistry. From the Amoco data the dyed fuel failed ΔP at a lower temperature than failure a visual rating. Most fuels fail visual at lower temperature than ΔP failure. Further study of why ΔP fails before the visual rating fails needs to be conducted. Recommendations for this would be to test the filter deposits for traces of dye or carbon in order to determine whether the pressure increase was caused by dye, carbon, or some other compound from the fuel.

Analyzing the data from both Amoco and Texaco upheld the hypothesis that dyed fuel would have an adverse effect on the thermal stability but not to the extent as anticipated. What has now come to light is that high sulfur diesel fuel is possibly the main contaminant in the aviation fuel. The source of contamination could be dyed diesel fuel or dye is adhering to the pipe walls. Once the source is established the companies should try to eliminate or decrease the amount of contamination. Further research should be conducted in order to distinguish between the problems

caused by the dye as opposed to the sulfur contamination. Research is currently being done in the form of an engine component test in order to determine long term effects of dye on the fuel system materials.

REFERENCES

CRC Group on Dye in Diesel Fuel, Minutes, Atlanta, GA, Dec. 6,1994

Dye In Aviation Turbine Fuel Group, Unconfirmed Minutes, Indianapolis, IN, June 20, 1995

Dye In Aviation Turbine Fuel Group, Unconfirmed Minutes, Chicago, IL, Oct. 11,1995

Dye In Aviation Turbine Fuel Group, Unconfirmed Minutes, Houston, TX, Dec. 5,1995

Group on Dye In Aviation Turbine Fuels, Unconfirmed Minutes, Chicago, IL, Oct. 26, 1994

Group on Dye In Aviation Turbine Fuels, Unconfirmed Minutes, Alexandria, VA, April 26,1995

Personal Communications, from Booth, Dr. David L., April 29, 1994

Personal Communications, from Harrison, William E. III, Oct .25, 1994

Personal Communications, from Makris, Nick, March 7, 1996

Personal Communications, from Makris, Nick, Feb. 9, 1996

Personal Communications, from Oppenheim, Lee Feb. 9, 1996

Personal Communications, from Zengel, Alan E., May 25, 1995

Zengel, Alan E., IASH, Newsletter No. 17, "Dyed Fuel Group", pg. 6, Feb. 1996

NEURAL NETWORKS AND DIGITAL IMAGE PROCESSING

Christopher R. Clark
Niceville High School
800 E John C. Sims Parkway
Niceville, FL

Final Report for 1996 High School Apprentice Program

Sponsored by:
Air Force Office of Scientific Research
Bolling Air Force Base, DC

and

Wright Laboratory

Mentor:
Paul L. McCarley

August 1996

Neural Networks and Digital Image Processing

Christopher R. Clark

Abstract

The areas of study presented are neural networks and digital image processing. These topics are explored using different approaches to determine their potential for use in future military sensor technology. Raw data taken from existing sensors was used to test the ability of conventional digital image processing techniques and neural networks to isolate and recognize potential targets in the input image.

The first task of the project involved porting an existing sensor model from Microsoft Excel to MathWorks' MatLab and then creating a Graphical User Interface front end for the model using Microsoft Visual Basic. This was to gain knowledge about the capabilities and programming languages of MatLab and Visual Basic which would be utilized throughout the project.

The next two tasks of the project entailed performing digital image processing and neural network processing on sensor-produced images for target recognition. The first of these tasks employed an Image MultiSpectral Sensing System, spectral deconvolution, and neural network filtering. The second task used Laser Radar and Pulse-Coupled Neural Networks.

Table of Contents

NeuroSeek System Model

Introduction

The NeuroSeek is currently being developed by Wright Laboratory and Pacific Advanced Technology[1]. It integrates state of the art infrared sensor system technologies into an infrared focal plane array (FPA) with dual color radiometric response (representing medium wavelength IR and long wavelength IR) which performs on-FPA smart neuromorphic analog image processing. The NeuroSeek will also interface with spectral image data from the Image MultiSpectral Sensing System (IMSS). This will allow the system to be used for day/night operation and target detection in a cluttered environment. The device will perform analog signal processing rather than the slower DSP-based methods that have been used in the past.

A system model was developed to test the performance of the sensor in different situations. The Microsoft Excel-based model takes user-defined input values, performs a series of calculations, and outputs realistic performance metrics for the sensor. This spreadsheet only deals with a single pixel of the array at a time. Since the sensor will be implemented with an array of 128-by-128 pixels, a model that takes all 16,384 pixels into account is more desirable. Thus, a matrix-based model was developed.

Conversion

Obviously, performing a series of complicated calculations on each of 16,384 inputs is very processor-intensive. Therefore, in order to implement such a system, a very quick matrix-manipulation algorithm is needed. MathWorks' MatLab provides such an algorithm.

---

[1] McCarley, Paul L., Mark A. Massie, and Buu L. Huynh, "The NeuroSeek Infrared Focal Plane Array: A High Density Two Color On-Chip Neuromorphic Processing Focal Plane Array for Motion Sensing Applications," Meeting of the Infrared Information Society Specialty Group on Passive Sensors, "Advanced System Concepts", 1996, Monterey, CA.

The first task at hand was to convert the Excel spreadsheet into a MatLab script file (M-file). The Excel spreadsheet uses cell addresses in its equations while MatLab requires variable names in its equations. So the Excel cell addresses were replaced by descriptive variable names when moving the equations to MatLab. In addition, the Excel model used a lookup table for a group of equations known as the Blackbody Calculations. Transferring these equations to MatLab required the development of some long and very complex formulas. Another issue in the conversion was the order in which all the calculations were performed. This was not a problem in the non-sequential spreadsheet, but is significant in the sequential M-file in which all the variables used in an equation must have been previously assigned a value. Ultimately, a working M-file was developed and the conversion process was successful.

Graphical User Interface

Since close to 30 different inputs must be provided to the model, an easy way of doing so was needed. Also, a good way to show the outputs was desired. Both of these goals were met by creating a graphical user interface (GUI) as a front end to the model. After a brief attempt at trying to create a GUI with MatLab code, the development was shifted to Microsoft Visual Basic. Visual Basic allows for rapid development of a standard Microsoft Windows GUI. It also supports Dynamic Data Exchange (DDE) permitting it to easily communicate with MatLab.

When the user runs the compiled Visual Basic program, a window with a menu appears. The user then selects the menu item "Blackbody Calculations" and he is asked which default values he would like to use—those for medium wavelength or those for long wavelength. After he chooses an option, an input dialog box consisting of a group of text boxes appears (Figure 1). The user may change any value he wishes or clear all values and start over.

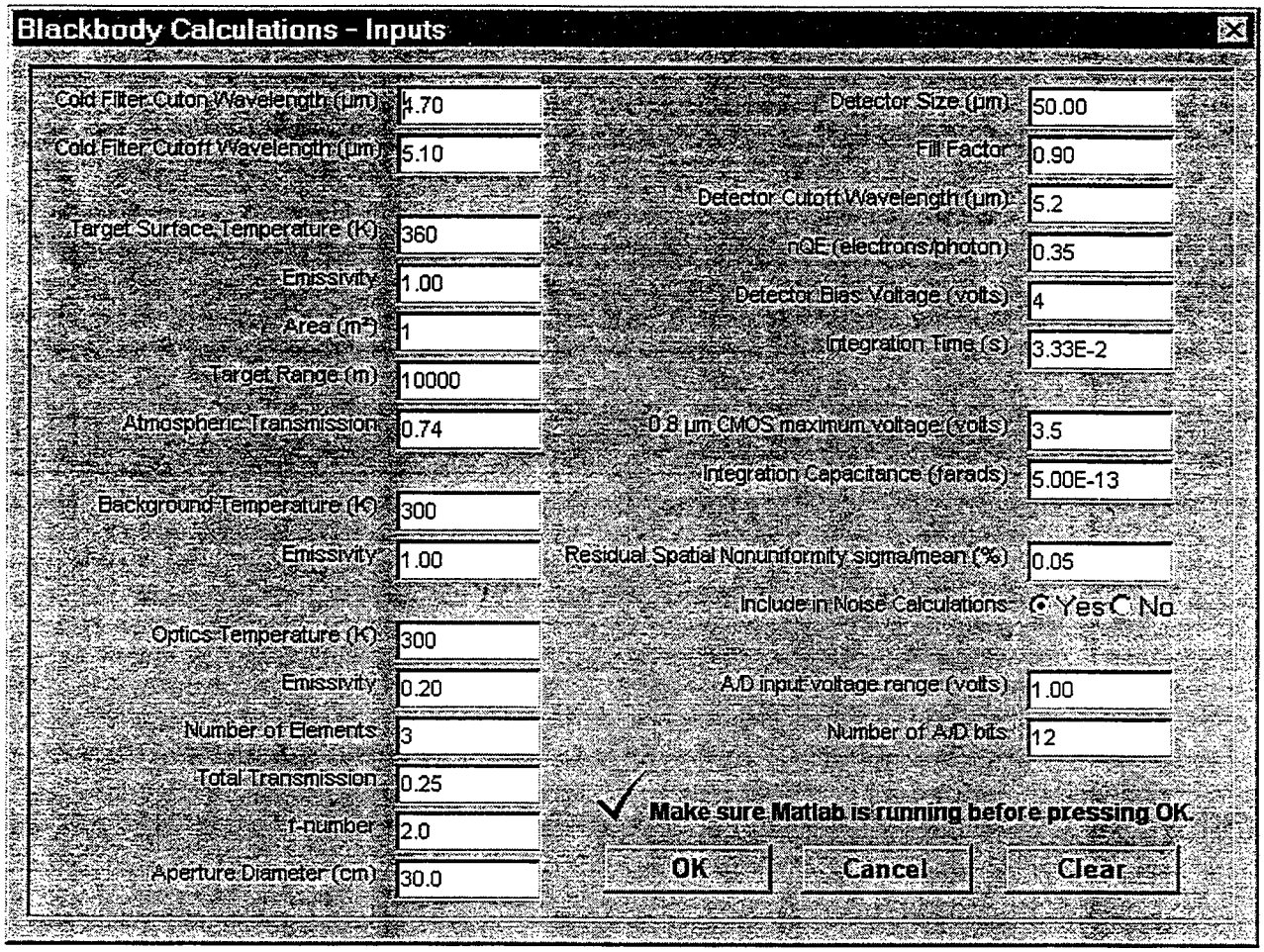

Figure 1: Input dialog box for NeuroSeek System Model GUI

When the user presses the OK button, the program sends all the input values to MatLab and performs the modeling calculations. Then MatLab sends the resulting performance metrics back to the interface program where they are displayed (Figure 2).

Conclusion

The graphical system model when used as shown here still assumes that the inputs are the same for all pixels in the sensor's array. But since it is MatLab-based, it could easily be modified to handle different values for each pixel with the addition of a pixel index value input. Each time the program was run, the user would specify a different index or range of indices to map the input values to an input matrix.

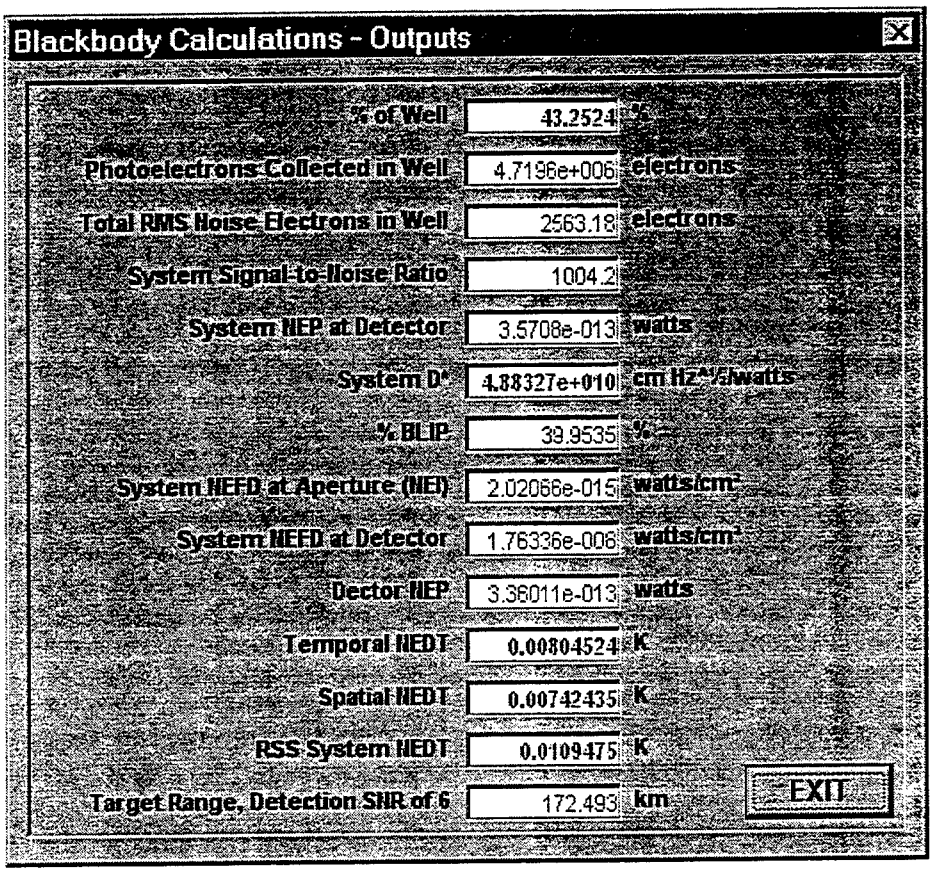

Figure 2: Output dialog box for NeuroSeek System Model GUI

IMSS and a Minefield Model

Introduction

The Imaging Multi-Spectral Sensor System (IMSS) is an infrared device used in target recognition applications. It uses infrared wavelengths of 3.5 to 4.9 micrometers to produce its output. IMSS moves through the infrared range in 90 equal increments at the rate of 30 wavelengths per second. This allows the system to be used for a variety of applications since different objects are seen best at different wavelengths of the infrared spectrum.

The developers of the aforementioned NeuroSeek designed their device to accept input from IMSS and wanted to see the type of data that would be

produced by the sensor. Pacific Advanced Technologies created a simulation minefield model consisting of pennies (representing the mines), a toy jeep covered in camouflage, and various clutter such as soil, grass, and leaves. They then ran the IMSS on the scene and saved the output on a computer. The data was sent to the author for testing.

Data Format and Pre-Processing

The data and a set of utility programs developed by PAT was received via a removable ZIP Drive disk. After inspection of the data files, it was determined that the data was in UNIX format and needed to be byte-swapped in order to be used by a Windows PC. This was achieved with the help of Mark Massie of PAT who sent a program that would perform the byte-swapping. Each data file consists of a header followed by a series of two-byte values representing the intensity levels of every pixel in the sensor's 256-by-256 array for each of the 90 wavelengths.

The raw data is not very useful without processing. The HyperPAT utility offers a function called JAN which performs spectral deconvolution on IMSS

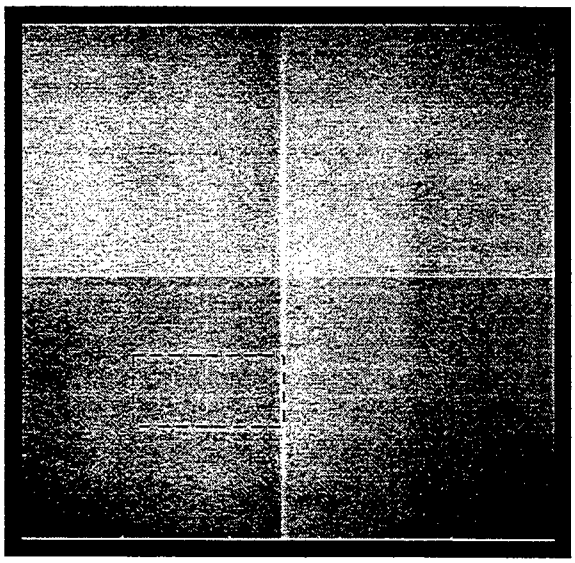

Figure 3: Processed IMSS data at 3.5 microns

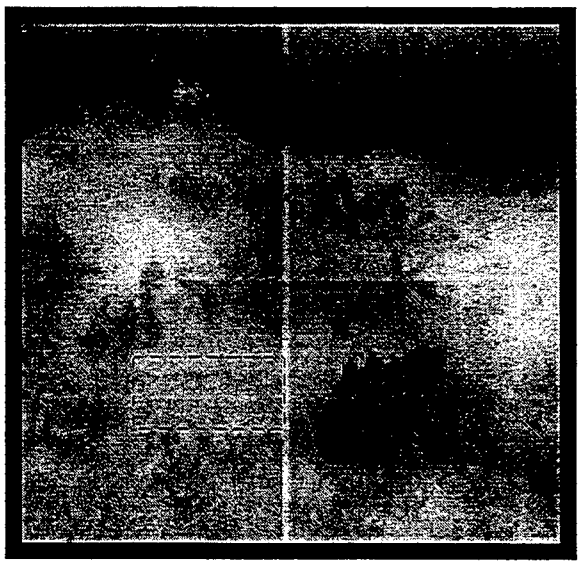

Figure 4: Processed IMSS data at 4.9 micrometers

images, making them viewable. Since JAN can only accept 128-by-128 input, the data had to be divided into four separate files in order to be processed. The JAN program takes over an hour to deconvolve a single file on a computer with a Pentium-90 processor.

Viewing the Data

A MatLab script file was written to read the processed data files and show gray-scaled images of the minefield model. The script file reads the data for a particular wavelength, or a frame, from the correct location in each of the four files and shows a single 256-by-256 image of the scene. Figures 3 and 4 show actual output of the M-file for different wavelengths. The lines that separate the quadrants of the images were the edges of the four files used by JAN and are a result of the filtering process performed. The area outlined by the dotted box in both images is the simulated minefield. The mines are barely visible in Figure 4. The camouflaged jeep can be seen in the exact middle of Figure 4.

Obviously, the wavelength has a significant effect on the image. It appears that more objects are visible at higher wavelengths. In order to investigate this idea further, a way to quickly view different wavelengths was needed. A program was written in Visual Basic to accommodate this task. The program is shown in Figure 5. The program allows the user to choose up to four files to view at once, use the scroll bar to adjust the current frame, copy the current frame to the Windows clipboard, and save the current frame to a bitmap file.

Neural Network-Based Image Processing

The final objective of a sensor system is to be able to find and recognize a target in the input image. There are many different ways to approach this. The use of neural networks to find targets is becoming very popular. The approach

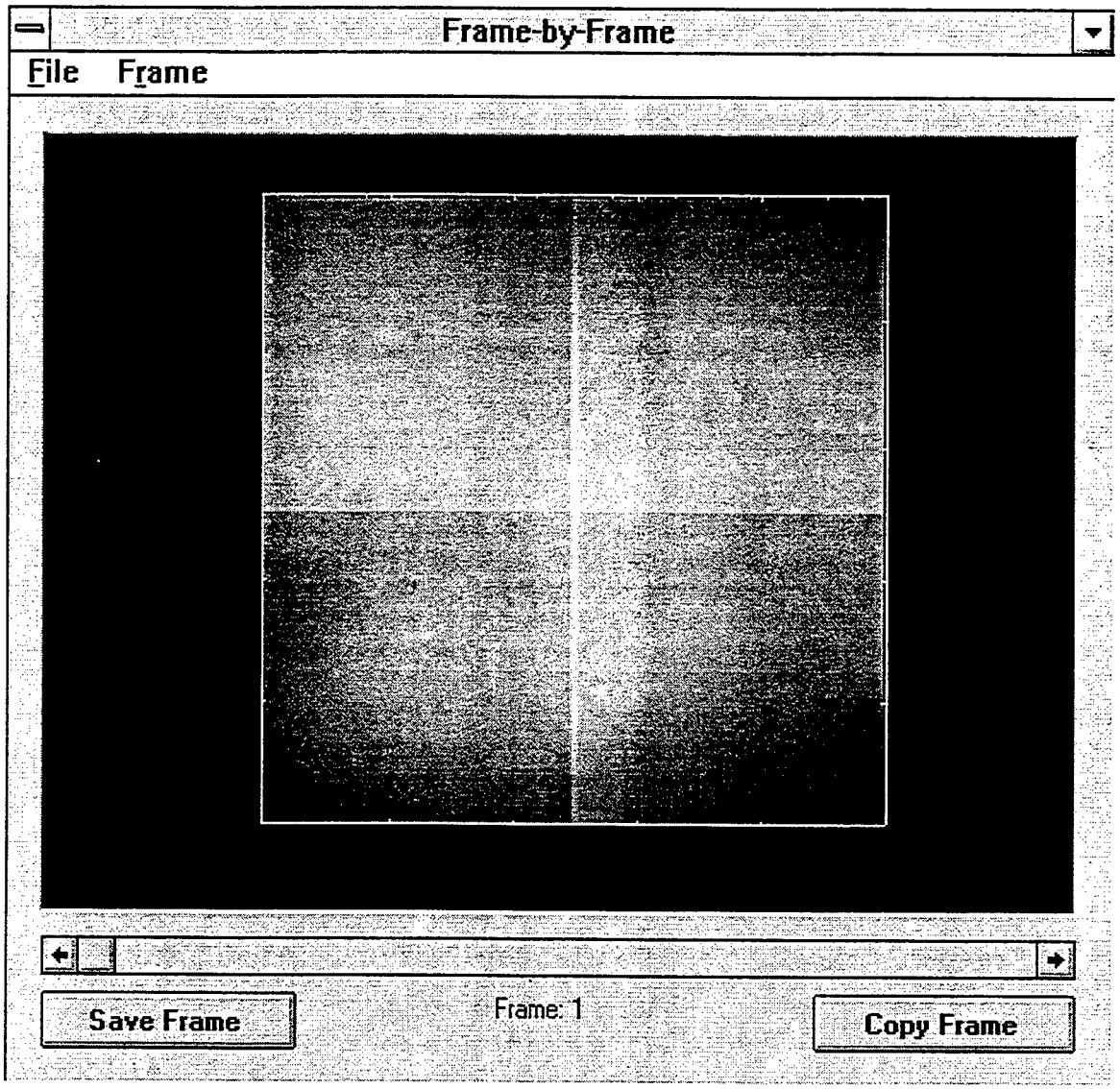

Figure 5: Visual Basic program for viewing processed IMSS data

discussed in this section involves the use of a neural network to obtain a filter, which is then convoluted over an input image using standard digital image processing techniques. Theoretically, the filtered image will have high output (white) in the areas of targets and low output (black) in all other areas.

To obtain a filter from a neural network, a target is needed. The neural network is then trained to output high values when it sees this object. To improve its robustness, the network should be trained on several different instances of the target object as well as several instances of non-target objects. A

neural network has a matrix of weight values that are multiplied by the input and then that output is passed through a transfer function. The network learns by adjusting these weights recursively until it comes up with a weight matrix that will output 1 when it is multiplied by the target image or it reaches a maximum number of iterations. When the network has finished training, the final weight matrix is used as the filter. If a network is well-trained it will have an output of very close to or equal to 1 when an exact copy of an image that it was trained on is filtered with the final weight matrix.

In this case we wanted to try to locate circular mines (pennies). So, we cut out several mines from the image in which they appeared best to use to train our neural network. Using a backpropagation algorithm in MatLab, we attempted to train a network to recognize our target. The training process was stopped when it was obvious that it would not get any closer to being perfectly trained. To test the filter we convoluted it over the image that the target images were taken from. The output was unsatisfactory—the locations of the mines were basically identified, but there were several other locations whose outputs very closely resembled the output for the mines.

Conclusion

The relatively small range of wavelengths used by IMSS limits its adequacy for target recognition. As previously shown, most objects appear better as the wavelength increases. This research confirms the theory of the NeuroSeek developers. The NeuroSeek will go up to at least 9 microns in wavelength. The neural network filter developed did perform up to expectations. This is due to the fact that the pennies in the image data are indistinguishable even by humans. This makes the chances of neural network recognition slim to none.

LADAR Images and Pulse-Coupled Neural Networks

Introduction

Laser Radar (LADAR) devices work like a conventional radio radar. They send out a laser signal and collect reflectance data to form an image. A LADAR image of a bridge taken from a plane is shown in Figure 6.

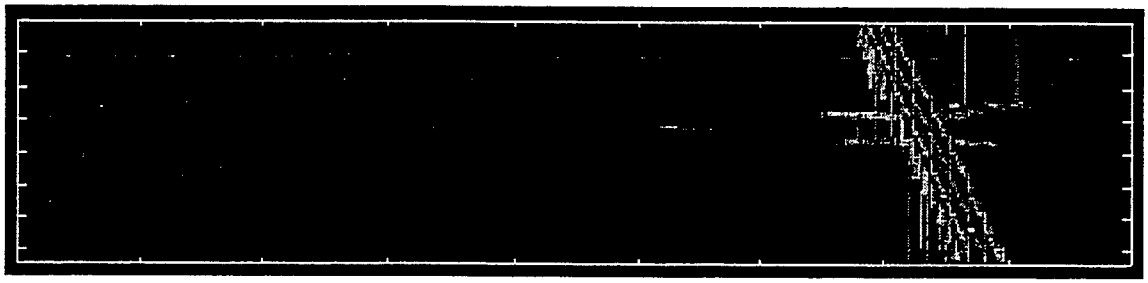

Figure 6: LADAR image of a bridge

Pulse-Coupled Neural Networks (PCNN) are designed to be invariant to all geometrical deformations of an image including size, position, rotation, and intensity. This means that the network will have the same output for an object no matter what size it is, where it is located in the image, the angle that it is positioned at, and the background that it is located in. If this is true, a target recognition application using a PCNN should be very successful.

PCNN Experiment

A PCNN works slightly different than most neural networks. It divides the input image into pulses of different intensities and sums the pulses to produce an output image. Another unique property of the PCNN is that it also outputs a plot of intensity versus time called a time signature. In theory, an object should have the same time signature in all situations. Classification is performed by correlating time signature of the desired target with the time

signature of the output image. A PCNN is similar to other network architectures in that it changes a type of weight matrix recursively.

To see how well a PCNN could perform, we tested it with several LADAR images. First, we ran the network with the image in Figure 6. The time signature output of this trial is shown in Figure 7. We ran the network again with another LADAR image of the same bridge taken from a different angle at a different altitude. This image had slightly different intensity values than the first image. The results of this trial are shown in Figure 8.

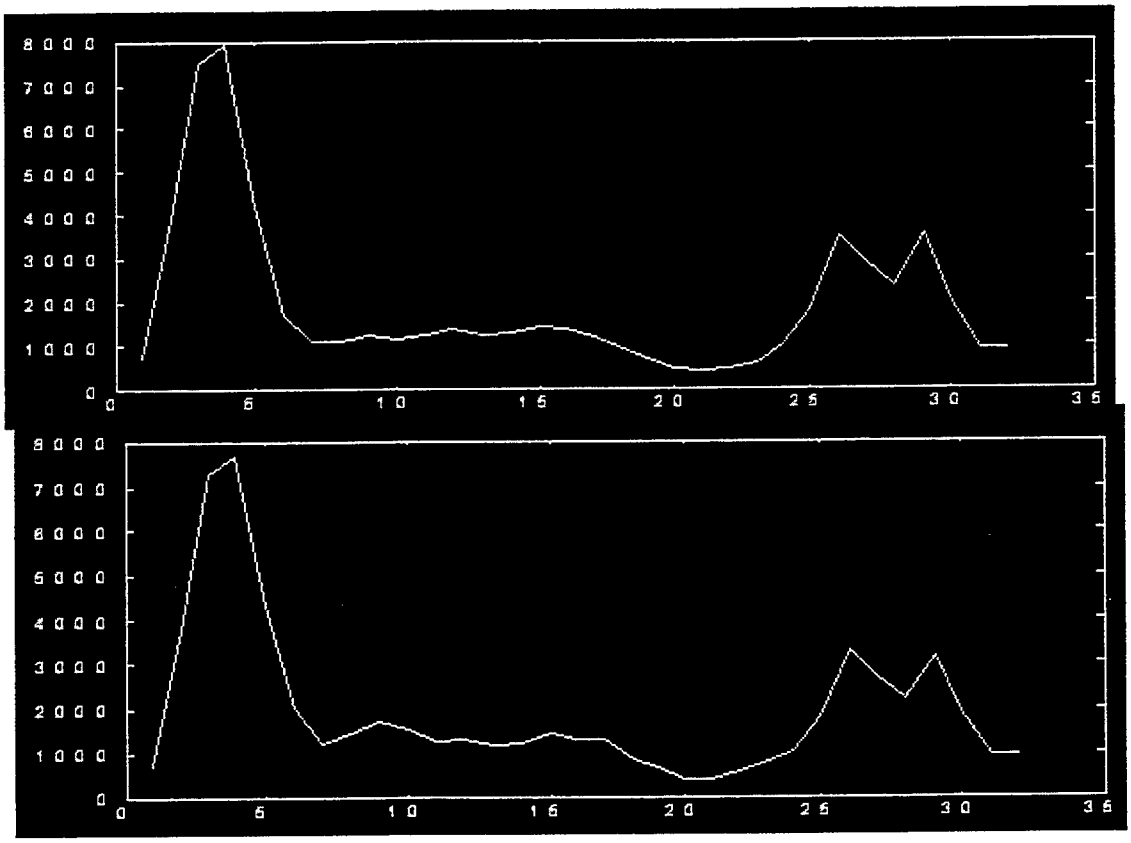

Figure 8: Time signature of a different image of the bridge in Figure 6

The time signatures of two different images of the same bridge are almost indistinguishable. The PCNN surpassed our expectations in terms of output quality, so we decided to test it with something seemingly a little harder—rotation. We rotated the second bridge 90 degrees and ran the network on the

resulting image. Again, the results were exceptional. Figure 9 is a plot of the auto-correlation of the image in Figure 6, the cross-correlation of the second image of the bridge with the image in Figure 6, and the cross-correlation of the rotated second image with the image in Figure 6. The graphs of the first and last of these plots were so close that they completely overlap. This plot represents a strong correlation between the three images. This is a very impressive feat for a neural network to achieve.

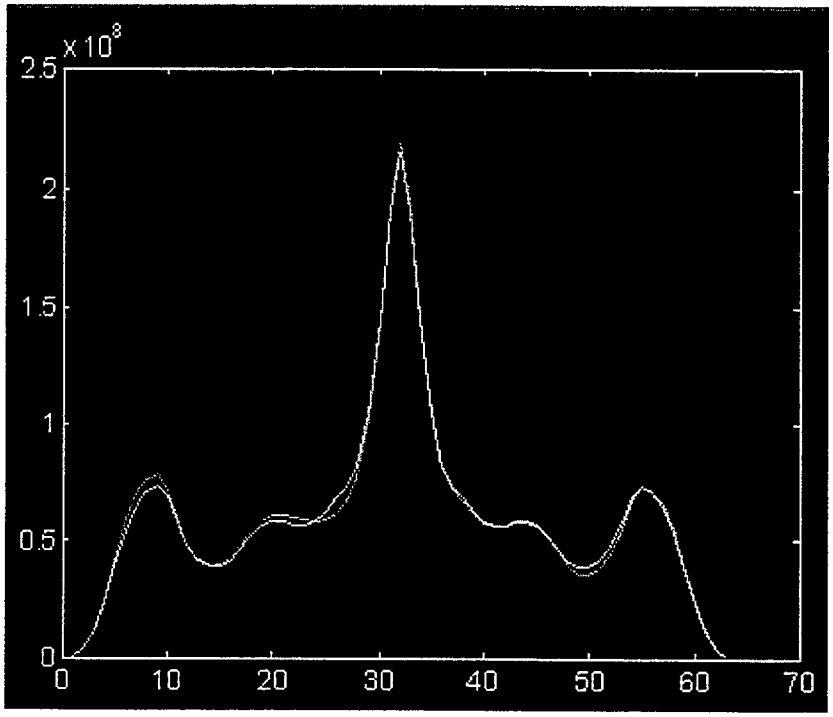

Figure 9: Graph of correlation between three images of the bridge

PCNN Code Optimization and Parameter Manipulation

The PCNN used in this project was a MatLab script file. This allowed us first to learn, and then to change how the network worked. After examination of the code, a way to optimize it was discovered. By reducing the number of calculations required in the main loop of the program the running time of the network was reduced from over 30 minutes to less than two minutes, or a greater

than 1000% increase in speed without sacrificing anything else. The decreased running time allowed for more extensive experimentation. The network has several adjustable parameters that affect the output. The effects of changing these parameters was unknown. In hopes of more thoroughly understanding the workings of the pulse-coupled neural network and thus producing even better output, a scientific experiment was organized.

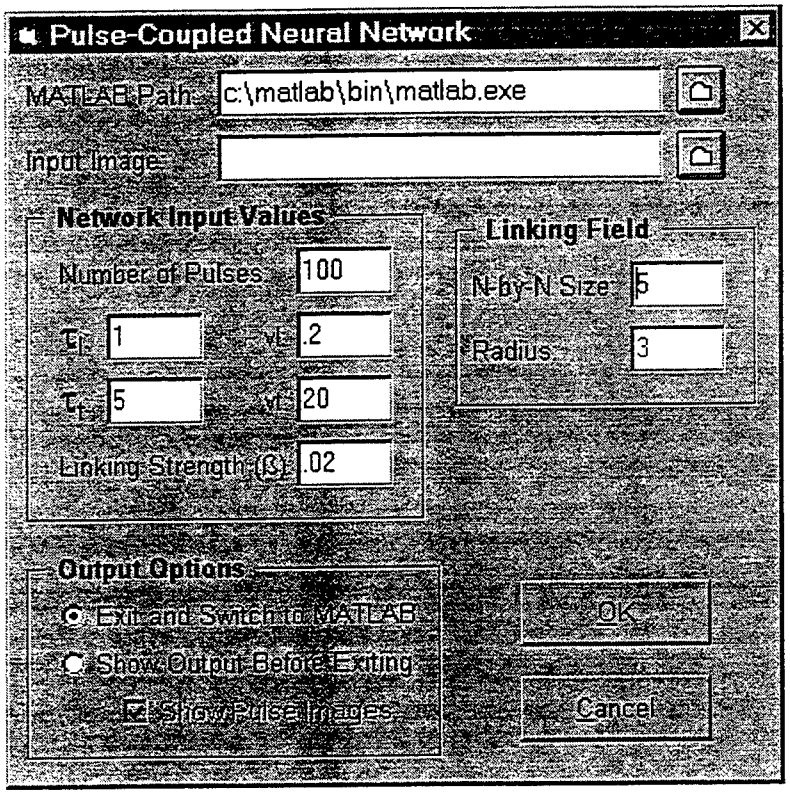

Figure 10: GUI to pass input parameters to MatLab PCNN

To facilitate changing the input parameter values of the network, a GUI was developed in Visual Basic to pass the desired variables to the MatLab M-file. The program is simple and was developed very quickly. The input interface with the default parameter values is shown in Figure 10. The program also gives the user the option to show the incremental pulses and the outputs in another window of the program.

The image in Figure 6 and its corresponding time signature in Figure 7 created with the default parameter values was used as the control of the experiment. The input parameters were changed one at a time in an attempt to determine their individual affect on the overall output. The default values were

scaled by a factor of 10 larger and smaller. The results of each trial were saved and compared. The findings of the experiment are shown in the table below.

Parameter	Effect on Output Image	Effect on Time Signature
Radius	None	Amplitude
Beta	Quality, Completeness	Slopes
τ_l	Contrast	Slopes
τ_t	Quality, Completeness	Number of cycles
v_l	Yet to be determined	Yet to be determined
v_t	Contrast	Number of cycles

Conclusion

The pulse-coupled neural network tested provides accurate target recognition despite changes in size, rotation, position, and intensity. The PCNN output almost identical time signature for significantly different images of the bridge. The output can be seen and would be relatively easy to classify. The presence of user-defined input parameters allows for a wide range of applications and the customization of the network to perform a particular task very well.

Maximal Length Sequences and Circuit Development

Allyn Crowe

Bellbrook High School
3491 Upper Bellbrook Dr.
Bellbrook, OH 45305

Final Report for:
High School Apprenticeship Program
Wright Laboratories

Sponsored By:
Air Force Office of Scientific Research
Bolling Air Force Base, DC

and

Wright Laboratories

August 1996

Abstract

Maximal Length Sequences and Circuit Development

During my tour this year I did many different tasks, but I concentrated on three. The first was designing a circuit and carrying it through most of the development stages. The second was modifying my program from last year. And the third major area of study was in computer repair and upgrading. I also used different computer programs in the lab area. Including Microsoft Word, Lab-View, Visio Technical, and Matlab. In the Appendixes are graphic aids.

Maximal Length Sequences and Circuit Development

Allyn J. Crowe

Many different areas of engineering interrelate with each other. In fact many areas are so closely related that different engineers in different jobs might end up doing the same thing. This holds true to Electrical Engineering and Computer Engineering. They are in description different fields, but when you look at the jobs that the engineers do you notice that the same job is sometimes done in both fields. This is how I was able to focus on some of the things that some people would not think an Electrical Engineer would do, such as computer programming. The computer is a very important instrument in the field of Electrical Engineering. This is due to its ability to solve complex mathematical equations in the time that it takes a person to write part of the equation down. Not only is the computer used for the math part of the field, but it also used to control instruments, extrapolate data from instrument readouts, and generate data for the engineer to feed into an instrument. This is one area that I learned more about and did some work in. The other major area that I worked in was that of circuit design. Circuit design is an involved process that has a great potential for error. On small mistake can destroy days, weeks, and even months of development. The potential for error can be reduced by simply moving slowly and double and triple checking your work.

Since this was my second tour in the same laboratory I had an idea of what I wanted to focus on. When I arrived for the beginning of my tour my mentor gave me several tasks to complete during my stay. To start off with I decided to do some CAD. I wanted to learn how to use a program called Visio Technical. This is a high powered CAD program that uses the Drag and Drop design. In this kind of program you use a template to start. Each template has its own group of stencils to go with it. In the stencils there are the complex shapes and other things that generally take longer to draw in conventional CAD programs. To use the items in the stencils you click and hold on the icon and then "drag" it over onto the drawing surface. It's just like moving icons around in the Windows environment. To become used to this program I was asked to do a floor plan of the lab area. The lab was right in the middle of a

move so I drew what the new lab floor plan would look like. I also added the floor tiles because that is how everybody in the building is used to seeing a floor plan. It is also how anything dealing with space is dimensioned. For example, if you where told to measure the size of the "control room" in the Lab you would say it was a 2x5 room. I finished the main floor plan in a couple of days. The hard part was putting the equipment on the drawing. I wanted to make this as useful as possible so I decided to put the location of all of the equipment on the plan. I did the control room first and then I had to wait for some walls to be moved so I could move all of the equipment around and then put it on the plan. But the wall movers did not come during my tour so I had to leave the drawing unfinished. The floor plan is located in Appendix A.

Next I decided to do the circuit design task. This had really interested me last year so I wanted to learn more about it. I knew some of the basics so I decided to jump right into a big project that I thought would take me some time to do. This was the project: I was to take a circuit through most of the stages of development. The circuit was a Digital Data Link. To start I was given one of the hard parts, the schematic. But that did not make this an easy task. I started off by bread boarding the circuit. Bread boarding out the circuit is building it using a solderless circuit board, called a breadboard, that you put all of the components on and find any errors in the schematic. In this case there were no major errors in the schematic diagram so I was able to proceed in the development.

The next step was probably the most time consuming one of all of the steps. This step was actually doing the layout of the circuit pathways and how each component went onto the circuit board. To do this I started by laying out the components on a piece of paper. I took the approximate size of each one and placed them according to how I would like them to sit on the board. On another sheet of paper I started to layout the actual paths of the circuit. I started with a piece of graph paper and a pencil. On the graph paper I placed dots that coincided with the leads on the components. Then using the schematic and the prototype I started to lay the pathways. I moved chips around many times and when I moved one I ended up moving more. All of this was to try to achieve the ultimate goal in circuit building, to not have any jumpers. It was not as easy of a task as I thought it would be. On the Encoder part of the circuit I had

only one jumper. The next part was the hardest though. I had to do the same for the decoder part of the circuit. The decoder was bigger and had more components. This meant that I had a much longer time ahead of me to work on this. I ended up only having three jumpers, we thought that was good considering this was only my second try at lying out a circuit. After I had the pathways drawn out on graph paper I decided to put them on the computer. I went back to the program that I had started my tour with. I used Viseo to layout the circuit paths on the computer so that I could include them in my report. I also did a layout of where all of the chips went on the top of the board.

With the most complicated part of the circuit done I had to transfer the circuit paths from paper to the circuit board. To do this you can use many different processes. Since this was going to be a one of a kind circuit we decided to use the dry transfer method. In this method you use something to cover the copper coating on the circuit board in the shape of the circuit pathways. I used a kit that is available through many different places. It included some dry transfer sheets of the pads and also a couple of rolls of the tape to layout the pathways. I started with the encoder again to learn how to use the things and then I moved onto the decoder. After I had laid out the pathways we etched the boards. When you etch a board you place it in a solution that takes the copper off the back of the circuit board. We used an etching solution that came with the dry transfer package. We mixed it up and then started etching the boards. It only took about twenty minutes to etch the encoder, but the decoder took about an hour. With this step complete it was time to move on to the next step.

The next step was to assemble the circuit. The first part of this step was to drill out the holes in the circuit board for the pins and leads of the components to go through. We did this using a small tool called a Dremel tool. It is basically a hand held drill, but it has a much higher RPM rate than a conventional drill allowing it to go through the circuit board with relative ease. With all of the holes drilled it was time to finish the assembly. I placed the parts on the board and soldered them one by one. This was a slow but relatively painless procedure. The hardest part was making sure that I put all of the components in the right way. After this was done all we had to do was try it out.

We had hoped that the circuit would work the first time, but it did not at least not completely. So the last step I had to do came into play. It was trouble shooting. The problem that I had to solve was that the Piezoelectric buzzer was not buzzing. All of the rest of the circuit worked out fine. We finally discovered that it was not a problem in the circuit it was a problem in a component. One of the resistors was labeled wrong. I needed a 150K ohm resistor and that is what the color coding on the outside of the resistor said it was, but it turned out that it was only a 15K ohm resistor. This caused the buzzer to only tick and not buzz.

The circuit turned out to do everything that we had designed it to do. We were able to link it together and after solving the minor problem above get it to do exactly as the prototype did. I really enjoyed working with the circuitry and hope to be able to do it some more in the future. I want to also learn about the different types of etching. The complete circuit drawings package is located in Appendix B.

My next project was physically simple compared to the circuit, but mentally it was a little harder. I had to take the program that I helped write last year and make some modifications and also some improvements. The first modification that I had to make was that I had to make the program so that you could input the initial fill in one number and have the program count the degree of the polynomial from that register. This was a simple task of having the initial fill inputted in a string instead of an array. Then I had the program count the number of bits in the string. After the program had that number I had it convert the string into an array so that I could patch the old program in with the new and not have to rewrite the entire program. Or so I thought. I ended up rewriting almost the whole program anyway.

The next change was another major change in the writing of the program. I had to take the program in which you entered the tap condition in about the same way as I used to enter the initial fill, and make it so you could enter the taps in Octal form instead of binary. This was a complicated task. To help me Mike Powell, another apprentice working in the lab, wrote an Octal conversion program. I made some cosmetic modifications and made it a stand alone program. Then I took it and modified it into a part of my program. After I had done this I had almost rewritten the program again.

After I had finished the modifications to my old program I wrote another one. The new program was noting special it was just a shell program for all of the programs that we were using in the lab to work with the Maximal Length Sequences. This included my Sequence program, named Sequence 2, the Octal conversion program, and a program that used the Berlycamp-Massey Algorithm to decode an M-Sequence. The Algorithm program was written by my Mentor James P. Stephens, SR.. After I had written the shell program we decide to compile the big programs so that they would run faster. With this done I was done with this project.

After I had modified the program I made a few little cosmetic changes. I really enjoyed working with the programming again. I had to review some of the things that I had learned last year about the Maximal Length Sequences, but I really enjoyed this project also. I got a chance to work closely with Mike since he was also working with the Maximal Length Sequences. Where I was encoding them he was using an ADI-DSP card to decode them using the program already mentioned, Massey's Algorithm. We helped each other out and both ended up completing our projects. The programs that I wrote or help write are located in Appendix C.

I had one final project while I was finishing up my tour. It was to overhaul a computer. I had worked with the same computer last year because it was having problems. They decided this year to order a new motherboard, hard drive, CD ROM drive, memory, and monitor for the computer. I got the honor of putting the whole computer together. I started with the motherboard and then move on through the rest of the computer parts. It did not take me very long to actually assemble the computer but that was the easy part. After I had the computer running I had to load all of the software onto it. While it was not a hard thing to do it was slow and time consuming. After I had all of the software loaded onto the computer we decided to try to put the computer on the local network. This was another slow process because the computer support department was already loaded down with new computers coming in that had to be put on the network so we had to wait our turn.

The amount of interaction between different areas of engineering is immense. Many Engineers that are in different fields can end up doing some of the same jobs. This can be anything from the

simplest task to a complex one. While on my tour this year I did many different tasks, I had a few big projects and a few small projects. Since this was my second tour I had already done some of the basics and could say a little more what I wanted to do. I was also able to work with another apprentice on a project where we were doing the same type of thing only he was doing one part and I was doing the other. I really learned a lot from my tour and I know that it will help me through my College years that are coming up. I know this since what I did last year helped me with my senior year of High School. I am glad that I had this wonderful opportunity.

Appendix A: Floor Plan done on Viseo Technical

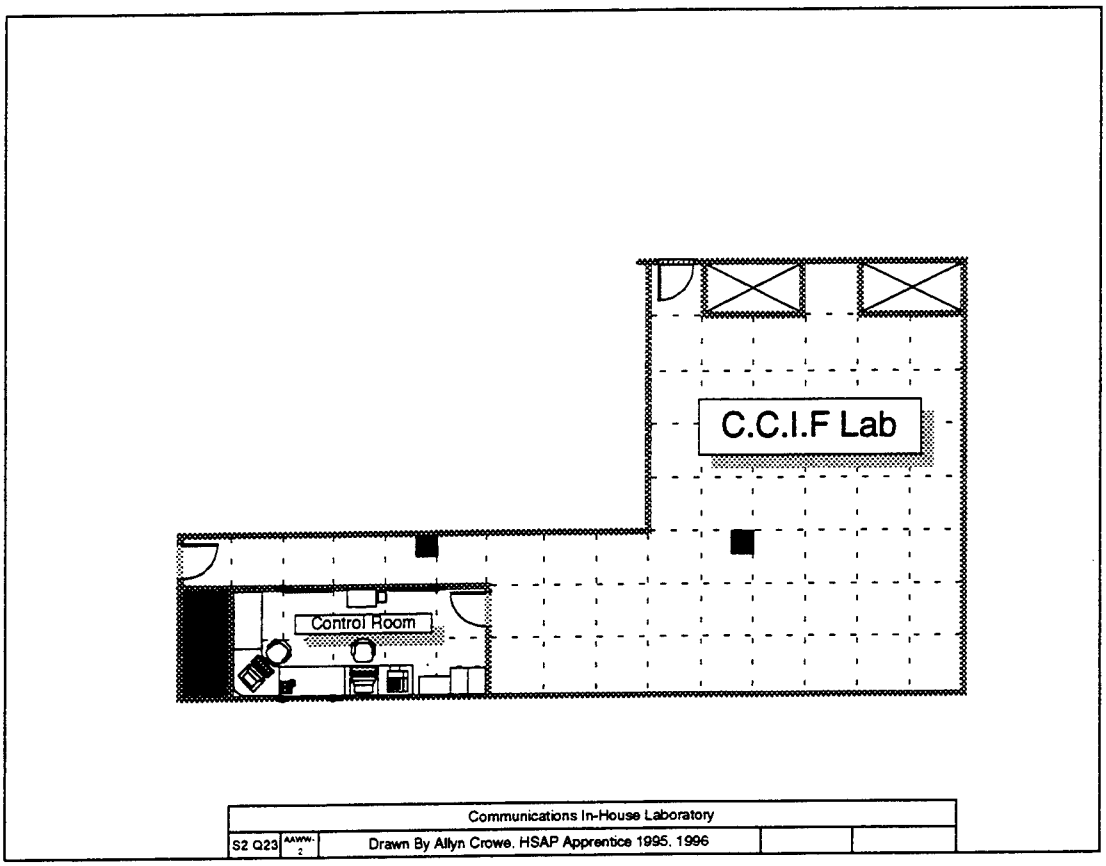

Appendix B: Complete Drawing package for the Digital Data Link.

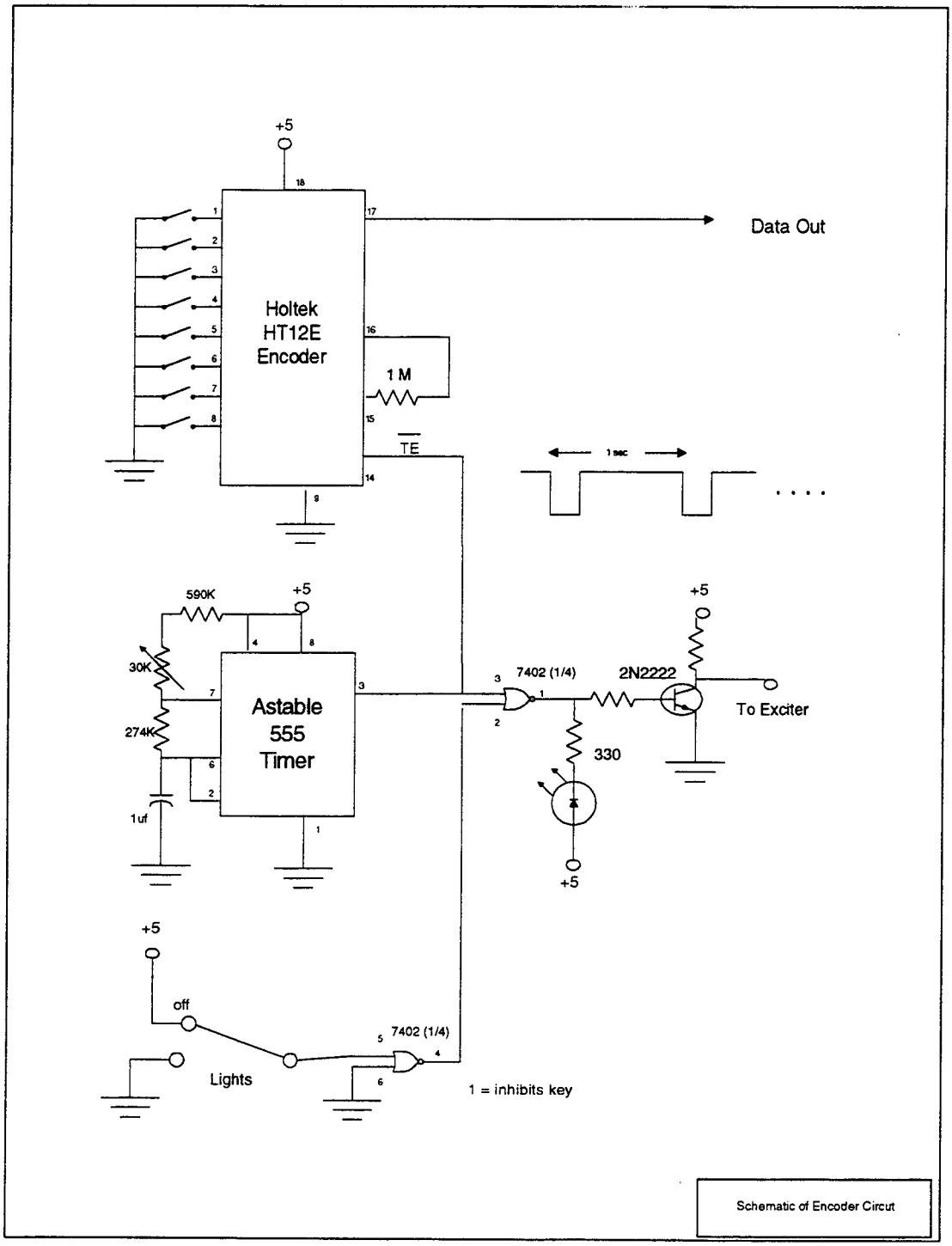

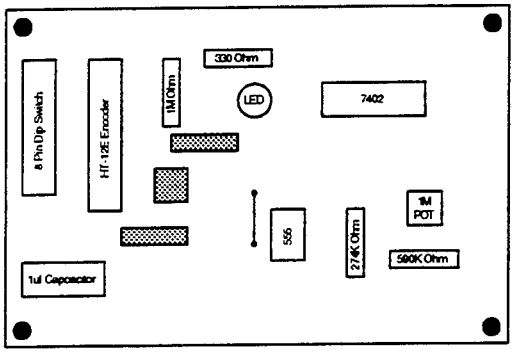

Encoder Circut Layout
Drawn By: Allyn Crowe
HSAP Apprentice 1995, 1996
7-9-96
Scale ~1:1

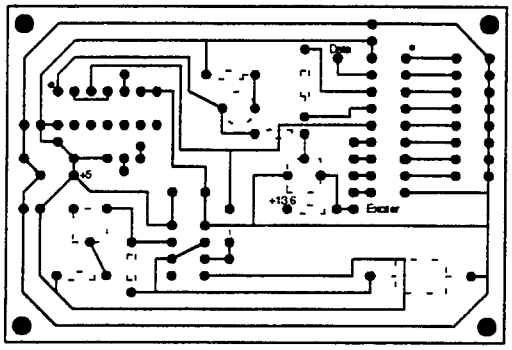

Encoder Circut Path Layout
Drawn By: Allyn Crowe
HSAP Apprentice 1995, 1996
7-3-96
Scale ~1:1

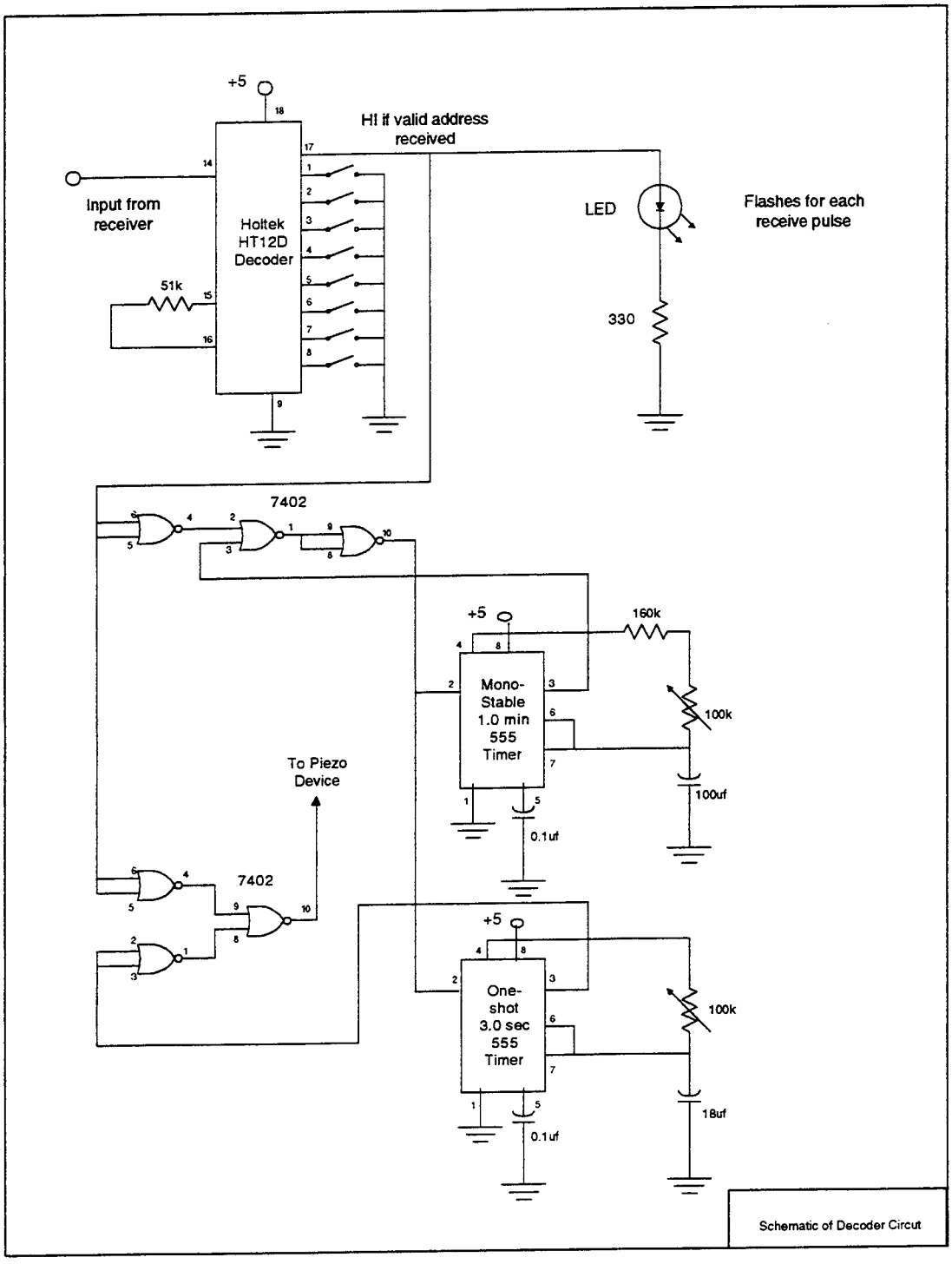
+5
18
HI if valid address
received
17
14
input from
receiver
Holtek
HT12D
Decoder
1
2
3
4
5
6
7
8
9
51k
15
16
LED
Flashes for each
receive pulse
330
7402
+5
160k
Mono-
Stable
1.0 min
555
Timer
100k
100uf
0.1uf
To Piezo
Device
7402
+5
One-
shot
3.0 sec
555
Timer
100k
18uf
0.1uf
Schematic of Decoder Circut

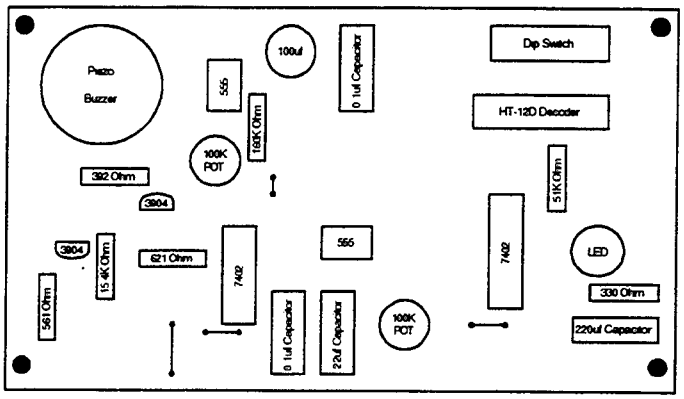

Overview of Decoder Circut
Drawn By: Allyn Crowe
HSAP Apprentice 1995, 1996
7-9-96
Scale -1:1

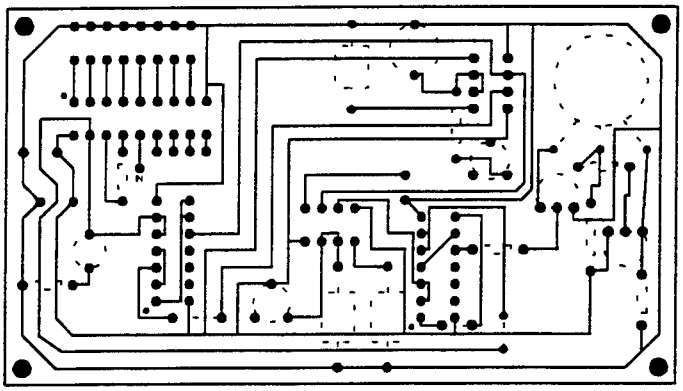

Decoder Circut Path Layout
Drawn By: Allyn Crowe
HSAP Apprentice 1995, 1996
7-8-96
Scale ~1:1

```
CLS
CLEAR
LOCATE 10
PRINT "*************************************************************************"
PRINT "*****   This is a program for generating Maximal Length              *****"
PRINT "*****   Sequences.  It was taken from the original                   *****"
PRINT "*****   program Sequence that was written by Allyn Crowe             *****"
PRINT "*****   and Jason Leopold.  This program was written by              *****"
PRINT "*****   Allyn Crowe with assistance from Michael Powell.             *****"
PRINT "*************************************************************************"
SLEEP 2
INPUT "PRESS ENTER TO CONTINUE"; Z$
CLS

INPUT "ENTER THE INITIAL FILL OF THE REGISTER "; IN$
    REM IN$ = STR$(IN)
    N = LEN(IN$)

12
INPUT "DO YOU WANT TO INPUT THE TAP CONDITION USING AN OCTAL NUMBER "; ans$
    IF ans$ = "N" THEN GOTO 7
    IF ans$ <> "Y" THEN GOTO 11

REM ***** This is the part of the program that converts the octal *****
REM ***** number to binary form.                                  *****
INPUT "ENTER THE OCTAL NUMBER FOR THE TAP CONDITION"; O
    O$ = STR$(O)
    LENGTH = LEN(O$)
    BIN$ = ""
    FOR CON = 2 TO LENGTH
        SECNUM = VAL(MID$(O$, CON, 1))
        BIT1 = INT(SECNUM / (4))
        NEXTPART = SECNUM MOD (4)
        BIT2 = INT(NEXTPART / (2))
        BIT3 = NEXTPART MOD 2
        BIN$ = RIGHT$(STR$(BIT3), 1) + RIGHT$(STR$(BIT2), 1) + RIGHT$(STR$(BIT1), 1) + BIN$
    NEXT CON

REM ***** This part of the program defines the arrays to be used,  *****
REM ***** calculates the number of bits that should be generated   *****
REM ***** for a m-sequence, and places all of the initial values   *****
REM ***** that are in string form into an array.                   *****
3
DIM R(N + 1), X(N + 1), T(N + 1), F(N + 1)
N1 = N + 1
L = 2 ^ N - 1
M = 0
FOR I = 1 TO N
R(I) = VAL(MID$(IN$, I, 1))
NEXT I
FOR I = 1 TO N
F(I) = R(I)
NEXT I
FOR I = 2 TO N1
T(I - 1) = VAL(MID$(BIN$, I, 1))
NEXT I

REM ***** This is the part of the program that identifies the  *****
REM ***** the number of taps.                                  *****
2
J = 0
FOR I = 1 TO N
IF T(I) = 1 THEN GOTO 6
5
NEXT I
```

```
REM ***** This is the actual calculation part of the program. It      *****
REM ***** uses the Exclusive Or function to generate the next bit.    *****
REM ***** It also prints the last bit in the register and counts      *****
REM ***** how many it has printed so it can check later to see if    *****
REM ***** the sequence it generated is an m-sequence or not.         *****
X(0) = 0
FOR K = 1 TO J
X(0) = X(K) XOR X(0)
NEXT K
R(0) = X(0)
PRINT R(N); " ";
M = M + 1
IF M = 2 * L THEN GOTO 10

REM ***** This part of the program shifts all of the bits in the  *****
REM ***** register over to the next register.                      *****
FOR I = N TO 1 STEP -1
R(I) = R(I - 1)
NEXT I

REM ***** This is the part of the program that checks the register  *****
REM ***** to see if it is the same as the initial register. If it   *****
REM ***** is not then it repeats back anmd does the whole process  *****
REM ***** again. If it is and it is the right length then it       *****
REM ***** tells you it is a m-sequence.                            *****
FOR I = 1 TO N
IF R(I) <> F(I) THEN GOTO 2
NEXT I
IF M = L THEN GOTO 1
PRINT : PRINT : PRINT "SEQUENCE IS NOT A M-SEQUENCE"
4
PRINT : PRINT "SEQUENCE IS "; M; " BITS LONG"
END
1
PRINT : PRINT : PRINT "SEQUENCE IS AN M-SEQUENCE"
GOTO 4

REM ***** This part of the program identifies where there are taps  *****
REM ***** and saves them so that it can work with them later.       *****
6
J = J + 1
X(J) = R(I)
GOTO 5

REM ***** This is the part of the program where you can enter the  *****
REM ***** tap condition in binary form instead of octal.           *****
7
PRINT "ENTER THE TAP CONDITION IN BINARY FORM STARTING WITH THE MOST"
INPUT "SIGNIFICANT DIGIT"; BIN$
Z$ = "1"
BIN$ = BIN$ + Z$
GOTO 3

10
PRINT "THIS SEQUENCE IS AN INDEFINITE SEQUENCE."
END

11
PRINT "YOU HAVE ENTERED AN INCORRECT RESPONSE MAKE SURE THE CAPS LOCK IS ON"
PRINT "AND TRY AGAIN."
GOTO 12
```

Octal Conversion Program:

```
CLEAR
CLS
REM octal2
REM ************************************************************
REM ******* This is a program used to convert octal numbers      *******
REM ******* to binary.  It was written by Micheal Powell,       *******
REM ******* and edited by Allyn Crowe.                          *******
REM ************************************************************
INPUT "Enter the Octal Number"; O
A$ = STR$(O)   'Puts the Octal number into a string
L = LEN(A$)    'defines the length
Bin$ = ""      'creates the string which will be used for the binary numbers
PRINT : PRINT "Octal number is:"
FOR con = 2 TO L  ' 2 because it reads strings with an extra bit on the front
REM ** This is the conversion part of the program **
  secnum = VAL(MID$(A$, con, 1))
  PRINT secnum;
  bit1 = INT(secnum / (4))
  nextpart = secnum MOD (4)
  bit2 = INT(nextpart / (2))
  bit3 = nextpart MOD 2
  Bin$ = Bin$ + STR$(bit1) + STR$(bit2) + STR$(bit3)
NEXT con
PRINT : PRINT : PRINT "Converted to Binary it is:": PRINT Bin$
END
```

Shell Program:

```
REM shell 1
CLS
CLEAR
REM ***************************************************
REM **   This is a program that incorporates several      **
REM **   different programs into one easy to use menu      **
REM **   system.  It uses the programs: Sequence, a        **
REM **   program to generate maximul length sequences,     **
REM **   and Massey's Algorithm, a program to find the     **
REM **   key and key length from a binary data string.     **
REM **   They are effectivly the opposit of each other     **
REM **   and can be used to decode a maximul length        **
REM **   sequence.                                         **
REM **                                                     **
REM **   This program was written by Allyn Crowe.          **
REM **   The program Sequenc2 was taken from the           **
REM **   original that was written by Allyn Crowe and      **
REM **   Jason Leopold.  It was written by Allyn Crowe     **
REM **   with assistance from Michael Powell.              **
REM **   The program Massey's Algorithm was converted      **
REM **   to basic by James Stephens.                       **
REM **   The Octal Conversion program was written by       **
REM **   Michael Powell and modified by Allyn Crowe.       **
REM ***************************************************
1
KEY OFF: SCREEN 0: WIDTH 80: CLS
LOCATE 10, 5
PRINT "          MAXIMUL LENGTH SEQUENCE TOOLS MENU"
PRINT "          1) GENERATE A SEQUENCE"
PRINT "          2) DECODE A SEQUENCE"
PRINT "          3) CONVERT AN OCTAL NUMBER TO BINARY"
PRINT "          4) EXIT"
PRINT : INPUT "          WHICH ONE DO YOU WANT TO DO "; A
IF A = 1 THEN CHAIN "SEQUENC2.bas"
IF A = 2 THEN SHELL "SR_MASY2.exe"
IF A = 3 THEN SHELL "OCTAL2.exe"
IF A = 4 THEN END
IF A < 0 THEN GOTO 2
IF A > 4 THEN GOTO 2
2
    CLS
    LOCATE 12, 5
    PRINT "   YOU HAVE ENTERED AN INCORRECT SELECTION, PLEASE TRY AGAIN."
    SLEEP 3
    GOTO 1
```

Polymerization Mechanisms for Electrodeposited Polypyrrole

Aaron Davis
High School Apprenticeship
Fuzes Branch

Wright Laboratory Armament Directorate
WL/MNMF
Eglin AFB, FL 32542-5434

Final Report for:
High School Apprenticeship Program
Wright Laboratory Armament Directorate

Sponsored by:
Air Force Office of Scientific Research
Bolling Air Force Base, Washington D.C.

August 1996

Polymerization Mechanisms for Electrodeposited Polypyrrole

Aaron Davis
High School Apprentice
Fuzes Branch
Wright Laboratory Armament Directorate

Abstract

Experiments were performed to determine possible mechanisms for the electropolymerization of the conductive polymer polypyrrole. The conditions required for electrodeposition of polypyrrole support electrolysis. It was conjectured that the hydrogen ion concentration around the growing polypyrrole affects the conductivity of the film. An electric field with positive or negative potential was used to alter the hydrogen ion concentration. The resulting conductive polymer films were then measured for conductivity and thickness.

Polymerization Mechanisms for Electrodeposited Polypyrrole

Aaron Davis

Introduction

Prior to the past several years synthetic polymers have been viewed purely as insulators. Now they are considered as a future source of electronic materials [1]. Polymers were first developed as non-conductive hydrocarbons because they satisfied applications which demanded low cost, light weight, and flexibility. Inherently conductive polymers [2] can also exhibit these characteristics. It is foreseen that someday conductive polymers will replace conventional materials in numerous applications ranging from electronic circuits and components to power transmission lines.

The conditions required for electrodeposition of the electrically conductive polymer polypyrrole from aqueous solution will tend to favor electrolysis (see Fig. 1). It is hypothesized that the mechanisms of electropolymerization of polypyrrole involve electrolysis which affects the concentration of free oxygen and hydrogen dissolved in the solution. The quality of the film seems to depend on the supply of free hydrogen released during electrolysis in aqueous depositions performed.

Discussion of Problem

Electrochemical polymerization is one of the best methods for synthesizing conductive polymers because their growth and thickness can be controlled [2]. Early reports of the electrosynthesis of polypyrrole suggested the use of non-aqueous solvents such as acetonitrile [3] or propylene carbonate [4,5]. These provisions have been found unnecessary for bulk preparations [6]. It is believed that the best results have been obtained via electrosynthesis from aqueous solution. The purpose of this project is to gain insight into the mechanisms for the electrodeposition of polypyrrole.

Methodology

During this project there were a few things that were held constant. The conductive polymer used was polypyrrole (PPY). This conductive polymer was doped with dodecylbenzenesulfonate (DBS). The dopant is a concentration of impurities that drastically modifies the electrical conductivity of the polymer at room temperature [1]. While the polymer type was constant for the duration of the project, the molarity of solution was altered. The first three solutions consisted of 0.1 M PPY and 0.1 M DBS. Subsequent solutions were both 0.05 M PPY and 0.05 M DBS. There has been previous documentation that there is no noticeable difference in the conductivity of the films made with different molar solutions [7].

The first task was to test the hypothesis that deposition conditions favored electrolysis. A study was performed to model the relationship between electrolysis current and voltage. In order to alter the hydrogen ion concentration it was decided to introduce an electric field. There were three "rafts" made for this purpose (see Fig. 2).

The rafts were to be tested with three variables. The first was whether the raft was between the electrodes or behind the anode. Second, the voltage varied from 0 volts to 1750 volts. A high voltage power supply was used for this. Finally, the polarity of the field was altered from negative to positive. Alternating current was used in four of the trials but the films were very powdery and there was no way to test them for resistance. After these experiments were completed electrolysis was performed again. This time raft #2 was present in the process. The current densities and voltages verified that electrolysis had taken place during deposition.

On each of the conductive films grown electrochemically a set of calipers was used to measure the thickness of the film. A Signatone (model S-301-4) four point probe and a Hewlett Packard (model HP 34401 A) multimeter were used to measure the resistance of each film.

Results

The first electrolysis experiments showed that hydrogen gas bubbles resulting from electrolysis are

evident from a lead cathode at about 2.25 volts. Again after all of the experiments were over electrolysis was performed to conform the measurements. Hydrogen was noticed coming from the cathode around 2.25 volts.

Second, films of PPY were electrodeposited in the presence of electric fields. Raft #1 was the first to be experimented with. The raft was placed behind the anode and a positive potential of 60 volts was applied. This experiment showed no difference in the conductivity of the PPY film than what was achieved in the control experiments. When the raft was placed between the electrodes with a positive potential of 60 volts there was still no significant change in film conductivity.

The first raft used with the high voltage supply was an experimental design that failed. It leaked out a steady stream of current that interfered with the procedure. Raft #1 also had its problems during the project and became useless. The primary raft used was raft #2. Multiple trials were carried out with raft #2 placed either behind the anode or between the electrodes. A positive potential chosen between 0 and 1750 volts was employed. The majority of the trials produced no noteworthy results. The conductivity of the PPY films resembled those of the control experiments.

Next raft #2 was used with a negative potential. The range of voltage remained the same, from 0 to 1750 volts. While the positive field showed very few results, not enough to draw any conclusions, the negative field did. The negative potential was placed between the electrodes and this upset the whole solution. The films made were very resistive. The resistance of films of identical size increased linearly with applied voltage (see Fig. 3). The raft was then placed behind the anode. The films produced from these experiments were less conductive than the average of the positive trials but it was still lower than three or four of the positive potential films.

A few trials were performed with alternating current but very poor film quality was the result. Only two of the films remained intact and could be used for conductivity measurement. The third film was very powder like. The resistance of the measurable films was unusually high, approximately two to three orders of magnitude higher than normal.

The last electrolysis trials produced results that were similar to the data obtained earlier. The

control experiment showed signs of hydrogen evolving from the cathode at 2.25 volts. This is the same voltage required to decompose the water with a 250-volt potential behind the anode. Electrolysis was observed at 3.25 volts when the raft was placed between the electrodes with the same 250-volt applied potential. Electrolysis was still observed at 2.25 volts despite the presence of a negative potential, using a raft either behind the anode or between the cathode.

Conclusion

Electrodeposition of PPY from aqueous solution requires two reactions to occur. First, there needs to be reduction of water taking place at the cathode to give off hydroxide ions (OH^-) and hydrogen gas (H_2). Second, the oxidation of pyrrole at the anode generates PPY and hydrogen ions (H^+). When the reduction of water occurs, hydrogen molecules are dispersed throughout the solution. The electropolymerzation of pyrrole robs the electrons from the hydrogen molecules, producing hydrogen ions which hover around the anode. The hydrogen and hydroxide ions maintain charge balance in the solution.

It could be possible that the generated hydrogen ions can attach to the water and form hydronium ions (H_3O^+) which are believed to have no adverse effect on the growing PPY. If too many hydrogen ions are present near the growing PPY layer, non-conducting polymer chains (oligomers) tend to form within it. This is the reason that a small amount of water in non-aqueous solutions results in a better film. With water, the excess hydrogen ions can be used up via the formation of relatively stable hydronium ions.

The rafts affect the hydrogen ion concentration in the presence of the growing PPY film. When the raft is positive it helps to neutralize excess hydrogen ions. The negative field does the exact opposite. With a negative potential between the electrodes, the hydrogen ions are prevented from combining with water molecules. The excess H^+ ions then remain near the anode and cause the growing PPY film to have lower conductivity associated with increased oligomer content. In order to form a PPY film with optimum conductivity it is necessary to remove all of the hydrogen ions from the surface sites as the electrodeposited PPY molecules form.

References

1. J. Mort, "Conductive Polymers," Science 208, 819 (1980).

2. M. Aldissi, Inherently Conducting Polymers, Noyes Data Corporation (Park Ridge NJ) 1993.

3. K. K. Kanazawa, A. F. Diaz, R. H. Geiss, W. D. Gill, J. F. Kwak, J. A. Logan, J. F. Rabolt and G. B. Street, J. Chem. Soc. Chem. Commun. 1979, 854.

4. S. Panero, P. Prosperi and B. Scrosati, Spectrochim. Acta 32, 1465 (1987).

5. T. Osaka, K. Naoi, H. Sakai and S. Ogano, J. Electrochem. Soc., Electrochem. Sci. and Technology 134, 285 (1987).

6. R. K. Bunting (private communication).

7. D. Harrison, "High Surface Area Conductive Polymers," High School Apprenticeship Program Final Report, August 1992 (Wright Laboratory Armament Directorate, Eglin AFB, FL) p. 18-1 to 18-6.

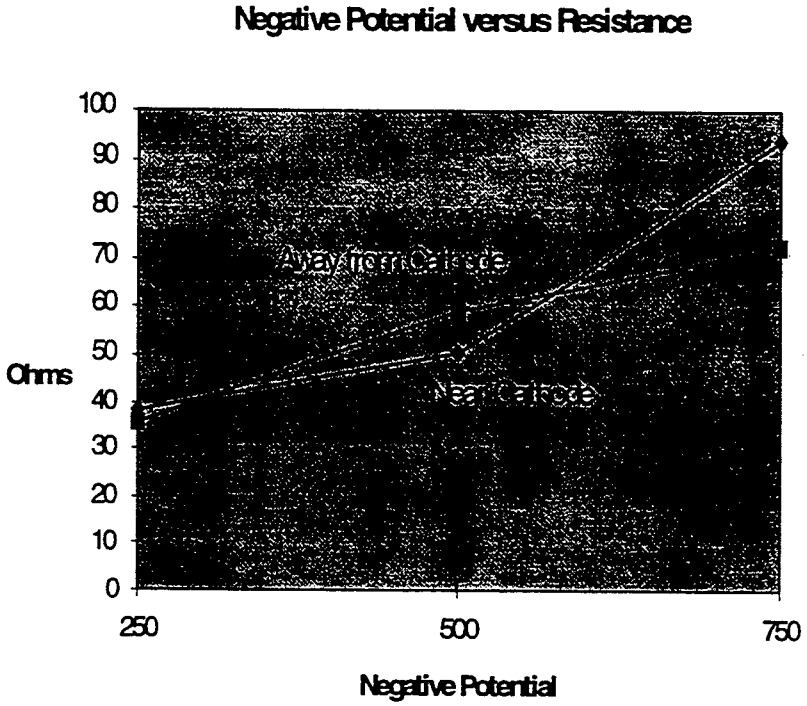

Figure 3. Graph of the negative potential versus resistance.

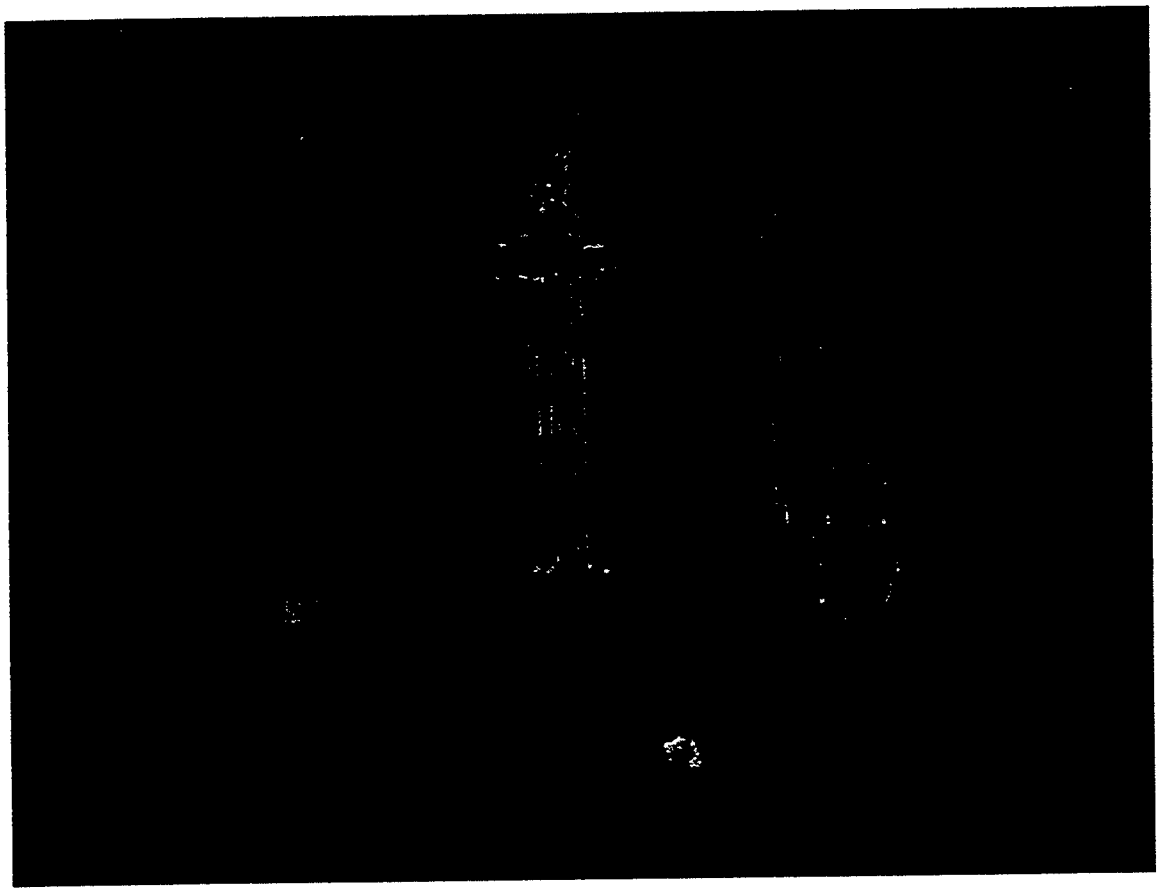

Figure 2. The three rafts used to apply electrostatic field (from left to right: #1, #2, and #3).

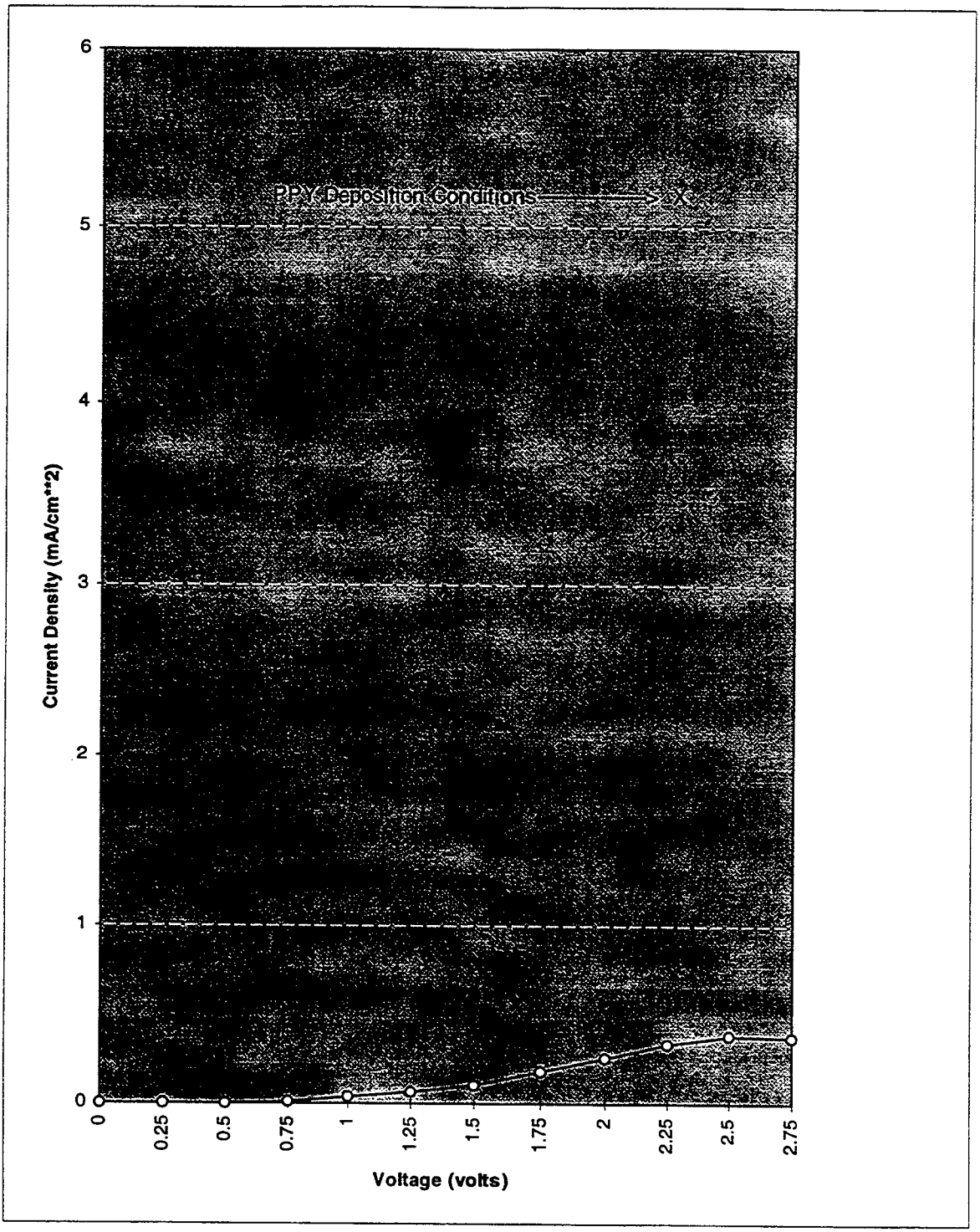

Figure 1. Current density versus voltage required for electrolysis (o) and electropolymerization (x).

Brad Day's report was not available at the time of publication.

INVESTIGATIONS OF THE IR BAND IN .1 MICRON INCREMENTS USING SYNTHETIC IMAGERY

Julie L. Deibler

Choctawhatchee High School
110 NW Racetrack Rd.
Fort Walton Beach, Fl. 32579

Final Report for:
High School Apprentice Program
Wright Laboratory

Sponsored by:
Air Force Office of Scientific Research
Bolling Air Force Base, DC
and
Wright Laboratory

August 1996

Investigations of the IR Band in .1 Micron Increments Using Synthetic Imagery

Julie L. Deibler

INTRODUCTION

Wright Laboratory's Irma software was used to investigate and generate multi-spectral infrared imagery. An investigation on how various objects in a scene change as you observe them at different wavelengths in the infrared was conducted. Irma models the spectral radiance of objects at various wavelengths and also takes into account the effects of the atmosphere at each wavelength. 120 synthetic images across the 1 to 12 micron IR spectral range in 0.1 micron increments were generated with Irma. Next a movie sequence of these images was generated to show how the IR signatures varies as the wavelength changes. This was done to observe the images at each wavelength. After Irma generated the scene radiance, it next accounts for the atmospheric effects by using either the HITRAN or LOWTRAN atmospheric attenuation models. As can be seen the atmosphere effectively blocks IR radiation from 5.5 to 7.5 microns and at 2.5 and 2.8.

PROCEDURE

Irma is the U.S. Air Force's premier research tool for high resolution, rendering, and signature prediction modeling that is used to generate synthetic imagery to develop and test aircraft sensors and smart, tactical weapons. Irma synthetically generates this type of required imagery at a fraction of the cost compared to conventional measurement techniques and is done from a desk top workstation in an office environment from the sensor's point-of-view. It is a

physics-based model possessing unique capabilities to address these weapon technology areas with pixel registration, common object geometry, and frame-to-frame correlation for different sensors. It is capable of integrating real, measured data with synthetically generated data. The thermal response module computes heat transfer of facet based target and background models and outputs the calculated facet temperatures or radiance for use by image generation and sensor effects modules.

Irma is capable of modeling the energy transfer both internal and external to the target's outer material layer. Optical and thermal properties of objects are specified with material IDs in the facet model files and indexed to the thermal properties file. The thermal properties file allows user definable operating conditions and temperatures for modeling thermal sources and sinks such as engines operating at different operating temperatures. Weather conditions are specified in the weather input file. The weather file contains not only weather conditions such as air temperature, relative humidity, wind velocity, and air pressure, but also data for the direct solar irradiance, earth albedo, skyshine, and earthshine radiance. Internal heat sources can be used to model effects such as engine heating. Environmental heat sources include direct and diffused solar heating, earthshine and skyshine heating, convective heat transfer, radiative heat transfer, and evaporative cooling. Irma can also provide multi-sensor correlated imagery for the emerging sensor fusion research technologies.

Irma consists of a number of computer programs tied together that run on a Unix workstation or personal computer and generates synthetic images from a sensor's view-point. Atmospheric transmittance data required by Irma for the IR region was produced using the software, Plexus. Next the output of Plexus needed to be put in a format that Irma could use. A Microsoft Excel spreadsheet software was used to do this.

SPECTRAL LOCATION OF ATMOSPHERIC ABSORPTION BANDS

For a 1000-ft. horizontal air path at sea level with 5.7mm precipitable water at 26°C temperature, within the wavelength interval from 1μ to 25μ.

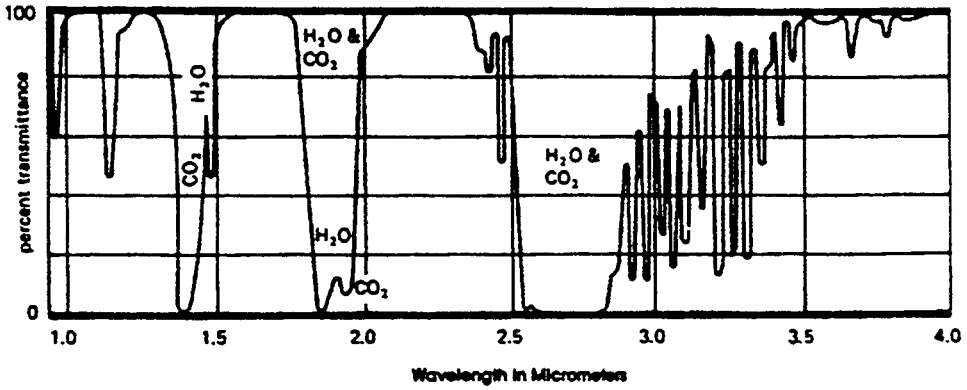

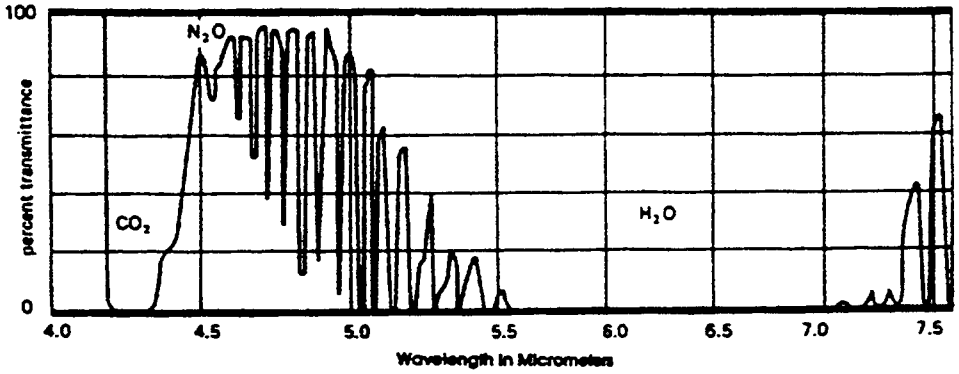

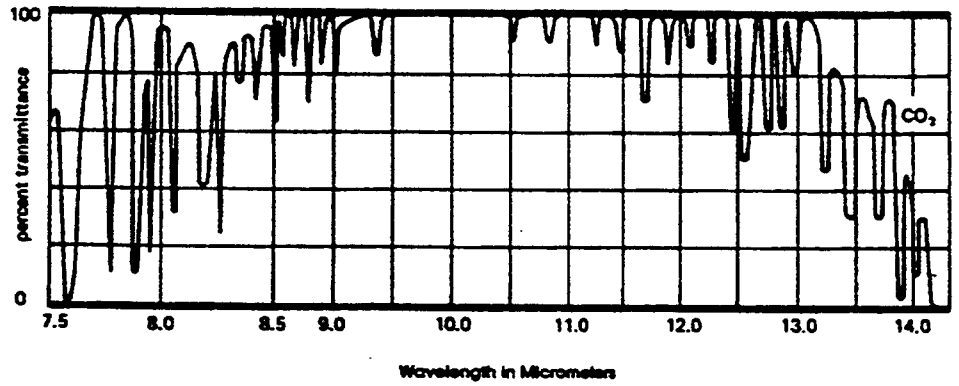

A scene that contained 17 trees, a T62 tank, and 2 bunkers was built first. Figure 2 is a gray scale image of the scene.

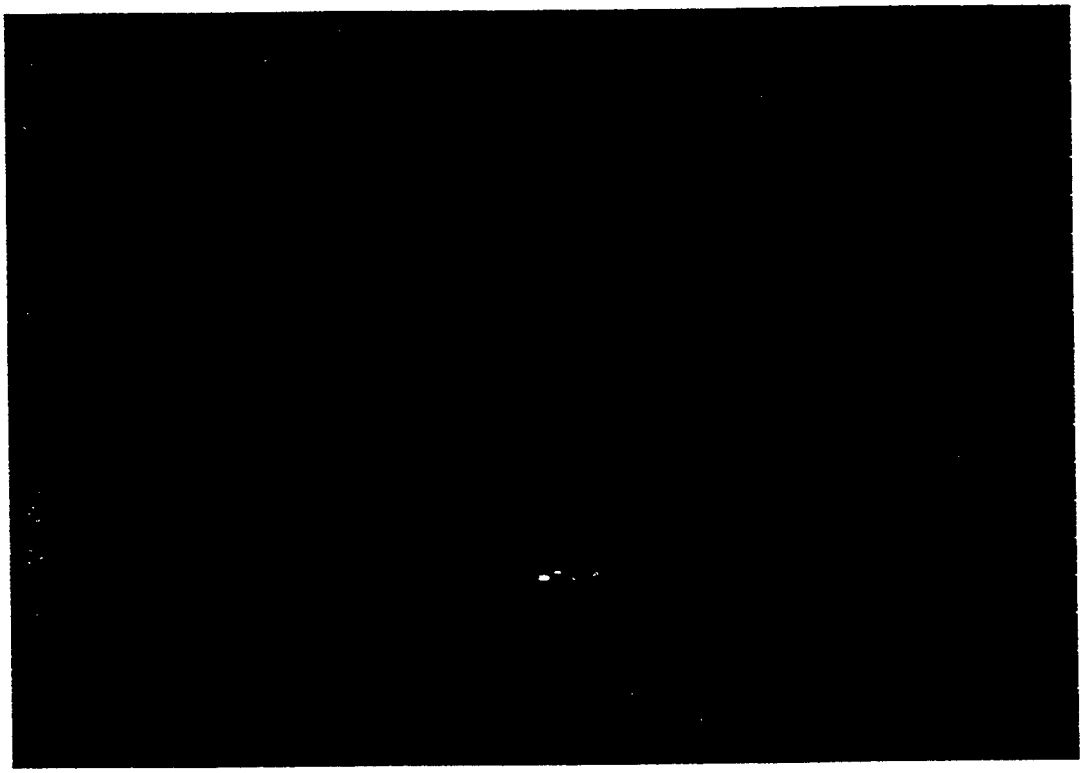

Figure 2. The original Irma image.

The material properties were assigned to each object. The trees were assigned wood, the bunkers, cement, and tanks appropriate metal. Next a spread sheet created with Plexus provided the necessary data to run the Irma program at .1 micron increments from 1-12 micron was developed. The intensity of each image was scaled from 0 to 256 to increase the contrast of the objects and make the images more meaningful. These images were then made into tagged image file graphics format type so that they could be used by the Wright Laboratory video tool on the silicon graphics computer to make a movie. Example images at 2.1, 3.6, and 9.4 micrometers are shown in figures 3,4,5.

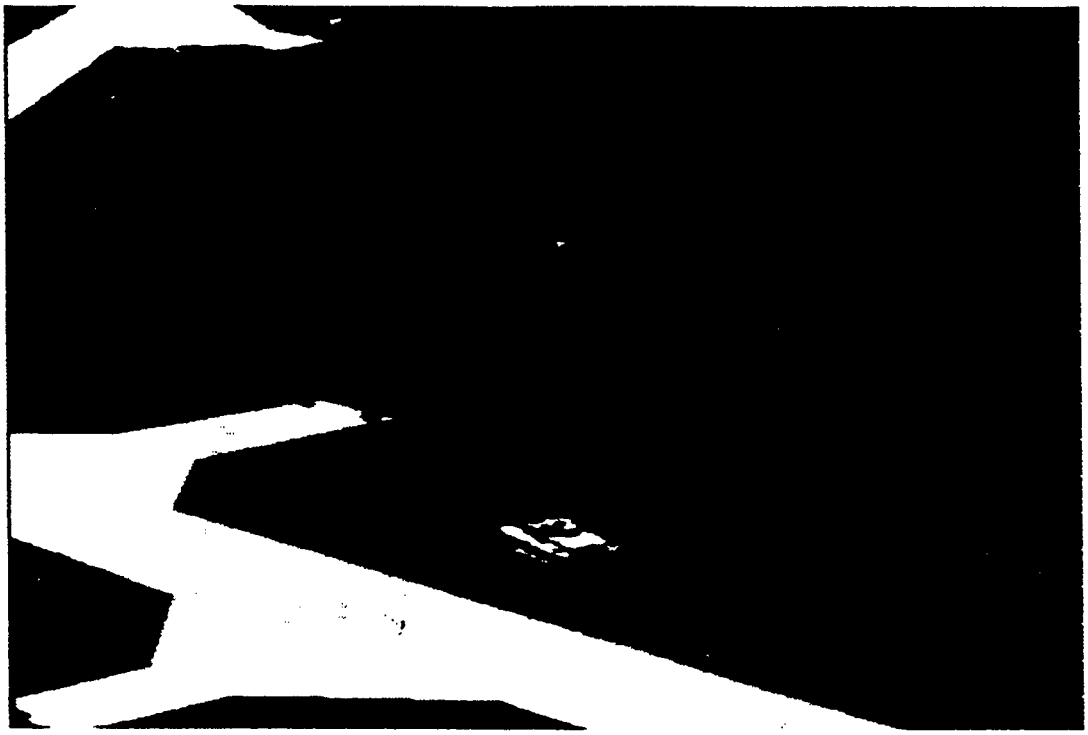

Figure 3. Irma image at 3.6 microns, the best wavelength for tank detection.

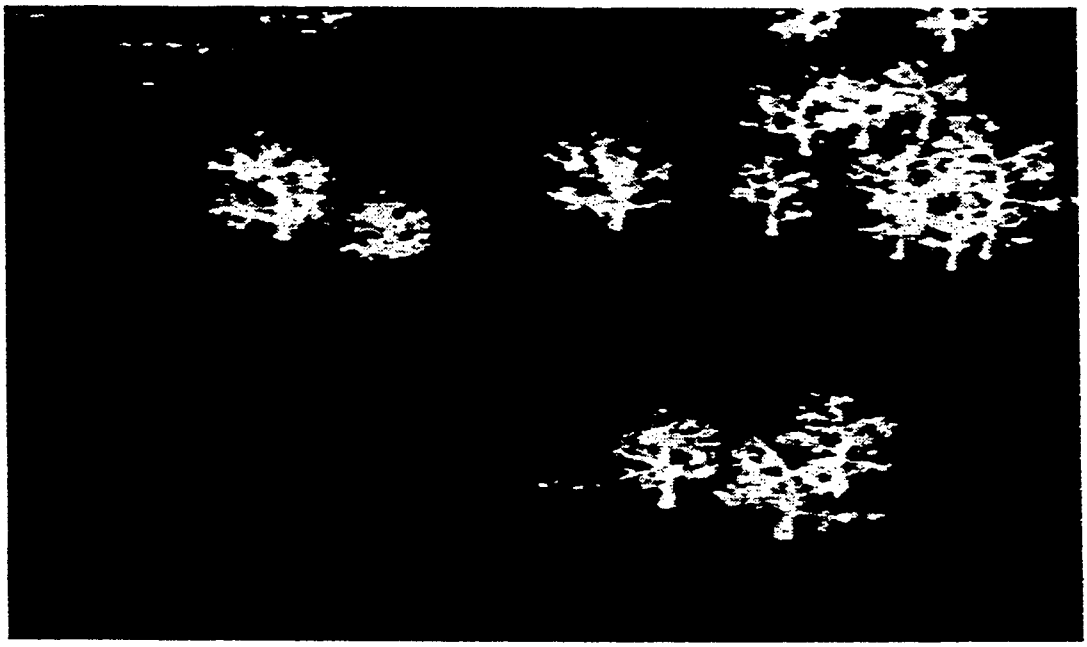

Figure 4. Irma image at 9.4 microns, the best wavelength for detecting the tank engine.

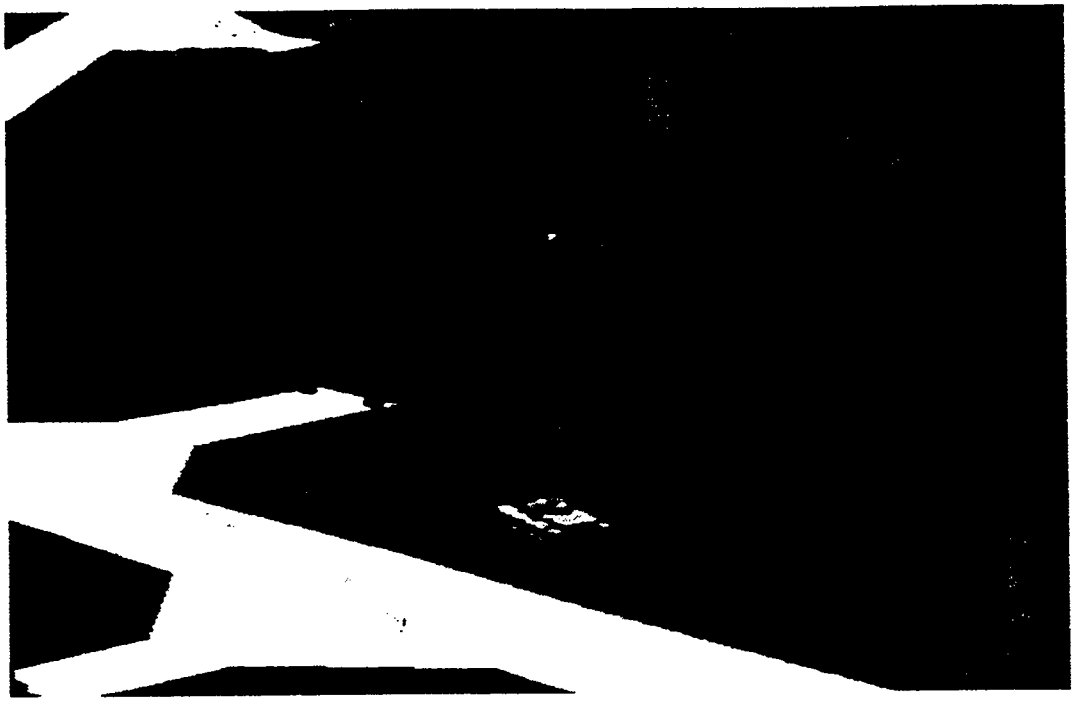

Figure 5. Irma image at 2.1 microns, the best wavelength for detecting the bunkers.

Everything is constant in each image only the wavelength changes. With the results of the Irma model a movie showing how the intensity changes with the wavelength was made. With this information, it was possible to determine which objects showed the most contrast at each specific wavelength.

RESULTS

The tank stands out the best at 3.6 microns, figure 3 the tank engine stands out the best at 9.4 microns, figure 4 and the bunkers stand out the best at 2.1 microns figure 5. One sequence of images was individually scaled to increase contrast, however; this effectively removed the atmospheric effects. In a second sequence, the entire set of images were scaled from 0 to 256 thereby shows the atmospheric effects. This sequence shows the image fading in and out as the atmospheric transmission changes.

CONCLUSION

Based on this analysis, if someone is trying to build a sensor to find various objects, it is possible to find the wavelength that the object shows up the best, just as if you were trying to find a red object, it would be best to have a red filter so all you see are the red objects. If you are trying to find a tank you would use a filter that only lets in 3.6 microns, or if you are looking for a bunker 2.1 microns.

ACKNOWLEDGMENTS

I would like to thank my mentor Lee Prestwood for all of his guidance and support this summer. I also thank Wright Laboratory for the opportunity to work here and providing the necessary equipment to do this project.

BIBLIOGRAPHY

Chenault, Flynn, McCarley. Thermal Response Modules for the Irma Signature Generation Code. August 23, 1995.

Blume, Vechinski, Witherspoon, Dubey, Flynn. Minefield Image Synthesis Tool. April 19, 1995.

Irma 4.0 User's Guide. November 21, 1995. WL/MNG.

MULTIPLE QUANTUM WELLS IN THE SEMICONDUCTOR MATERIAL $GaAs/Al_xGa_{1-x}As$ and COMPUTATIONAL CHEMISTRY

Cindi L. Dennis

Beavercreek High School
2660 Dayton-Xenia Rd.
Beavercreek, OH 45434

Final Report for:
High School Apprenticeship Program
Wright Laboratory

Sponsored by:
Air Force Office of Scientific Research
Bolling Air Force Base, Washington DC

and

Wright Laboratory

July 1996

MULTIPLE QUANTUM WELLS IN THE SEMICONDUCTOR MATERIAL $GaAs/Al_xGa_{1-x}As$

Cindi L. Dennis

Introduction

The term semiconductor indicates that under certain conditions, the material will conduct electricity and under different conditions, it will act as an insulator. For example, in this experiment, as the sample cooled down, its resistance increased dramatically (Fig. 1.1) because fewer electrons (or holes) have the necessary energy (provided by the temperature) to be excited from their ground states into higher energy conducting states. As the temperature decreases, more electrons (or holes) are "frozen" into the ground states of the impurity atoms. Thus, this material acts as a semiconductor, conducting better under certain conditions than others.

To make a semiconductor, holes or free electrons (which are the mobile charged particles required to conduct electricity) are necessary. Since, a pure material is not usually desirable, the semiconductor is intentionally doped with an impurity to provide the holes or electrons. There are two types of dopants, p-type and n-type. If the semiconductor is doped with an element that has more electrons in its valence orbitals than the material it is replacing in the lattice, the semiconductor

Fig. 1.1 Resistance versus Temperature for KGE10GB-A

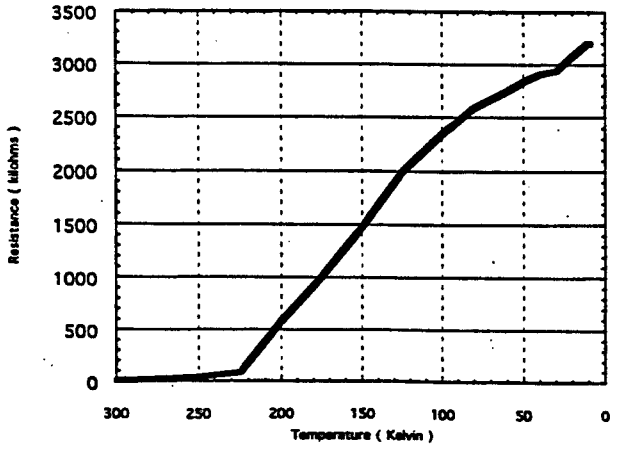

is called n-type (negatively charged). If the semiconductor is doped with an element that has fewer electrons than what it is replacing in the lattice, it is called p-type (positively charged). For example, in this semiconductor of GaAs, the dopant is beryllium. This makes it a p-type semiconductor because beryllium has fewer electrons than the gallium it is replacing.

By doping a material and then freezing out almost all of the electrons (or holes), a detector can be formed from a semiconductor. In this experiment, an infrared detector is formed due to the creation of quantum wells in the $GaAs/Al_xGa_{1-x}As$. Quantum wells are formed when there is a conduction or valence band offset in energy at the heterostructure interface. This energy offset is due to a difference in the bandgap between the alternating compositions. Interfaces are created by sandwiching a layer of a small band gap material between two layers of wide band gap material. Due to the thinness of the layers and the heterojunctions at the interfaces between the materials, the electrons are trapped within the wells and the energy levels in them show the quantum effects associated with electron confinement. Therefore, the continuous levels associated with a macroscopic thickness become discrete allowed energy levels in the very thin layers.

The actual values of the discrete energy levels in the quantum wells are determined by the thickness and the depth of the well. (The depth of the well is controlled by the aluminum concentration.) The allowed electron or hole energies are quantized by the presence of two potential energy barriers formed by the wide bandgap material. As a result, the depth of the well is the band discontinuity of the two materials, called conduction band discontinuity for electrons and valence band discontinuity for holes. Further control of the discrete energy levels is provided by varying the well width. Wider wells contain more bound states that are closer in energy than the bound states in narrower wells.

Molecular beam epitaxy and metalorganic chemical vapor deposition make it possible to deposit the multilayer heterojunctions that form the quantum wells. These two processes can form abrupt interfaces between atoms and control the dopant concentration in individual monolayers only a few Angstroms thick. This allows what is called "band-gap engineering," which can be used to precisely control the characteristics of the quantum wells.

When many quantum wells are grown on top of one another, two different types of structures can be formed depending on the thickness of the barrier layer. Multiple quantum wells are formed when the barrier layers are thick enough that the electron wave functions in adjacent quantum wells do not overlap. If the barrier walls are thin enough that tunneling between walls is significant, then the structure is called a superlattice. The concept of the superlattice was first proposed by Esaki and Tsu in 1969. [2] In a superlattice, the electron wave functions overlap and the discrete electron transitions in the isolated wells become minibands (Fig. 1.2).

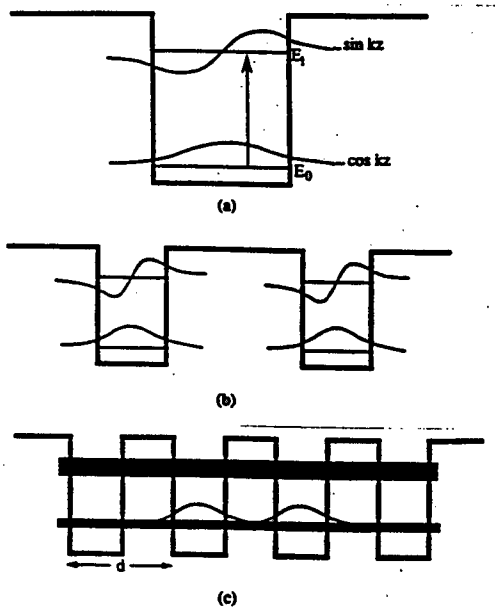

Fig. 1.2 A schematic representation of GaAs/AlGaAs conduction bands. (a) Two bound energy levels and wave functions are in a finite isolated quantum well; the vertical arrow indicates a possible transition between these levels, which is known as the *intersubband transition*. (b) A multiple quantum well structure is formed by choosing thick barrier layers. (c) Periodic potential wells of a period *d* superlattice form where the energy levels in each quantum well are overlapped to form minibands.

The properties of a superlattice are controlled by the artificial periodicity introduced by the multilayer structure. They can be varied by the choice of materials for the heterojunctions and also by barrier and well thickness. The internal strain field of a heterostructure constructed from two semiconducting materials with mismatched lattice constants can be used to shift the band structure of the superlattice to form what is known as a strained-layer superlattice. Two types of superlattices, type I and type II, can be formed. Type I superlattices have both band edges of the smaller bandgap material below those of the wide band gap material (i.e. the conduction and valence bands are formed in the same layer). In type II superlattices, the top of the valence band layer lies above the bottom of the conduction band of the other layer producing a staggered band offset.

Absorption of certain wavelengths of infrared radiation results from the interband transitions in the semiconductor. The transitions in GaAs/$Al_XGa_{1-X}As$ are a direct result of the impurity level of beryllium ($10^{18}/cm^3$). If the material is not doped, then no photon absorption occurs because there are no electrons or holes in the ground state. The absorption strength thus depends upon the number of electrons in the ground state as well as the number of unoccupied excited states. Specifically, long-wavelength infrared radiation absorption in GaAs/$Al_XGa_{1-X}As$ is caused by the intersubband transition between the ground state and first excited state in the quantum wells. This can be a bound-to-bound transition or a bound-to-continuum transition (Fig. 1.3). As an optical excitation mechanism in infrared detectors, the bound-to-continuum transition is favored. This transition is caused by two intersubband states, one bound within the quantum well and the other lying slightly above the potential barrier surrounding the well. This transition is formed by narrowing the width of a well with two intersubbands within it, causing the

upper one to move to the top of the well. Infrared response is usually a broad band in the case of a bound-to-continuum transition.

A narrow band and stronger photoresponse can be obtained by designing the quantum well so that the excited subband is just below the top of the barrier conduction band. In the latter case, the electrons will tunnel through a small potential barrier. At very high energies, the electrons in the extended continuum states become more like free electrons, causing a slow decrease in the absorption. Therefore, more energies are allowed and more infrared radiation wavelengths can provide enough energy to excite the electrons. However, this results in more noise which can only be eliminated by cooling most infrared detectors down below 70K. Above 70K, there is enough thermal energy available to excite the electrons into tunneling through the barrier walls, causing a significant dark current.

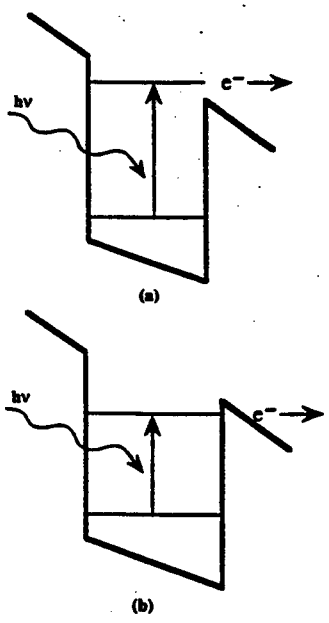

Fig. 1.3 Bound-to-continuum transition (a) and bound-to-bound transition (b) in a GaAs/AlGaAs quantum well structure under an applied electric field.

Problem

It has been shown that p-type multiple quantum wells eliminate the gratings that are necessary for n-type multiple quantum wells to detect incident light rays. Current research on the p-type multiple quantum well structure is choosing the theory that best matches the experimental data. By determining the theory that gives the most accurate energy for the bandgap, detectors can be designed to meet specific requirements such as the range it detects in. This is done by matching photoluminescence data with the experimentally determined energy gap. Future research will optimize the dopant density and thickness of the well size.

Methodology

The GaAs/$Al_xGa_{1-x}As$ multiple quantum well structures were grown using molecular beam epitaxy. A heavily doped GaAs epitaxial contact layer was grown onto a GaAs substrate. Next, the GaAs/$Al_xGa_{1-x}As$ multiple quantum well structure was grown. Then another heavily doped GaAs epilayer was grown to serve as a top electrical contact. This layered structure was then etched into mesas 4mm x 4mm, and indium solder was used to bond gold wires to the top and bottom contact layers.

Following this lengthy manufacturing process, the sample was mounted into the spectrometer using vacuum grease to attach it to the coldhead. The gold wires were indium soldered to external wires for measurement of the photoresponse, an electrical current. A vacuum was then pulled on the sample, allowing it to be cooled down in a vacuum to a temperature of 9 Kelvin. Measurements were made using a long wavelength infrared beam to excite electrons in the heavy hole 1 level to the light hole 2 level. Tests were run using different voltages and different temperatures up to approximately 70 K where thermal excitation of the electrons or holes began to override the response from the infrared excitation.

Results

As the voltage is increased, the signal strength increases until the electric field has induced all mobile electrons to move. Then, increasing the bias has no effect. In addition, a zero bias produces a sudden drop in the middle of the slow descent from the peak. The cause of this sudden drop is only conjecture at this time and will require further investigation to explain.

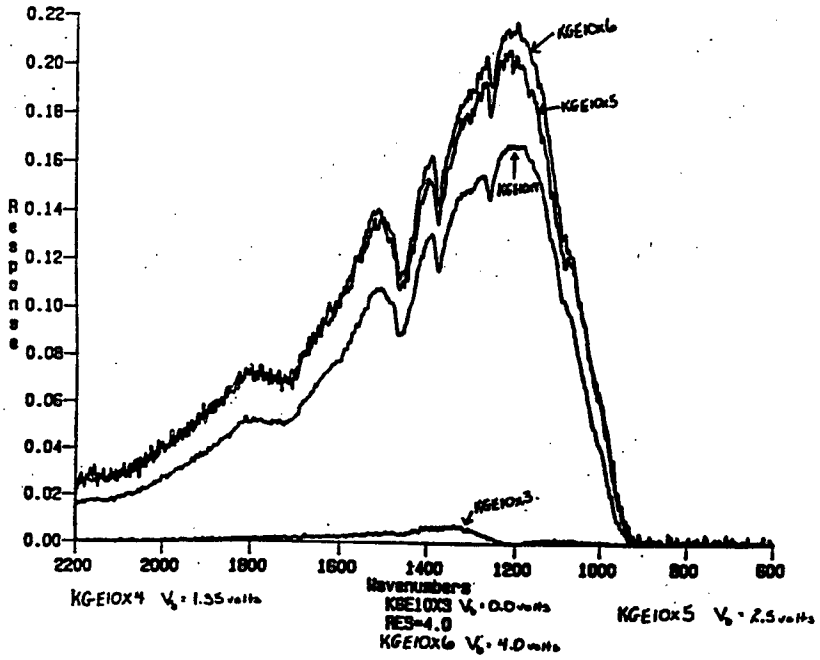

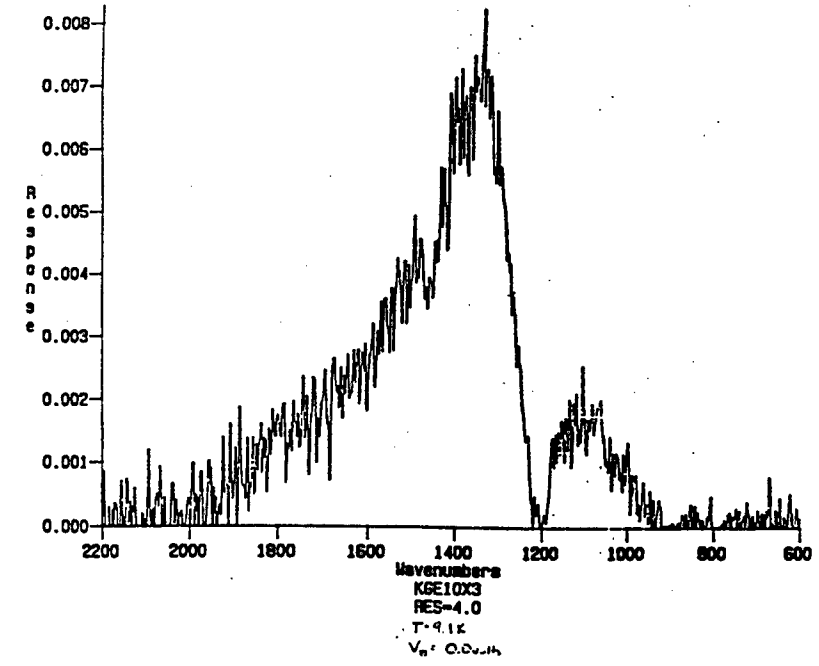

As the temperature rises, the amount of background noise increases as the signal strength decreases. The clear photoresponse degenerates into a noisy, weak peak as the temperature rises from 8.9K to 51 ±2K at a constant bias of 2.5 volts. The intervals were approximately 10K apart.

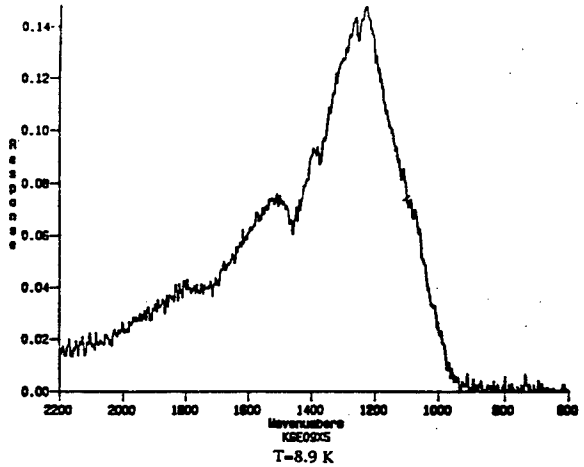

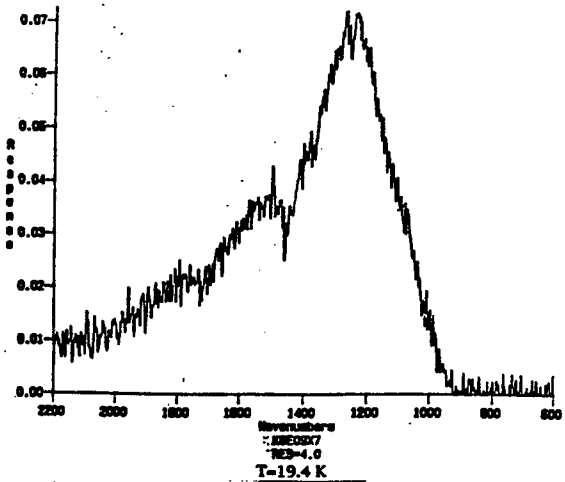

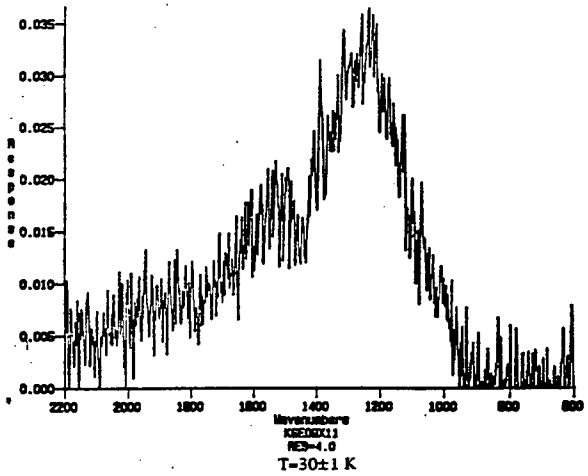

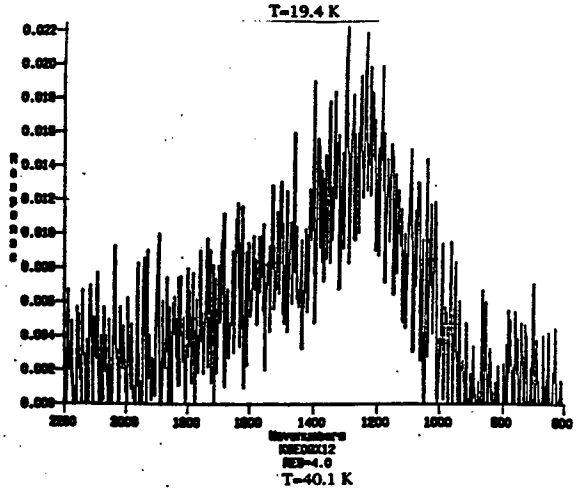

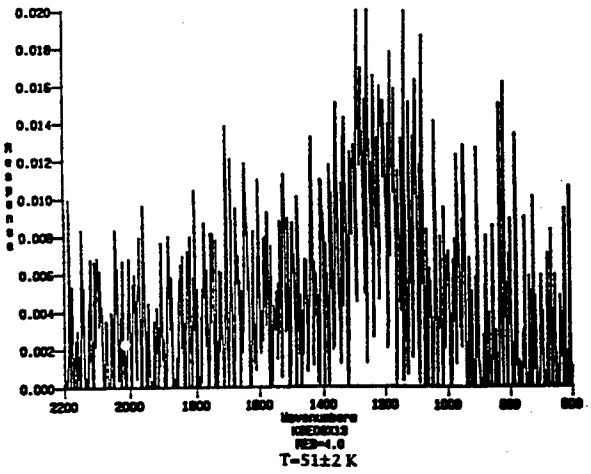

The current theories calculate the energy of the peak in electron volts based upon well width and aluminum composition. By matching photoluminescence data with the experimentally determined energy gap, the parameters for a detector in a certain range can be determined and then the detector can be made. The formulas are: Model A = 1.427x, 38:62; Model B = 1.247x, 40:60; and Model C = 1.427x, 40:60. The ratio refers to the aluminum concentration over the gallium concentration. This gives the band gap between the first heavy hole level and the second light hole level. The results are below.

MQW Variables		PL Results		Theory	
Well Width	Al Composition	Peak	Model A	Model B	Model C
40	30	1.68	1.683	1.672	1.682
30	30	1.677	1.683	1.672	1.682
60	30	1.652	1.658	1.6497	1.658
42	28	1.636	1.639	1.632	1.638
50	32	1.611	1.611	1.606	1.6104
50	32	1.601	1.611	1.606	1.6104
45	30	1.615	1.622	1.617	1.622
48	33.4	1.628	1.626	1.6203	1.625
55	32	1.595	1.599	1.5956	1.599
56	29.2	1.6095	1.609	1.604	1.608
50	30	1.619	1.609	1.604	1.608
50	30	1.616	1.609	1.604	1.608
50	30	1.613	1.609	1.604	1.608
57	37	1.602	1.601	1.599	1.602
76	15	1.551	1.557	1.555	1.557
76	15	1.548	1.557	1.555	1.557
75	30	1.57	1.568	1.566	1.567
75	30	1.561	1.568	1.566	1.567
75	30	1.554	1.568	1.566	1.567
75	30	1.551	1.568	1.566	1.567

Note: The shaded boxes indicate that the data was determined by X-ray diffraction.

Conclusion

When the calculations were run comparing the experimental energy of the peak value with the calculated value, the best match of data came using Model C. However, Model A is also within the range of experimental error and therefore, more conclusive tests are needed before either model can be judged the best with certainty.

References

1. Dr. Gail J. Brown, mentor, Wright Laboratory, WL/MLPO, Wright Patterson Air Force Base.

2. Esaki, L., and Tsu, R., *IBM Journal of Research and Development*, Vol. 14, 1970, p. 61.

3. Manasreh, M. O. , Editor, *Semiconductor Quantum Wells and Superlattices for Long-Wavelength Infrared Detectors*, Artech House, Boston, Mass, 1993, pp. 1-15.

4. Bube, Richard H. , *Electrons in Solids: An Introductory Survey*, Academic Press, Inc. Harcourt Brace Jovanovich, Publishers, New York, 1988, pp. 226.

COMPUTATIONAL CHEMISTRY

Cindi L. Dennis

Introduction

Several different approaches were used in this study. It involved three energy minimization algorithms as well as two semi-empirical energy algorithms. Each of these provided information about the molecules.

Energy Minimization - There are several different algorithms that can be used to minimize a structure (i.e. find the lowest energy form). The three most common algorithms are Steepest Descents, Conjugate Gradients, and Newton-Raphson. Two of these depend upon a line search. The line search is basically a one-dimensional minimization along a given direction. If the given direction is the gradient, then the one-dimensional surface can be expressed parametrically by a new one-dimensional coordinate, α

$$x' = x + \alpha \frac{\partial E}{\partial x} | xy$$

$$y' = y + \alpha \frac{\partial E}{\partial y} | xy$$

where (x', y') are the coordinates along the line away from the current point, (x_o, y_o), in the direction of the gradient at (x_o, y_o), $(\partial E/\partial x, \partial E/\partial y)_{x_o, y_o}$.

The general strategy of the line search is to converge on the actual minimum by successive iterations. It extracts all energy from one direction before moving on to the next. As a result, the gradient at the minimum of the line search must be perpendicular to the previous direction. However, due to the number of function evaluations needed to find a one-dimensional minimum (three to ten), line searches are inefficient.

In **Steepest Descents**, the line search direction is simply taken as the gradient. After each line search, the old direction is replaced with the gradient at the new point and the process is started all over again. However, this method leads to oscillations on the way to the minimum, causing it to retrace progress made earlier. As a result, the best time to use Steepest Descents is for the initial search for the minimum. It is efficient with large gradients. Only as the gradients approach zero at the minimum does Steepest Descents become inefficient due to the overcorrection for previous directions' deviations from the path to the minimum.

Conjugate Gradients attempts to eliminate the primary flaw of Steepest Descents by preventing the next direction vector from retracing progress already made. It produces a set of mutually conjugate directions so that each successive step continually refines the direction toward the minimum.

In this algorithm, $\mathbf{h}_{i+1}$ is the new direction vector leading from the point i+1 and is determined by adding the gradient at the point (i+1 , $\mathbf{g}_{i+1}$) to the previous direction $\mathbf{h}_i$ scaled by a constant γ_i.

$$\mathbf{h}_{i+1} = \mathbf{g}_{i+1} + \gamma_i \mathbf{h}_i$$

γ_i is a scalar defined as:

$$\gamma_i = \frac{g_{i+1} \bullet g_{i+1}}{g_i \bullet g_i}$$

This direction is then used to replace the gradient in the line search equations and a new line search is conducted. This means that the next gradient $\mathbf{g}_{i+1}$ will be perpendicular to all previous gradients and the new direction $\mathbf{h}_{i+1}$ will be conjugate to all previous directions. The following equation is another form of the one above for γ, when the function is a quadratic and where dE_i/dx and dE_i/dy are the derivatives of E at point i.

$$\gamma = \frac{(dE_b/dx)^2 + (dE_b/dy)^2}{(dE_a/dx)^2 + (dE_a/dy)^2}$$

Conjugate Gradients is the best algorithm for large systems where performing the calculations for the Newton-Raphson style algorithm is impractical if not impossible. However, derivations of the two equations for Conjugate Gradients assume that the function being minimized is quadratic. For a function that is not, Conjugate Gradients will minimize *ad infinitum* without ever converging.

Newton-Raphson uses not only the gradient (direction), but also the curvature of the function provided by the second derivative to minimize the function. The curvature is used to predict where the function will change directions (i.e. pass through a minimum). Since the complete second derivative matrix defines the curvature in each gradient direction, the inverse of the second derivative matrix multiplied by the gradient will contain a vector that will lead directly to the nearest minimum. The equation for this is

$$r_{min} = r_o - A_o^{-1}.\nabla V(r_o)$$

where $\mathbf{r}_{min}$ is the predicted minimum, $\mathbf{r}_o$ an arbitrary starting point, and A_o the matrix of second partial derivatives of the energy with respect to the coordinates at $\mathbf{r}_o$. When the function is a quadratic, A_o is a Hessian matrix given by:

$$A_o = \begin{pmatrix} \frac{d^2E}{dx^2} & \frac{d^2E}{dydx} \\ \frac{d^2E}{dxdy} & \frac{d^2E}{dy^2} \end{pmatrix}$$

By using this method, the minimum can be found without line searches and only a single evaluation of the gradient and the second-derivative matrix.

However, there are several problems with this algorithm. First, the terms in the Hessian matrix are difficult to derive and computationally costly for molecular force fields. When the structure is not harmonic and far from its minimum, the minimization can become unstable and diverge rapidly, especially if the initial

forces are too big (i.e. the path is too "flat"). Furthermore, the storage requirements for the Hessian matrix are huge and when the number of atoms in the molecule becomes greater than one thousand, it becomes impossible to calculate given the limits of today's computers.

Often, due to the disadvantages of this algorithm, a variation of the Newton-Raphson method is used, called "quasi-Newton-Raphson." It was developed by Fletcher and Powell.[2] It calculates the Hessian matrix numerically using only first-derivative information rather than the second-derivatives. As a result, the algorithm is faster, but because the second-derivative information is built up slowly, it behaves like Steepest Descents in the beginning and Newton-Raphson as the structure approaches the minimum. In principle, the quasi-Newton-Raphson method is no faster than Conjugate Gradients. However, in practice, it is less sensitive to line search convergence, and therefore, will converge faster without line searches. Newton-Raphson is the preferred method over quasi-Newton-Raphson only when a precise minimum is required (i.e. 10^{-8}).

Monte Carlo Search - Monte Carlo, used for the probable docking sites calculations, samples the conformational energy surface at random. It emphasizes the prediction of long-range residue-to-residue contacts when the secondary structure is well predicted in advance or is closely constrained to the observed secondary structure. It also assumes that the native structure of that molecule is the minimized form.

Semi-Empirical Calculation - MOPAC is a "general-purpose semi-empirical molecular orbital package for the study of solid state and molecular structures and reactions."[5] The semi-empirical Hamiltonians used to calculate the molecular orbitals, the heat of formation, and its derivative with respect to molecular geometry were MNDO, MNDO/3, AM1, and PM3.

Problem

In terms of stability, proteins may be more appropriate than other matrix molecules for non-linear optical substitution. Since fifteen dyes were to be used as the radiation absorbers, the probable locations of the dockings of those dyes with the peptide needed to be determined. This would later enable researchers to determine some of the chemical properties of these compounds and if they are appropriate for laboratory use in developing laser-impervious safety glasses.

Methodology

Two molecular simulation programs were used, Quanta and Cerius^2. These were used to build the molecules. Then, CHARMm was used to minimize the molecules using one of the three methods listed in the introduction. Electron delocalization was determined through MOPAC, and the probable docking sites were determined from Monte Carlo calculations in Quanta. The Monte Carlo Search method was Random Minimization. It had a torsion angle window of 2 and used Rigid Body Manipulation. The Rigid Body Manipulation window was 0.5. Further, the number of trials was 4000 and the maximum number of fails was 75.

The peptide used was sixteen amino acids long with a NH_2 patch on the lysine end and the secondary conformation of a parallel Beta sheet. It was formed in the following pattern: Alanine-Glutamate-Alanine-Glutamate-Alanine-Lysine-Alanine-Lysine-Alanine-Glutamate-Alanine-Glutamate-Alanine-Lysine-Alanine-Lysine-NH_2. The fifteen dyes were Tropaeolin O, 4-(2-Pyridylazo) Resorcinol, Murexide, Methyl Orange, Indigo Carmine, Ethyl Orange, Congo Red, Eriochrome Black, Evans Blue, Ponceau S, Tetraphenyl Porphyrin Tetrasulfonate, Acid Fuchsin, Methylthymol Blue, Pyrocatechol Violet, and Xylenol Orange. For the structural formulas of the fifteen dyes, see page 17-20.

Results

After minimization, 4-(2-Pyridylazo) Resorcinol had the following energies:

Bond Energy = 0.4351 kcal/mole

Angle Energy = 1.7939 kcal/mole

Dihedral Energy = 0.0577 kcal/mole

Improper Energy = 0.0010 kcal/mole

Lennard-Jones Energy = 3.5273 kcal/mole

Electrostatic Energy = 3.2727 kcal/mole

Constraints, etc. Energy = 0.0000 kcal/mole

Total Energy = 9.0878 kcal/mole

MOPAC produced the following data for 4-(2-Pyridylazo) Resorcinol:

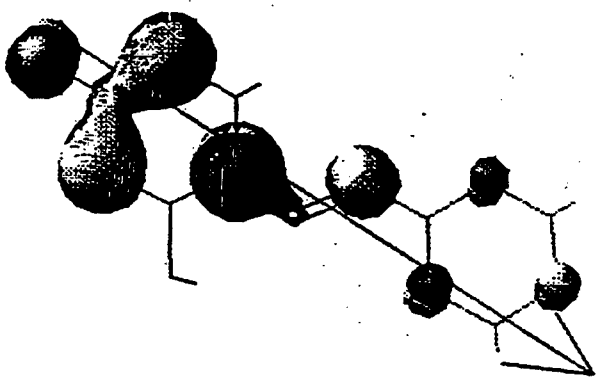

Highest Occupied Molecular Orbitals

Dipole Moment

Lowest Unoccupied Molecular Orbitals

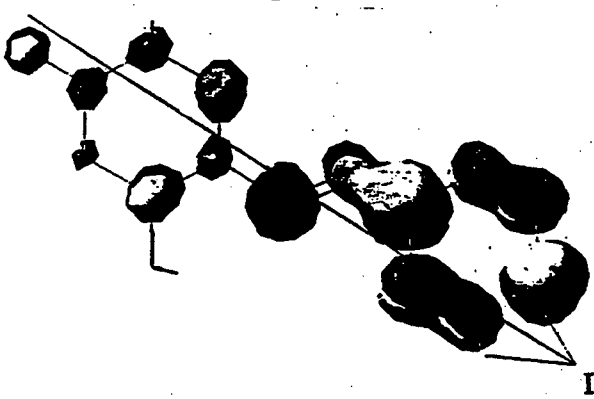

Dipole Moment

The energies of the dockings for all fifteen molecules in the three locations are:

Docking By:	Alanine	Glutamate	Lysine	No. of Atoms
Dyes (Charge)				
Tropaeolin O (-1)	-1111.7173	-1078.7384	-1172.9596	28
Resorcinol (-1)	-1076.3616	-1055.3501	-1137.9343	24
Murexide (-1)	-1129.7214	-1117.8064	-1206.9463	27
Methyl Orange (-1)	-1107.9359	-1086.0045	-1173.3257	35
Indigo Carmine (-2)	-1039.0066	-1004.0872	-1131.1775	36
Ethyl Orange (-1)	-1107.5929	-1082.0359	-1185.0048	41
Congo Red (-2)	-1125.5137	-1161.806	-1201.4877	68
Eriochrome Black (-1)	-1082.7469	-1086.838	-1171.0627	43
Evans Blue (-4)	-869.7891	-848.8464	-1004.7145	82
Ponceau S (-4)	-923.4253	-896.8184	-1146.5905	56
Porphyrin (-4)	-954.9188	-912.9128	-1030.2922	92
Acid Fuchsin (-2)	-984.5026	-990.0526	-1119.1124	59
Methylthymol Blue (-5)	-627.8403	-558.7028	-756.5714	92
Pyrocatechol Violet (-1)	-869.7348	-888.0487	-970.5681	39
Xylenol Orange (-5)	-639.7795	-637.8573	-775.0123	80

Conclusions

The most probable docking site for all of the dyes is by a lysine. This is due to the fact that it is line with the peptide, causing the greatest separation between atoms and therefore, the lowest energy. However, depending upon the charge and orientation of the molecule with respect to the peptide, the next most probable docking site was either the alanine or the glutamate. If the dye had a charge greater than two, then it favored alanine over the glutamate. However, when the charge was less than two, then its structure determined the more favorable docking site. If the rings were grouped close together, then it favored the glutamate. However, if the rings were stretched out in a line, then it favored the alanine.

The electron delocalizations occurred primarily along the double bonds, where more electrons would be shared between atoms than with a typical single bond. However, delocalizations also occurred between atoms where one had a much stronger "pull" than the other one such as between an oxygen and a hydrogen.

References

1. Dr. Ruth Pachter, mentor, Wright Laboratory, WL/MLPJ, Wright Patterson Air Force Base.

2. Fletcher, R., *Practical Methods of Optimization*, Volume 1, John Wiley & Sons, New York, 1980.

3. Fasman, Gerald D., *Prediction of Protein Structure and the Principles of Protein Conformation*, Plenum Press, New York, 1989, pp. 319-328.

4. The results published were generated using the programs CHARMm and/or QUANTA. These programs have been developed by Molecular Simulations, Inc.

5. The results published were generated using the program Cerius$^{2™}$. This program was developed by Molecular Simulations Incorporated.

6. "MOPAC 93.00 Manual", J. J. P. Stewart, Fujitsu Limited, Tokyo, Japan (1993).

The Dyes

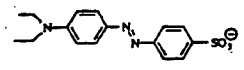

Ethyl Orange

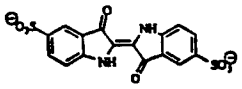

Indigo Carmine

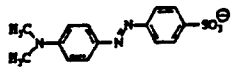

Methyl Orange

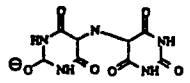

Murexide

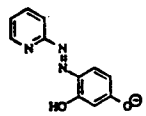

4-(2-Pyridylazo)Resorcinol

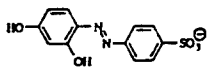

Tropaeolin O

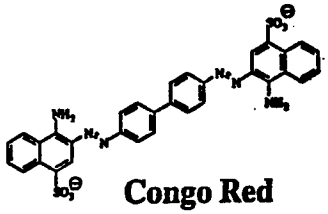

Congo Red

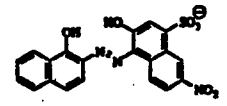

Eriochrome Black

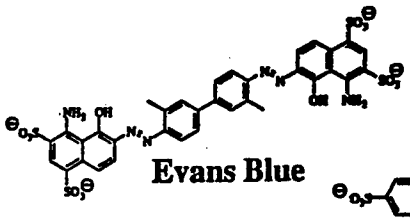

Evans Blue

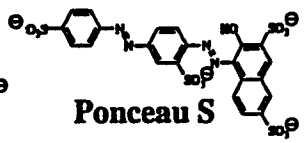

Ponceau S

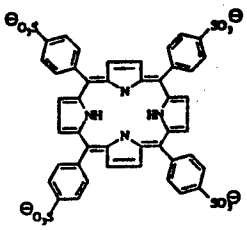

Tetraphenyl Porphyrin Tetrasulfonate

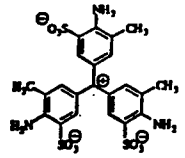

Acid Fuchsin

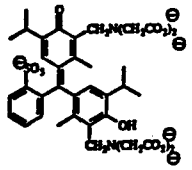

Methylthymol Blue

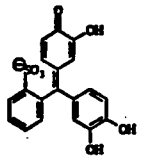

Pyrocatechol Violet

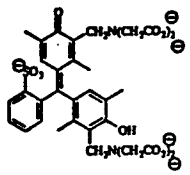

Xylenol Orange

EXHAUST FAN MEASUREMENTS WITH A WEDGE PROBE

Mark Fecke

Chaminade-Julinne High School

Final Report for High School Apprenticeship Program
Wright Laboratory

Sponsored by
Air Force Of Scientific Research
Bolling Air Force Base, DC

And
Wright Laboratory

August 1996

Abstract

The measurements that were taken of the exhaust fan using a wedge probe helped to corroborate the data received from the PIV system. From that final analysis, it was found that the fan was stalled in the original configuration based on the flow angle readings. The fan came fully unstalled when the hood was taken off. The flow was further increased when the inlet screen was removed as seen by increased velocity (or pitot pressure). A description of the inlet and outlet velocity and flow angle was obtained with the fan operating in the high flow condition which can be used by PIV researchers for comparison with their results. The axial velocity and flow angle can be compared in **Appendix A**.

Introduction

One of the most challenging and time consuming problems in experimental fluid mechanics is measuring the overall flow field properties such as the velocity, vorticity, and pressure fields because it is very important to know the flow structures in turbomachinery. That problem is answered with the new technique called the Particle Imaging Velocimetry or PIV. One thing that makes it so useful is the fact that it is non-intrusive. There are efforts underway to make PIV measurements in turbomachinery. This technique has just started to take off. It is still only in Phase 1 which is to make measurements in a low speed, axial-flow exhaust fan. The purpose of this summer apprenticeship for me was to provide a means to corroborate velocity measurements made by the research PIV system.

The application of the PIV to the measurements of the velocity in a field involves two steps. The first is to create a selected plane of surface within the flow field. The orientation of this plan should be such that it contains the dominant flow direction. The plane itself is created by seeding the flow with small tracer particles which are illuminated with a sheet of coherent light. The laser sheet is formed by focusing the laser beam first with a long focal length spherical lens and then diverging the beam in one dimension with a cylindrical lens. The light scattered by the tracer particles in the illuminated plane provides a moving pattern. When the seeding concentration is low, the instantaneous pattern consists of resolved, diffraction-limited images of the particles. When the concentration increases, the images overlap and interfere to produce a random instantaneous pattern and, taken in quick succession, is used to record the data. When the time interval between exposures is appropriately chosen, the tracer particles will have moved only a few decimeters, far enough to resolve their motion but less than the smallest length scale of the flow. The information on the fluid velocity is stored on a photographic image and can be retrieved by subsequent analysis.

In the second step the local fluid velocity is derived from the ratio of the measured spacing between the images of the same particle, of speckle grain, and the time between exposures. The recorded image is a complicated random pattern. There are many methods of converting the information contained in the picture to flow field data such as velocity, streamlines, or vorticity. These methods can be broken into two broad categories. In the first, the distance between particle pairs is evaluated directly. The second category covers those techniques that evaluate the particles' image spacing indirectly. They exploit the property that all particles in a small reign are displaced roughly the same distance between exposures.

Approach

In the approach there are three main things that have to be described. The first is the procedures, the second is the calculation, and the third is the description of the test apparatus. Over all there were six different full runs on the outlet and five full runs on the inlet side. Each run was different in some way, but very similar in others. A run consisted of 20 different points on the outlet side and 13 points on the inlet side. This was because of the poswition of the metal plate in **figure 3**. The points were taken every 7/16 of an inch. The probe had marks on it so that the person running the test could tell how far to insert the probe. On the outlet side the probe went to the center line. The procedure below tells how one full run was completed .

As stated earlier, there were 6 full run of the outlet and 5 full runs of the inlet. Out of the 5 complete runs, that means using an inlet and outlet, only two used the nulling way to find the flow angle and the others used the peaking method to find the flow angle. There were two methods used because it was found that leaks made it hard to measure low pressure. The flow angle is the first thing to be found because the probe can only extrapolate the data if it is directly in the center of the flows path. The two ways to find flow angles are nulling which consists of opening valve 2 and 3 and trying to zero them or 1 and 3 are open and you find where 1-3 is the highest. It should also be noted that the assumption was made that port 2 and 3 measure static pressure exactly. The drawings in **figure 1** show this.

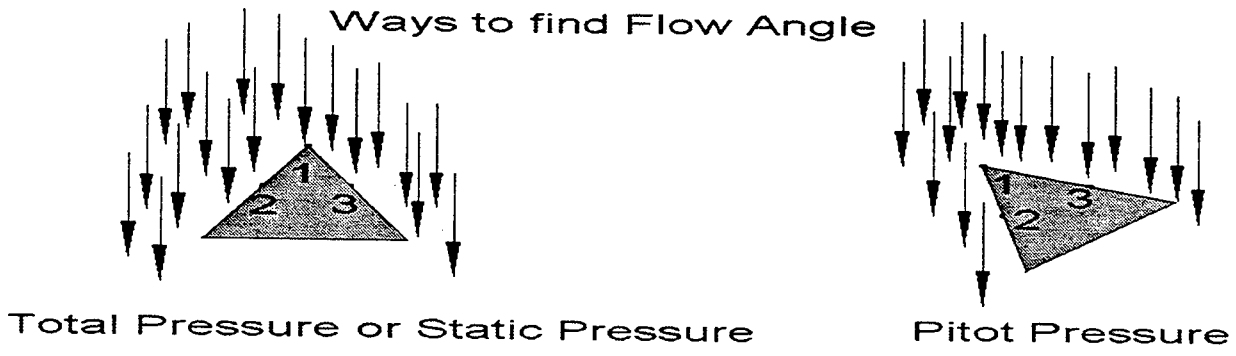

Figure 1. Shows how the flow angle is found and the ways flow flows into the probe.

Procedures

1. Turn on exhaust fan
2. Put the probe in the outlet side of the compressor case
3. Turn on the motor

4. Push in probe to the first hash mark

5. 2 different ways to find flow angle

5a. Nulling Method

1. Open valves 2 and 3
2. Zero the manometer
3. Take **flow angle** reading
4. Open valves 1 and 0(atmospheric)
5. Take **Pt** reading
6. Open valves 1 and 3
7. Take **pitot pressure** reading
8. Push probe into next hash mark
9. Repeat steps 1-8 until done
10. Turn off motor
11. Put probe in the inlet side
12. Push probe to the first hash mark
13. Turn on motor
14. Repeat steps 1-8 until done

5b. Peaking method

1. Open valves 1 and 3
2. Peak the manometer
3. Take **flow angle** reading
4. Take **pitot pressure** reading
5. Open valves 1 and 0
6. Take **Pt** reading
7. Push probe into next hash mark
8. Repeat steps 1-7 until done
9. Turn off motor
10. Put probe in inlet side
11. Push probe to the first hash mark
12. Turn on motor
13. Repeat steps 1-7 until done

Calculation

Once the data points were acquired, then the data was used to calculate three more data points. The calculations found the velocity, the volumetric flow rate and the total pressure. The calculation that was done on total pressure was done to double check the data. These three calculation are seen below. The first is dealing with finding the Volumetric Flow Rate (VFR). To find the VFR you have to have a velocity.The equation for velocity is in the equation for VFR. It is broken up into some separate equations. The first two are of the area the flow has to cover, and the total pressure in inches of water.

$$A = \left(\frac{18}{12} * \frac{1}{2}\right)^2 \pi \approx 1.7671\ ft^2$$

$$V = \frac{4640}{(1.7671 * 60)} \approx 43.76\ \frac{ft}{sec}$$

$$q = \frac{1}{(2 * g_c)} \rho V^2$$

$$g_c = 32.174$$

$$p = \rho R T$$

$$T = 519^0\ R$$

$$P = 14.7\ psi$$

$$R = 53.35$$

$$\rho = \frac{p}{R T} = \frac{(14.7 * 144)}{(53.35 * 519)} \approx 0.0765$$

$$q = \frac{1}{(2 * 32.174)} * 0.0765 * 43.76^2 \approx 2.277\ psf$$

$$2.277\ \frac{lbf}{ft^2} * \frac{1}{144}\ \frac{ft^2}{in^2} * 2.307\ \frac{ftH_2O}{psi} * 12\ \frac{inH_2O}{ftH_2O} \approx 0.438\ inH_2O$$

Calculation 1. Total amount of water need in manometer for run

$$A = \left[\left(\frac{18}{12} * \frac{1}{2}\right)^2 - \left(\frac{4\frac{13}{16}}{12} * \frac{1}{2}\right)^2\right] * \pi \approx 1.6409\ ft^2$$

$$V = \frac{4640}{(1.6409 * 60)} \approx 47.13\ ft/sec$$

$$\rho = \frac{(14.7 * 144)}{(53.35 * 519)} \approx 0.0765$$

$$q = \frac{1}{(2 * 32.174)} * 0.0765 * 47.13 \approx 2.655\ psf$$

$$2.655\ \frac{lbf}{ft^2} * \frac{1}{144}\ \frac{ft^2}{in^2} * 2.307\ \frac{ftH_2O}{psi} * 12\ \frac{inH_2O}{ftH_2O} \approx 0.510\ inH_2O$$

Calculation 2. Same as **Calculation 1** except the hub is taken into consideration in this one

$Pitot(R)$ = water in inches read from the manomiter

$$q = Pitot(R) * \left(\sin\left(\frac{(\pi * 11.56)}{180}\right) * 2\right)$$

$$V = \sqrt{\frac{(2 g_c q)}{\rho}}$$

$$V_x = V \cos\alpha$$

$$A = \frac{\pi(r_2^2 - r_1^2)}{144}$$

$$VFR = V_x A$$

*note that the case has a radius of 9 inches. r_2 begins with 9 and then is subtracted by $\frac{7}{16}$.

The data points were taken every $\frac{7}{16}$ of an inch starting at the edge of the case.

Calculation 3. The calculation below was used to get the VFR.

$$Pitot(R) = 1.2$$

$$q = 1.2 * \left(\sin\left(\frac{(\pi * 11.56)}{180} \right) * 2 \right) \approx 0.4810$$

$$V = \sqrt{\frac{(2 * 32.174 * (\frac{(\pi * .4810)}{180}))}{.07283}} \approx 47.019 \ ft/sec$$

$$V_x = 47.019 * \cos(\frac{40 * \pi}{180}) \approx 36.0188$$

$$r_2 = 9$$

$$r_1 = .5(8.125 * 8.5625) \approx 8.3438$$

$$A = \frac{\pi (9^2 - 8.3438^2)}{144} \approx 0.2483$$

$$VFR = 0.2483 * 36.0188 \approx 8.9440 \ CFM$$

Calculation 4. An example of the VFR calculation with the first data point taken from **Outlet III** is shown above

$$\rho_{o2} - \rho_{o1} = \rho_{o1} \left\{ \left[\frac{*\eta * r * \varpi}{(c\rho * T_{o1} * g_c * J)} * (V_{\theta 2} - V_{\theta 1}) + 1 \right]^{\frac{\gamma}{\gamma - 1}} - 1 \right\}$$

ρ_{o2} = the total pressure of the outlet

ρ_{o1} = the total pressure of the outlet

$V_{\theta 2} = V_2 \sin \alpha_2$ (V is the velocity of outlet along with the flow angle that corresponds to the same point

$V_{\theta 1} = V_1 \sin \alpha_1$ (is the same as above)

$c\rho = 0.24$

$assume \eta = 0.7$

r = radius in feet

$\varpi = 2187$ rpm

$T_{o1} = 530° R$

$g_c = 32.174$

$J = 778$

$\gamma = 1.4$

Calculation 5. This equation was used to find the total pressure at one point.

The data that was calculated can be seen in **Appendix A.**

Description of test apparatus

There are three basic things included in this test apparatus. The first is the exhaust fan. The second is a test facility, or lab where the test can be run. In this case it was at Wright Patterson Air Force Base in Bldg.450. The third and finial thing needed is the testing materials, materials that are needed to gather, record, and analyze. In this case it would be a wedge probe, a manometer, and a computer. There were four pieces of date that were need to make this test useful.

The four measured quantities include Pt (or total pressure), Flow angle, Pitot (or the total pressure minus the static pressure), and how far was in the probe. All four of these quantities measured were using a wedge probe with the help of an inclined water manometer. The wedge probe was named for its wedge shaped hull. The probe has an opening at the top of the wedge which is used for total pressure. There are also two other openings on either side, equidistant from the opening at the top. One adaptation to the probe was the addition of an angle scale, which was referenced against the tip of the wedge which was assumed to be parallel to the flat base at the end of the probe.

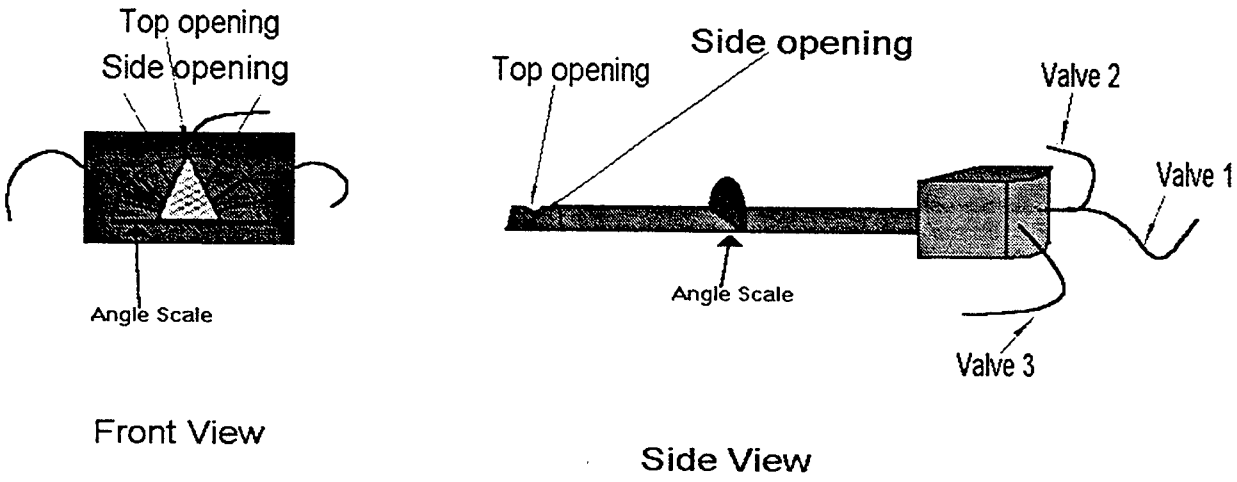

Figure 2. A front and side view of the probe.

The probe was not the only thing used. A water manometer was used in conjunction with the probe. One problem that was experienced was that the test only required two inches of water at the maximum. and the manometer went up to six. To get more precise, the manometer was inclined to increase its sensitivity.

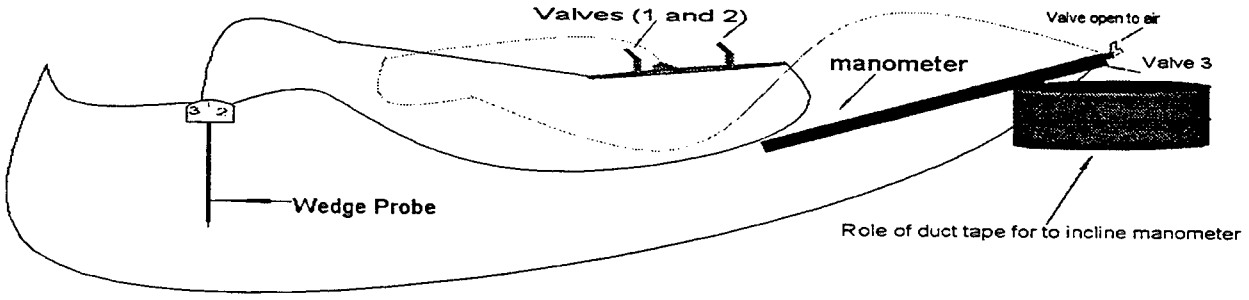

Figure 3. Shows the way the probe and the manometer were set up

The way the manometer could work like this is that a person could read the water level from the manometer and then take that number and multiply it by the SIN of angle of elevation times 2 as seen below

h = height of water column

s = measured valve

θ = angle of inclination

$h = s\sin\theta$

Calculation 6. Shows how the calculation that the data had to go through to be data from a vertical manometer

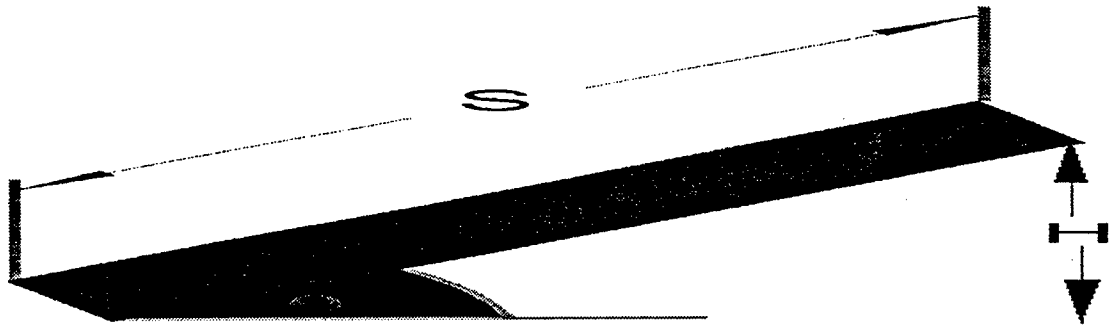

Figure 4. Shows where the letters in **Calculation 6.** came from

Besides the instrumentation there was the test subject, which was an industrial grade exhaust fan. The dimensions of the exhaust fan were needed for referencing the probe.

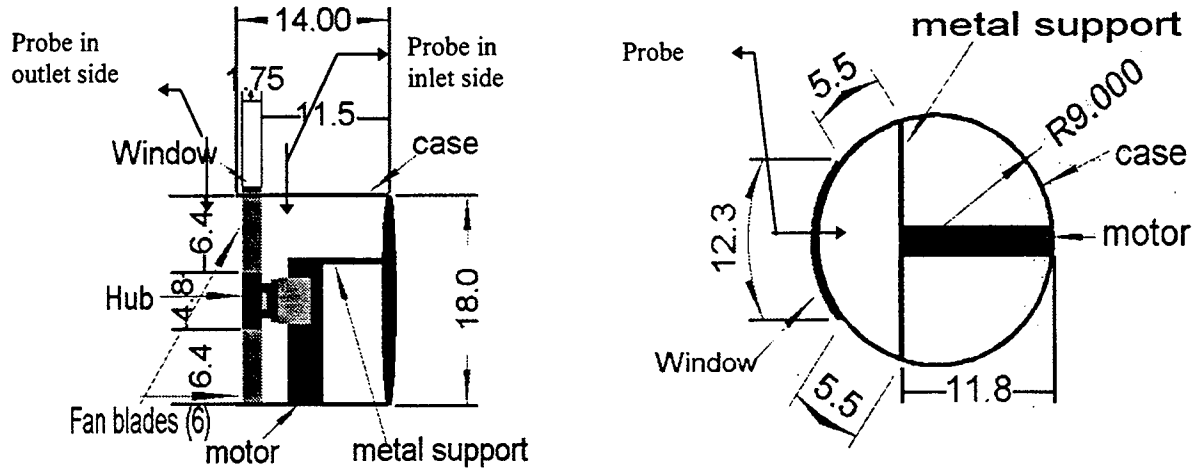

Figure 5. Show the dimensions of the case and fan.

Beside the case and the compressor there was also a hood on the outlet side of the case that led the air to a vent. The vent was 10 inches in diameter twenty feet away was an identical vent that was was plugged up during the early runs. Beside having a hood on the outlet side, there was also a mesh gate on the inlet side of the case for safety reasons. This prevented anything from entering into the case.

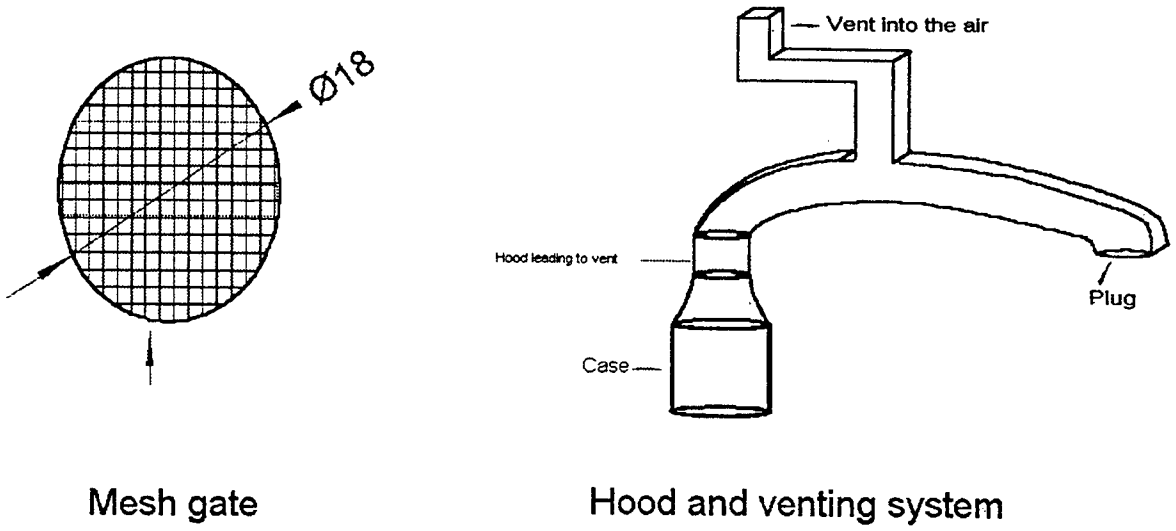

Mesh gate

Hood and venting system

Figure 6. Shows the hood, the plug, and the mesh gate.

There are two other notable features on the case. They are the transmitter window and receiver window. They are used in the PIV system that was talked about earlier. The pictures which show these windows and also shows the probe in the case itself can be ound on the last page in **Appendix B**. The probe was stuck in the case at two spots, one below the blades(or window) and one above the blades(or window).

Interpretation of results

The charts you will see below have six columns. The first column "**Radius (in.)**" tells what the radius in inches of the probe is inside the case. For example, 8.5625 means that it is .4375 inches inside the case. Another way to look at it would be that the radius from the center of the case radius to the end of the probe is 8.5625 inches. The second column "**Pt (in. of H20)***" tells the total pressure in inches of water that was read from the manometer. The total pressure as seen above is when the 1 valve is open and the 0 valve or atmospheric valve is open. The manometer measures the difference between the pressure inside the case and the pressure out side the case. In the center of the flow path is were the pressure is going to be higher. The third column "**Pt(I)A**" is the Actual total pressure that there was. Since an inclined manometer was used, the readings off the manometer would have to be put through the calculation seen in **Calculation 6**. The next column "**Angle ° I**" states the flow angle measure in degrees off of the angle scale on adapted to the probe. The next column "**Pitot (I)R**" is the Pitot pressure that was read off the manometer. The Pitot pressure as seen above is when valve 1 and 3 are open and the reading is the

difference between these two. When the probe is directly in the center of the flow path then that is when the pressure is at its highest point. The last column "**Pitot (I)A"** is the Actual Pitot pressure that would be seen if it was on a vertical stand.

The first run was taken with everything on and in plane. The hood ,exhaust fan, and mesh gate were on. In the first full run, the data that was taken showed that the flow angle was very high for both the inlet and outlet. As seen below the first outlet run has a flow angle that is greater then 90 degrees. Since that is very improbable, it was plain to see that something had gone wrong. The problem could be many things. The problem could be a leak in the line some where or maybe the fan was operating in a stalled state. A leak check was done on the tubing that ran from the probe to the manometer. There was one leak that was found and subsequncialy fixed.

Radius (in.)	Pt (in. of H20)*	Pt(I)A	Angle ° I	Pitot (I)R	Pitot (I)A
8.5625	4.6	1.843623	69	1.5	0.6011815
8.125	4.35	1.743426	76	1.33	0.53304759
7.6875	4.15	1.663269	81	1.25	0.50098458
7.25	4	1.603151	87	1.25	0.50098458
6.8125	3.92	1.571088	91	1.31	0.52503184
6.375	3.9	1.563072	92	1.35	0.54106335
5.9375	3.82	1.531009	94	1.51	0.60518937
5.5	3.78	1.514977	95	1.58	0.63324451
5.0625	3.7	1.482914	96	1.8	0.7214178
4.625	3.6	1.442836	93	2	0.80157533
4.1875	3.45	1.382717	85	2.2	0.88173286
3.75	3.2	1.282521	82	2.45	0.98192978
3.3125	2.94	1.178316	76	2.67	1.07010307
2.875	2.52	1.009985	73	2.8	1.12220546
2.4375	1.95	0.781536	70	3	1.202363
2	1	0.400788	75	3.02	1.21037875
1.5625	-0.3	-0.120236	77	2.95	1.18232361
1.125	-1.8	-0.721418	79	2.6	1.04204793
0.6875	-3.8	-1.522993	84	1.7	0.68133903
0.25	-5.6	-2.244411	92	0.55	0.22043322

Chart 1. It is the outlet part of Run 1.

During the first outlet run, the flow angle was extrapolated using the Nulling method. During the first inlet run the peaking method was used to find the flow angle. It didn't to make much difference because as seen below the inlet flow angle goes form -95 to 95. The flow angle in the inlet should stay around zero since the flow is just getting sucked up and there is really not much in the way so the flow should be almost totally vertical.

Radius (in.)	Pt (in. of H20)*	Pt(I)A	Angle ° I	Pitot (I)R	Pitot (I)A
8.5625	1	0.400788	-95	4	1.60315066

8.125	1	0.400788	-97	4	1.60315066
7.6875	0.3	0.120236	-97	3	1.202363
7.25	-0.5	-0.200394	-85	2	0.80157533
6.8125	-0.9	-0.360709	-73	1.9	0.76149656
6.375	-1.6	-0.64126	-27	1.9	0.76149656
5.9375	-1	-0.400788	-19	1.9	0.76149656
5.5	-1	-0.400788	0	1.9	0.76149656
5.0625	-0.9	-0.360709	10	1.9	0.76149656
4.625	-1	-0.400788	20	1.85	0.74145718
4.1875	-1	-0.400788	40	1.45	0.58114211
3.75	-1	-0.400788	55	1.22	0.48896095
3.3125	-1.4	-0.561103	95	1.1	0.44086643

Chart 2. Inlet part of Run 1

The second run was done in a similar fashion as the inlet side of the first run. The flow angle was found by peaking the pitot pressure. The only major physical difference was that a plug was taken out of the other side of the exhaust fan to allow more air in the exhaust pipes. In this run the outlet flow angle looked a little better than before, but the inlet side was still just as bad as before.

Radius (in.)	Pt (in. of H20)*	Pt(II)A	Angle ° II	Pitot (II)R	Pitot (II)A
8.5625	4.1	1.643229	50	2.2	0.88173286
8.125	3.65	1.462875	55	2.2	0.88173286
7.6875	3.5	1.402757	65	2.12	0.84966985
7.25	3.4	1.362678	70	2.1	0.8416541
6.8125	3.45	1.382717	75	2.2	0.88173286
6.375	3.33	1.334623	80	2.4	0.9618904
5.9375	3.5	1.402757	85	2.6	1.04204793
5.5	3.2	1.282521	75	2.9	1.16228423
5.0625	2.9	1.162284	71	3.2	1.28252053
4.625	2.55	1.022009	65	3.3	1.3225993
4.1875	2.05	0.821615	62	3.4	1.36267806
3.75	1.95	0.781536	62	3.9	1.5630719
3.3125	1.3	0.521024	58	3.9	1.5630719
2.875	0.85	0.34067	55	4	1.60315066
2.4375	0.1	0.040079	60	3.85	1.54303251
2	-1	-0.400788	58	3.55	1.42279621
1.5625	-1.7	-0.681339	68	2.55	1.02200855
1.125	-3.1	-1.242442	73	1.7	0.68133903
0.6875	-4.3	-1.723387	76	0.7	0.28055137
0.25	-4.8	-1.923781	77	0.2	0.08015753

Chart 3. Outlet part of Run 2

Radius (in.)	Pt (in. of H20)*	Pt(II)A	Angle ° II	Pitot (II)R	Pitot (II)A
8.5625	1.5	0.601181	-107	4.3	1.72338696

8.125	1	0.400788	-103	4.2	1.68330819
7.6875	-0.8	-0.32063	-95	2.8	1.12220546
7.25	-1.55	-0.621221	-85	1.5	0.6011815
6.8125	-1.6	-0.64126	-80	0.7	0.28055137
6.375	-1.7	-0.681339	-35	1.3	0.52102397
5.9375	-1.6	-0.64126	-10	1.8	0.7214178
5.5	-1.1	-0.440866	-6	2	0.80157533
5.0625	-1.3	-0.521024	7	2.05	0.82161471
4.625	-1.2	-0.480945	15	1.95	0.78153595
4.1875	-1.1	-0.440866	30	1.4	0.56110273
3.75	-1	-0.400788	50	1.15	0.46090582
3.3125	-0.75	-0.300591	75	1.3	0.52102397

Chart 4. Inlet part of Run 2

In the third run the plug was still out but the hood that lead to the exhaust vent was taken off and the flow angle was still found by peaking the pitot pressure. It was hoped that this would keep the exhaust fan from becoming stalled since the data to this point said it was stalled. It was believed that the exhaust fan was stalled because of the wild flow angle. When a exhaust fan is stalled it means that there is too much back pressure coming back and the forward flow or upward flow is not able to go up due to the back pressure. A stalled fan is like two people pushing on a peddle in opposite direction. The bike doesn't go anywhere or is stalled because the pressure applied to going forward is halted due to the equal pressure going the opposite way. The picture below shows this graphically. During this run, the flow angle this time was not nearly as bad as it had been. The inlet and outlet were starting to show sings this it wasn't in a stalled state any more. Notice the inlet angle dropped from + or - 90 to +20 and -5.

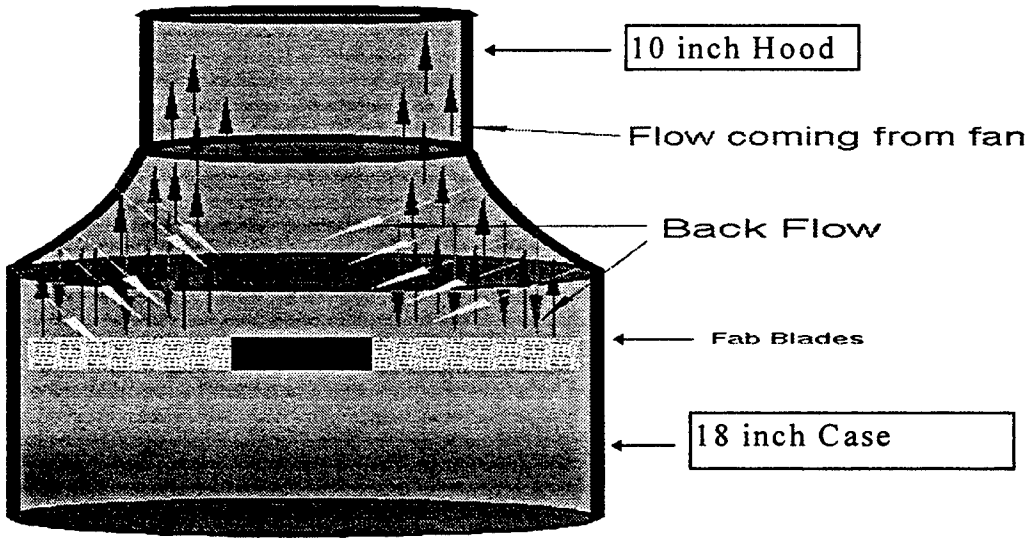

Figure 7. Shows what was happening to the fan during the first and second run

Radius (in.)	Pt (in. of H20)*	Pt(III)A	Angle ° III	Pitot (III)R	Pitot (III)A

8.5625	0.6	0.240473	40	1.2	0.4809452
8.125	0.92	0.368725	52	1.3	0.52102397
7.6875	0.6	0.240473	39	1.2	0.4809452
7.25	0.4	0.160315	30	1.23	0.49296883
6.8125	0.9	0.360709	35	1.2	0.4809452
6.375	0.4	0.160315	15	1.65	0.66129965
5.9375	0.5	0.200394	15	1.9	0.76149656
5.5	0.55	0.220433	12	2.05	0.82161471
5.0625	0.45	0.180354	15	2	0.80157533
4.625	0.65	0.260512	15	1.9	0.76149656
4.1875	-0.05	-0.020039	15	1.4	0.56110273
3.75	0.3	0.120236	25	1.6	0.64126026
3.3125	0.5	0.200394	30	1.25	0.50098458
2.875	-0.45	-0.180354	25	1	0.40078767
2.4375	-0.5	-0.200394	30	0.9	0.3607089
2	-0.3	-0.120236	55	0.75	0.30059075
1.5625	-0.6	-0.240473	60	0.8	0.32063013
1.125	-0.8	-0.32063	70	0.7	0.28055137
0.6875	-1.2	-0.480945	77	0.6	0.2404726
0.25	-1.5	-0.601181	80	0.3	0.1202363

Chart 5. Outlet part of Run 3

Radius (in.)	Pt (in. of H20)*	Pt(III)A	Angle ° III	Pitot (III)R	Pitot (III)A
8.5625	-1.95	-0.781536	-5	0.2	0.08015753
8.125	-1.9	-0.761497	3	0.3	0.1202363
7.6875	-2	-0.801575	10	0.4	0.16031507
7.25	-1.95	-0.781536	15	0.72	0.28856712
6.8125	-1.6	-0.64126	15	1	0.40078767
6.375	-1.5	-0.601181	10	1.5	0.6011815
5.9375	-1.6	-0.64126	17	1.75	0.70137841
5.5	-1.6	-0.64126	23	1.9	0.76149656
5.0625	-1.3	-0.521024	15	2.3	0.92181163
4.625	-1.3	-0.521024	10	2.35	0.94185101
4.1875	-1.8	-0.721418	13	1.8	0.7214178
3.75	-2.1	-0.841654	17	0.65	0.26051198
3.3125	-2	-0.801575	20	0.1	0.04007877

Chart 6. Inlet part of Run 3

The fourth run was done with the hood off, and the bottom mesh off. This was done because it was thought that the mesh gate might be creating a near stall situation. The outlet angles were much more centrally located during this run. The plug and hood were still off. Peaking the pitot pressure was still used as the way to find the flow angle.

Radius (in.)	Pt (in. of H20)*	Pt(IV)A	Angle ° IV	Pitot (IV)R	Pitot (IV)A
8.5625	1.8	0.596464	38	2	0.66273739
8.125	2.05	0.679306	40	2.2	0.72901113
7.6875	2.4	0.795285	35	2.1	0.69587426
7.25	2.8	0.927832	35	2.6	0.86155861
6.8125	1.7	0.563327	7	4.5	1.49115913
6.375	2.3	0.762148	15	4.5	1.49115913
5.9375	1.55	0.513621	10	4.9	1.62370661
5.5	1.55	0.513621	10	4.8	1.59056974
5.0625	1.6	0.53019	20	4.5	1.49115913
4.625	0.75	0.248527	20	4.1	1.35861166
4.1875	0.6	0.198821	30	3.5	1.15979044
3.75	0.9	0.298232	40	2.8	0.92783235
3.3125	0.3	0.099411	35	2.3	0.762148
2.875	-0.1	-0.033137	35	1.8	0.59646365
2.4375	-0.6	-0.198821	40	1.5	0.49705304
2	-0.9	-0.298232	38	1.3	0.43077931
1.5625	-1.6	-0.53019	30	0.9	0.29823183
1.125	-1.75	-0.579895	35	0.8	0.26509496
0.6875	-2.1	-0.695874	30	0.4	0.13254748
0.25	-2.2	-0.729011	50	0.4	0.13254748

Chart 7. The outlet part of Run 4

The inlet side in this run is not fully complete. The inlet side of this run was actually done before the inlet. There had to be a quick survey of the effect the mesh gate had on the compressor. It was late in the day and there was not enough time to make a full run. The quick servey did show that the flow angle was staying linear.

Radius	Pt	Pt(IV)A	Angle	Pitot(IV)R	Pitot(IV)A
8.5625	-3	-0.994106	-3	1	0.3313687
7.25	-2.2	-0.729011	0	1.6	0.53018991
5.5	-0.4	-0.132547	0	3.9	1.29233792
4.1875	-2.4	-0.795285	3	3.7	1.22606418

Chart 8. The inlet part of Run 4

The fifth run was run very similar to the fourth in that the flow angle was found by the peaking of the pitot pressure again. The difference in the runs was that the fifth run was a complete run of both inlet and outlet, and two valves, two and three, were switched. This was because there was a notion that there might be a leak in one of the tubes. Valve two does not get used a lot because it is on the same valving mechanism as valve 1 which gets used all the time. This is shown is **Figure 3.** A trend that has been noticed is that the total pressure is turning negative faster than the run in the past. When it says there is a (-) pressure reading, it means that for example the total pressure inside the case is less than the atmospheric pressure. Some of this pressure loss is contributed to the fact

that the flow closer to the hub is really unstable so the flow angle will not stay constant and the pressure that is being taken in by the probe is not the absolute highest pressure.

Radius (in.)	Pt (in. of H20)*	Pt(V)A	Angle ° V	Pitot (V)R	Pitot (V)A
8.5625	1.7	0.563327	38	2.2	0.72901113
8.125	1.5	0.497053	25	2.6	0.86155861
7.6875	2	0.662737	21	3.2	1.06037983
7.25	1.7	0.563327	12	4.1	1.35861166
6.8125	2.2	0.729011	10	4.4	1.45802226
6.375	2.7	0.894695	15	4.5	1.49115913
5.9375	1.9	0.629601	7	4.9	1.62370661
5.5	2	0.662737	10	4.7	1.55743287
5.0625	0.8	0.265095	10	4.5	1.49115913
4.625	1.35	0.447348	20	4.2	1.39174852
4.1875	1	0.331369	20	3.7	1.22606418
3.75	-0.15	-0.049705	15	2.8	0.92783235
3.3125	-0.5	-0.165684	15	2.1	0.69587426
2.875	-0.45	-0.149116	25	1.8	0.59646365
2.4375	-0.95	-0.3148	21	1.4	0.46391617
2	-1.55	-0.513621	15	1	0.3313687
1.5625	-1.6	-0.53019	30	0.9	0.29823183
1.125	-1.75	-0.579895	48	1	0.3313687
0.6875	-1.7	-0.563327	55	1	0.3313687
0.25	-2	-0.662737	80	0.45	0.14911591

Chart 9. Outlet part of Run 5

Radius (in.)	Pt (in. of H20)*	Pt(V)A	Angle ° V	Pitot (V)R	Pitot (V)A
8.5625	-2.4	-0.795285	-10	1.55	0.51362148
8.125	-2.7	-0.894695	10	2.2	0.72901113
7.6875	-2.4	-0.795285	7	2.6	0.86155861
7.25	-2.2	-0.729011	5	3.3	1.0935167
6.8125	-1.4	-0.463916	2	3.5	1.15979044
6.375	-0.9	-0.298232	-1	3.8	1.25920105
5.9375	-0.5	-0.165684	0	3.9	1.29233792
5.5	-0.4	-0.132547	0	4.05	1.34204322
5.0625	-0.45	-0.149116	2	4.35	1.44145383
4.625	-1.1	-0.364506	2	3.65	1.20949574
4.1875	-2.6	-0.861559	7	2.2	0.72901113
3.75	-3.5	-1.15979	10	1.1	0.36450557
3.3125	-4.2	-1.391749	17	0.4	0.13254748

Chart 10. Inlet part of Run 5

Since the last run provided data that was pretty reliable, the sixth and final run was done the same way except that the flow angle was done a different way. The flow angle was extrapolated by using the nulling method, the method that was used for the first run of the outlet. This way was chosen so that if there was data the was far off from the

last run, then it would be known that there was something wrong somewhere. If it wasn't to far off then the two runs could be compared and then an answer could be found to what the capabilities of the machine are.

Radius (in.)	Pt (in. of H20)*	Pt(VI)A	Angle ° VI	Pitot (VI)R	Pitot (VI)A
8.5625	2.1	0.695874	50	1.6	0.53018991
8.125	2.1	0.695874	45	1.8	0.59646365
7.6875	2.5	0.828422	35	2.6	0.86155861
7.25	3	0.994106	20	2.85	0.94440078
6.8125	3.1	1.027243	27	3.1	1.02724296
6.375	3.1	1.027243	25	3.2	1.06037983
5.9375	3.1	1.027243	27	3.3	1.0935167
5.5	2.9	0.960969	28	3.25	1.07694826
5.0625	2.7	0.894695	32	3.1	1.02724296
4.625	2.4	0.795285	32	3	0.99410609
4.1875	2	0.662737	40	2.6	0.86155861
3.75	1.3	0.430779	30	1.9	0.62960052
3.3125	0.8	0.265095	45	1.6	0.53018991
2.875	0.4	0.132547	50	1.3	0.43077931
2.4375	0.15	0.049705	57	1.05	0.34793713
2	0	0	65	1	0.3313687
1.5625	-0.35	-0.115979	70	1.1	0.36450557
1.125	-0.7	-0.231958	75	1	0.3313687
0.6875	-1.4	-0.463916	82	0.5	0.16568435
0.25	-2	-0.662737	89	0.3	0.09941061

Chart 11. Outlet part of Run 6

Radius (in.)	Pt (in. of H20)*	Pt(VI)A	Angle ° VI	Pitot (VI)R	Pitot (VI)A
8.5625	-2.3	-0.762148	-12	1.3	0.43077931
8.125	-2.1	-0.695874	-9	1.8	0.59646365
7.6875	-1.7	-0.563327	-5	2.1	0.69587426
7.25	-1.5	-0.497053	-2	2.4	0.79528487
6.8125	-1.1	-0.364506	0	3.1	1.02724296
6.375	-0.8	-0.265095	-1	3.4	1.12665357
5.9375	-0.4	-0.132547	0	3.8	1.25920105
5.5	-0.3	-0.099411	2	4.1	1.35861166
5.0625	-0.4	-0.132547	0	4.15	1.37518009
4.625	-0.9	-0.298232	0	3.5	1.15979044
4.1875	-2.6	-0.861559	5	2.2	0.72901113
3.75	-3.85	-1.275769	-5	0.7	0.23195809
3.3125	-4.2	-1.391749	10	0.3	0.09941061

Chart 12. Inlet part of Run 6

Once all the data had been collected and calculated, then it was time to sit down and compare what had happened in each test and use that data to make a summery of what went on. The first run was ruled out for any comparison because the data was way off what it should have been and the fact that there was a leak in the number 2 valve. The first run was also a practice run because the person doing the test had never done that technique for

finding flow angle before and there a large margin for error. The forth run was also ruled out for comparison because it was not a full complete run.

Once the bad runs were thrown out, the rest could be used in a comparison. The second, third, and fifth run were compared because they all found the flow angle by peaking the pitot pressure. Then the fifth and sixth run were compared because they were both done under the same conditions except that the flow angle was found a different way in both. To show what happened during the test the axial velocity (or Vx) and the flow angle were compared. The inlet and outlet on each of the runs would be compared.

In comparison of the flow angle in Runs second, third, and fifth as seen in **Graph 1** in **Appendix B,** the second run is the one that is farthest away from the other two. In the outlet part of run two the flow angle is somewhat parallel to three and five that means that there is some pressure loss accruing some where along the probe or the tubing. The inlet is a different story. In the inlet comparison seen in **Graph 2** in **Appendix B** the inlet goes from +75 to -107. It dives right through three and five. Some of this might be that the compressor was still in a stalled state or at least still running with a very heavy load on it. In **Graph 3** and **Graph 4** in **Appendix B** that deal with axial velocity, the fifth run is always higher than the other two and the second run is always the lowest. This is because of the different changes from one test to an other. Run five and six are the only time in which the mesh gate and hood were off. The third run was an improvement from run two because it did increase the velocity and the fact that the flow angle was constant relative to run five. The velocity of run five increased in the range of 30 -60 % over run 3. In all three of these runs the flow angle was found by peaking the pitot pressure. Finding the flow angle this way is less accurate then nulling or zeroing it. This is because the manometer reacted very slowly to the turn of the wedge probe, and so the manometer moved slowly and it was still moving when the reading was being taken. There is a greater range of error for peaking it because like a mountain there are two side to any point except the peak. Since the manometer took so long to react, the peaking method was even worse than it had to be because the flow angle reading would be taken when the water was on a downward motion.

The comparison between run five and six tried to show this to some effect, but theee was not enough runs done to make an accurate conclusion. What can be said is that the velocity increased with the hood and mesh gate off and the flow angle of the inlet stayed around zero in **Graph 5** in **Appendix B.** This is what it should do because the flow was just being sucked straight up. The outlet flow angle was a different story. Run six had a higher flow angle and lower velocity under the same condition which means that the nulling method was worse, when logically it

should be more accurate. The flow angle was not as high as run two but was still higher then five as seen in **Graph 6** in **Appendix B.** The inlet velocities were almost the same, as seen in **Graph 8** in **Appendix B,** which would be expected because the test were run under the same conditions except that the flow angle was determined a different way. The outlet seen in **Graph 7** in **Appendix B** is what is expected if you saw the flow angle. Since the velocity is higher, the peaking method worked better when taking in to consideration everything else was the same in both tests. This is because the velocity is at its highest point at the center of the flow which is what the measurement of the flow angle was for. The closer the flow angle is to the correct flow angle the higher the probability the velocity will be higher assuming everything else is the same.

In an overall finial summery, it was found that the fan was stalled in the original configuration based on the flow angle readings. The fan came fully unstalled when the hood was taken off. The flow was further increased when the inlet screen was removed as seen by increased velocity (or pitot pressure). A description of the inlet and outlet velocity and flow angle was obtained with the fan operating in the high flow condition which can be used by PIV researchers for comparison with their results. The axial velcoity and flow angle can be compared in **Appendix A.**

Appendix A

The first column tells what run it is by looking to the right of the **V**, and it tells the velocity in feet per second at a certain radius. The second tells the Volumetric Flow Rate measure in cubic feet per second. The number at the bottom of the second column that is in bold and underline type is a total sum of the VFR that is then multiplied by sixty. The third column tells the axial velocity which can be found in the calculation above. The fourth is the total pressure measure in inches of water that was calculated by the last equation. The fifth column is the total pressure measured in inches of water that was actually taken. The number is the total pressure of the outlet minus the total pressure of the inlet. The sixth column is the flow angle. This is inserted here so you can compare the flow angle with axial velocity. The seventh and finial column tells the radius in inches inside the case. There will only be one "**Pt (C)**" and "**Pt (A)**," because it takes the outlet minus the inlet and there is only one answer for each run.

V1 (ft/sec)	VFR (in CFM)	Vx	Pt (C)	Pt (A)	Angle ° I	Radius (in.)
52.569083	4.67800214	18.839124	6.740784	1.442836	69	8.5625
49.5006148	1.85740463	11.975336	6.329394	1.342639	76	8.125
47.9887877	1.1016815	7.5071569	5.442768	1.543033	81	7.6875
47.9887877	0.3476034	2.5116006	4.587603	1.803544	87	7.25
49.1270199	-0.1114922	-0.857319	4.202148	1.931797	91	6.8125
49.8714111	-0.2118018	-1.74042	2.850038	2.204332	92	6.375
52.7440222	-0.4170117	-3.679164	2.486705	1.931797	94	5.9375
53.9527164	-0.493697	-4.702214	1.721268	1.915765	95	5.5
57.5865452	-0.5817149	-6.019352	1.384952	1.843623	96	5.0625
60.7015485	-0.280476	-3.17679	1.094122	1.843623	93	4.625
63.6643211	0.44355614	5.5487907	0.735689	1.783505	85	4.1875
67.1843027	0.66935044	9.3503282	0.60412	1.683308	82	3.75
70.1359046	1.07292373	16.967487	0.447088	1.739418	76	3.3125
71.8230407	1.15248144	20.999099			73	2.875
74.3439102	1.18314609	25.427187			70	2.4375
74.5913116	0.73707502	19.305732			75	2
73.7217745	0.49465387	16.583872			77	1.5625
69.2104138	0.28360955	13.206049			79	1.125
55.9640625	0.07677451	5.8499064			84	0.6875
31.8321606	-0.0049465	-1.110883			92	0.25
	719.827341					

Chart A-1. The outlet side of Run 1

Data Analysis for Redesign of the 105mm Blast Diffuser

Landon W. Frynire

Laurel Hill School
8078 4th Street
Laurel Hill, FL 32567

Final Report for
High School Apprentice Program
and
Wright Laboratory at Eglin

Sponsored by:
Air force Office of Scientific Research
Bolling Air Force Base, DC

and

Wright Laboratory

August 15, 1996

Data Analysis for Redesign of the 105mm Blast Diffuser

Landon W. Frymire
Laurel Hill School

Abstract

A more advanced diffuser is needed by the Air Force for use on the AC - 130 Gunship's 105mm gun. To fill this need, blast overpressure tests were conducted on three types of diffusers and a bare muzzle without a diffuser. The three types of diffusers tested consisted of a baseline diffuser (currently in use), an extended diffuser with holes, and an extended diffuser with a shroud covering the holes. A blast arena was set up around the muzzle of a 105mm gun, which is mounted on a gun truck. This arena consisted of fifteen free air probes designed to record blast overpressure signatures. After the raw data from the tests was recorded, it was then condensed in order to place emphasis on the initial peak pressure. Comparisons of the refined data will enable designers to develop a new diffuser for the AC - 130 Gunship.

Data Analysis for Redesign of the 105mm Blast Diffuser

Landon W. Frymire

The AC - 130 Gunship is an attack plane in use by the United States Air Force Special Operations Command. The Gunship is armed with a 105mm cannon, a 40mm gun, and two 20mm guns. The 105mm gun is capable of firing at various angles depending on the aircraft's position. However, the 105mm gun with the current diffuser is limited in how close it can be positioned to the wing due to the overpressure generated by its firing. In an effort to bring the gun closer to the aircraft, the Aeroballistics Section of Wright Laboratory's Armament Directorate, Eglin Air Force Base, FL, was tasked with developing several new diffuser designs to minimize excessive overpressure. Despite a diffusers effectiveness, it must also be light enough so as to not effect the current aircraft's load capabilities. The test results would also serve to validate computer models of muzzle blast to optimize new diffuser designs.

Firing of the 105mm gun by the AC - 130 was simulated by the Aeroballistic Section's gun truck. The gun truck is a modified cement truck with a 105mm gun mounted on the back (Figure 1). Around the gun muzzle,

fifteen free air probes were positioned to gather blast overpressure data created by the primary and secondary blast waves. Probes were positioned around the muzzle at the following angles: fifteen, thirty, forty five, and ninety degrees (Figure 2). The probes were also placed at distances of three, six, nine, ten and one half, and twelve feet from the center of exit from the diffuser (Figure 2).

For the tests described herein, a total of eleven shots were fired. For each shot the fifteen probes were used. Shots one and two were with the baseline diffuser; shots three, four, and five were with a bare muzzle without a diffuser; shots six, seven, and eight were with the extended diffusers with holes; and finally shots nine, ten, and eleven were with the extended diffuser with holes with a shroud over the holes. For each shot, each individual probe was gathering data. This raw data was compiled and plotted on graphs by a support contractor.

The raw data was received from the support contractor, and was then plotted on a graph with a reduced scale focusing on the initial blast overpressure. This condensed data from each probe was then plotted on one graph according to diffuser type and shot number. To do this, the data from each diffuser type needed to be "averaged" to give a better representative blast overpressure as well as smooth out any "noise" in the raw data signal. For

example, Figure 3 shows the initial blast overpressure vs. time for probe one. Here, only the data of shots one and two are shown as they are of the baseline diffuser. Also shown in Figure 3 is a "smooth" data trace which attempts to eliminate the noise of the raw data.

Once this averaged smooth data was plotted for each diffuser, all the results can be plotted on one graph to compare the performance of each diffuser. This is shown in Figure 4. Here we see for probe one the four data traces that represent the three diffusers tested plus the bare muzzle.

Once the data had been compared, it was discovered that no one diffuser was able to reduce the overpressure consistently. The results varied for each diffuser depending on the probe's location. For example, the bare muzzle with no diffuser had a lower overpressure at probe one (Figure 4), which was located three feet from the center of exit from the muzzle; at probe number eight (Figure 5) which was six feet from the muzzle, the bare muzzle had a higher overpressure than all three of the diffuser designs.

In addition to the actual tests, computer simulations are being performed. When the information from those simulations are complete it should help shed some light on the different diffuser designs.

In conclusion, the blast overpressure tests on the 105mm cannon were completed for various blast diffusers. The data analysis showed a wide variation in overpressure with diffuser type and location. Comparisons with the computer simulations will be analyzed as soon as the computations are complete. It is hopeful that these results will aid in further comparison of the three diffuser designs. Also in the future, an investigation of aircraft location with respect to the muzzle will be done to further develop an optimal design.

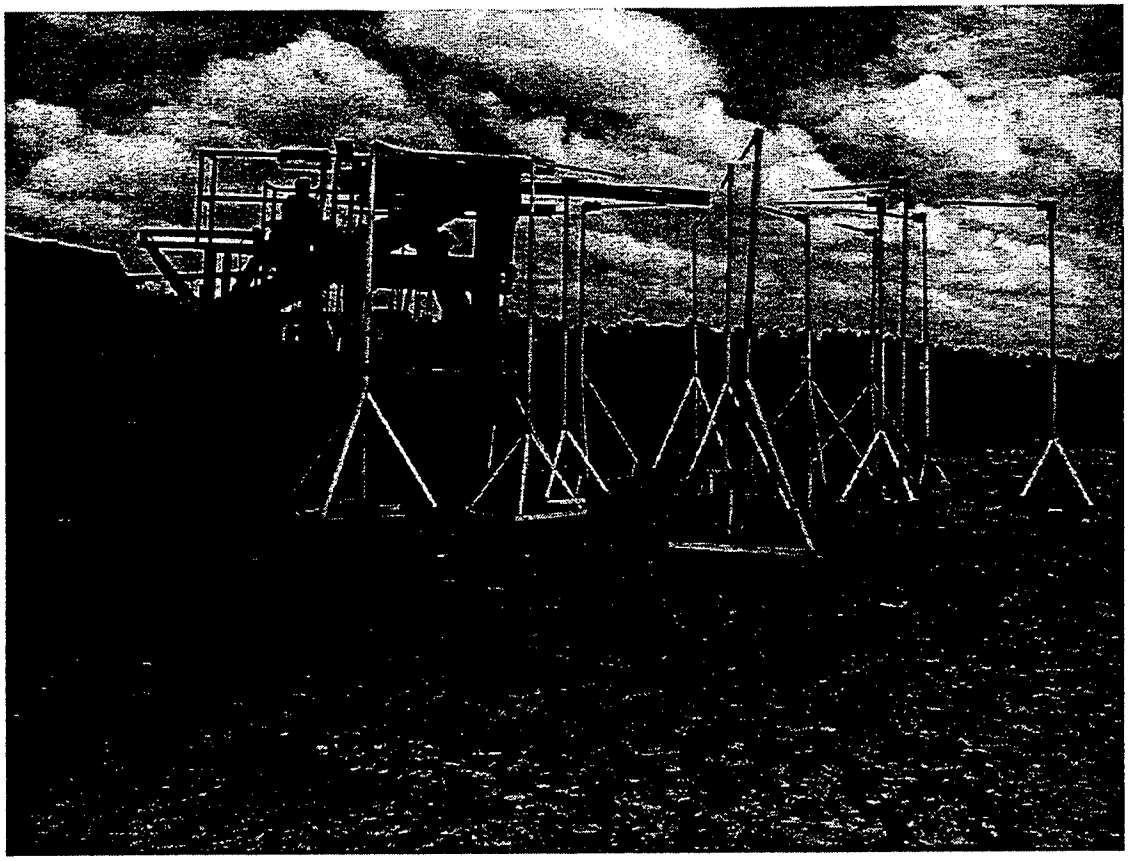

Figure 1. Gun Truck \Blast Arena

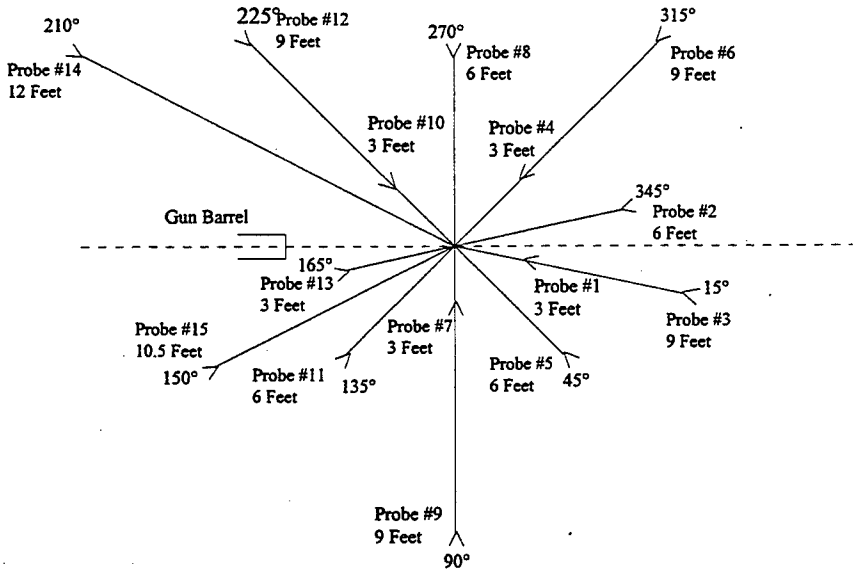

Figure 2. Pressure Probe Location

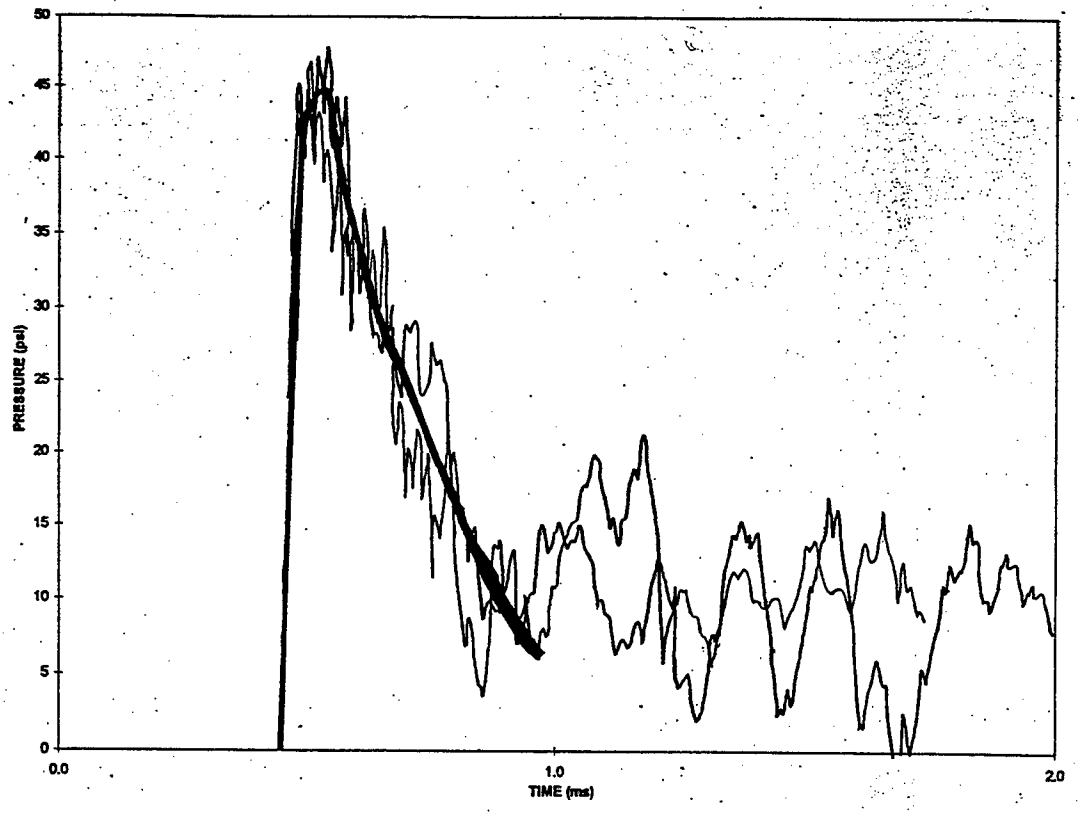

Figure 3. Pressure vs. Time, Probe 1, Shots 1& 2

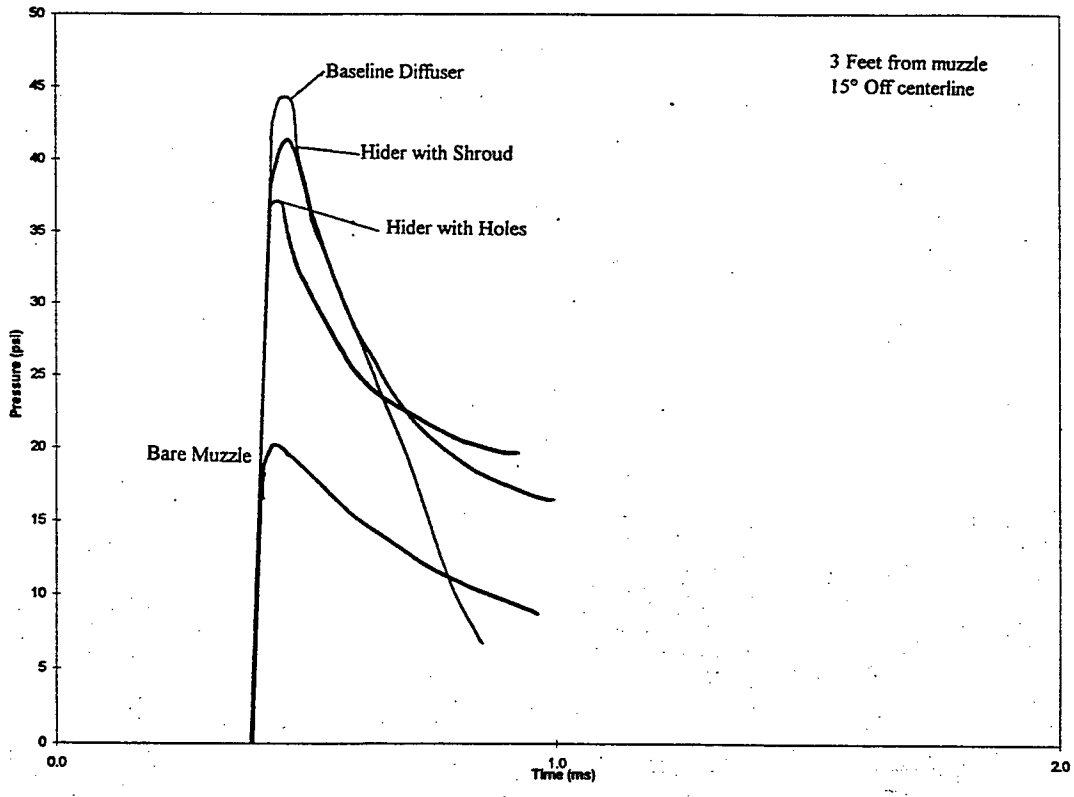

Figure 4. Pressure vs. Time, Probe 1, All Diffuser Designs

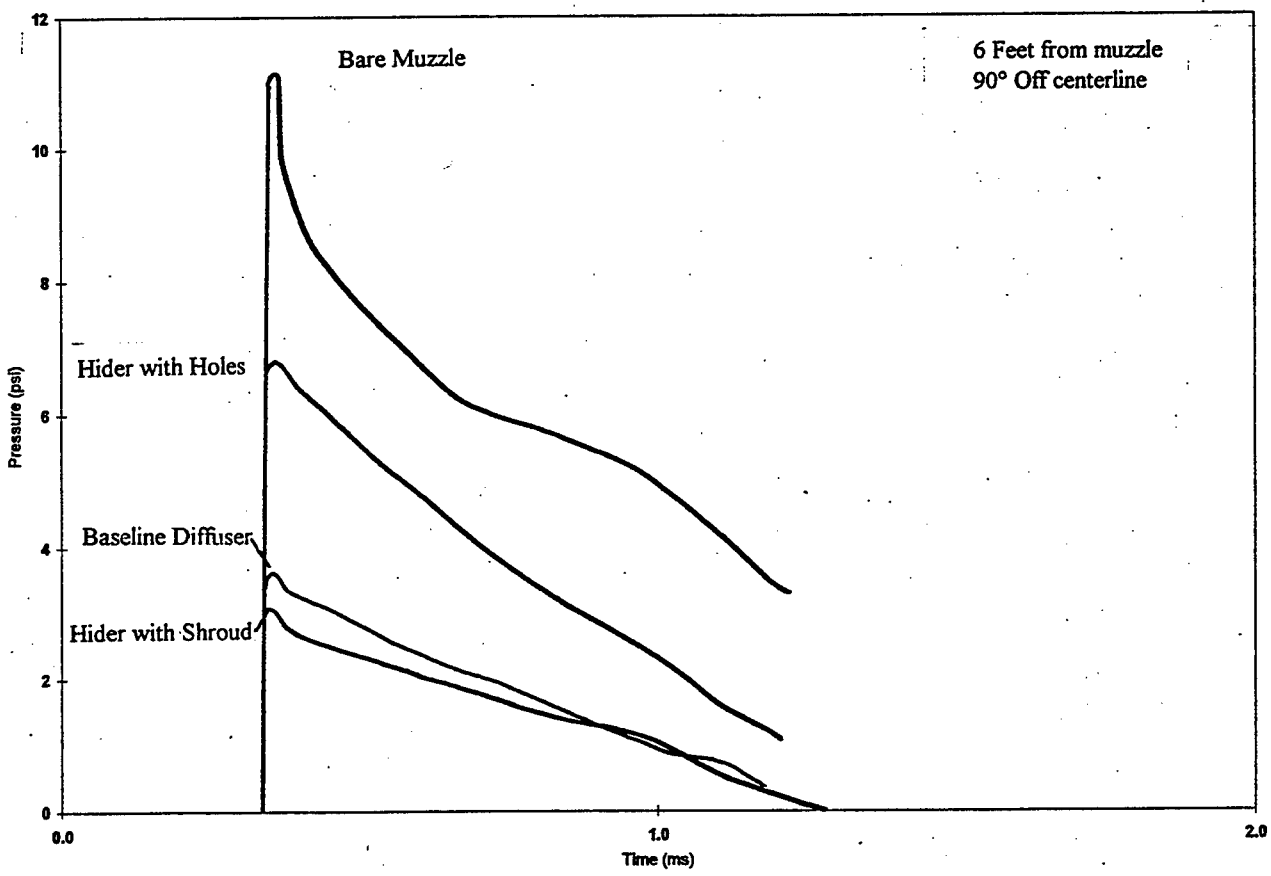

Figure 5. Pressure vs. Time, Probe 8, All Diffuser Designs

THE CREATION OF MOVING AND STATIONARY ACQUISITION AND RECOGNITION AND INFARED VISUAL DATA WEB PAGES

Jenny R. Garringer

Miami Trace High School
3722 State Route 41 NW
Washington Court House, Ohio 43160

Final Report for:
High School Apprentice Program
Wright Laboratory

Sponsored by:
Air Force Office of Scientific Research
Bolling Air Force Base, DC

and

Wright Laboratory

August 1996

THE CREATION OF MOVING AND STATIONARY ACQUISITION AND RECOGNITION AND INFARED VISUAL DATA WEB PAGES

Jenny R. Garringer
Miami Trace High School

Abstract

The Moving and Stationary Target Acquisition and Recognition (MSTAR) and infrared visual data images were converted to various formats and then placed on a web page. The creation of the MSTAR web page started by transferring photographs of 14 targets from a PhotoCD, using a Silicon Graphics Indy machine. These images were reduced in size and resolution. They were then placed onto a web page using Hypertext Markup Language (HTML.) The infrared visual data images were converted to the JPEG format using NIH Image and GIF Converter on a Macintosh computer. These images were also put onto a web page using HTML. The conversion of all images took a long time and was very tedious work. I learned a great deal about HTML and the creation of web pages. These are things that I probably would not have learned without this program.

THE CREATION OF MOVING AND STATIONARY ACQUISITION AND RECOGNITION AND INFARED VISUAL DATA WEB PAGES

Jenny R. Garringer

Personal Web Page

I began my tour by first getting used to a UNIX based machine. After I finally became accustomed to a UNIX machine, I started creating a personal web page. I learned how to take images from other sites and use them in my own home page. I also experimented with the HTML language by using it to do various functions such as creating hypertext links to other sites and creating tables and forms. This page was not posted on the server because it just served as an introduction to HTML. It was very helpful in that respect.

MSTAR Data Page

The second project was to create a web page using MSTAR photographs. There were a total of 14 different targets. Each target was photographed at 45 degree intervals at an elevation angle of 15 degrees around its circumference. Photographs were also taken of the right side of each target at the elevations of 30 and 45 degrees. Each of these images had to be transferred from a PhotoCD and then reduced in size and resolution. After all of the approximately 230 images were reduced they were converted to the JPEG format because it was the most compressed format available. These images were then transferred onto a web page where they were inserted into a table. Thumbnail size icons also had to be made for each target.

The web page contains three frames. The first frame contains the icons and names of the 14 targets. When one of the targets is selected its table will come up in the second frame. When a certain angle is selected a picture of the target at that angle will appear in the third frame.

If the password is known this page may be viewed at:

http://www.mbvlab.wpafb.af.mil/MBVDATA/TARGETS/index.htm

Group Web Page

The third project was to create a group home page. This page contains a short biography of each of the participants in the program from our area. After each participant had written their biography, they were compiled onto a web page. Each of the participants were then photographed using a digital camera. Our pictures were then inserted onto the web page containing our biographies.

Infrared Visual Data Web Page

The fourth and final project was to create a web page for the infrared visual data. Five different targets were photographed at five different elevations over a 24 hour period. They were photographed using mid wavelength infrared and long wavelength infrared during the months of August and December, 1994. There were approximately 2,500 images that needed to be converted to the JPEG format. These images were first converted to the PICT format via NIH Image 1.52. The images were then converted to the JPEG format using the program GIF Converter 2.3.3. These images were then transferred onto a web page very similar to the MSTAR data page. The first frame allows one to choose whether he/she wants the month of August or December. The list of the five targets then appear in the second frame. When one of the targets is chosen a table appears. Here one can choose which hour out of the 24 hour period they would like to view. When an hour is chosen, the mid wavelength and the long wavelength images appear in the fourth frame. There is also a function that allows one to view all of the images in sequence over the 24 hour period. Each hour's images are shown for a period of seven seconds.

Conclusion

My experience while working at Wright-Patterson Air Force Base has been quite rewarding. I learned a great deal about HTML that I had not been exposed to previously. I also became very familiar with the process of converting images to a variety of different formats. The information that I learned over the summer will be very beneficial in the future and I am glad that I had the opportunity to experience this program.

References

Castro, Elizabeth. HTML for the World Wide Web. Berkeley, CA: Peachpit Press, 1996.

December, John and Mark Ginsburg. HTML and CGI Unleashed. Indianapolis, IN: Sams.net Publishing, 1995.

Smith, Bud and Arthur Bebak. Creating Web Pages for Dummies. Chicago, IL: IDG Books Worldwide, 1996.

Stauffer, Todd. HTML By Example. Indianapolis, IN: Que Corporation, 1996.

A STUDY OF THE LUBRICATING PROPERTIES OF COMMERCIAL LUBRICANTS WITH RESPECT TO RELATIVE HUMIDITY

Douglas S. Ginger

Centerville High School
500 East Franklin St.
Centerville, OH 45459

Final Report for:
High School Apprentice Program
Wright Laboratory

Sponsored by:
Air Force Office of Scientific Research
Bolling Air Force Base, DC

and

Materials Directorate
Wright Laboratory

August 1996

A STUDY OF THE LUBRICATING PROPERTIES OF COMMERCIAL LUBRICANTS WITH RESPECT TO RELATIVE HUMIDITY

Douglas S. Ginger
Centerville High School

Abstract

The effectiveness of lubricants on the wear of steel in a controlled environment was studied. To simulate a system experiencing relative motion, a Cameron-Plint tribometer was used along with highly polished steel disks and cylinders. The environmental relative humidity was strictly controlled and varied between test runs from one to ninety-five percent to determine the impact humidity has on the wear and frictional properties of the lubricant. With the temperature kept at a constant 150°C throughout the tests, experimental results indicate that a significant correlation exists between the relative humidity of the air around the sample with friction and wear.

A STUDY OF THE LUBRICATING PROPERTIES OF A BASE FLUID IN DIFFERENT HUMIDITIES

Douglas S. Ginger
Centerville High School

Introduction

With the development of machines with interacting moving parts, the development of lubricating materials to prevent wear from damaging the machines is a must. As machines and equipment become more complex and more delicate, new better protecting and specialized lubricants need to be developed. Modern-day science continues to pose similar problems within the mechanical field as new lubricants are needed for the space and aerospace industries. The development of new lubricants, as with any new material, necessitates the need for extensive testing. The testing of various environmental conditions was a natural result of this procedure. If variations in the environmental conditions, in this case the relative humidity, alter the performance of a lubricant, such information could help to lead to an improved understanding of the chemistry operative and/or under what conditions the lubricant was suitable to be used.

Methodology

Using commercially available fluids, the testing was done using a Cameron-Plint tribometer simulating boundary lubrication conditions incorporating a specially modified test chamber used to control the environmental conditions. A steel cylinder was slid across a similar steel disc in a reciprocating manner in order to produce a wear scar under boundary lubrication conditions. A 250N load was placed on the cylinder to aid in the formation of the wear scar. The temperature of the test sample was kept at a constant 150°C in these experiments. The relative humidity of the test chamber was varied from test to test to determine the impact humidity had on the wear and frictional properties of the lubricant. The relative humidity was varied using either the injection of dry air into the test chamber for tests with a relative

humidity lower than the ambient level or an ultrasonic humidifier for the tests with a relative humidity higher than ambient. A data acquisition system, taking measurements every thirty seconds, was used to measure and record the temperature and relative humidity of the sample and to observe the friction and electrical resistance between the steel cylinder and disk. The electrical resistance was used to help determine whether or not the development of a film occurred. A high electrical resistance was an indicator that little metal to metal contact was occurring and thus the formation of a film occurred. Likewise, a low electrical resistance indicated significant metal to metal contact and thus the lack of a film. The wear area was determined by measuring the average length and width of the wear scar on the cylinder at the end of each test run.

Results

Testing produced results indicating that relative humidity does indeed have a significant impact on the formation of a film on the steel and thus a significant reduction in the wear. As the humidity is increased from one to twenty percent the frictional force and wear scar size each decreased dramatically and the electrical resistance, thus indicating formation of a film, increased.

Figure 1 shows the effect of the relative humidity on friction. When the humidity is between one and ten percent the coefficient of friction is relatively high (ca. 0.13). As the humidity is increased to twenty percent, however, the coefficient of friction drops sharply to 0.11 and remains between 0.11 and 0.12 for all test runs between twenty and ninety-five percent.

Figure 1

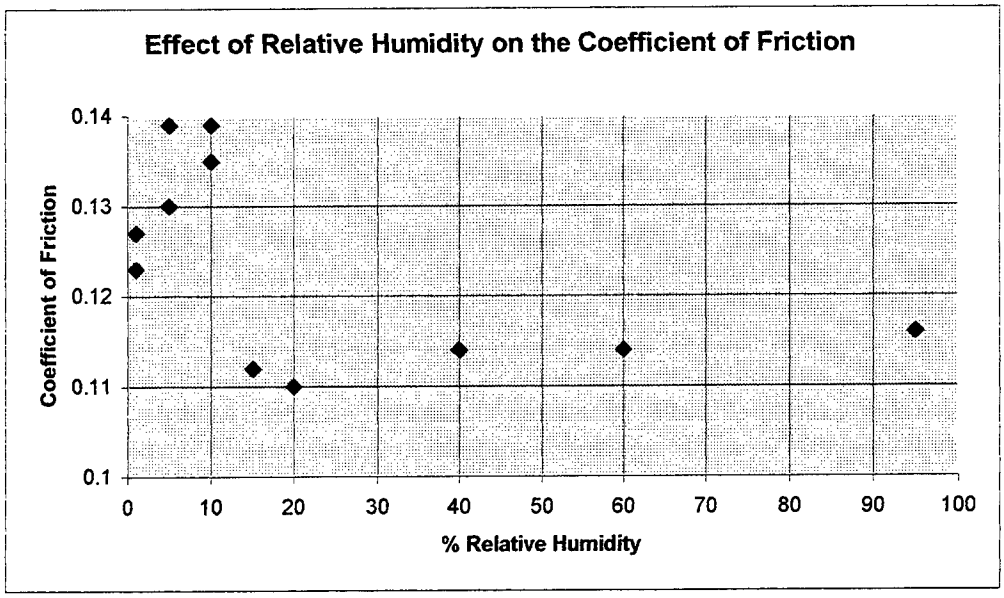

Figure 2 shows the effect of relative humidity on the wear scar. Perhaps one of the more significant indicators of the effectiveness of the lubricant, the wear scar was relatively large when the relative humidity was between one and twenty percent with values between three to over four square millimeters. Again, as the relative humidity was raised to twenty percent, the wear scar results decreased dramatically (from over three square millimeters to under one square millimeter for all humidity levels greater than twenty percent).

Figure 2

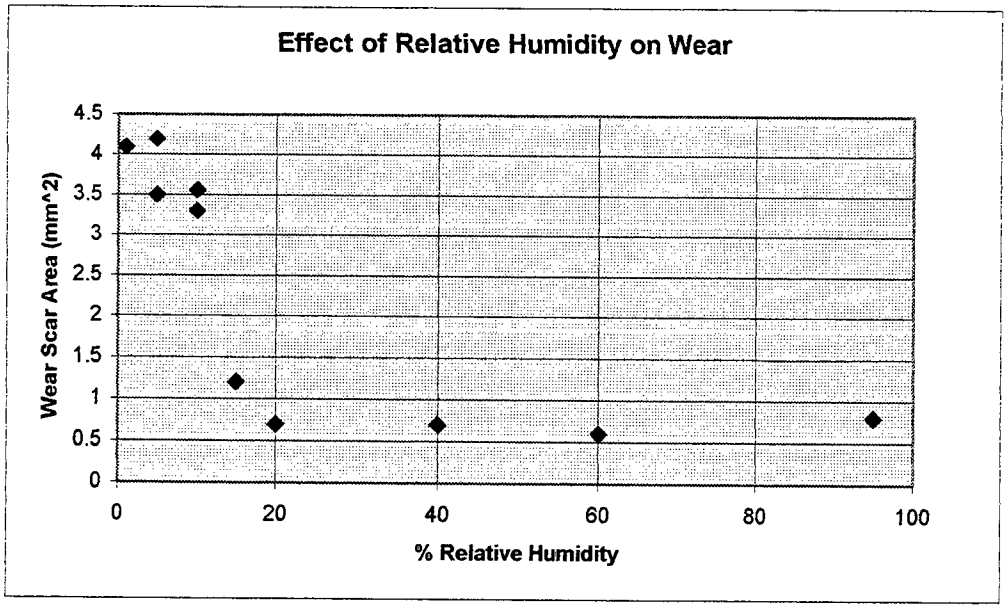

Figure 3 shows more clearly the dramatic reduction in wear scar area produced when the relative humidity is increased above twenty percent.

Figure 3

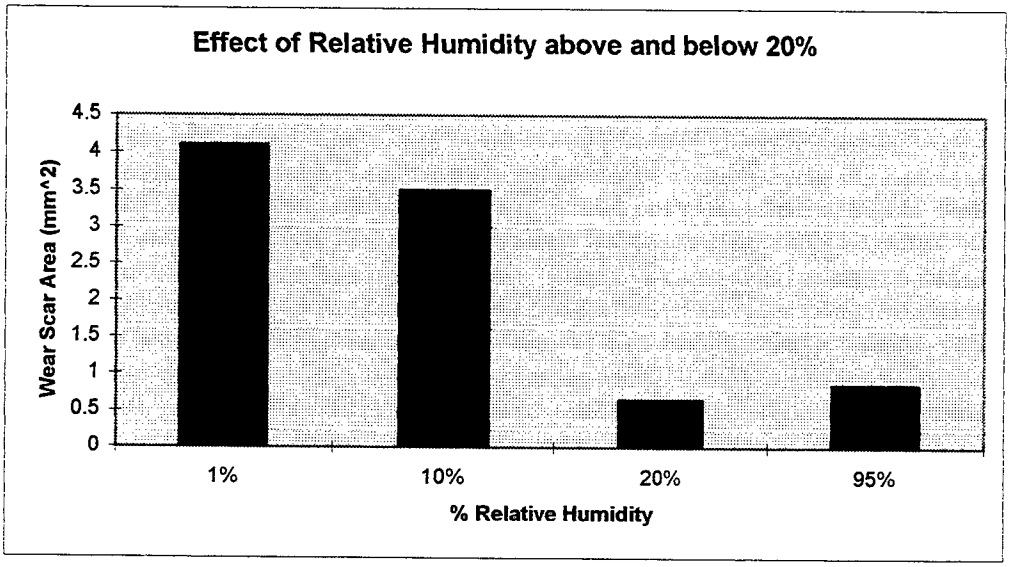

The percent of relative humidity seemed to have a direct impact on the electrical resistance. On tests run around ninety-five percent relative

humidity, the electrical resistance hovered between ten-thousand and one-hundred-thousand ohms. On tests run around one percent relative humidity, the resistance was much less, around one-hundred to one-thousand ohms. The electrical resistance is determined by the amount of metal to metal contact between the two steel materials, and the metal to metal contact is mainly determined by the extent of the formation of a film on the steel, thus the percent of relative humidity seems to directly impact the formation of a film on the steel disks.

Discussion

It has been shown that there is a correlation between low levels of humidity and the high friction and wear scars observed with several types of commercial perfluoropolyalkylether lubricants. The explanation of this phenomenon is best left to the chemists. The atmospheric water may play some sort of role in the formation of the protective film on the steel, or the atmospheric water may in some way protect the lubricant itself from decomposition or chemical alteration. Further study on this topic is needed if the true nature of what is happening is to be understood, but all further testing of similar lubricants needs to be strictly monitored and controlled regarding the atmospheric humidity at the test site.

Conclusions

In many commercial lubricants, the presence or absence of atmospheric humidity has a dramatic impact on the wear and frictional properties of the lubricants when used under boundary lubrication conditions. The atmospheric humidity interacts either in the formation of the protective film on the steel or in protecting the lubricant from changing its chemical structure or decomposing into a less effective substance. This property of some lubricants necessitates the careful control of humidity in all lubricant testing to help to ensure controlled and consistent results from season to season and

laboratory to laboratory or the understanding and modification with additives to avoid these limitations.

Julie Glaser's report was not available at the time of publication.

PITOT PROBE MEASUREMENTS OF AIR FLOW THROUGH A DUCT AND DIFFUSER

Robert J. Glaser III

Carroll High School
4524 Linden Avenue
Dayton, Ohio 45432

Final Report for:
High School Apprentice Program
Wright Laboratories

Sponsored by:
Air Force Office of Scientific Research
Bolling Air Force Base, DC

and

Wright Laboratories

August 1996

ABSTRACT

Testing has been conducted on a generic inlet and diffuser test section that was designed to simulate the air flow delivery to a combustor sector. The airflow exiting the diffuser must have a uniform velocity or momentum profile. This momentum or dynamic pressure leaving the diffuser has a tremendous impact on the combustion air entering into the combustor and thus the operation of the combustor. The ununiformity of the air entering into the combustor can manifest itself in poor combustor stability as well as a decrease in combustion efficiency and an increase in flame length. Velocity measurements using a pitot static probe have been obtained at various locations in the test section to determine the distribution of air through the rig. The probe was traversed to obtain a full compliment of data for which to interpret the trends. Based on the data obtained, adjustments were made to condition the flow to effect the flow distribution of air entering and exiting the diffuser.

PITOT PROBE MEASUREMENTS OF AIR FLOW THROUGH A DUCT AND DIFFUSER

INTRODUCTION

A pitot probe is a probe designed to measure two types of pressure in an air flow to determine the velocity of the flow. One pressure is called total pressure or stagnation pressure. This pressure is the pressure obtained when the flow is decelerated to zero velocity by a frictionless process. This measurement is taken at the tip of the probe shown in figure 1. The other type of pressure, thermodynamic or static pressure, is the pressure that an object moving at the same velocity as the air being measured would experience. This measurement is taken on the sides of the probe shown in figure 1. These pressures are measured using a water manometer. The air flow velocity can be calculated when the delta p (the difference between total pressure and static pressure), static pressure, and the air temperature are known. There are however, many problems that could introduce error into these measurements. Even the mere presence of the probe can change the pressures being

measured. Yaw angle (the angle between flow axis and the probe) can affect static pressure as much as 8% with just a 15 degree yaw angle. Interaction between adjoining probes, probe supports, and duct walls can also influence the accuracy of the measurements.

Pitot Probe (Fig. 1)

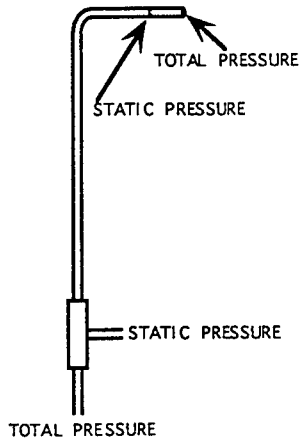

A profile of flow velocities in a duct can be obtained by traversing a pitot probe across the duct opening. Several compiled profiles can show a realistic three dimensional depiction of air velocities through a pipe or duct. Ideally, air flow velocities would be constant across the crossectional area of the duct. In reality however, air velocities are substantially lower near the duct walls due to friction effects. This area of lower velocities near the duct walls is known as the boundary layer.

Through a process called conditioning these velocity variations can be minimized. Conditioning can be done in many ways. Rounding of sharp edges in the inlet section, putting screens and or honeycombs in the inlet section are more typical ways of conditioning the flow of the inlet.

Conditioning of the flow through ducts and pipes has many applications in industry. In burner systems, research applications including wind tunnels, cooling research for heat transfer, systems for research in gas turbine engines as well as various systems such as compressors, turbines, and combustors all require stable continuous flows.

In jet turbine engines, a diffuser attached to the exit of the compressor discharge delivers air flow to the combustor. The purpose of the diffuser is to reduce the velocity of the air exiting the duct with as little pressure loss as possible. Reducing the pressure loss is important in jet turbine engines

because substantial energy is put into pressurizing the air in the compressor and this stored energy is to be released as thrust not losses in the diffuser. The velocity must be reduced so that the combustor can mix fuel with the air and burn it as efficiently as possible. The diffuser must also deliver a smooth and stable flow to the combustor dome. With present technology, it is not possible to decrease the velocity without the pressure loss. A trade off must be made to reduce the velocity to an acceptable level while giving up some pressure. In most diffusers, the velocity decrease is achieved by increasing the cross-sectional area of the flow while minimizing the flow separation.

DISCUSSION OF PROBLEM

The problem was to determine if the velocity profile of the air at the entrance and exit of the diffuser was smooth and stable. Then to make any modifications to the inlet section necessary. To accomplish this, a way of measuring velocity in the duct and diffuser had to be found. A pitot probe was used to do this. A method of moving the probe quickly and accurately to different locations for data acquisition had to be implemented. The yaw angle of the pitot probe must be as close to zero as possible, and the probe must be handled with care so as to avoid damaging it.

METHODOLOGY

Through the use of a pitot probe, a three dimensional velocity profile was created. This was done by traversing the probe across each opening and taking measurements at 0.25 inch horizontal increments. The test section was mounted on a three axis traverser which is accurate to one ten thousandth of an inch. The traverser was used to move the rig to each location where each data point was to be taken. The yaw angle was measured to be certain that it was zero both horizontally and vertically. Five of these sets of data were taken across each opening. One at the centerline, one at 0.125 inches above the centerline, one at 0.25 inches above the centerline, one at 0.125 inches below the centerline, and one at 0.25 inches below the centerline were taken for the inlet to the diffuser. One at the centerline, one at 0.15 inches above centerline,

one at 0.30 inches above centerline, one at 0.15 inches below centerline, and one at 0.30 inches below centerline were taken for each opening at the exit of the diffuser.

The test rig consisted of a pipe which terminates into a plenum section which leads to the tapered duct (as shown in Figure 2). The air flow was controlled by using an orifice plate with 60 psi constant upstream pressure and a 7 psi pressure drop across the orifice plate. The pressure readings generated by the pitot probe were measured with a water manometer in inches of water. These pressure readings were then converted into velocities through a mathematical conversion process done on a spreadsheet. Graphs were produced from the data in the spreadsheet, and then the data could be analyzed.

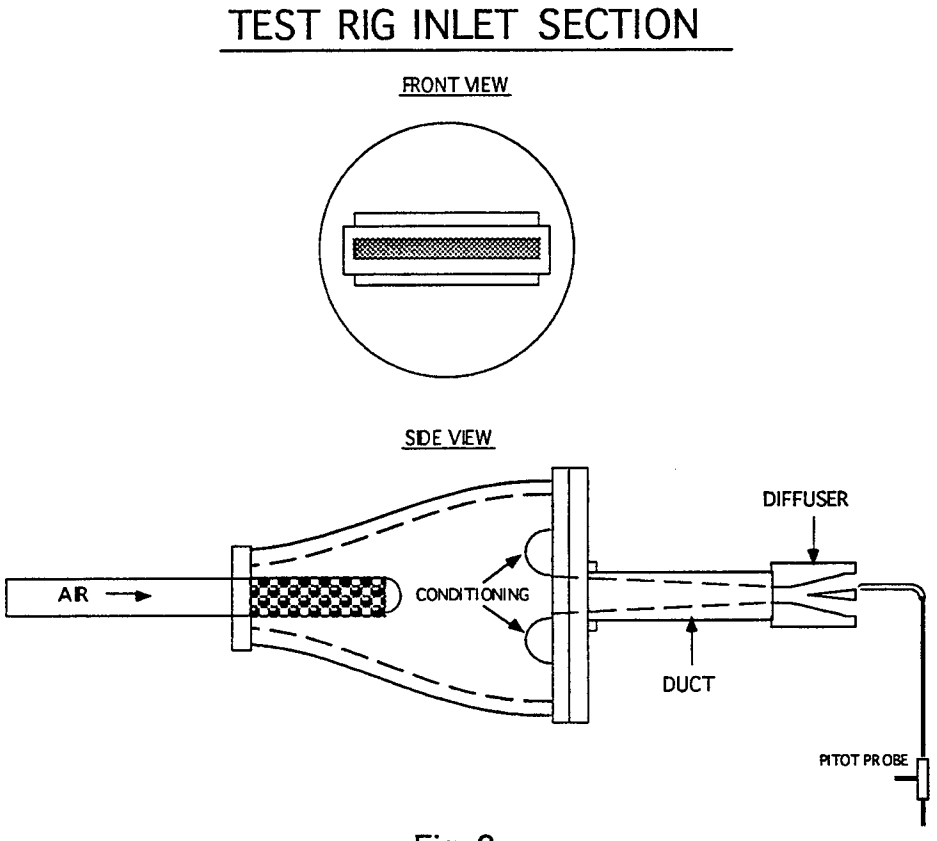

Fig. 2

RESULTS

The velocity profile for the entrance to the diffuser appears to be both smooth, stable, and constant across the crossectional area of the duct (Fig 3). The low measurements at the walls (-3 inches and 3 inches) is due to the boundary layer that exists in all pipes and ducts and cannot be avoided. The positive side of the graph shows that the velocities are higher on the right side of the duct exit as you are facing it.

The velocity profile at the exit of the diffuser passages is substantially higher near the center of the diffuser exit (Fig 4 and 5). There is even a small area at the top and bottom of the diffuser exit where the velocities taken were negative. This means that air was actually flowing backwards into the diffuser exit. This small area of recirculation may cause flame stability problems in the combustor. Flow separation in the diffuser causes turbulence in the form of shedding. It is important to have a constant velocity across the opening at the exit of the diffuser to maintain good flame stability in the combustor.

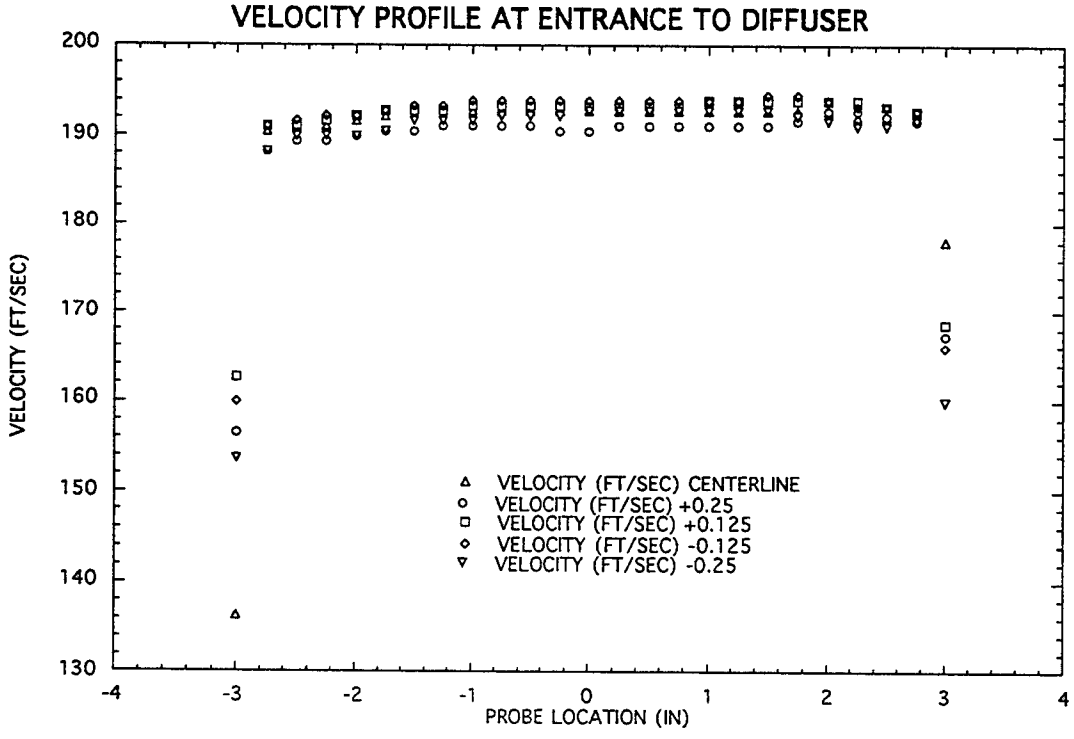

Fig.3

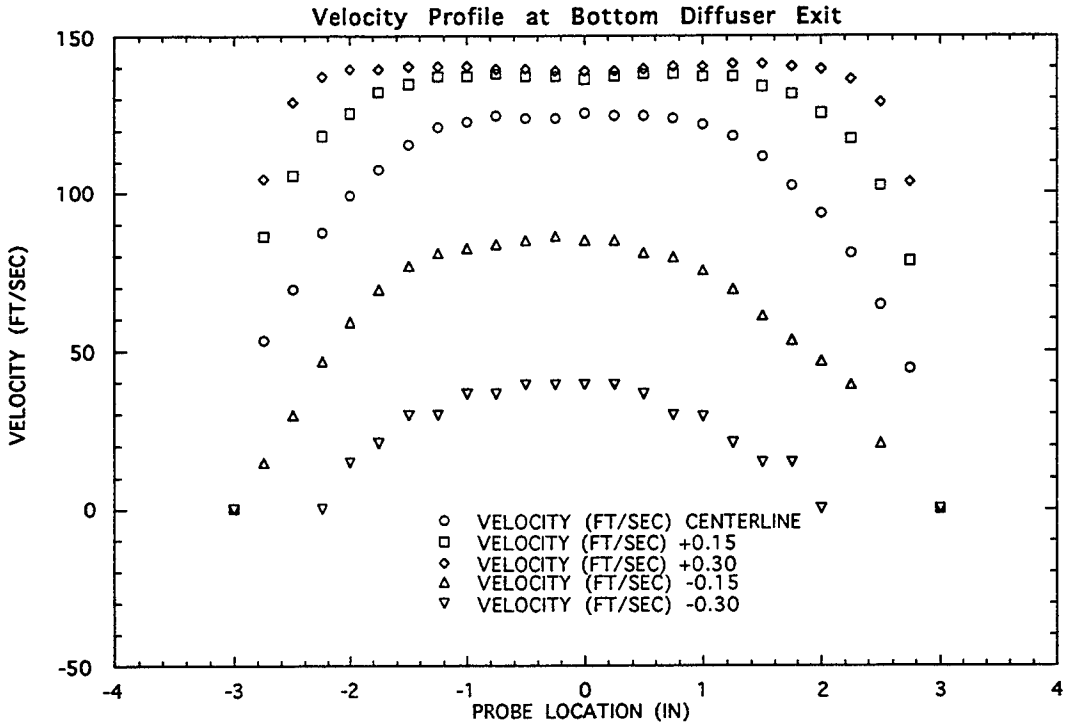
Velocity Profile at Bottom Diffuser Exit
VELOCITY (FT/SEC)
PROBE LOCATION (IN)
VELOCITY (FT/SEC) CENTERLINE
VELOCITY (FT/SEC) +0.15
VELOCITY (FT/SEC) +0.30
VELOCITY (FT/SEC) -0.15
VELOCITY (FT/SEC) -0.30

Fig. 4

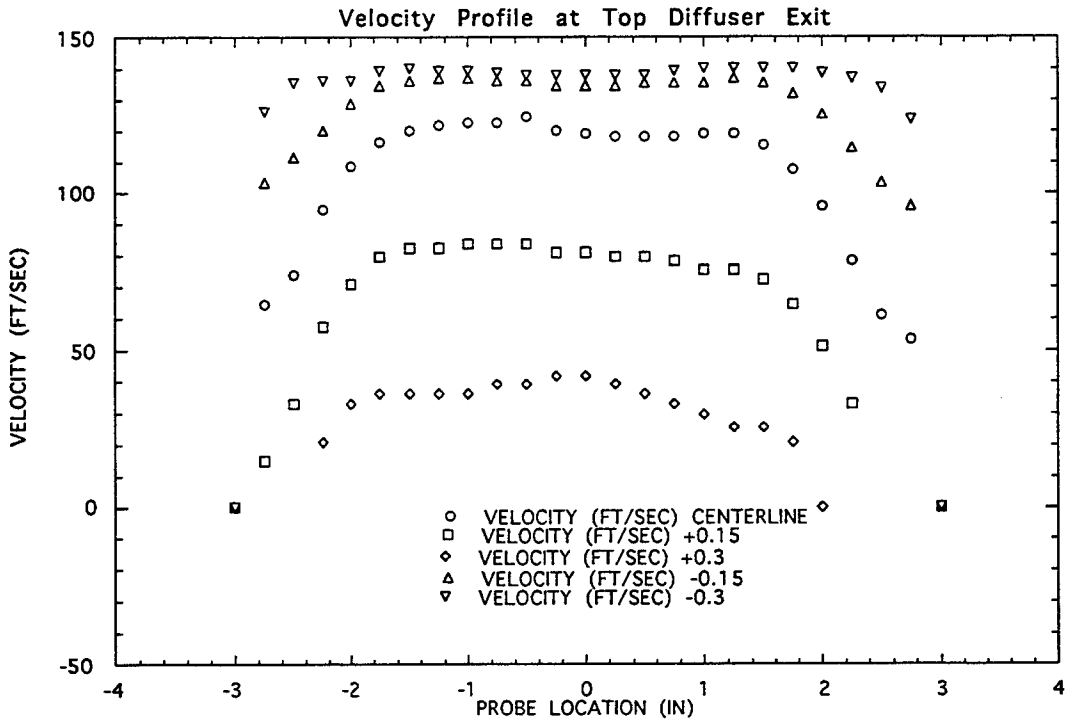
Velocity Profile at Top Diffuser Exit
VELOCITY (FT/SEC)
PROBE LOCATION (IN)
VELOCITY (FT/SEC) CENTERLINE
VELOCITY (FT/SEC) +0.15
VELOCITY (FT/SEC) +0.3
VELOCITY (FT/SEC) -0.15
VELOCITY (FT/SEC) -0.3

Fig. 5

CONCLUSION

The data collected shows that the flow into the diffuser is extremely good, it is flat, smooth, and stable. This means that the diffuser is getting a favorable velocity profile. At the diffuser exit however, the velocities are much higher near the center of the diffuser. This is indicative of both flow seperation and streamlining of the incoming flow. To correct this the diffuser angle would to be decreased to avoid the flow seperation. The streamlining effects must be accounted for in a different manner, the placing of verticle struts in the diffuser will provide for an increase in effective exit blockage which will tend to distribute the air flow better and in turn reduce the streamline effects. The struts are to be designed and will be added, however further testing will be required and consequently will not be reported in this paper. This modification should correct the problem identified by the data collected during this experiment.

REFERENCES

Interview: Dale T. Shouse, Combustion Research Program Manager, Aero Propulsion and Power Division, WPAFB Ohio.

Arthur H. Lefebvre, *Gas Turbine Combustion*, Hemisphere Publishing Corporation, New York, 1983.

Beckwith, Buck, Marangoni, *Mechanical Measurements,* Third Edition, Pittsburgh, 1981.

Robert W. Fox, Alan T. McDonald, *Introduction to Fluid Mechanics,* Third Edition, John Wiley & Sons, New York, 1985.

Robert D Zucker, *Fundamentals of Gas Dynamics*, Matrix Publishers, London, 1977.

DEVELOPING AN AUTOMATIC NEURAL NETWORK TRAINING ALGORITHM AND USING NEURAL NETWORKS AS CIRCUIT SIMULATOR MODELS

Stephen M. Govenar

Beavercreek High School
2660 Dayton-Xenia Road
Beavercreek, OH 45434

Final Report for:
High School Apprentice Program
Wright Laboratory

Sponsored by:
Air Force Office of Scientific Research
Bolling Air Force Base, Washington DC

and

Wright Laboratory

August 1996

DEVELOPING AN AUTOMATIC NEURAL NETWORK TRAINING ALGORITHM AND USING NEURAL NETWORKS AS CIRCUIT SIMULATOR MODELS

Stephen M. Govenar
Beavercreek High School

Abstract

The HP Libra circuit simulator has a feature called Senior that enables user-defined elements to be created and used in the program. A neural network training program developed last year, named nnw, was modified to output C source code for a Senior element and for a standalone neural network program. An automatic neural network training algorithm was then developed, and the nnw program was modified to include this.

DEVELOPING AN AUTOMATIC NEURAL NETWORK TRAINING ALGORITHM AND USING NEURAL NETWORKS AS CIRCUIT SIMULATOR MODELS

Stephen M. Govenar

Introduction

Neural networks can be used to find the relationships among sets of data, and make predictions from other inputs using these relationships. A neural network consists of an input layer, a hidden layer, and an output layer of neurons. Weights connect each neuron of one layer to each neuron of the next layer. All of the inputs to a neuron are multiplied by the connecting weights, summed, and put through an activation function, the value of which is the output of the neuron. In this case, a two-layer feed-forward network was used, with the error backpropagation training algorithm using the delta learning rule. The activation function used was

$$f(net) = \frac{2}{1+e^{-\lambda net}}$$

The nnw program written last year that implements neural network training and testing was modified and used as a base for two other programs that were created.

Standalone Neural Network Program

To make it easy to compute outputs from a neural network trained by the nnw program, a standalone program was created. This program gives the user the option of either entering one network input vector at the keyboard, or reading a large number of inputs from a file. The outputs

are written to unix standard output, which is normally the screen but can be redirected to a file. The standalone program was built around the test function from the nnw program, with unnecessary parts removed. Network parameters and the weights used in training the network were stored in the source code as constants.

A validation process was carried out to ensure that the standalone program produces the same outputs as the nnw program. The following results were found on both the HP and sun platforms. "Nnw 1st run" refers to the outputs obtained with the nnw program immediately after training. "Nnw 2nd run" outputs were obtained after exiting and restarting the nnw program and reading in the saved weights. "Standalone" outputs were obtained from the standalone program created by the nnw program after training.

For the training data, the results were the same for all three of nnw 1st run, nnw 2nd run, and standalone (with very small errors due to rounding). The correlation between all of the outputs from nnw 1st run and nnw 2nd run was 1.0, as was the correlation between the outputs from nnw 1st run and the standalone program. Graphs were plotted for the first and last outputs. The small error (ex. Average Relative Error of 0.000069% between HP nnw 1st run and 2nd run for the first output) was introduced when the weights were saved in a file with 5 decimal places, causing rounding to occur.

For the test data, the same results were obtained with nnw 1st run and nnw 2nd run (correlation = 1.0), but results from the standalone program were different (ex. correlation of 0.949156 and ARE of 11.9% between HP nnw 1st run and standalone for the first output). This was because the standalone program was created using max/min values from training data to scale the test data, but the nnw program scaled the test data using max/min values from the test data. The standalone program would have given different results if it had been created after loading test data, instead of after training. The results from the standalone program were better than the results from the nnw program (ARE between desired and computed first output of 4.7% compared to 12.1%).

This was fixed by storing the max/min values from the training data in the weight file when the weights are saved. These max/min values are read when the weight file is read, and these values will be used for scaling the test data and for creating the standalone program.

To test this fix, a 3rd run of the nnw program was made, reading in a weight file that had the max/min values of the training data in it. The results were exactly the same as the results from the standalone program (ARE of 0%).

Libra Senior Element

A linear Libra senior element that used a neural network to model an inductor was made. To create this element, an example element file was

copied and modified. The example file was for a nonlinear element and parts of it had to be changed to work with a linear element. Network parameters and the weights used in training the network were stored in the senior element source code as constants. The linear analysis function that Libra calls, nnwelem_y, was created by copying the test function from the nnw program, removing the parts that were not needed. Code was added to interface with Libra. The frequency is passed into nnwelem_y by Libra and is converted into MHz. The other network inputs are copied from a Libra parameter structure. The neural network outputs are S-parameter magnitude/angle pairs. To return these to Libra in the form it wants, the S-parameters are converted to real and imaginary components, and then the Libra function s_y_convert is called to convert the S-parameters to Y-parameters. Debugging messages were added to the senior element, but they are off by default.

Automated Source Code Generation

After the standalone program and Libra senior element source code was finished, options were added to the nnw program to generate these source code files using current neural network weights. To accomplish this, a function called make_wgt_code was written that writes the current weights and the max/min arrays that are used for scaling to a source code file in the form of C constants. Then two more functions, make_stand_code, and make_libra_code, were written. Make_stand_code writes the remainder of the standalone program source code to the file that make_wgt_code started. This is done with one large fprintf

statement, with all of the source code hardcoded into the nnw program. A small program called inc was written to put source code into a form suitable for simply being pasted into the fprintf statement. make_libra_code works the same way as make_stand_code, but also prompts for the element name and input labels, and uses loops to write variable portions of the source code, in addition to the hardcoded code.

Auto Training Algorithm

An automatic neural network training algorithm was developed by Greg Creech and implemented in the nnw program. This algorithm started training the network with a small number of hidden layer neurons, and added another hidden neuron when the difference between the errors of two consecutive training epochs dropped below a user defined value. The algorithm then tested the network, and decided that the best network had been found when the difference between two test errors was below a specified value.

A second auto training algorithm was then developed that was believed to give better results and be more general. This algorithm did both the training and testing of the network at the same time. At the end of each epoch the ratio of the training error to the testing error was calculated. After another epoch, a ratio of the two error ratios was computed. If this ratio, called O^1hl, was below a user defined value, the network had stopped improving, and another hidden neuron was added. The above process was then repeated until another hidden neuron needed to be added, and O^2hl was calculated. If the ratio of O^1hl/O^2hl, called ro_hl, was less than a user defined value, this network was the best, and the training stopped.

When this auto training algorithm was tested, the part that decided when to add a new hidden neuron worked well, but the section that determined when to stop the training did not. The value of ro_hl went up and down

in a small range of values, and never got near the cutoff point. However, the training log file that this algorithm produced still provided a good estimate of the optimum number of hidden neurons.

Appendix A

NNW User's Guide

==========

NNW is a program written in C that simulates a two-layer feed-forward neural network. It consists of the files nnw.c, nnw.h, and Makefile, and reads its data from various files, usually including a network parameter file, network info file, input vector file, and output vector file. They may have any filenames, but the following convention has been used so far: if the data being tested was from inductors, a prefix like 'ind' would be chosen, and the four files mentioned above would be named indnet.dat, indinfo.dat, indin.dat, and indout.dat.

Compiling

To compile NNW, an ANSI C compiler is required. Edit the Makefile if necessary and type 'make hp' to compile on an HP, or 'make sun' to compile on a sun (using gcc). No changes to the Makefile should normally be needed. The compiled binary is named 'nnw'.

Data Files

Network Parameter File

The network parameter file contains constants used in the neural network (except for the number of inputs). It should look like:

```
eta 0.01
lambda 0.2
emaxcum 0.01
cyclemax 200000
J 1
K 1
p_iter_dev 1.0005
p_hl_dev 0.99
train_epoch 500
```

The values can be given in any order, and the names are not case sensitive. If a parameter is not given in this file, the values in the above example are used as defaults. The definition of each network parameter is:

eta - learning constant used in delta weight calculations
lambda - steepness factor in the network's activation function
emaxcum - for regular training, desired cumulative error of the network; training will stop when the error
drops below this value
cyclemax - for regular training, maximum number of cycles to train
When emaxcum or cyclemax is reached, a menu appears allowing the user to alter parameters and
continue or stop training.
J - for regular training, number of neurons in the hidden layer for auto training, number of hidden neurons
to start with
K - number of neurons in the output layer
p_iter_dev - percent iteration deviation; in auto training, a new hidden layer neuron will be added when
ro_gen drops below this value
p_hl_dev - percent hidden layer deviation; auto training will stop when ro_hl drops below this value; the
best network has then been found
train_epoch - number of cycles in one training epoch; in regular training, this controls how often the
training errors are displayed on the screen. in auto training, it
also controls how often errors and ro_gen are calculated

Network Information File

The network information file describes the number of neurons in the input layer, and the number of patterns. The first two entries in this file are the number of lines in the file (number of patterns + 1) and the number of words in the file. The rest of the file is ignored. The

number of inputs, or I, is calculated by second_number/first_number. The UNIX command wc can be used to create this file, as in "wc -lw indin.dat > indinfo.dat". If indin.dat contained 16 patterns with 4 (68/17) inputs, the resulting file would look like this:

```
17 68 indinput.dat
```

Input Vector (Data) File

The input vector file consists of one header line describing the inputs, and then all of the inputs for the network separated by tabs, one pattern per line. An example would be

```
*Width Spacing Length  Turns
10         10          200       1.5
1e+1    1e+1       2e+2     2.5e+0
....etc....
```

The words in the header are not used by the program, but must exist, and there should be one word per input.

Output Vector (Data) File

The output vector file contains the desired outputs for the network, and uses the same format as the input vector file (including the one line header).

Running the Program

To begin program execution, one must type 'nnw' at the shell prompt. nnw takes no command line arguments. The appropriate options are then selected from different menus. The function each menu option performs is described below.

Main Menu

When the program is started, the weights are initialized to random values between -0.125 and 0.125, and the main menu of NNW appears, and looks like this:

1. Load training patterns
2. Weight operations
3. Shuffle patterns
4. Edit network parameters
5. Train the neural network
6. Auto train the neural network
7. Test the neural network
8. Calculate sensitivities
9. Calculate correlations
10. Create a linear Libra model using current weights
11. Create a standalone neural net program using current weights
12. Quit the program

Each option is described below.

Load Training Patterns

This prompts the user for the network parameter, network info, input vector, and output vector files. The network parameters are set, and their values are displayed. The input and output vectors are read in, and the inputs and outputs are normalized, or scaled down, to values between -0.9 and 0.9. The normalized vectors are written to the files normalin.dat and normalout.dat (for checking purposes; these files are not used again by the program).

Weight Operations

This allows the user to randomize the network weights, store the current weights in a file, and read in weights from a file. The max/min arrays used by nnw to scale the data are also written to or read from a weight file.

Shuffle Patterns

This shuffles the input/output patterns, which should be done for the best training. The shuffled patterns are written to the files shuffin.dat and shuffout.dat (again, for checking purposes; they are not used again by the program).

Edit Network Parameters

This displays a menu with options to read a new network parameter file, save the parameters to a file, and alter the parameters.

Train the Neural Network

This starts training the neural net. Interrupting the program, usually by pressing CTRL-C or sending the SIGINT signal to the program, displays a menu that allows you to change the values of eta, lambda, emaxcum, cyclemax, and the display frequency (the variable train_epoch), and either continue or stop training. The current cycle number, cumulative network error, and root mean square normalized error are displayed every train_epoch cycles, which defaults to 500. If the error drops below emaxcum, or the cycle number reaches cyclemax, training is stopped and this menu appears. If you want to continue training, emaxcum and/or cyclemax need to be changed. You may stop training temporarily to return to the main menu and save the weights, test the network, etc., and continue training where it left off.

Auto train the neural network

Auto training can be used to easily see what number of hidden layer neurons provides the best neural network. Before using this option, training patterns must first be loaded. This option then prompts for the test info, input, and output files, and a filename to use for a training log. The auto training algorithm then begins. Every train_epoch cycles, ro_gen is calculated. If ro_gen drops below p_iter_dev, another hidden neuron is added to the network. ro_hl is then calculated, and if this value drops below p_hl_dev the best network has been found, and training stops. You can then save the weights using

the option in the main menu. As in regular training, CTRL-C brings up a menu allowing you to change the values of network parameters, or stop training.

Test the Neural Network

This displays the following menu.

1. Test network using training vectors
2. Test network using different test vector files
3. Quit to main menu

The first option tests the net using the currently loaded training patterns. The second option tests the net using patterns loaded in from another set of input/output vector files. The user is prompted for a network info file. If a network parameter file has not been read, lambda and J (number of hidden neurons) are prompted for. Then the input vector and output vector files are prompted for and read. After this, for both testing options, filenames for the results and errors to be written to are prompted for. The neural network is then tested by putting the test inputs into the network, using the current weights and writing the desired and actual outputs to the result file, separated by tabs, one pattern per line (as D1 O1 D2 O2 etc.). Errors for the network's actual versus desired outputs are written to the error file in the following format (all numbers on a line are separated by tabs). First, the percent error for each output of each pattern, one pattern per line. Then, the average percent error for each output, on one line. Next, a blank line, and then the squared error for each output of each pattern, one pattern per line. Then, the mean square error for each output, on one line. Another blank line follows, and the next line contains the value of r (output correlation) as a percentage for each output. Another blank line, and then on one line, the value of R squared as a percentage for each output.

Calculate Sensitivities

This prompts for a result filename, calculates the sensitivities (or importances) of the inputs to outputs, and writes them to the result file. The mean square average, absolute, and maximum sensitivities are written to the file in that order, each using the following format. First, a table of sensitivities, outputs horizontal from left to right, and inputs vertical, top to bottom. Then, the sorted average input sensitivities, along with the gap between successive values. Next, for each output, a sorted list of input sensitivities, with their gaps.

Calculate Correlations

This prompts for a result filename and calculates the input/output correlations, and the input/input correlations. The correlations measure how each output varies as each input varies. A value of 1 means they vary in the same way and are exactly correlated, and a value of -1 means they vary in exactly reverse ways. A value of 0 means they are not correlated at all. The result file will contain the input/output correlation matrix in a table, outputs horizontal from left to right, and inputs vertical, top to bottom. Then a blank line, and the input/input correlation matrix.

Create a linear Libra model using current weights

This creates a source code file containing a neural network that can be compiled as a "senior" model in the Libra circuit simulator. As input, the network will use frequency plus any number of user defined parameters. The network will output 8 S-parameters.

This option prompts for a source code filename and then asks if you want a passive or active model. In the active model, the neural network has 8 outputs, one for each S-parameter. In the passive model, the network has 5 outputs, s11m, s11p, s21m, s21p, s22p, and the following relationships are assumed be true: s12 = s21, s22m = s11m.

Next the program prompts for the element name. It can be up to 8 characters. The program prompts for labels for each input (except the first one, which must always be frequency), and then writes the source code to the filename specified. The network parameters, current weights, and max/min arrays used for scaling are written into this file as constants.

Create a standalone neural net program using current weights

This creates a source code file containing a standalone neural network program. The program prompts for a source code filename and then writes the source code to the file. The network parameters, current weights, and max/min arrays used for scaling are written into this file as constants. The resulting source code file can be compiled with a command line like

```
cc -Aa -O3 -s -o filename filename.c -lm
```

on an HP. For gcc, the following line will work:

```
gcc -O2 -s -o filename filename.c -lm
```

When running the standalone program, it gives the option of entering one input vector interactively, or reading the inputs from a file. For the first choice, the inputs are entered by the user, separated by a space (or carriage return). For the second option, the user is prompted for the number of patterns in the file, and then for the filename to read. The network outputs are written to stdout, which is normally the screen, but can be redirected to a file (the prompts are written to stderr and will not be redirected).

Recommended Use

In normal use, the user should load the training patterns, shuffle the patterns, and begin training. The weights should be saved either periodically or whenever the error seems small. The network could be

tested each time the weights are saved, or after all the training has finished, loading in the saved weight files for each test. The sensitivities could be used to determine which inputs are not very important in affecting the output, and could possibly be omitted to speed up network training.

ANALYSIS OF THE FLAME-OUT PARAMETER ON AN EXPERIMENTAL COMBUSTOR

WEB PAGE DESIGN USING HTML PROGRAMMING

Neil Griffy

Broookville High School
106 Hill Street
Brookville, Ohio 45309

Final Report for:
High School Apprentice Program
Wright Laboratory

Sponsored by
Air Force Office of Scientific Research
Bolling Air Force Base, DC

and

Wright Laboratory

August 1996

Phase 1

Analysis of the Flame-out parameter on an Experimental Combustor

The analysis of the flame-out procedure on a combustor was studied. Results previously obtained from the General Electric J79 turbojet, were compared to those of the test combustor. This analysis is one of a series of analyses used by Dr. Keith Numbers at Wright Patterson Air Force Base. The purpose of this analysis is to simulate the flame-out procedure of the combustor. As the plane is flying through the air, air and fuel are constantly mixing. If a gust of wind is induced into the combustor, then the air-fuel ratio changes. If the air is moving faster than the fuel can burn, then the result causes a flame-out, and the burner efficiency equals zero. Due to the differences in engines, the results differed by a small amount. Several qualities of the combustor were taken into account: air mass flow, mass fuel flow, pre- and post combustion pressures, pre- and post combustion temperatures, pre- and post combustion density, pre- and post combustion Mach number, pre- and post combustion total energy, pre- and post combustion velocity, post combustion mass flow rate, burner efficiency, and flame-out parameter. Using a set of values consisting of time, air mass flow, fuel mass flow, pre- combustion pressure, and pre- combustion temperature, all values were calculated using a FORTRAN program.

The analysis was conducted using a program written in the FORTRAN language. A source code listing is listed in the appendix. The program operated by asking the user to enter an input file. This input file consisted of the five values listed above. After this was completed, the program would then ask the user to enter an output file. This created a user defined file that all the data would be stored in. After the input and output files were entered, the program would run all the data through a series of equations and interpolations. Each individual number per unit of time would be run through the equations as it was called for. After the program is finished with the equations, the solutions are then written to the output file. This output file can then be read as text and be graphed. These graphs can also be found in the appendix. All work was done on a Silicon Graphics Workstation.

As was suspected, the tested data compared to the J79 data differed slightly. Most of the data followed the same curve as the J79, but was slightly higher in value. Although some test data did match the J79 values near the beginning of the test, the curves separated. This separation occurred at approximately 18 seconds, and the conditions were Mass air flow = 33.800, Mass fuel flow = .906, Pressure = 13227.339, Temperature = 888.716.

Phase 2

Web Page Design using HTML programming

During the second phase of my tour, I designed and created World Wide Web pages for various branches and groups, in the Flight Dynamics Directorate. Such groups and branches include: Aeromechanics Integration Branch, Airframe Propulsion Integration Group, Airframe Weapons Integration Group, Airframe Aerodynamics Integration Group, Experimental Operations Branch, Experimental Operations Group, Advanced Diagnostics Group, and various other points of contact and information pages. This was necessary because of the restructuring of the various branches and groups.

HTML is a computer language specifically designed for web page design on the World Wide Web computer server. It involves a series of commands to do a task just as any other program. HTML's abilities range from inserting titles and pictures, to linking to other web pages and utilizing e-mail. HTML code is viewed using any default text editor. When the code is run, it can be viewed with Netscape Navigator. Netscape Navigator comes in several different versions. In my programming I used Netscape Navigator version 2.01. An sample of HTML code is shown in the appendix, along with the actual page.

For the branch pages, I began the page with the branch title. I then inserted a picture that had relation to the branch. I followed this picture with information about the branch. After this was completed, I listed links to the group web pages. This allows the user to go directly to the group page desired, without having to enter a location. After this I then displayed the branch address and created a link to a points of contact page. This page allows the user to click on a desired name of a person in that branch. By clicking this name, Netscape then brings up an e-mail window with the chosen person's e-mail address.

The group pages are much like the branch pages, but have links to facilities within the group. In the example page I have included, I have highlighted the links to the other pages. In the link to the Philip P. Antonatos Subsonic Aerodynamic Research Facility (SARL), there is also a link to a page about Philip P. Antonatos.

Appendix

```
      program com
c*****************************************************************
c*                          CONSTANTS                            *
c* H.V.= fuel heating value (BTU/lb) = 18400 BTU/lb              *
c* hf- fuel energy entering combustor, 147.5 BTU/lb              *
c* R- gas constant, 1716 ft. lbs./slug degrees Rankin or 53.3    *
c* GAMMA- 1.4 for "cold section", 1.3 for "hot section"          *
c* Cp- .24 for "cold section", .276 for "hot section"            *
c*****************************************************************
      character*25 datain, dataout
      real Mi1, Mf, M1, Mi2, M2, K1, K2, M2NEW,
     +mop1, mop2, tm1, tm2, tau
      pi = acos(-1.0)
      HV = 18400.0
      hf = 147.5
      R = 53.3
      g = 32.2
      XJ = 778.0
      eta = 1.0
      GM1 = 1.4
      Cp1 = .24
      A1 = 1.3
      write(6,*) 'Enter the input file'
      read(5,7) datain
7     format (a)
      write(6,*) 'Enter the output file'
      read(5,8) dataout
8     format (a)
      open (unit = 10, file = datain, status = 'unknown')
      open (unit = 20, file = dataout, status = 'unknown')
      read (10,*)
1     continue
      read (10,*, end = 1002) time, Mi1, P1, T1 , Mf
      Mi1 = Mi1 * 42.405 / 33.75
      write (6,*) '***************TIME****************'
      write (6,*) '       ',time,'in seconds'
      write (6,*) '************Cold Section************'
      write (6,*) 'Mass flow rate of air (lbs. / sec.)'
      write (6,*) Mi1
      write (6,*) 'Mass flow rate of fuel (lbs. / sec.)'
      write (6,*) Mf
      write (6,*) 'Pressure (lbs./ft^2)'
      write (6,*) P1
      write (6,*) 'Temperature (degrees Rankin)'
      write (6,*) T1
      write (6,*) 'Duct area (ft^2)'
      write (6,*) A1
      A2 = A1
      RH1 = (P1 / R / T1)
      write (6,*) 'Density equals '
      write (6,*) RH1,' lb / ft^3'
      V1 = Mi1 / RH1 / A1
      write (6,*) 'Velocity equals'
      write (6,*) V1,' ft / sec'
      M1 = V1 / sqrt((GM1 * R * g * T1))
      write (6,*) 'Mach number equals'
      write (6,*) M1
      ht1 = Cp1 * T1 + V1**2 / 2.0 / g / XJ
      write (6,*) 'Total energy equals'
      write (6,*) ht1,' BTU / lb'
      FOP = P1 * T1 / V1
      af = Mi1 / Mf
      call flameout (Mi1, Mf, flm, af)
         if (FOP .le. flm) then
             eta = 0.
             write (6,*) 'Fuel-Air Ratio equals'
```

```
            write (6,*) af
            write (6,*) 'Burner efficiency equals'
            write (6,*) 'FLAME OUT'
         else
            write (6,*) 'Fuel-Air Ratio equals'
            write (6,*) af
            write (6,*) 'Burner efficiency equals'
            call efficiency(Mi1, Mf, T1, P1, A1, b, pter, mop2)
            if  (mop2.eq.0) then
                goto 80
            endif
            call burner (pter, eta)
         endif
80     if (time.eq.0) then
          mop2 = .98
          t2 = 0
          goto 85
       endif
       tau = 10
       tm1 = tm2
       tm2 = time
       mop1 = mop2
       mop2 = mop1 + (tm2 - tm1) / tau * (eta - mop1)

85     write (6,*) mop2
c       write (6,*) tm1,'tm1'
c       write (6,*) tm2,'tm2'
c       write (6,*) mop1,'mop1'
       GM2 = 1.3
       Cp2 = .276
       write (6,*) '***********Hot Section***********'
       Mi2 = Mi1 + Mf
       write (6,*) 'Mass flow rate'
       write (6,*) Mi2,' lb. / sec.'
       write (6,*) ''
       K1 = (P1 + RH1/g * V1**2)
       K2 = K1
       ht2 = (Mi1*ht1+Mf*hf+mop2*Mf*HV)/(Mi2)
       M2 = 0.
100    Continue
       T2 = ht2 / Cp2 / (1.0 + (GM2 - 1.0) / 2.0 * M2**2)
       P2 = K2 / (1.0 + GM2 * M2**2)
       RH2 = P2 / R / T2
       V2 = Mi2 / RH2 / A2
       M2NEW =  V2 / SQRT(GM2 * R * g * T2)
       IF (abs(M2new-M2) .lt. 1.e-4) then
          goto 200
       else
          M2=M2new
          goto 100
       endif
200    continue
       write (6,*) T2,'temp'
       write(6,*) ''
       write (6,*) V2,'Velocity ft / sec'
       write (6,*)
       write (6,*) RH2,'density'
       write (6,*) ''
       write (6,*) A2,'duct area'
       write (6,*) ''
       write (6,*) 'Pressure'
       write (6,*) P2,' lbs / ft^2'
       write (6,*) ''
       write (6,*) 'Total energy'
       write (6,*) ht2,' BTU / lb.'
       write (6,*) ''
```

```
      write (6,*) 'Mach number equals'
      write (6,*) M2NEW
      write (6,*) ''
      write (20,17) time, P1, P2
17    format (18f15.5)
1000  goto 1
1002  END
      Subroutine efficiency (Mi1, Mf, T1, P1, A1, b, pter, mop2)
      real Mf, Mi1, Mistoi
      D1 = .16666667
      Mistoi = Mi1 / (14.78 * 3.73)
      phi = Mf / Mistoi
      b = 220.0 * (SQRT(2.) - abs(alog((phi / 1.03))))
      pter = P1**1.75 * A1 * D1 * (exp((-T1/b)) / Mi1)
      write (6,*) Mistoi,'mistoi'
      write (6,*) phi,'phi'
      write (6,*) b,'b'
      write (6,*) pter,'pter'
      if (b.le.0) then
        mop2 = 0
      endif
      return
      END
      subroutine burner (pter, eta)
      dimension param(27)
      dimension effi(27)
      data param /0, .25, .4, .5, .625, .75, .875, 1, 1.25, 1.5, 2,
     +2.5, 3, 3.5, 4, 5, 7, 10, 15, 23, 35, 53, 80, 120, 180, 270, 600/
      data effi /0, .1, .18, .3, .6, .75, .84, .87, .895, .91, .928,
     +.943, .952, .96, .97, .98, .98, .98, .98, .98, .98, .98, .98,
     +.98, .98, .98/
      x0 = pter
         if (pter .gt. param(27)) then
            eta = effi(27)
            goto 20
         endif
      do 10 i = 1, 27
         if (param(i) .gt. pter) then
            x2 = param(i)
            x1 = param(i-1)
            y2 = effi(i)
            y1 = effi(i-1)
            eta = ((y2 - y1) / (x2 - x1) * (x0 - x1)) + y1
            goto 20
         endif
10    continue
20    return
      END
      subroutine flameout (Mi1, Mf, flm, af)
      dimension pram(15)
      dimension fair(15)
      real Mi1, Mf
      data pram /300000, 75000, 40000, 22000, 10000, 6000, 4000, 2800,
     +2500, 2700, 3300, 5000, 8000, 12000, 60000/
      data fair /3, 5, 7, 10, 20, 35, 50, 80, 110, 150, 200, 300, 400,
     +500, 600/
      x0 = af
         if (x0 .gt. fair(15)) then
             flm = pram(15)
             goto 40
         endif
         if (x0 .lt. fair(1)) then
             flm = pram(1)
             goto 40
         endif
25    do 30 q = 1, 15
```

```
          if (fair(q) .gt. x0) then
              x2 = fair(q)
              x1 = fair(q-1)
              y2 = pram(q)
              y1 = pram(q-1)
              flm = (y2 - y1) / (x2 - x1) * (x0 - x1) + y1
              goto 40
          endif
30      continue
40      return
        END
```

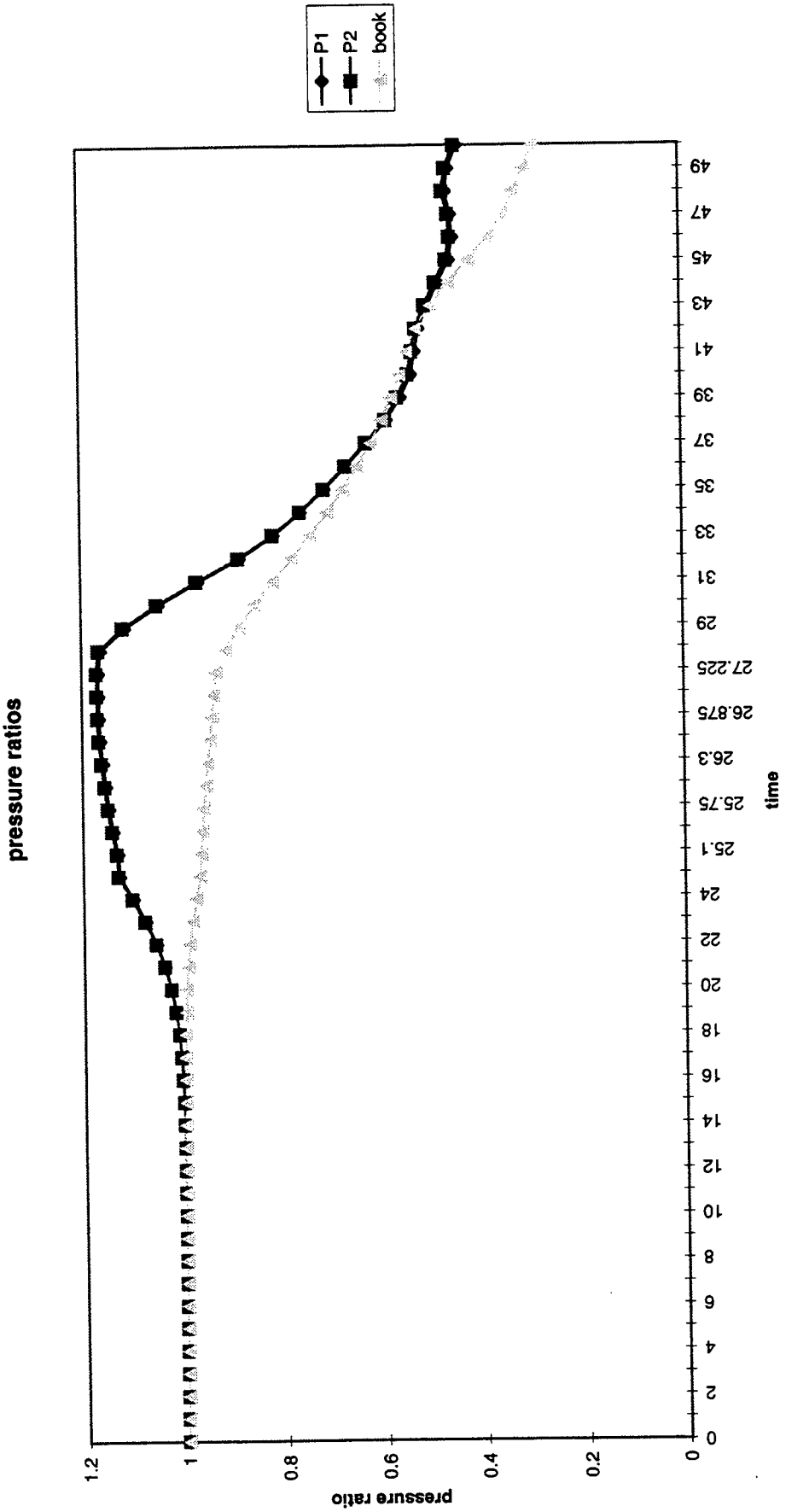
pressure ratios
P1
P2
book
pressure ratio
1.2
1
0.8
0.6
0.4
0.2
0
time
0
2
4
6
8
10
12
14
16
18
20
22
24
25.1
25.75
26.3
26.875
27.225
29
31
33
35
37
39
41
43
45
47
49

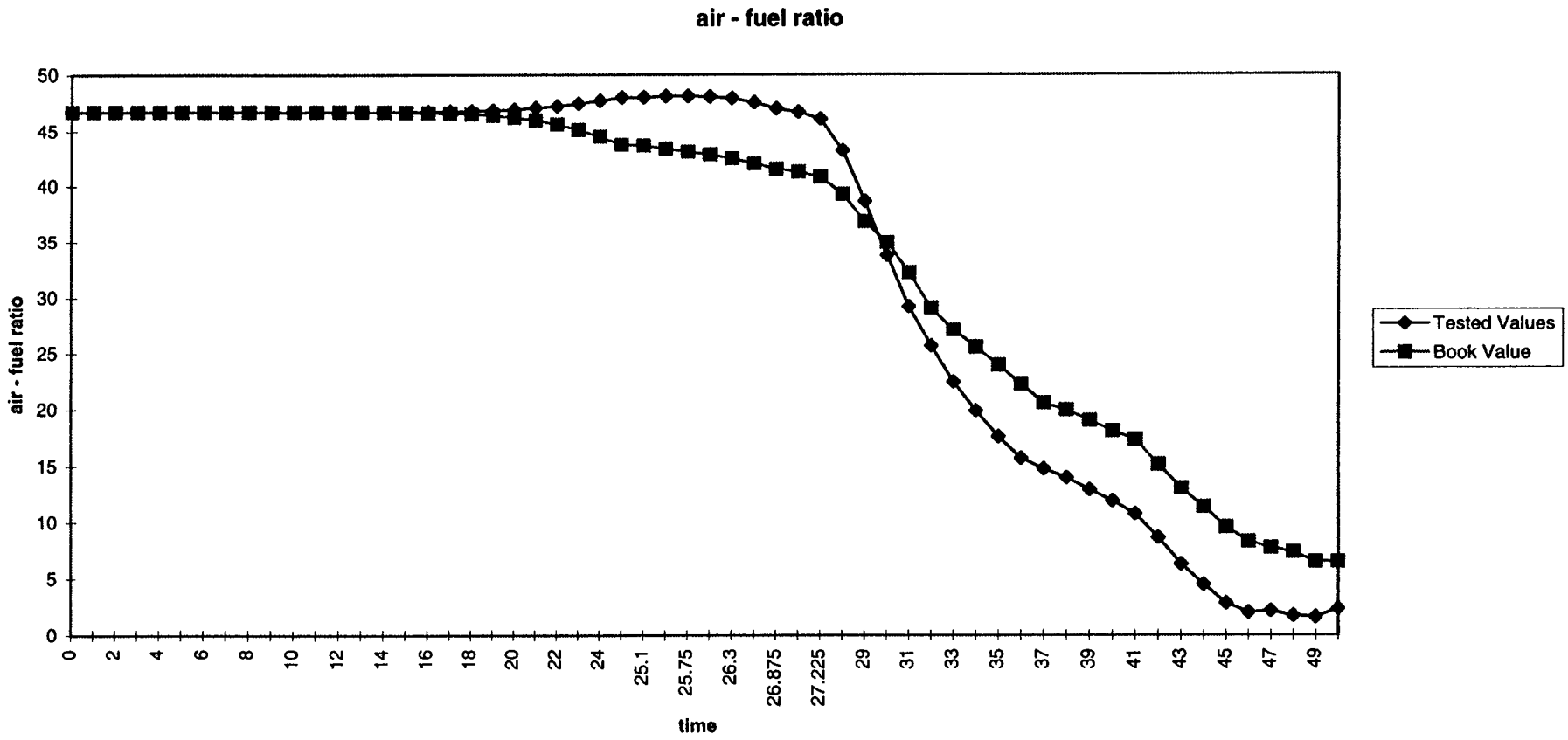
air - fuel ratio
air - fuel ratio
time
Tested Values
Book Value
0
5
10
15
20
25
30
35
40
45
50
0
2
4
6
8
10
12
14
16
18
20
22
24
25.1
25.75
26.3
26.875
27.225
29
31
33
35
37
39
41
43
45
47
49

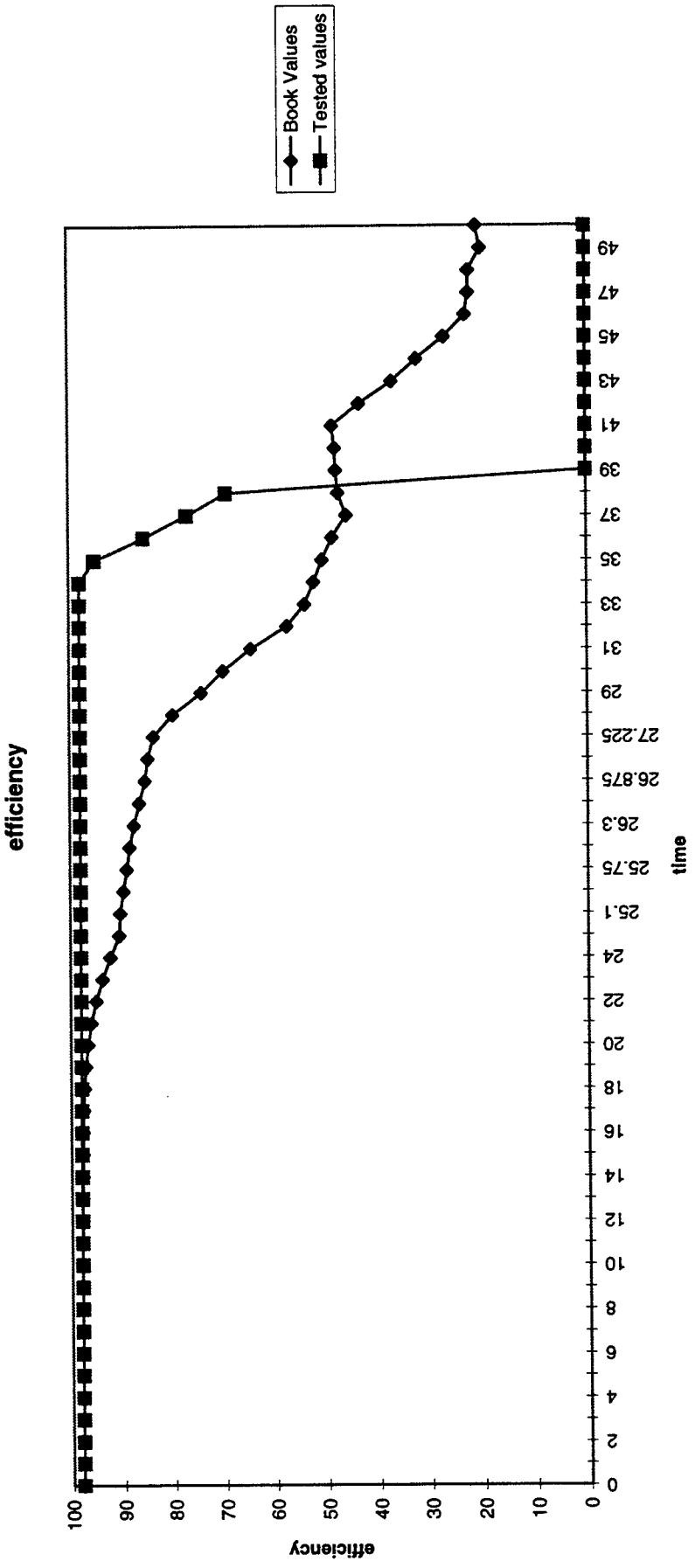
Book Values
Tested values
efficiency
time
efficiency
0
2
4
6
8
10
12
14
16
18
20
22
24
25.1
25.75
26.3
26.875
27.225
29
31
33
35
37
39
41
43
45
47
49
0
10
20
30
40
50
60
70
80
90
100

EXPERIMENTAL OPERATIONS GROUP

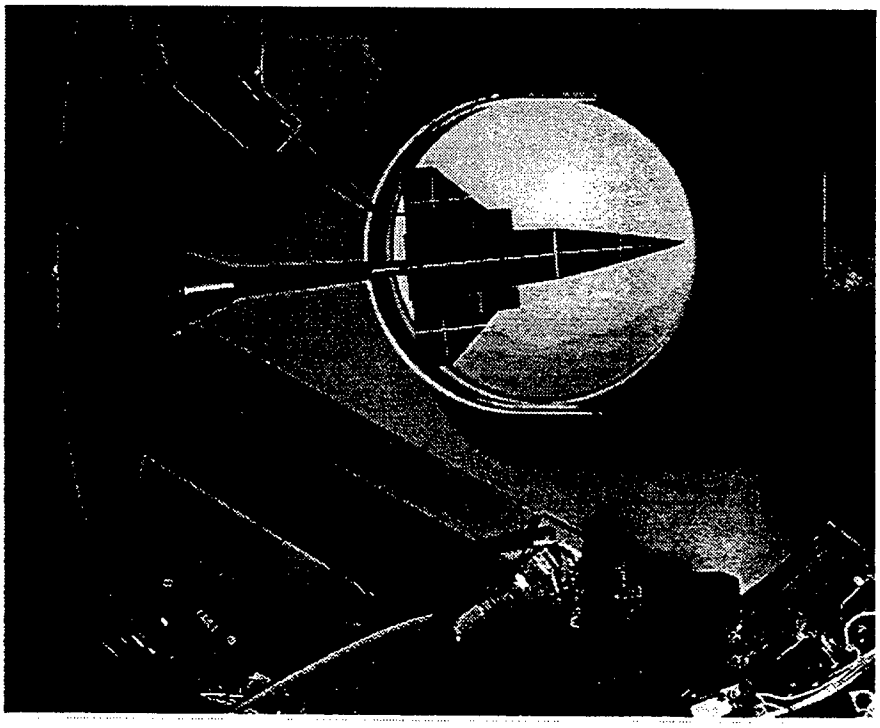

Our Mission...

"Our mission is to lead the research, development and application of a broad range of experimental technologies. We produce new technology components and provide the tools and expertise for assessment, evaluation and transition of this technology as appropriate to DoD, government, industry and academia, in the interest of the United States Air Force."

Our Technology...

The Experimental Operatoins Group of the Flight Dynamics Directorate is responsible for advancing aerodynamics by the use of wind tunnel testing. We conduct aerodynamic research in six in-house test facilities at Wright-Patterson Air Force Base. The facilities we now support include:

- Philip P. Antonatos Subsonic Aerodynamic Research Laboratory (SARL)
- Two-Foot Trisonic Gasdynamics Facility (TGF)

- Mach 3 High Reynolds Number Facility
- Mach 6 High Reynolds Number Facility
- 20 Inch Hypersonic Wind Tunnel
- Two-Foot Hydrodynamic Test Facility

Our customers include the USAF using commands and other USAF organizations, Defense and Civilian Industries, National Laboratories, NASA, and Academia.

In these days of declining budgets, we utilize IR&D and university "leverage" to develop technology required by the USAF. This is accomplished by acting in concert with industry and academic partners as well as innovative use of resources, faciltities and people. We look for opportunities to participate in cooperative programs, as well as to provide technical support. We are responsible for specific experimental and computational methodologies and have our own in-house areas of research interest. Opportunities will result from a continued expansion of our database and the development of new innovative dual use technologies to meet USAF and industry, including the private sector needs.

Technology Transfer...

Bunches of information about the wonders of tech xfer. programs.

Points of Contact...

The Experimental Operations Group is in Room A117 of Building 450 which is located on Wright-Patterson AFB, Area B. Our mailing address and phone numbers are:

WL/FIMI, Bulding 450
2645 Fifth Street, Suite 7
Wright-Patterson AFB, OH 45433-7913
(513) 255-6207 voice
(513) 476-4210 fax

For further information, please see our Points of Contact list.

Last updated by Lt. Jeff Hank

Time	Mi1	P1	T1	Mf
0.0000	33.7177	13080.9382	885.6200	.9066
1.0000	33.7177	13080.9382	885.6200	.9066
2.0000	33.7177	13080.6711	885.6143	.9066
3.0000	33.7177	13080.6711	885.6143	.9066
4.0000	33.7177	13080.6711	885.6143	.9066
5.0000	33.7177	13080.6711	885.6143	.9066
6.0000	33.7177	13080.9382	885.6200	.9066
7.0000	33.7177	13081.2054	885.6257	.9066
8.0000	33.7177	13081.7397	885.6370	.9066
9.0000	33.7177	13082.5412	885.6540	.9066
10.0000	33.7177	13084.1441	885.6880	.9066
11.0000	33.7220	13086.2813	885.7334	.9066
12.0000	33.7220	13089.7543	885.8071	.9066
13.0000	33.7264	13095.3646	885.9261	.9066
14.0000	33.7307	13104.1807	886.1131	.9066
15.0000	33.7394	13118.0727	886.4076	.9066
16.0000	33.7524	13140.2465	886.8771	.9066
17.0000	33.7697	13174.7094	887.6057	.9066
18.0000	33.8000	13227.3388	888.7158	.9066
19.0000	33.8433	13306.6835	890.3835	.9066
20.0000	33.9082	13423.1628	892.8188	.9066
21.0000	34.0035	13586.6611	896.2118	.9066
22.0000	34.1247	13805.4604	900.7071	.9066
23.0000	34.2763	14080.6293	906.2889	.9066
24.0000	34.4581	14403.0844	912.7316	.9066
25.0000	34.6617	14748.7819	919.5253	.9066
25.1000	34.6833	14783.5120	920.2015	.9066
25.4500	34.7396	14902.3956	922.5076	.9066
25.7500	34.7483	15003.6470	924.4614	.9066
26.0000	34.7093	15080.8546	925.9449	.9066
26.3000	34.6010	15156.9935	927.4026	.9066
26.6000	34.3542	15219.2405	928.5904	.9066
26.8750	33.9559	15247.8260	929.1347	.9066
27.0000	33.7350	15252.1004	929.2160	.9066
27.2250	33.2804	15257.4435	929.3177	.9066
28.0000	31.2193	15197.8681	928.1829	.9066
29.0000	27.9198	14557.4995	915.7804	.9066
30.0000	24.3606	13670.5476	897.9414	.9066
31.0000	21.0958	12616.8914	875.6405	.9066
32.0000	18.5194	11539.4585	851.4150	.9066
33.0000	16.2159	10641.8204	829.9656	.9066
34.0000	14.3323	9916.2296	811.6616	.9066
35.0000	12.6739	9285.2114	794.9485	.9066
36.0000	11.2926	8711.8985	779.0448	.9066
37.0000	10.6258	8171.9798	763.3686	.9066
38.0000	10.0759	7662.7839	747.8911	.9066
39.0000	9.3008	7282.6235	735.8496	.9066
40.0000	8.5864	6999.7072	726.5936	.9066
41.0000	7.7507	6896.0514	723.1354	.9066
42.0000	6.2265	6787.3196	719.4678	.9066
43.0000	4.5162	6540.7363	710.9920	.9066
44.0000	3.2172	6253.0112	700.8085	.9066
45.0000	2.0351	5957.2715	689.9862	.9066
46.0000	1.4635	5862.4318	686.4344	.9066
47.0000	1.5415	5906.7794	688.1003	.9066
48.0000	1.2341	6037.6849	692.9661	.9066
49.0000	1.1431	5967.9577	690.3838	.9066
50.0000	1.6757	5733.6634	681.5458	.9066

0.00000	46.72890	252.33148	12897.21094
1.00000	46.72890	281.25943	12897.21094
2.00000	46.72890	310.18738	12896.94043
3.00000	46.72890	339.11533	12896.94043
4.00000	46.72890	368.04327	12896.94043
5.00000	46.72890	396.97119	12896.94043
6.00000	46.72890	425.89914	12897.21094
7.00000	46.72890	454.82709	12897.48145
8.00000	46.72890	483.75500	12898.02441
9.00000	46.72890	512.68298	12898.83691
10.00000	46.72890	541.61090	12900.46484
11.00000	46.73485	570.59485	12902.61328
12.00000	46.73485	599.52563	12906.13574
13.00000	46.74095	628.51953	12911.80859
14.00000	46.74691	657.51770	12920.73438
15.00000	46.75896	686.59021	12934.78809
16.00000	46.77699	715.74426	12957.22656
17.00000	46.80096	744.98792	12992.11035
18.00000	46.84295	774.48254	13045.36133
19.00000	46.90296	804.25275	13125.64453
20.00000	46.99290	834.48480	13243.47266
21.00000	47.12498	865.38904	13408.80469
22.00000	47.29295	896.92920	13630.44434
23.00000	47.50305	929.24170	13908.51270
24.00000	47.75500	962.37158	14234.20410
25.00000	48.03717	996.18408	14583.17480
25.10000	48.06710	999.60498	14618.21875
25.45000	48.14513	1011.17651	14738.24512
25.75000	48.15719	1020.24316	14840.62207
26.00000	48.10314	1026.77625	14918.86816
26.30000	47.95305	1033.21899	14996.31055
26.60000	47.61101	1036.46167	15060.27344
26.87500	47.05901	1035.32593	15090.82813
27.00000	46.75287	1033.79211	15096.06738
27.22500	46.12284	1029.49097	15103.36328
28.00000	43.26640	999.64697	15051.84473
29.00000	38.69366	933.49969	14419.54199
30.00000	33.76102	841.27185	13540.61230
31.00000	29.23638	736.42273	12493.29688
32.00000	25.66578	1131.86194	11419.38477
33.00000	22.47339	361.66400	10526.49023
34.00000	19.86294	90.96600	9805.69336
35.00000	17.56458	30.99819	9211.22949
36.00000	15.65026	31.49922	8712.43652
37.00000	14.72615	32.40000	8172.37500
38.00000	13.96405	33.30000	7663.04395
39.00000	12.88985	20.47507	7181.03809
40.00000	11.89977	-65.08588	6901.40674
41.00000	10.74159	-178.88663	6805.16211
42.00000	8.62922	-427.98691	6711.51758
43.00000	6.25894	-803.60962	6481.37842
44.00000	4.45867	-1214.36951	6206.29639
45.00000	2.82042	-1781.19507	5922.96045
46.00000	2.02824	-2212.98584	5834.81104
47.00000	2.13634	-2189.10400	5878.38623
48.00000	1.71032	-2506.95947	6013.69629
49.00000	1.58421	-2648.53931	5944.81982
50.00000	2.32233	-2197.59766	5702.66504

```
<HTML>
<BODY BGCOLOR="#ffffff" TEXT="#000000" LINK="#FF0000" VLINK="#787878">
<HEAD>
<TITLE>Experimental Operations Group</TITLE>
</HEAD>
<CENTER><H3>
<FONT SIZE=+7>E</FONT>XPERIMENTAL
<FONT SIZE=+7>O</FONT>PERATIONS
<FONT SIZE=+7>G</FONT>ROUP
<P></H3>
<BODY>
<IMG SRC="/net/ind11/griffynp/pictures/mach6-2.jpg">
<P>
</CENTER>
<P>
 
<p>
<img src="/net/ind21/hankjd/http/misc/jet_lr.gif">
<p>
<H2>Our Mission...</H2>
<I>"Our mission is to lead the research, development and application of a broad
range of experimental technologies.  We produce new technology components
and provide the tools and expertise for assessment, evaluation and transition
of this technology as appropriate to DoD, government, industry and academia,
in the interest of the United States Air Force."</I>
<p>
<img src="/net/ind21/hankjd/http/misc/jet_lr.gif">
<P>
<H2>Our Technology...</H2>
The Experimental Operatoins Group of the
<A HREF="http://www.fim.wpafb.af.mil/FI/fi.html">Flight Dynamics
Directorate</A> is responsible for advancing aerodynamics by the use of wind tun
nel testing.
We conduct aerodynamic research in six in-house test facilities at Wright-Patter
son Air Force Base.
  The facilities we now support include:
<UL>
<IMG SRC="/net/ind21/hankjd/http/misc/yellowball.gif"><A HREF="/net/ind11/griffy
np/html/sarl.html">
Philip P. Antonatos Subsonic Aerodynamic Research Laboratory (SARL)</A>
<BR>
<IMG SRC="/net/ind21/hankjd/http/misc/yellowball.gif"><A HREF="/net/ind11/griffy
np/html/tgf.html">
Two-Foot Trisonic Gasdynamics Facility (TGF)</A>
<BR>
<IMG SRC="/net/ind21/hankjd/http/misc/yellowball.gif"><A HREF="/net/ind11/griffy
np/html/mach3.html">
Mach 3 High Reynolds Number Facility</A>
<BR>
<IMG SRC="/net/ind21/hankjd/http/misc/yellowball.gif"><A HREF="/net/ind11/griffy
np/html/mach6.html">
Mach 6 High Reynolds Number Facility</A>
<BR>
<IMG SRC="/net/ind21/hankjd/http/misc/yellowball.gif"><A HREF="/net/ind11/griffy
np/html/20inch.html">
20 Inch Hypersonic Wind Tunnel</A>
<BR>
<IMG SRC="/net/ind21/hankjd/http/misc/yellowball.gif"><A HREF="/net/ind11/griffy
np/html/hydro.html">
Two-Foot Hydrodynamic Test Facility</A>
</UL>

<P>
Our customers include the USAF using commands and other USAF organizations,
<A HREF="industry.html">Defense and Civilian Industries</A>,
<A HREF="http://www.fim.wpafb.af.mil/sites.html">National Laboratories</a>,
```

```
<A HREF="http://hypatia.gsfc.nasa.gov/NASA_homepage.html">NASA</A>, and
<A HREF="http://www.fim.wpafb.af.mil/sites_edu.html">Academia</A>.

<P>
In these days of declining budgets, we utilize IR&D and university "leverage"
to develop technology required by the USAF.  This is accomplished by acting
in concert with industry and academic partners as well as innovative use of
resources, faciltities and people.  We look for opportunities to participate
in cooperative programs, as well as to provide technical support.  We are
responsible for specific experimental and computational methodologies and have
our own in-house areas of research interest.  Opportunities will result from a
continued expansion of our database and the development of new innovative dual
use technologies to meet USAF and industry, including the private sector needs.

<P>

<img src="/net/ind21/hankjd/http/misc/jet_lr.gif">
<p>
<H2>Technology Transfer...</H2>
<P>
Bunches of information about the wonders of tech xfer. programs.
<P>
<img src="/net/ind21/hankjd/http/misc/jet_lr.gif">
<P>
<H2>Points of Contact...</H2>

The Experimental Operations Group is in Room A117 of Building 450
which is located on Wright-Patterson AFB, Area B.  Our mailing address and
phone numbers are:
<P>
<ADDRESS><UL>
WL/FIMI, Bulding 450<BR>
2645 Fifth Street, Suite 7<BR>
Wright-Patterson AFB, OH 45433-7913<BR>
(513) 255-6207   voice<BR>
(513) 476-4210   fax<BR>
</UL></ADDRESS>
<P>
For further information, please see our
<A HREF="./eogpoc.html">Points of Contact</A> list.
<P>
<img src="/net/ind21/hankjd/http/misc/jet_lr.gif">
<P>
Last updated by <A HREF="mailto:hankjd@fim.wpafb.af.mil">Lt. &nbspJeff Hank<
/A>
</BODY>
```

Observation of de Gaussing Through Repeated Thermocycling of Samarium Cobalt Magnets

Shaun R. Guillermin

Chaminade - Julienne High School
505 S. Ludlow Street
Dayton, Ohio 45402

Final Report For:
High School Apprenticeship Program
Wright Laboratory

Sponsored by:
Air Force Office of Scientific Research
Bolling Air Force Base, DC

and

Wright Laboratory

August 1996

Observation of deGaussing Through Repeated Thermocycling of Samarium Cobalt Magnets

Shaun R. Guillermin
Chaminade Julienne High School

Abstract

An experiment was designed to study the deGaussing of Samarium Cobalt magnets when thermocycled repeatedly from room temperature to 400 degrees Celsius. At specified intervals, certain magnets will be removed from the test bed and analyzed for loss of Gauss strength. Elapsed time for the project is three thousand cycles, or approximately one hundred and sixty seven days. A preliminary study is presented, detailing design, construction and operation of the test apparatus. Plots of initial heating and cooling cycle tests, as well as actual thermocycling data from the test bed, are included. At this early stage, sufficient data has not been accumulated for publishing.

Table of Contents

Observation of deGaussing Through Repeated Thermocycling of Samarium Cobalt Magnets

Shaun R. Guillermin

1:1 Introduction

In nearly all research and development programs there are a multitude of factors which can alter the expected outcome of experimental data. One such variable is temperature; Environmental temperature fluxes can cause changes ranging from negligible expansion and contraction to changing physical properties of components and materials. The problem is even further compounded when 'real world' conditions subject materials to repeated cycles of heating and cooling. The effects can degrade performance, weaken objects and their natural properties, or even damage them beyond use. Thorough investigation is required to fully understand this phenomenon and to enable designers to account for it in their work.

In this particular case, the problem applies to samarium cobalt magnets. Over time, questions have been raised whether this type of magnet will lose magnetic strength, or deGauss, when subjected to repeated cycles of thermal stress. The Thermal Technology Section at Wright Patterson Air Force Base has accepted a contract to design an experiment that will carry out high temperature thermocycling of samarium cobalt magnets over extended periods of time. These magnets will be examined to observe the possible loss of Gauss strnegth.

2:1 Test Parameters and Experimental Test Set-up

The contract specified the testing of sixteen magnets. Each cubic magnet measures 0.11 inches, with a mass of between 0.203 to 0.207 (see table 1) grams. Thermocycling parameters require that they be heated from room temperature (approximately 23 degrees Celsius) to 400 degrees celsius within ninety seconds. The temperature must remain at 400 for thirty one minutes (a 2 percent error in either direction is acceptable). Then, the magnets are allowed to cool to room temperature for eight and a half minutes. The process is repeated continually. The test apparatus must be capable of producing 3,000 cycles automatically and without variation. Total elapsed time for this test is one hundred and sixty seven days. At specified intervals, certain magnets magnets will be removed for Gauss testing and not replaced (see table2).

2:2 Test Set-up

Experimental set-up was left to the discretion of Wright Lab researchers. Initial designs consisted of two flat "baskets" made from #40 copper mesh screen and measuring approximately five inches square. Each held eight units, and was covered with a mesh overlay (magnets were spaced 2.25" apart to prevent the possibility that magnetic attraction could alter test results- all materials used were non-magnetic). Heating was accomplished with resistance wire heaters made from 0.015" nichrome wire shielded by 0.092" ceramic tube. Tubing was cut into twenty four, four inch lengths that were spaced evenly above and below the specimens and tied to the outside of the mesh with 36 awg copper wire (see fig. 1). Preliminary testing, using a 110 vac Variac Autotransformer as a power source, revealed that the thermal mass of the heating elements was too great, preventing heating within the allotted time.

The final design (see fig. 2) consists of six separate heating elements, each capable of holding three magnets. The elements are constructed from a 4.5 by 1.5 inch pieces of #16 copper screen. Three pieces of #100 mesh copper, .75 by 1.5 inches, are evenly spaced on the screen and sewn with 0.010" copper wire. Each smaller piece is cut so that, when folded, it can securely hold one specimen. The entire unit is then folded lengthwise to form a half inch diameter roll. This design provides lower thermal resistance as well as improved airflow. Heater wiring was changed also. The same wire was used, but the ceramic insulation was exchanged for Omega Nextel fiberglass sleeving. The heater was wrapped evenly around the screen roll (see fig. 3).

The heater and Variac are controlled by a Fuji PYZ4 microprocessor and a Macromatic SS-63122 dual output, repeat cycle timer (see table 3 for settings). Both connect to a 15 ampere DPDT relay which is energized by the controller (see fig. 4).

To cool the heater assembly, a 4.5" muffin fan was mounted 2" above the work surface using 0.75" aluminum angle stock. This stock extends eight inches above the fan to provide mounting points for the individual elements. Phenolic strips 0.125" and 0.0625" thick were cut and assembled to form two grids that fit into slots in the aluminum. Heaters were secured to these grids with 0.010" copper wire.

The three elements on each level of the stand are wired in series, and both rows are wired together in parallel so

that each heating element draws approximately 100 watts. The purpose of this is to provide a low relative resistance which allows for better accuracy and control. The

nichrome wire used in the heating elements has a resistance of 2.580 ohms per foot, with each element containing four feet of wire. If the elements were wired completely in series, total resistance would be approximately 60 ohms. This would require maxaimum output from the Variac and increase the time it takes to heat the magnets to 400 degrees C. Also, higher voltage values increase the response time of the temperature controller, as it has less control over the higher current. Limiting the system to 600 watts results in a lower voltage requirement and higher accuracy while still providing enough power for quick response times.

Data acquisition was accomplished via six type K (chromel-alumel) thermocouples (see fig. 5). The second thermocouple is the control point, and relays information to a Fuji microprocessor controller. The Fuji then uses that information to adjust temperature accordingly. The remaining five are wired into a Fluke Datalogger, where data is stored on disk. All thermocouples were mounted within 0.10" of a magnet, with the exception of the control point.

It is attatched directly to a magnet by magnetic attraction. This magnet is used for control and measurement purposes only, and is not one of the sixteen observed subjects.

Safety is of particular concern in theis experiment. It is a continuously running life test, and will go unsupervised for long periods of time. For this reason, a Newport Dual Output 10 amp controlled relay was wired in series with the Fuji controller and the 15A main relay. It utilizes a type J thermocouple to read temperatures in the second heater element. If they exceed the programmed setpoint of 450 degrees C, the unit will open an internal relay which prevents the main relay from energizing, effectively shutting down the experiment and stopping any potential

problems. The relay is programmed to latch open and will not close until the unit is manually reset.

3:1 Experimental Data

At this time, the experiment is running successfully with no apparent problems. However, as it is still in the

early stages , no deGaussing data has been collected yet.

Included are preliminary time/temperature plots for the heating and cooling cycles of the apparatus. Both fall well within the specications set forth in the task description.

Table 1: Magnet Mass and Position (in grams)

Lower Level			Upper Level		
0.204	0.205	0.205*	0.203	0.203	0.204*
0.205	0.205*	0.206	0.204	control pt.*	0.204
0.206*	Empty	0.207	0.204*	0.204	0.204
FRONT			FRONT		

Note: * Denotes location of thermocouple

Table 2: Schedule of Samarium Cobalt Magnet Removal

Approximate Elapsed Time (Days)	Hours Accumulatede @ 400 degrees Celsius	# of Cycles	# of Magnets Removed
3	50	25	2
6	100	50	2
17	300	150	4
28	500	250	2
56	1000	500	4
167	3000	1500	2

Table 3: Settings of Programmable Equipment

3:1 Fuji PYZ4 Microprocessor Temperature Controller

Primary Menu		Secondary Menu	
Main setpoint	400 degrees C	Control action	0
Proportional band	10.5	Input type	3 (type T thermocouple)
Integral time	75 seconds	Digital Filter	2
Derivative	20	Input range:	
Low alarm	395	Lower limit	0
High alarm	395	Upper limit	1000
Cycle time	1	Alarm type	79
Hysteresis	0.0	Alarm hysteresis	1
Heater break alarm	0	Decimal point resolution	0
Autotuning	0	Load (heater) voltage	100
		Process variable offset	0
		Setpoint variable offset	0
		C/F selection	0

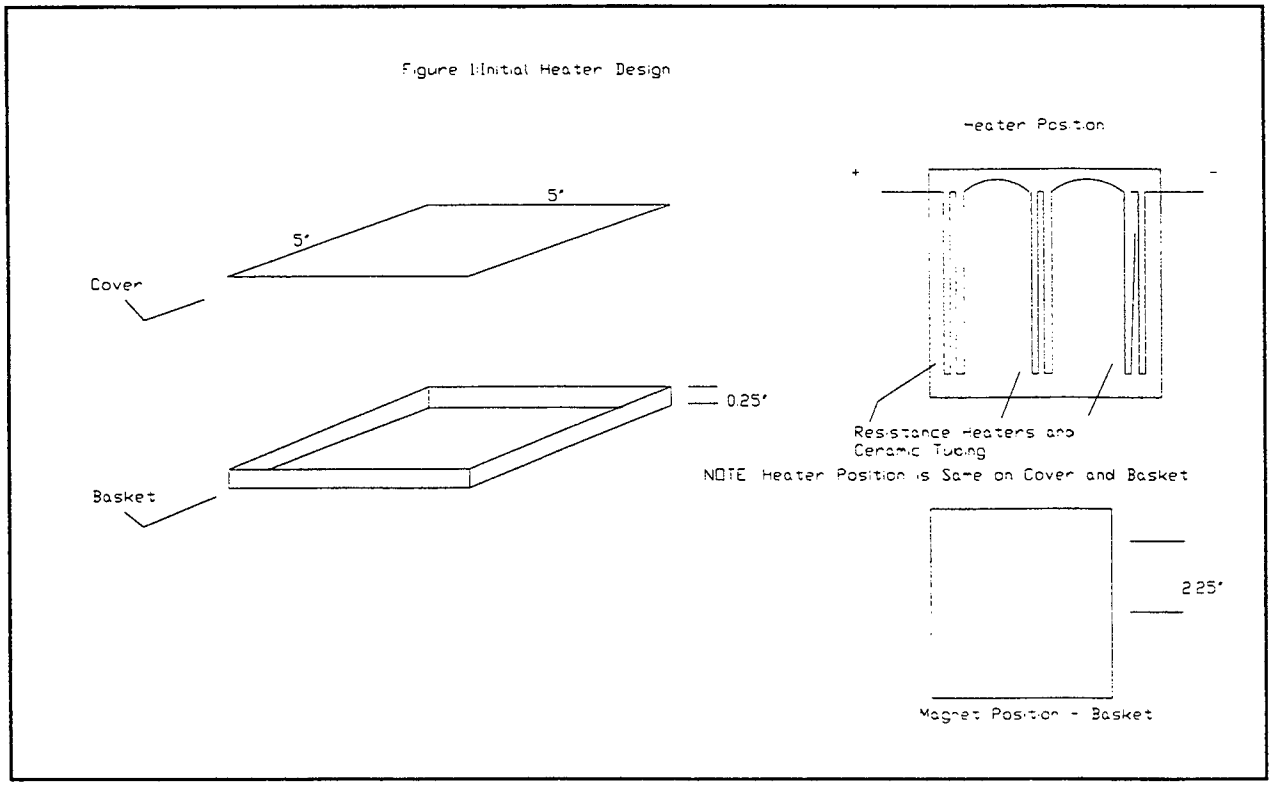
Figure 1:Initial Heater Design
Heater Position
+
-
5"
5"
Cover
0.25"
Basket
Resistance Heaters and
Ceramic Tubing
NOTE Heater Position is Same on Cover and Basket
2.25"
Magnet Position - Basket

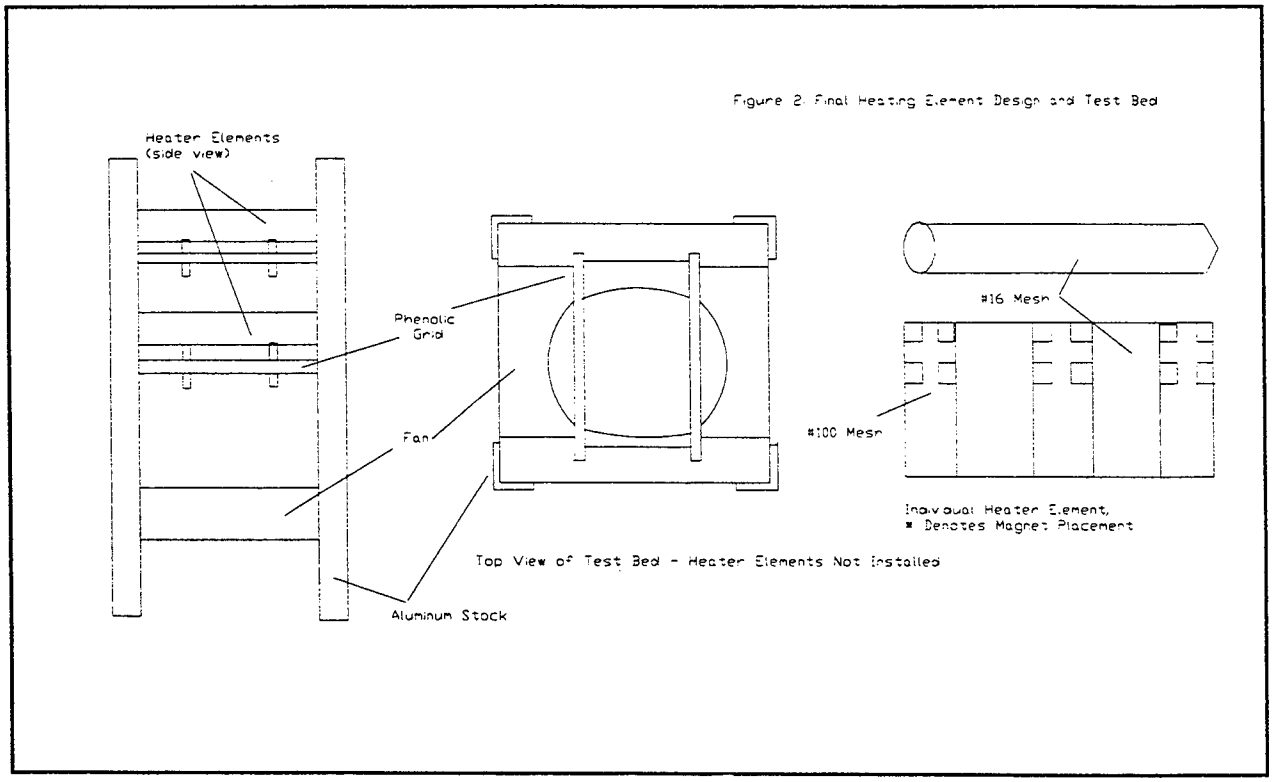
Figure 2: Final Heating Element Design and Test Bed
Heater Elements
(Side View)
Phenolic
Grid
Fan
Aluminum Stock
Top View of Test Bed - Heater Elements Not Installed
#16 Mesh
#100 Mesh
Individual Heater Element,
* Denotes Magnet Placement

Figure 3: Resistance Heater Detail

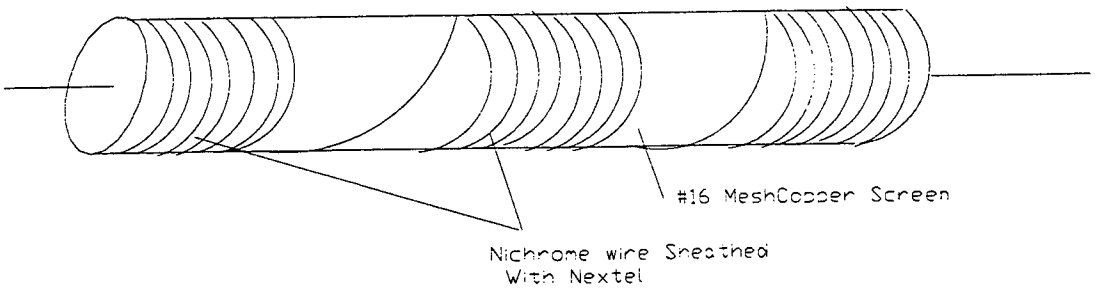

Figure 4 Schematic of Experimental Apparatus

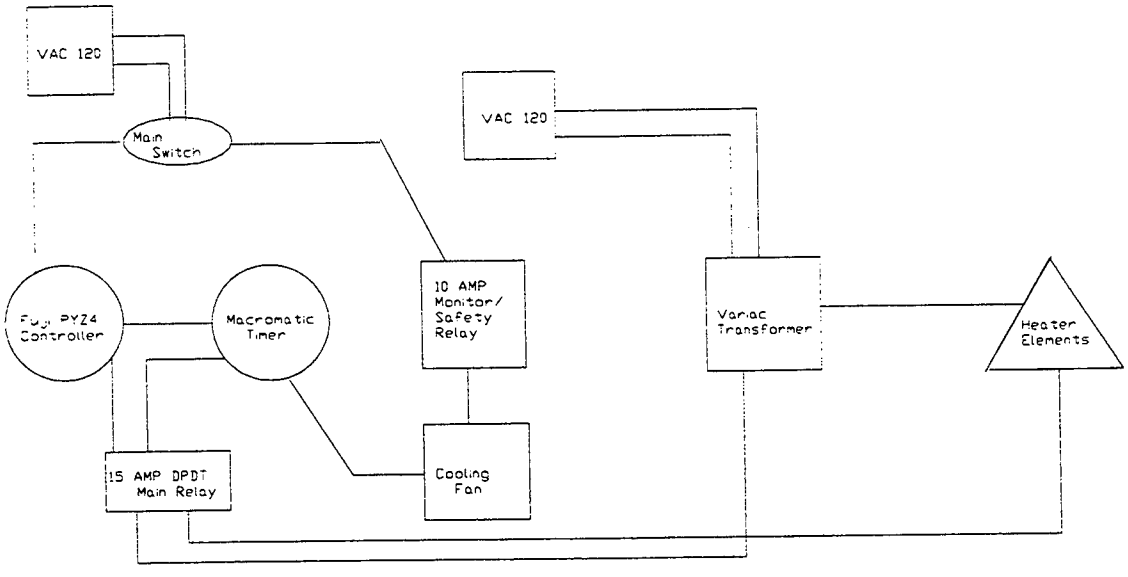

Figure 5: Thermocouple Locations in Heater Elements

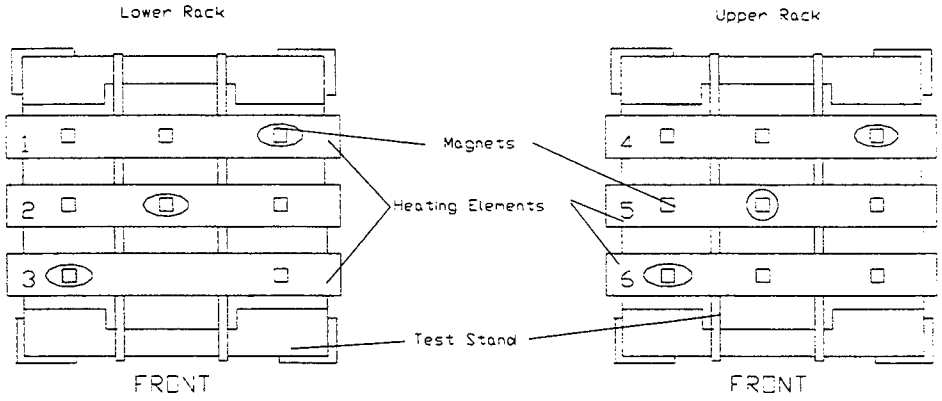

Note: Denotes control point thermocouple position

Denotes thermocouples positioned near magnets

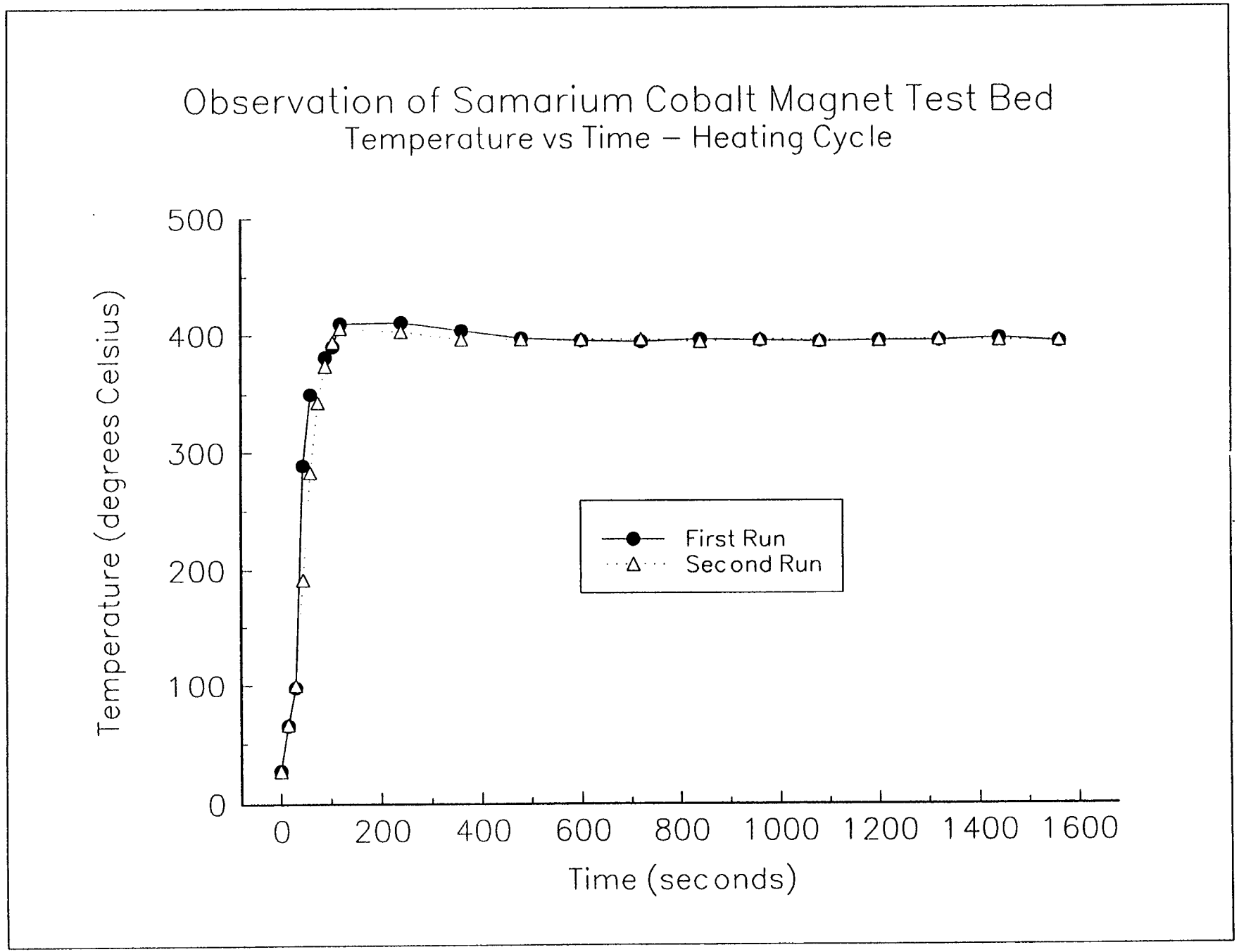
Observation of Samarium Cobalt Magnet Test Bed
Temperature vs Time – Heating Cycle
Temperature (degrees Celsius)
500
400
300
200
100
0
0
200
400
600
800
1000
1200
1400
1600
Time (seconds)
First Run
Second Run

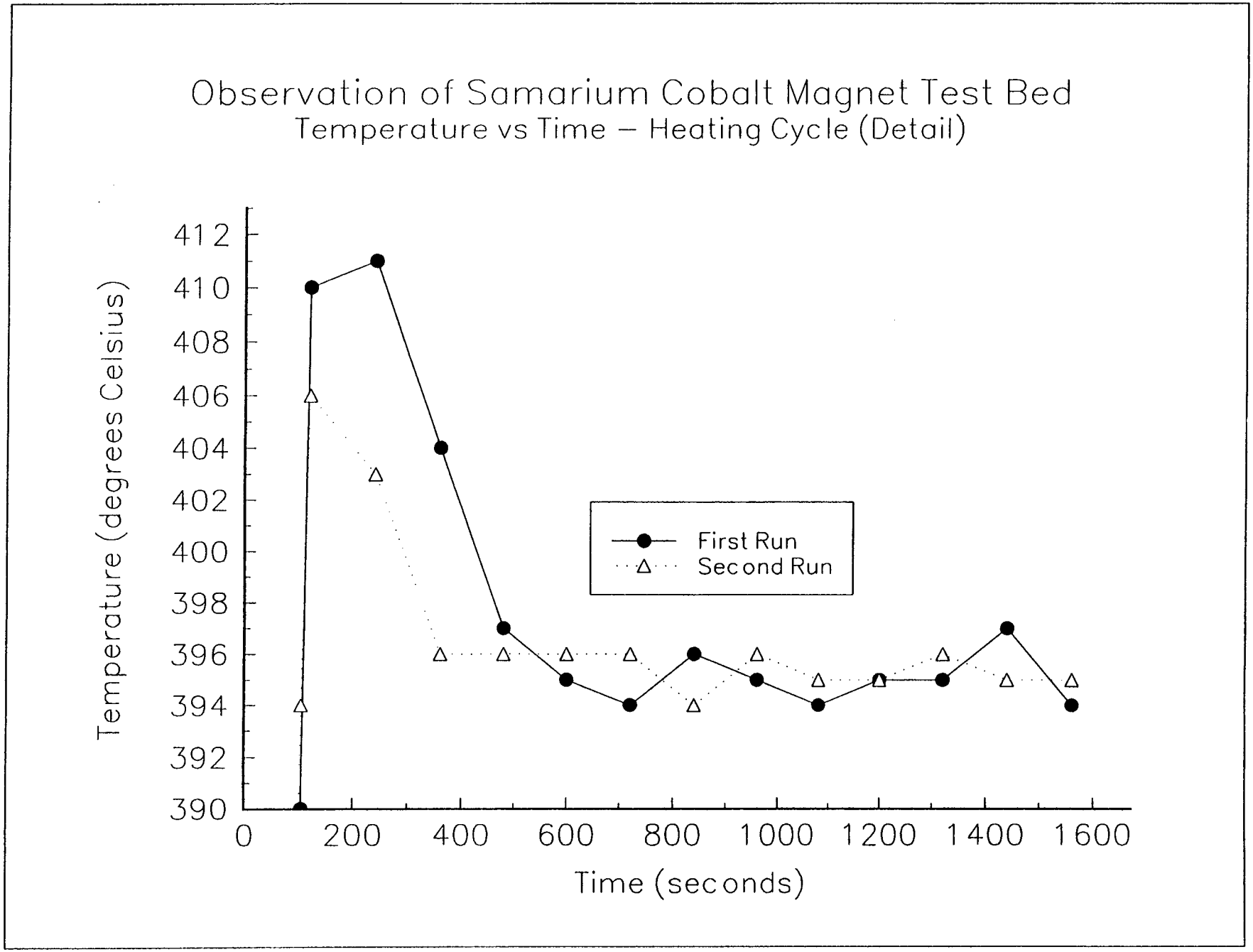
Observation of Samarium Cobalt Magnet Test Bed
Temperature vs Time – Heating Cycle (Detail)
Temperature (degrees Celsius)
412
410
408
406
404
402
400
398
396
394
392
390
0
200
400
600
800
1000
1200
1400
1600
Time (seconds)
First Run
Second Run

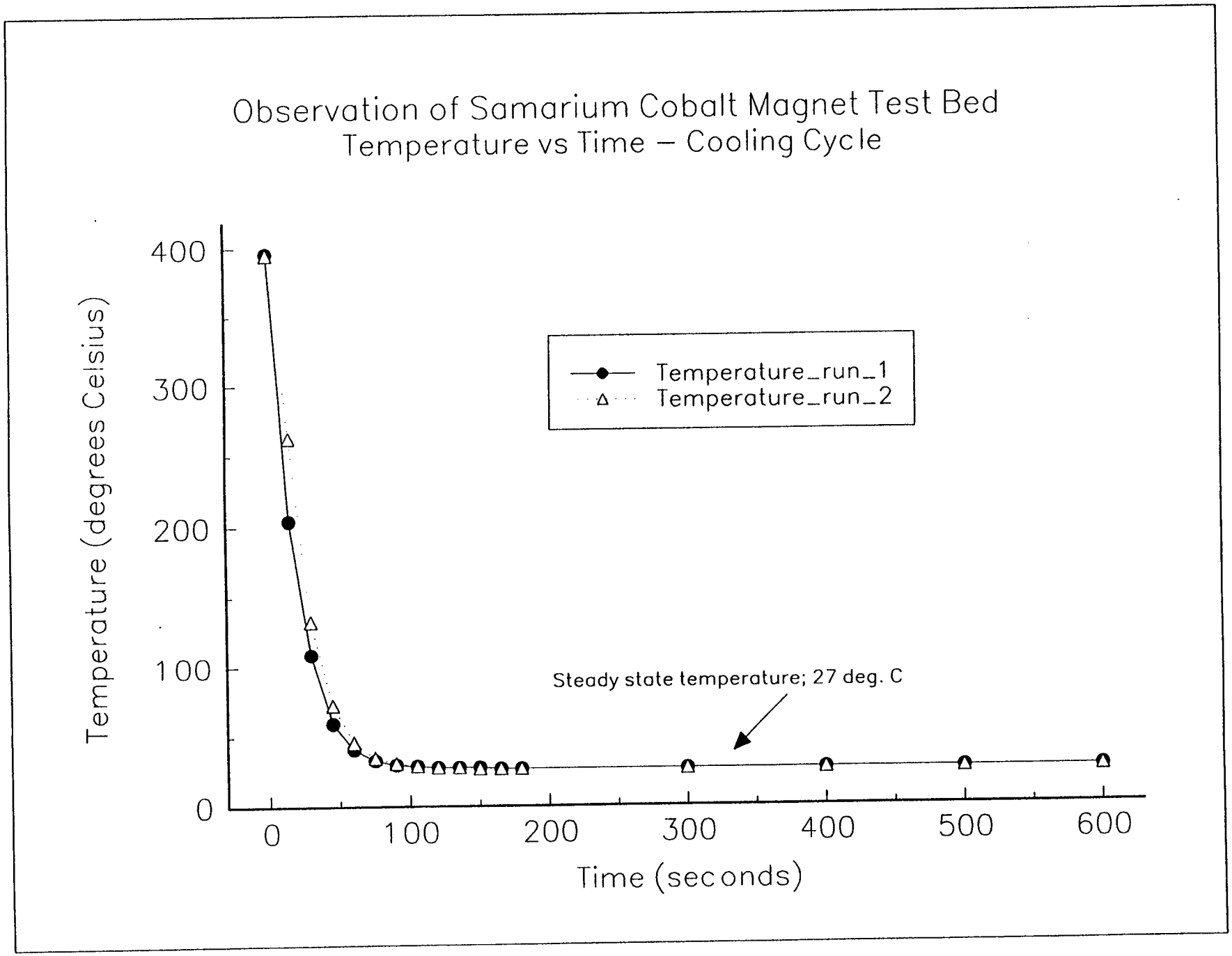
Observation of Samarium Cobalt Magnet Test Bed
Temperature vs Time – Cooling Cycle
Temperature (degrees Celsius)
400
300
200
100
0
Temperature_run_1
Temperature_run_2
Steady state temperature; 27 deg. C
0
100
200
300
400
500
600
Time (seconds)

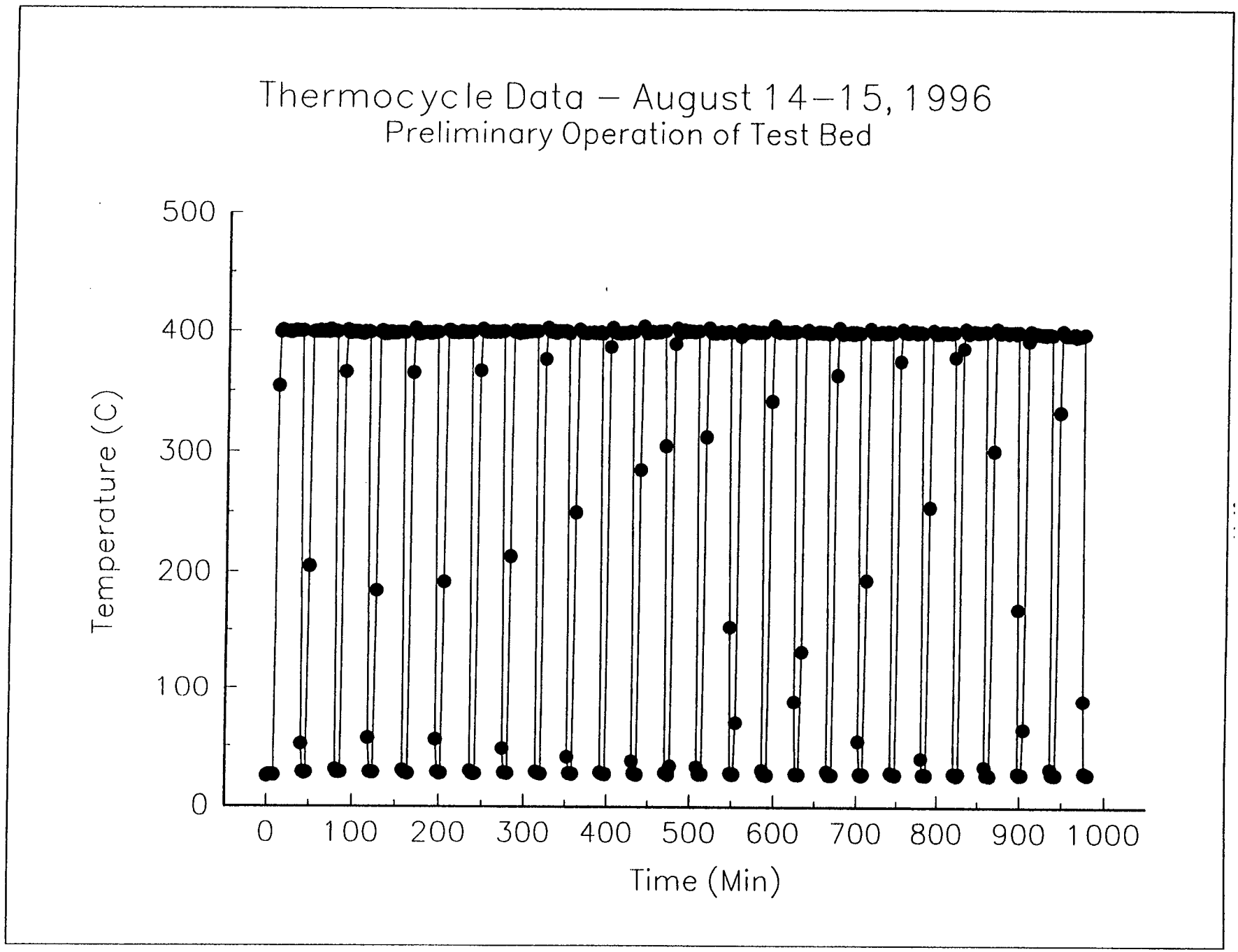
Thermocycle Data – August 14–15, 1996
Preliminary Operation of Test Bed
Temperature (C)
500
400
300
200
100
0
0
100
200
300
400
500
600
700
800
900
1000
Time (Min)

THE STUDY OF THE NEOTAM* COMPUTATIONAL MODEL

Angela C. Helm

Carroll High School
4524Linden Avenue
Dayton, OH 45432-0367

Final Report for:
High School Apprentice Program

Sponsoring Laboratory:
Wright Laboratory-WL/AACT

Sponsored by:
Air Force Office of Scientific Research
Bolling Air Force Base, Washington DC

and

USAF Wright Laboratory

09 August 1996

THE STUDY OF THE NEOTAM COMPUTATIONAL MODEL

Angela C. Helm
Carroll High School

ABSTRACT

This paper involves research that was done on the NATO NEOTAM (NATO electro-optic target analyzing model) computational model. This model is set in a Khoros Cantata environment. This platform uses the GUI (Graphical User Interface) format. It allows the user to interact in a graphics atmosphere with the information that deals with the NATO model. Unfortunately, this program is not yet user friendly. NEOTAM phenomonologists are trying to develop ways to make the program easy for unexperienced users to run the model successfully. The purpose of this research was to use the model, and as an unexperienced user, comment on parts that were not user friendly. In order to do this successfully, a basic learning of aerial targeting and what it involves had to be attained. Numerous weeks were spent studying the concepts of infrared aerial targeting, and it's application to modeling and simulation. After this was done, this acquired knowledge was applied to the NEOTAM model. Comments were made on how this program could be improved. The primary work done was to design GUI style glyphs (a way to portray information graphically) with the information that existed in a text form.

TABLE OF CONTENTS

A STUDY OF THE NEOTAM* COMPUTATIONAL MODEL

Angela C. Helm

INTRODUCTION

The use of the electromagnetic spectrum is advancing the ways that targeting sensors are used in the military today. The electromagnetic spectrum is an arrangement of the various electro- magnetic radiations in order by wavelength or frequency. These radiations, in order, by increasing wavelength, are: gamma rays, X-rays, ultraviolet, visible, infrared (near, mid-wave, long wave, millimeter-wave), and radio. The visible wavelength is dealt with every day by the human eye. Visible radiation is the wavelength band where human eyes operate. Any wavelength between 0.4 and 0.7 micrometers (μm) is within the visible wavelength.

Infrared (IR) wavelengths cannot be seen by the naked eye without the aid of mechanical devices. The infrared range is between 0.7μm to 24.0μm. Within this range there are four subdivisions; near, mid-wave, long wave, and millimeter-wave. Most of the EM radiation used for viewing in the visible and near IR bands are reflected off of the objects being viewed. In the mid-wave and long-wave bands, the user can also "see" an object by it's emitted radiation. In the thermal IR bands, objects are seen by a combination of reflected and self-emitted radiation.

In aerial targeting, the use of sensors operating in infrared frequency bands is giving our aircrews a great advantage over their opponents by:
1.) allowing the aircrew to detect another aircraft before it reaches visual range.
2.) allowing the aircrew to determine if an aircraft is enemy or ally.
As these techniques are perfected, it becomes easier to detect and destroy enemy targets at safe distances. This fine discrimination also prevents fratricide.

A target seen with a particular sensor has a "signature". A signature is a set of observable characteristics of a target which give it a unique identity. Knowing that the infrared frequency band portrays images by their emitted heat, the signature of a target presented in a thermal image is determined by the pattern of radiance. An example of a signature may be a targeted aircraft having one of its "hot parts" located midway on the left side. The pilot may know that his own vehicle has the same feature as the targeted aircraft. From this information, the pilot can deduce that the object being targeted is probably one of his own ships.

Automated means for classifying targets based on signatures are presently being developed. Electromagnetic spectrum targeting uses modeling and simulation in research and development for actual aerial targeting situations. A model is a representation of an object or process that is being studied, and has similar, if not exact, properties of that object or process. This paper involves modeling being used to test how certain aspects of a sensor system will react to different anticipated conditions.

In targeting, there is a distinct difference between detecting a target and recognizing a target. The difference being that, detection of an object is plainly realizing that a target is present. Recognition of an object is first detecting that a target is present, finding it's signatures, and using these to determine if it is an enemy or ally. Automatic recognition of a target based on signatures involves a series of sophisticated algorithms that operate on powerful computers. Algorithms are a set of mathematical rules used to solve a problem in a finite number of steps.

Signatures play a significant role in the targeting process. It is vitally important that the air crew, vehicle designer, and the sensor designer all know and understand signatures and what influences them. Although signatures are very important, they are also highly variable. Different conditions can affect the way signatures look. These conditions may not be easy for a human to detect, but they are the basis for a sensor's reliability.

Contrast is also very important to the success of EO sensor prediction. Being able to distinguish between the targeted object and it's background is an essential step in targeting. Many things contribute to the way signatures may look to a sensor. One is weather sensitivities: the way the environment affects electromagnetic activity. An important weather sensitivity occurs in background. Some background settings include: grass, soil, trees, roads, towns, and cities. These settings, depending on which ones are present, affect the electro-optical (EO) sensor's ability to produce dependable results. If the background makes it difficult for the flight crew see objects that are in the visual wavelength, then the IR sensor usually is able to pick up the image without trouble.

Another weather sensitivity that EO sensors have to compensate for are atmospherics. Atmospherics include clouds, humidity, wind speed, air temperatures, smoke, and dust. Clouds interfere with the performance of IR and visible systems. They tend to obscure atmospheric transmission and suppress target-background contrast. Humidity absorbs many wavelengths, making it hard for the sensor to detect images well. Wind speed shakes the airframe causing the sensor to produce an unstable image. Air temperatures create shimmer distortion in images causing an image that is fuzzy or comes into focus in waves. Smoke and dust reduce the contrast through absorption, they also cause path radiance.

Cirrus clouds exist in two forms, normal cirrus and sub visual cirrus. Cirrus are high altitude clouds characterized by this white filaments or narrow bands of ice crystals. Sub cirrus clouds are invisible when

viewed from the azimuth and zenith angles. The azimuth angle is defined as the angle of horizontal deviation that is measured clockwise. The zenith angle is defined as the point on the celestial sphere vertically above a given point or observer. The point which these clouds can be seen is horizontally along the line of sight. When looking at a sub cirrus cloud from it's line of sight, it can reach for great distances. If looking at it from an angle, the person can see nothing. This type of weather conditions has proved to be very threatening to the pilot and the performance of the aircraft because of unexpected cloud cover.

A third category of weather sensitivities is the climate of the region that the aircraft is operating in. Examples of these climates include solar insolation (solar radiation), latitude, longitude and solar zenith and azimuth angles. In order to fly an aircraft to the best of its ability, the weather conditions must be considered. In most cases, several of the weather sensitivities mentioned are present when an aircraft is in use. The more weather sensitivities present, the more obstacles the IR sensors have to contend with.

In this program, the NATO model will be tested using the NEOTAM (NATO Electro-Optical Targeting Analysis Model) system. This is a modeling and simulation system that involves software which computes and displays aircraft and missile signatures on UNIX platforms. The NEOTAM system allows users to run individual models against certain aspects of the signature modeling problem. This allows a detailed and diverse study of the ways the target signature will react to different conditions and in turn how the sensor systems will perform in these conditions. This program allows for each smaller study to be linked together into a combination of all the influences in an end-to-end targeting situation.

End-to-end networking is seen as a complete view of a problem, and a complete approach in solving it. (see diagram on end-to-end networking, page 27-13) Modeling can cover either a very narrow or a very extensive study. Instead of a model researching only one aspect of the IR targeting process, a model will look at all of the conditions present and analyze them as a whole. This type of networking is far more beneficial in learning how the sensor will react with it's environment.

PURPOSE

The purpose of this research paper was to design a way to simplify operation of the Khoros Cantata NEOTAM software. In doing this, the NEOTAM model did not have to run successfully. Running the model was not the main focus of this research. The focal point was developing a user friendly model that is easy for a new user to run. In order to make the system easier to use, GUI- style glyphs were edited or created. GUI means Graphical User Interface and a glyph is a function that creates a small interactive icon that stores all the information that was produced for the user in a text form. This is a style that lets the user interact with the program in a graphics environment. This interaction is helpful for the inexperienced user to run the model. It helps experienced users work quickly and interpret outputs without error. In designing the GUI glyphs, the information was taken from a text from and put in to a GUI style format. This was to be done to all of the models that did not preexist in a glyph format.

PROBLEM

The problem under this research topic was that the NEOTAM computational model was not yet user friendly. The model was ready to be run successfully, but it was difficult for inexperienced users to run the program. Due to this problem, ways to help the system to become more user friendly had to be developed. This task involves a series of people, ideas and contributions for a successful outcome. The improvement to the NEOTAM computational model lie within the development of GUIs.

METHODOLOGY

In researching this project, a series of steps were taken. The first step in beginning this experimentation was to gather information pertaining to the infrared targeting process. Once this was done, a basic understanding of electromagnetic sensor technology and how it applied to aircraft targeting, was acquired. This new information was then put to use by applying it to small scenarios and coming up with answers to those scenarios.

Next, we had to receive a SunSparcs station the computer equipment that was required to run this

program. The equipment necessary was a SunSparc station. On this Computer, the NEOTAM model was to be run through the Khoros program. The cantata program uses a GUI format. The GUI format is a conglomeration of icons and graphics that help a user to run a program with visual aids. These visual aids provide an understandable procedure for running the program.

Khoros Cantata program was installed into the SunSparc Station. Cantata introduces a workspace which allows the user to create the desired environment in which the model will be tested. To do this, the user must go to the icon which holds the particular aspect of the environment that is to be altered. This done, the user will be allowed to edit the information given and finally glyph the item. Glyphing is a process which takes the inputted information and turns it into a small icon in the workspace. Once the information is to this point, it can be connected together with other glyphed material and run together as a network.

In most SunSparc stations that are installed, it is expected that the FORTRAN 77 library is already in the system. For some unknown reason, this was not the case. In order for the Cantata program to be run correctly, this library had to first be installed. This hindered the research of this program for about two weeks. After the installation was complete, another obstacle arose. In order to create glyphs from the information that was still in text form, a technical document telling what the text meant had to be received. This was not received until the last two weeks of research. During that waiting time, the Khoros Cantata program was modified.

DATA / RESULTS

The start date for collecting data was July 10, 1996. On this day, the NEOTAM program was installed into the SunSparc Station computer. Once up and running, the program was able to be accessed. When logging on as a new user, an option for a "shell tool" was presented to the user. This option was not clear as to what it is. Recommendation: add a help option to this window to inform a new user on how the shell tool may be used. Experienced users may choose to simply disregard the option after first learning the information.

Once the user decides to proceed with or without the shell tool, the Cantata screen appears. This is where the networking for the model will take place. In making a network, a series of glyphs must be made. These glyphs are then connected together by clicking on the connector arrows. (A line should appear showing that a good connection was made.) The problem here was that the connector arrow and the screen background were the same color. Thus, the user had no way of knowing if the connection was completed. To fix this problem, a programmer must change the color palette. Recommendation: the

program should have a preset color for the screen which is different than the one for the arrows to be able to make a distinction between the two.

Before running the network of connected glyphs, the variables of each glyph can be changed as desired. Once the conditions are set, the user will then "turn on" or run the network. In doing this for the first time, errors saying that the program could not read the file were encountered. It was noted later that the installation of the NEOTAM program was incomplete. Two weeks of effort were required to track the some problems to missing libraries, files and documents in the operating system and models. It was later discovered that the library was not a problem with the NEOTAM model, but with the SunSparc station.

Some of the modifications suggested about the NEOTAM model have to deal with package completeness. In order to produce effective results from this program, the system should have an easy installation package with a complete list of the software that is needed. This will speed the initial start-up of the program. A new user that has little to no experience with the Cantata program is likely to have problems in being able to use i t to it's greatest extent. This is why there should be a small tutorial at the beginning of the program to help the new users to begin their exploration of Cantata with out stumbling along the way.

In the NEOTAM package that was given for this particular research project, only the sub models CET and REP could be run. In the beginning of the testing, this was not known. Had I known earlier that those were the only models that could be run together, it would have saved a lot of time that could have been well spent exploring the NEOTAM model. In order to prevent this same thing from happening to other people, each package should be clearly marked telling what aspects of the NEOTAM model were installed into that particular program.

In each GUI glyph, there is a help option. This is a very helpful item when trying to understand the functions of each sub model. Unfortunately, these help functions are not yet completed. It is important for the new user to be able to rely on this function for help. Inside these help menus, there should be a section that explains what other models should be run with the particular model being used, and what order would be best for them to be in.

In creating the GUI glyphs, many things can be said. Trying to understand the information that existed in text form was difficult. The technical document which was recieved helped explain what each line number represented. Without this documentation, it would have been impossible to create glyphs for the rep sub model. This documentation should be attached to the NEOTAM package that is sent to the user.

CONCLUSION

In conclusion to this project, it can be said that the NEOTAM computational model needs much editing due to the fact that it is not user friendly . Throughout the eight week period of research, is was discovered that modeling is essential to the success of targeting sensors. Before a targeting sensor can be used, numerous studies must first take place to test it's reliability. This has to be done with not only the NEOTAM computational model, but with every model used in research and development.

Researching this topic on modeling has resulted in many outcomes. The most important result was, that it is essential to the success of the program to have a user friendly program. Creating GUI formats for the text information is a good way to do just that.

REFERENCES

1. Capps, W.L, et al. The Aircraft Infrared Measurements Guide, report JTCG/AS. 81-c 002. March 1983.

2. Electro-Optic Model for Aerial Targeting, version 2.00 (EMAT 2.00) User Manual; Horizons tech, inc. San Diego,1991. (Controlled-Distribution Limited)

3. Fligor, Patrick D, et al. Electromagnetic Radiation Signatures From 0.2 to 14.0μm for Target and Background Materials and Scene Energy Sources For Naval Night Sensing. Washington DC: Technology Inc., July 1970.

4. Schaibly, John. Dr. NEOTAM* 0.P.1 (Preliminary) User Guide and Tutorial. San Diego: Horizons Technology, Inc., April 1996.

5. Weiss, Richard A., and Randy K. Scoggins. Infrared Target Background Analytical Models US Army technical report E1-98-11, SWOE report 89-3. Engineer Waterways Experiment Station, Vicksburg, MS. Aug.1989. (Controlled-Distribution Limited)

6. Wolfe, William L., Handbook of Military Infrared Technology. Office of Navel Research Department of the Navy, Washington, D.C.,1965.

7. Various unpublished reports, papers, videos and presentations were also a source of documentation throughout this research paper. As supervisors, William Lanich, and Mary Anne Gualtieri along with others aided in the progression of this report. This research topic was also aided by my colleague, Disha J. Patel.

PLUME TESTING (GUI)

(click on whole number coordinate for to see values)

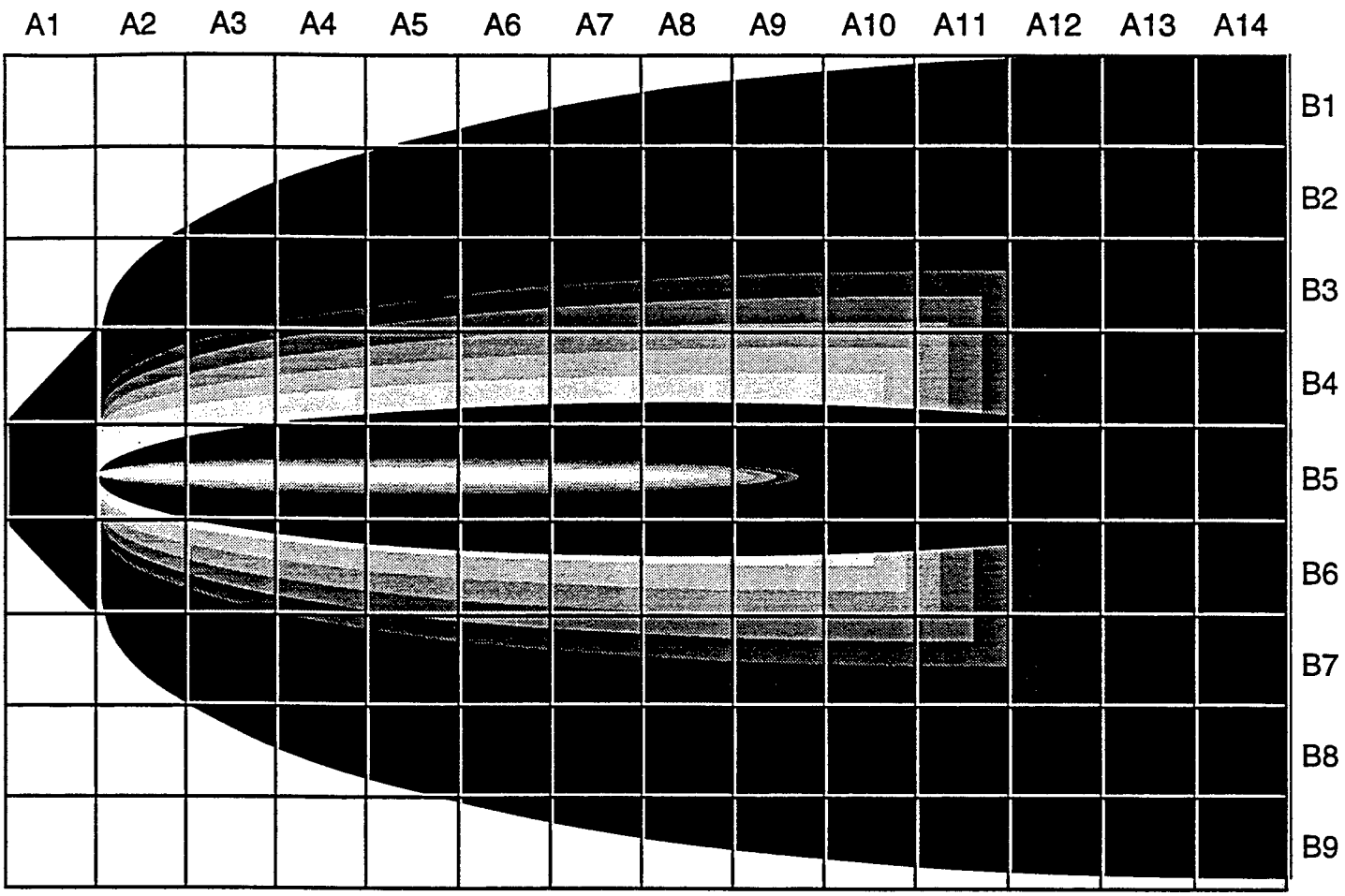

GLYPH
RUN
SAVE
HELP
QUIT

TEMP
N2
H2
CO
CO2
H2O
H
OH
HO2
PBO
O2
O

*This GUI representation is a map of the temperature or species concentration data in the rep.dat output file.

*This will allow the user to access a section of the plume by simply selecting that area, as opposed to changing the information in the text editor.

AEM*AT Signature Factors

FACTOR not all are independent	TARGET (hardbody emitted / reflected, plume)	PATH signal loss, additive noise, modulation	BACKGROUND clutter geometry, spectral content, intensity
Illumination			
• **sunshine — current / history** bearing, elevation (ToD), clouds	reflection, glints, heating	path radiance	reflection, heating, clutter: glints (water, cultural detail), shadows
• **skyshine — current / history** bearing, clouds, surface condition	reflection, heating	path radiance	reflection heating
• **cloudshine — current / history** type, altitude, coverage	reflection, heating	path radiance	reflection, heating
Meteorology			
• **humidity — current / history**	skin heating, hot parts temp, plume spectrum	spectral xmsn	transpiration, soil moisture, (cultural detail = target factors)
• **air temp — current / history**	skin heating, engine temp, plume	spectral xsmsn	transpiration, soil moisture (cultural detail = target factors)
• **airspeed / wind — current / history**	skin heating (total/differential), plume geometry, wake, hot parts	vapor/aerosol sources (cultural detail = target factors)	transpiration, soil moisture
• **clouds — current / history**	contrast reversals	signal loss, contrast loss,	clutter, rad trap (contrast reduct, hi temps), modulation
• **hardbody construction**	skin $\varepsilon/\alpha/\rho$, internal conduction, thermal mass		cultural detail = target factors
• **surface coating & condition**	aero skin heating, $\varepsilon/\alpha/\rho$		cultural detail = target factors
• **internal stores (fuel cells, e.g.)**	differential skin heating		cultural detail = target factors
• **external stores**	additive signatures, drag affects flying factors		
• **fuel type**	plume spectral signature, tgt size (vis/subvis contrails)	visual/subvisual contrails (attenuation)	visual/subvisual contrails (clutter
)Flying Factors			
• **altitude — current / history**	skin heating, engine temp, xmsn		sky/horizon/terrain
• **speed — current / history**	skin heating, engine temp,		sky/horizon/terrain
• **attitude wrt flight vector — current / history**	differential skin heating		
• **attitude wrt LoS**	radiation pattern		pointing, stabilization
• **throttle setting — current / history**	plume, hot parts, aero heating	water vapor, "cirrus", aerosols	water vapor, "cirrus", aerosols

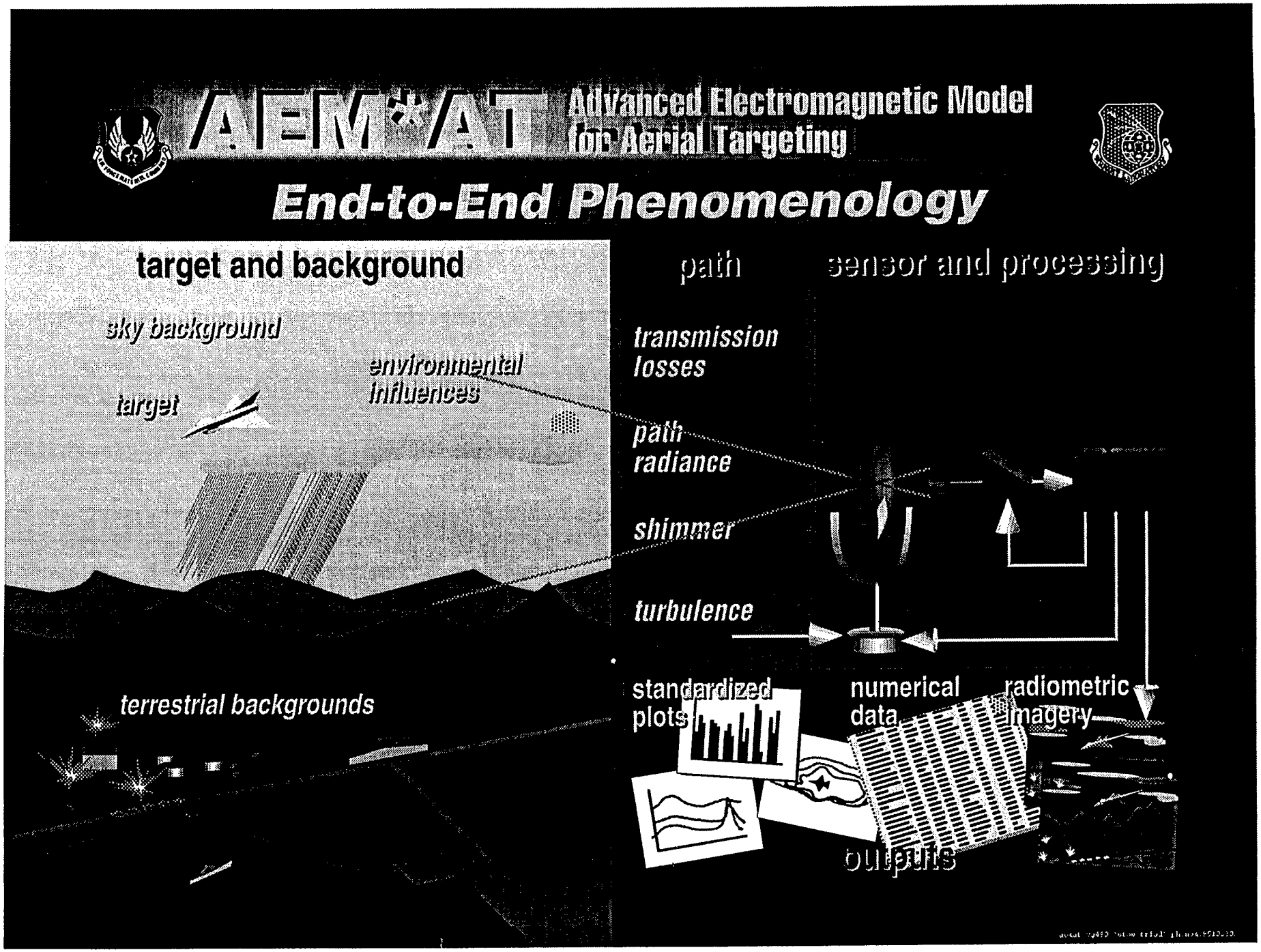
AEM*AT
Advanced Electromagnetic Model for Aerial Targeting
End-to-End Phenomenology
target and background
path
sensor and processing
sky background
environmental influences
target
transmission losses
path radiance
shimmer
turbulence
terrestrial backgrounds
standardized plots
numerical data
radiometric imagery
outputs